Vol. 8 No. 1
April 2024

ISSN 2579-5821
e-ISSN 2579-5546

S3 sinta
Science and Technology Index

Jurnal Geocelebes

Published by:
Geophysics Department
Hasanuddin University
Makassar, Indonesia

JURNAL GEOCELEBES
Geophysics Department | Faculty of Mathematics and Natural Sciences | Hasanuddin University

Volume 8 Number 1, April 2024

P-ISSN: 2579-5821
E-ISSN: 2579-5546

Published by:
Geophysics Department, Math and Natural Science Faculty
Hasanuddin University

JURNAL GEOCELEBES
Volume 8 Number 1, April 2024

ISSN: 2579 – 5821 (Print)
ISSN: 2579 – 5546 (Online)
URL address: http://journal.unhas.ac.id/index.php/geocelebes

Diterbitkan berkala dua kali setahun oleh/ **Published periodically two times annually by**
Dept. Geofisika Universitas Hasanuddin/ **Geophysics Dept., Hasanuddin University**

Dewan Redaksi/ Editor Board

Sekretariat/ Secretariat:
Departemen Geofisika, FMIPA Universitas Hasanuddin
Gedung MIPA, Kampus Unhas Tamalanrea - Jalan Perintis Kemerdekaan, Makassar, Sulawesi Selatan, 90245.
E-mail: geocelebes@sci.unhas.ac.id

Jurnal Geocelebes is a scientific journal published by the Department of Geophysics, Hasanuddin University. This journal is intended as a means of scientific publication in the field of geophysics ranging from theoretical topics to geophysical applications in various fields topics. The articles are original research results, reviews of recent advances in a particular topic, case studies of geophysical applications or reviews of software related to geophysics. Papers should be sent to the editorial website in softcopy using the template provided. Each accepted paper will be reviewed for eligibility through a rigorous reviewing process by the Editorial Board.

Contents

JURNAL GEOCELEBES

Volume 8, Number 1, April 2024

ISSN: 2579 – 5821 (Print)
ISSN: 2579 – 5546 (Online)

URL: http://journal.unhas.ac.id/index.php/geocelebes

Preface

Jurnal Geocelebes managed by the Department of Geophysics, Faculty of Mathematics and Natural Sciences, Hasanuddin University Makassar has entered its eighth year. The Editorial Board expresses gratitude to God Almighty for this achievement and expresses gratitude for the commitment of the Editorial Board, in carrying out this mandate. In particular, the Editorial Board expresses its gratitude and highest appreciation to all authors who have submitted their scientific works and to the Reviewers who have been willing to take the time to provide constructive suggestions and corrections to each article in each issue of the Jurnal Geocelebes.

In the edition of Volume 8 Number 1 April 2024 there are ten articles. The articles published generally discuss the implementation of the role of geosciences, especially geophysics in natural resource exploration and other fields that are in accordance with the focus and scope of the field published by the Jurnal Geocelebes. The language used in this volume and in the future is English, which shows that Jurnal Geocelebes deserves to be an international journal in the future. Jurnal Geocelebes welcomes participation from academics, researchers, industry practitioners, students, and others in the field of geosciences in both theoretical and application perspectives, both related to the subsurface (lithosphere) and above the surface (atmosphere), which of course will go through a series of processes namely submitting, editing, and reviewing.

The Editorial Board of Jurnal Geocelebes is open to suggestions and constructive criticism for future improvements. All suggestions and criticisms can be sent via email geocelebes@sci.unhas.ac.id

Makassar, April 2024

The Editorial Board of Jurnal Geocelebes

ISSN: 2579-5821 (Print)
ISSN: 2579-5546 (Online)
URL address: http://journal.unhas.ac.id/index.php/geocelebes
DOI: 10.20956/geocelebes.v8i1.28144

Jurnal Geocelebes Vol. 8 No. 1, April 2024, 1 – 10

Investigation of Sediment Layer Thickness Estimation at Bengkulu University Hospital Based on Microtremor Data

Andre Rahmat Al Ansory, Hana Raihana, M. Farid*, Arif Ismul Hadi

Geophysics Study Program, University of Bengkulu, Indonesian

*Corresponding author. Email: mfarid@unib.ac.id

Manuscript received: 7 August 2023; Received in revised form: 15 September 2023; Accepted: 17 November 2023

Abstract

Bengkulu is the capital of Bengkulu Province and is in the subduction zone between the Eurasian and Indo-Australian plates. Bengkulu is also close to the major faults of Sumatra, namely the Musi fault, the Ketahun fault, and the Manna fault. Therefore, regional planning and infrastructure development for earthquake mitigation is necessary. The purpose of this study is to estimate the thickness of the sedimentary layers in the construction zone of Bengkulu University Hospital during the earthquake attenuation phase. This study is conducted by surface geological analysis using the HVSR method; data analysis using microtremor data. The microtremor data were analyzed using the HVSR method to obtain the amplification value (A_0) and the dominant frequency (f_0). HVSR analysis gave dominant frequency (f_0) values from 5.1 to 5.8 Hz, amplification (A_0) from 1.64 to 5.91 times, and dominant period (T_0) from 1.49 to 2.81 seconds. The values of A_0, f_0, T_0 are interpreted with reference to the literature and surface geology as a moderate risk of seismic vulnerability, characterized by moderate to weak sedimentation and moderate amplification values.

Keywords: A_0; f_0; microtremor; sedimentary rocks; T_0.

Citation: Al Ansory, A. R., Raihana, H., Farid, M., & Hadi, A. I. (2024). Investigation of Sediment Layer Thickness Estimation at Bengkulu University Hospital Based on Microtremor Data. *Jurnal Geocelebes,* 8(1):1-10, doi: 10.20956/geocelebes.v8i1.28144

Introduction

Bengkulu is the capital of Bengkulu Province and is located at the subduction zone between the Indo-Australian and Eurasian plates. Bengkulu is close to the Great Sumatra Fault, which are the Ketahun section, the Manna section and also the Musi section (Irsyam et al., 2017).

Bengkulu Province itself is located at the coastal area of Sumatra Island that is directly facing Indian Ocean. Within last 10 years, the climate change effects had resulted several impacts to the environment in several areas around Indian Ocean, including Bengkulu City, the capital city of Bengkulu Province (Mase et al., 2022).

This situation makes Bengkulu subject to frequent earthquake disturbances (Lestari & Susiloningtyas, 2022). Tectonic plates move continuously and can be felt on the surface of the earth in phenomena called seismic tectonic events (Mase, 2017).

The Eurasian plate moves relatively southeastward very slowly, averaging about 0.4 cm, colliding with an oceanic plate, the Indo-Australian plate, at a speed of 7 cm per year in a relatively northern direction (Silitonga et al., 2023).

This of course makes Bengkulu Province very vulnerable to earthquake events. Regional governance and the development of facilities and infrastructure that are oriented towards earthquake disaster

mitigation need and must be applied in areas prone to earthquake disasters.

Referring to this condition, the local government should be carefully considering the earthquake aspect for the spatial plan in Bengkulu City. The actions to define the spatial plan should cover safety, convenience, productivity based on hazard mitigation is prioritized. Natural Disaster Agency of Bengkulu Province or BPBD mentioned that the revised spatial plan is also destined to support Bengkulu City as the tourism and educating area and as the trading area in the coastal area of Western Sumatra Island, nationally and regionally (Farid & Mase, 2020).

Bengkulu University is one of the universities located in Bengkulu City. Bengkulu University always strives to provide great benefits to the community, one of which is by building health and education facilities in the form of Bengkulu University Hospital.

The principle of development in this hospital is to apply the principle of sustainable development which is become a public place that can be used for a long time. An environmental carrying capacity or "sustain" is very important in a sustainable development which is a way to keep what we have and must remain.

A step to keep the Bengkulu University Hospital sustainable is to build these public facilities based on the application of earthquake disaster mitigation, considering that the location of the hospital itself is in an area that is vulnerable to earthquake disasters.

The initial stage is to know the character of the sedimentary rock layer found at the construction site of this hospital. Where a layer that has a low frequency value and a high amplification value can cause a response to a larger wave to cause a stronger shock to the building on the surface of the earth (Ryanto et al., 2020).

Information on the frequency values of rock formations is important to reduce the effects of shaking in buildings that have similar frequency values when earthquakes occur (Saputra et al., 2022).

Geophysics is a branch of science that is utilized in order to obtain information about the state of subsurface structures. The subsurface of sedimentary rocks can be identified using the microtremor method (Moustafa et al., 2022).

In this study using the analysis of estimating the thickness of the sedimentary layer structure at the bottom of the top using microtremor data by considering the geological conditions at the construction site of the Bengkulu University Hospital. The purpose of this study is to estimate the thickness of the sedimentary rock layer at the construction site of the Bengkulu University Hospital, as part of the preparedness stage in the event of an earthquake disaster. This study was also carried out to support the robustness of the building.

Materials and Methods

The Horizontal to Vertical Spectral Ratio (HVSR) method is one of the methods that can be used to utilize microtremor data. It can generate the dominant frequency value and amplification of the soil in an area, to compute the seismic vulnerability index and the thickness of the sedimentary layer. The purpose of this study was to determine the level of seismic vulnerability in the study area by making a map of the distribution of the dominant frequency value, amplification factor, seismic vulnerability index, shear wave velocity

and sediment layer thickness (Isburhan et al., 2019).

The microtremor data is obtained from the 3 (three) component short-period digital seismometer, which consists of 2 (two) horizontal components (north-south direction and east-west direction) and 1 (one) vertical component. The data is stored in digital waveform with sampling rate 100 Hz, and it must be transformed into frequency domain so the spectral ratio can be analyzed. The process of transforming the data from time domain into frequency domain is called Fast Fourier Transform (FFT) (Amirudin et al., 2023).

The HVSR value is the peak of the spectrum at the dominant frequency at one measurement point. HVSR also calculate the amplification as the micro zonation parameter. The amplification factor is mostly influenced by the wave velocity and rock density, if the wave velocity is getting lower, the amplification will be larger (Asnawi et al., 2020).

The sites' resonance frequency and peak amplitude can be obtained without any high energy sources, both naturally occurring (earthquake activities) and manmade ones (Imposa et al., 2018).

This research was conducted at the construction site of the Bengkulu University Hospital, using the microtremor method with a total of 15 measurement points, with a space between measurement points of 15 meters. The research survey design map can be seen in Figure 1.

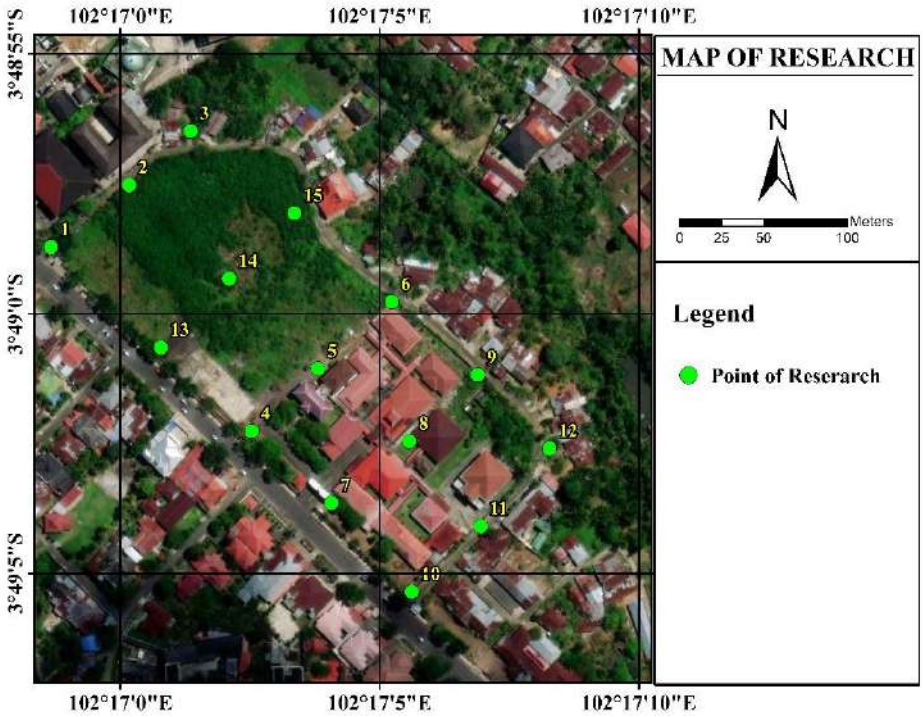

Figure 1. Map of Research Location

Initial data obtained from microtremor measurement results in .csv format After that it was converted to saf. After being replaced, continued with processing using the Geophysical Signal Database for Noise Array Processing (GEOPSY) version 3.4.2 application with HVSR analysis.

The research procedure is broken down into stages, which are field data acquisition sessions, data processing and data interpretation and analysis. The data collection method uses the single station microtremor method. Measurements in the field used the 3D Geophone / Surface Gemini 2 tool, with a measurement time of

30 minutes with a sampling rate 200 Hz (PASI, 2013).

The length of time of this measurement aims to obtain the maximum frequency value distribution. The measurement results are recorded in the form of a signal in .csv format on the device.

Interpretation is done by analyzing data from the results of processing with the HVSR method, which are data analysis of the dominant period (T_0), dominant frequency (f_0) and amplification (A_0) (Ghuge, 2023). The interpretation uses literature data, geological data, so that more accurate interpretation results can be obtained (Mase et al., 2021).

Results and Discussion

The results of this research data processing produce 2 types of curves. This type of clear peak curve dominates over the multi-peak curve where only one point out of 15 measurement points is a multi-peak curve (Dal Moro & Panza, 2022). The clear peak curve is an ideal curve for processing microtremor data because the reliability of clear peak curve data has been verified according to the European SESAME Project. In this case, the characteristic frequency obtained from the peak curve analysis can be considered as the natural frequency of the site. Data analysis using the HVSR method refers to the research results of SESAME for reliable data (Mohamed et al., 2021).

This type of clear peak curve dominates over the multiple peak curves where only one point out of 15 measurement points is a multiple peak curve. The clear peak curve is an ideal curve for processing microtremor data because the reliability of clear peak curve data has been verified according to the European SESAME Project. In this case, the characteristic frequency obtained from the peak curve analysis can be regarded as the natural frequency of a site.

Research that has been conducted with the same concept has been conducted by Hesti et al. (2021) that the results obtained in the UNILA Hospital area, the research area is a vulnerable area when an earthquake occurs characterized by thick and soft sedimentary layers and medium amplification values.

Distribution map of dominant frequency value analysis (f_0)

Based on data processing with the HVSR method, the distribution map of dominant frequency values is obtained as shown in Figure 3, which is interpreted that the area of Bengkulu University Hospital has a dominant frequency value ranging from 5.1 - 5.8 Hz. The dominant frequency value of an area indicates the level of sediment thickness and rock type as described in Table 1. The distribution of dominant frequency values in the research area ($5.1 < f0 < 6$ Hz) according to Haryanto et al. (2020) and Ridwan et al. (2021) is an area with type II classification with an indication that the thickness of surface sediments is in the middle category of 10 meters and is included in tertiary rocks. Medium sedimentary rock layers have a moderate risk of earthquake shaking.

Distribution map of dominant period value analysis (T_0)

Based on the dominant period value distribution map in Figure 4, it can be interpreted that the Bengkulu University Hospital area has a dominant period value between 1.49 - 2.81 s. The grouping of soil types refers to the value of the dominant period according to Omote-Nakajima (Haryanto et al., 2020) divided into 4 types, which are type I with a frequency value between 0.05-0.10 s which indicates the character of hard sedimentary rock types, type II with a period value of 0.10-0.25 s indicates the character of medium sedimentary rocks, type III with a period

value of 0.25-0.4 s indicates the character of soft sedimentary rock types, and type IV with a period value of more than 0.4 s indicates the character of very soft sedimentary rock types. The distribution of the dominant period value in the Bengkulu University Hospital area is T_0>0.4 s. The area is an area with type III classification according to Omote-Nakajima (Haryanto et al., 2020) with an indication of the character of very soft sedimentary rock types in the form of alluvial rocks, which are formed from delta sedimentation, top soil, mud. Based on data from the geological map, the research area is an alluvial deposit consisting of sand, clay, and gravel. Areas with soft sedimentary layers on the earth's surface are vulnerable to earthquake shocks.

Distribution map of amplification value analysis (A_0)

Based on the amplification value distribution map in Figure 5, it can be interpreted that the Bengkulu University Hospital Development area has an amplification value ranging from 1.64-5.91 times. The soil amplification zone according to Meng et al. (2023) can be divided into 4 risk descriptions, which are low risk category with amplification value (0<A_0<3 times), medium risk category with amplification value (3<A_0<6 times), high risk category with amplification value (6<A_0<9 times), and very high-risk category with amplification value (A_0>9 times).

Based on the results of the amplification calculation value in the Bengkulu University Hospital Development Area ranges from 1.64-5.91 into the medium category, so it can be said that the Bengkulu University Hospital Development Area is included in an area with a medium risk category against earthquake shocks

Table 1. Soil classification based on natural microseismic frequency value by Kanai ((Ridwan et al., 2021).

Classification soil		Natural	Kanai Classification	Description
Type	Class	Frequency		
IV	I	6.67 – 20	Tertiary rocks or older. Consists of Hard rock sandy, gravel, and others.	Thickness sediment surface very thin, dominated by rock hard rocks.
III	II	4.0 – 10	Tertiary rocks or older. Consists of Hard rock sandy, gravel, and others.	Thickness sediment surface in category medium 5-10 m.
II	III	2.5 – 4	Alluvial rocks with thickness of more than 5m thick. Composed of sandy gravel, sandy hard clay, loam, and others.	Thickness sediment surface in category thick, about 10-30 m
I	IV	< 2.5	Alluvial rocks which formed from the sedimentation of delta, top soil, mud, and others. Depth ≥ 30m	Thickness sediment surface very thick
I	IV	< 2.5	Alluvial rocks which formed from the sedimentation of delta, top soil, mud, and others. Depth ≥ 30m	Thickness sediment surface very thick

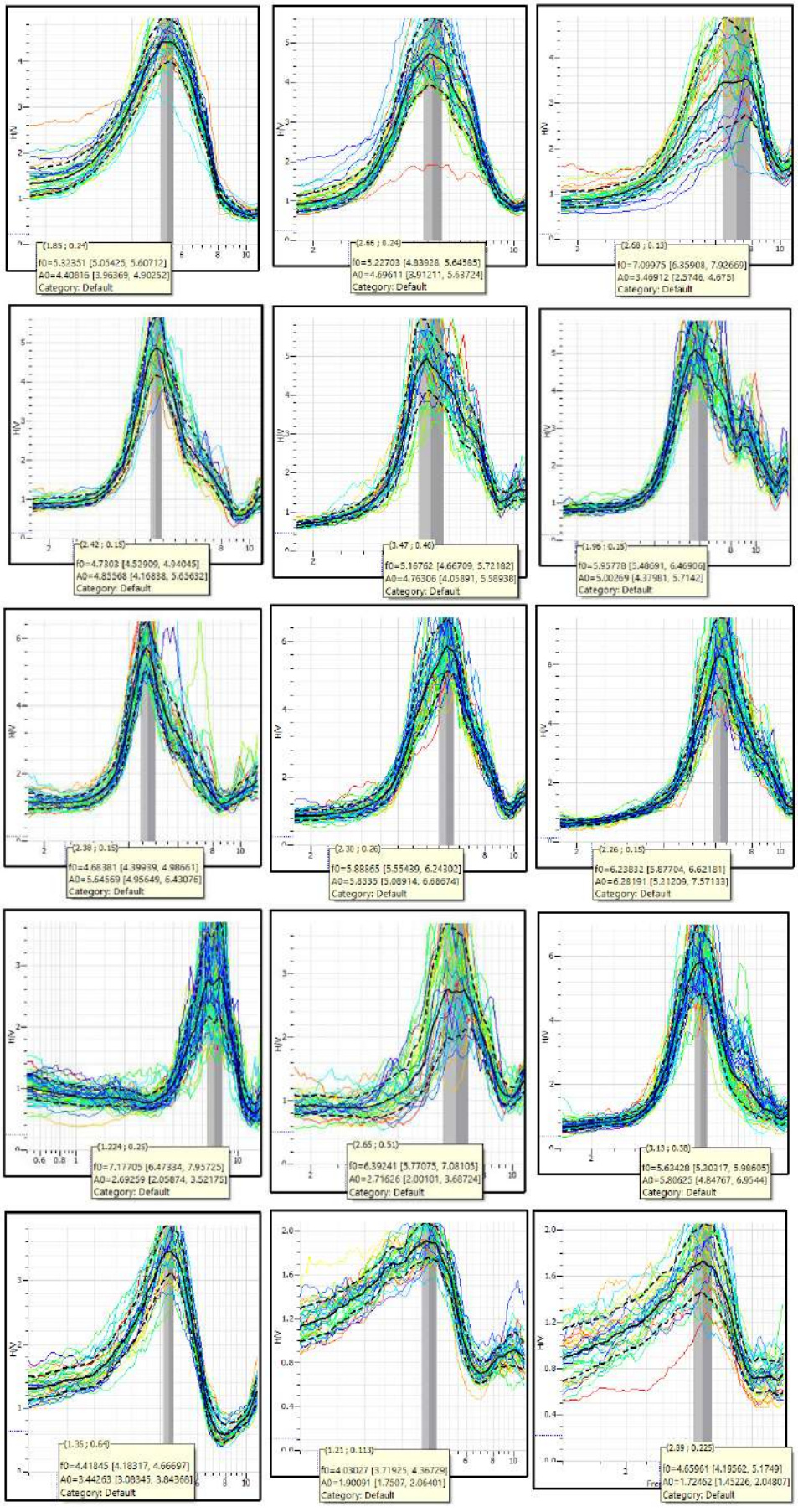

Figure 2. The curve of microtremor data processing results of HVSR method in 15 measurement points.

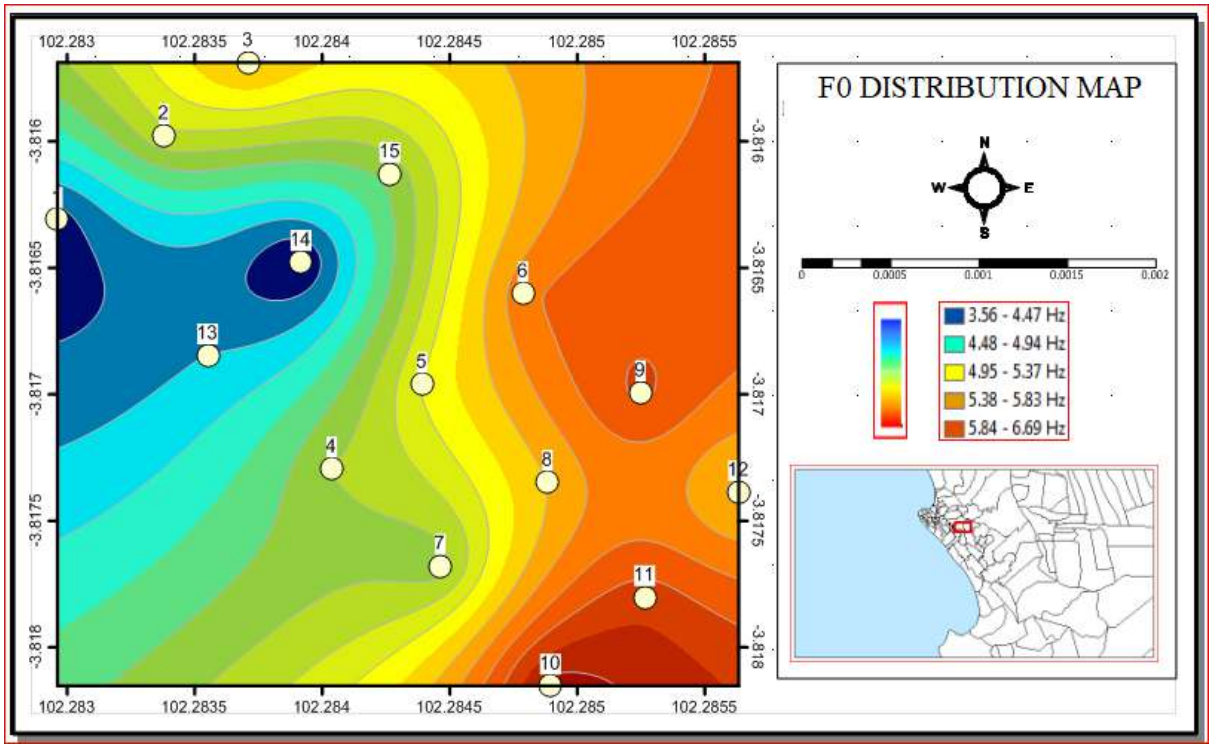

Figure 3. Distribution map of dominant frequency (f0).

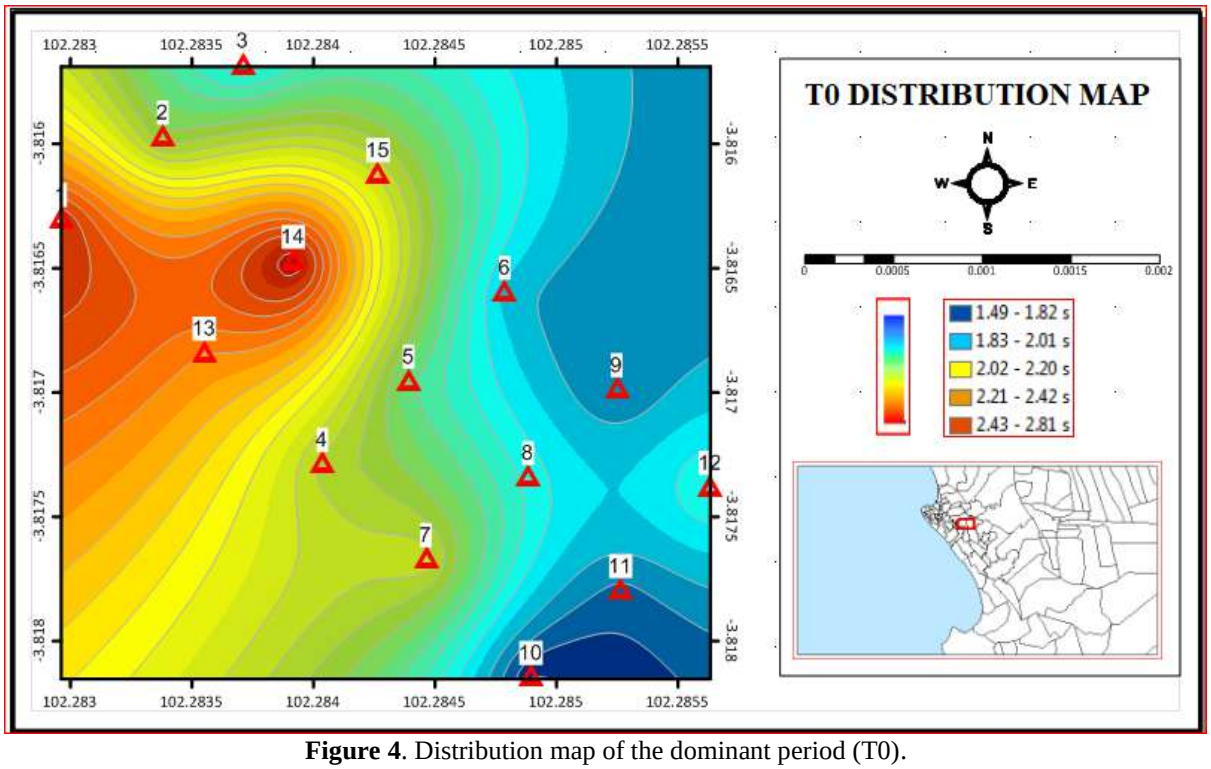

Figure 4. Distribution map of the dominant period (T0).

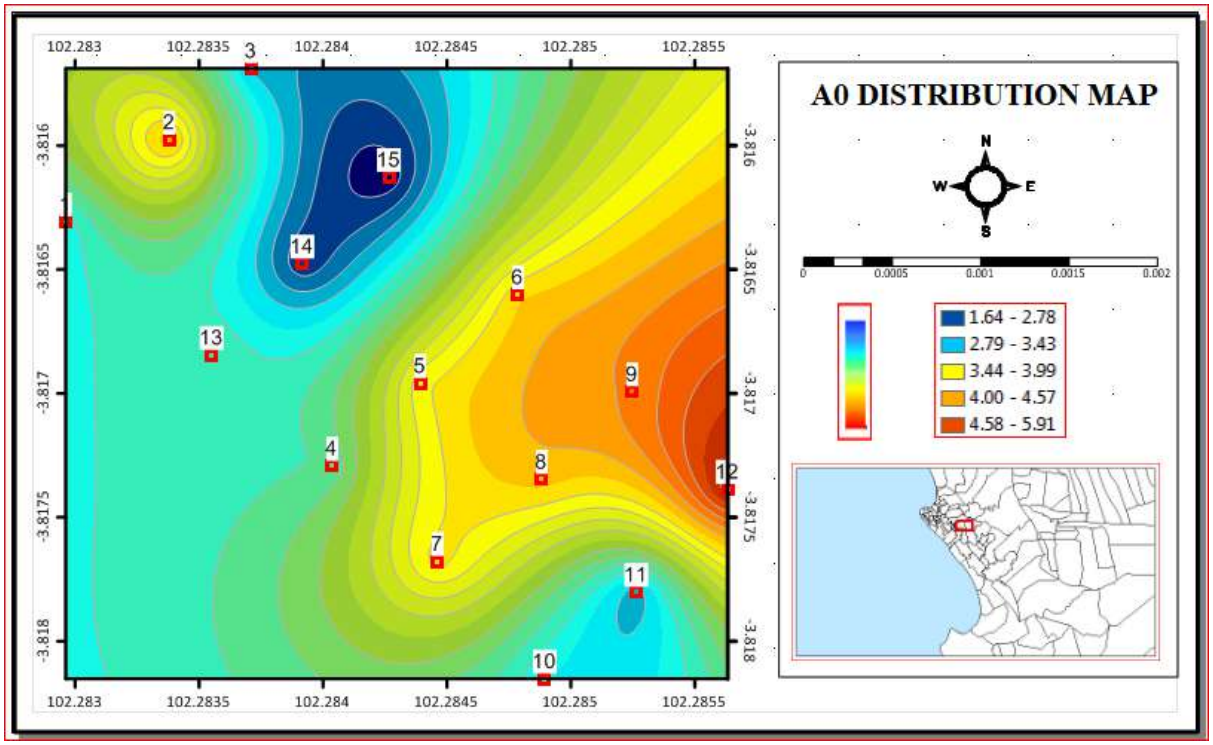

Figure 5. Amplification distribution map (A0).

Conclusion

First, the natural frequency value in the Bengkulu University Hospital area ranges from 5.1 - 5.8 Hz. This shows that the Bengkulu University Hospital area is in the class II type III soil classification, which is composed of alluvial rocks formed from sedimentation with a thickness of about 10 meters. The second one, the research area includes areas that have a moderate risk of vulnerability when an earthquake occurs, characterized by medium and soft sedimentary layers and medium amplification values.

Acknowledgements

Thanks to friends who have helped this research so that it can provide extraordinary information to all circles. Thanks also to the supervisor who has helped and provided advice on this paper.

Author Contribution

The preparation of this research journal, each author is divided into several job desks for collecting literature sources and preparing journals by Hana Raihana. Making research survey design, data processing by Andre Rahmat. Observers and supervisors in writing this journal are M. Farid and Arif Ismul Hadi.

Conflict of Interest

The authors declare no conflict of interest.

References

Amirudin., Madrinovella, I., & Sopian. (2023). Seismic Vulnerability Analysis Using the Horizontal to Vertical Spectral Ratio (HVSR) Method on the West Palu Bay Coastline. *Journal of Geoscience, Engineering, Environment, and Technology*, 08(02), 23–34.

Asnawi, Y., Simanjuntak, A. V. H., Umar, M., Rizal, S., & Syukri, M. (2020). A Microtremor Survey to Identify Seismic Vulnerability Around Banda Aceh Using HVSR Analysis. *Elkawnie: Journal of Islamic Science and Technology*, 6(2), 342–358. https://doi.org/10.22373/ekw.v6i2.7886

Dal Moro, G., & Panza, G. F. (2022). Multiple-peak HVSR curves: Management and statistical assessment. *Engineering Geology*, 297, 106500. https://doi.org/10.1016/j.enggeo.2021.106500

Ghuge, D. L. (2023). *Application of the HVSR Technique to Map the Depth and Elevation of the Bedrock Underlying Wright State University Campus, Dayton, Ohio*. Wright State University. http://rave.ohiolink.edu/etdc/view?acc_num=wright1683237719091288

Farid, M., & Mase, L. Z. (2020). Implementation of seismic hazard mitigation on the basis of ground shear strain indicator for spatial plan of Bengkulu city, Indonesia. *International Journal of GEOMATE*, 18(69), 199–207. https://doi.org/10.21660/2020.69.24759

Haryanto, Y., Hu, H.-T., Han, A. L., Hidayat, B. A., Widyaningrum, A., & Yulianita, P. E. (2020). Seismic Vulnerability Assessment Using Rapid Visual Screening: Case Study of Educational Facility Buildings of Jenderal Soedirman University, Indonesia. *Civil Engineering Dimension*, 22(1), 13–21. https://doi.org/10.9744/ced.22.1.13-21

Hesti., Suharno., Mulyasari, R. & Hidayatika, A. (2021). Analisis Karakteristik Lapisan Sedimen Berdasarkan Data Mikrotremor di Area Rumah Sakit Pendidikan UNILA. *Jurnal Geofisika Eksplorasi*, 7(2), 150–159. https://doi.org/10.23960/jge.v7i2.123

Imposa, S., Lombardo, G., Panzera, F., & Grassi, S. (2018). Ambient vibrations measurements and 1D site response modelling as a tool for soil and building properties investigation. *Geosciences (Switzerland)*, 8(3), 1–21. https://doi.org/10.3390/geosciences8030087

Irsyam, M., Widiyantoro, S., Natawidjaja, D. H., Meilano, I., Rudyano, A., Hidayati, S., Triyoso, W., Hanifa, N. R., Djarwadi, D., Faizal, L., & Sunarjito. (2017). *Peta Sumber dan Bahaya Gempa Indonesia tahun 2017*. Kementrian Pekerjaan Umum dan Perumahan Rakyat.

Isburhan, R. W. P., Nuraeni, G., Ry, R. V., Yudistira, T., Cipta, A., & Cummins, P. (2019). Horizontal-to-Vertical Spectral Ratio (HVSR) Method for Earthquake Risk Determination of Jakarta City with Microtremor Data. *IOP Conference Series: Earth and Environmental Science*, 318(1), 012033. https://doi.org/10.1088/1755-1315/318/1/012033

Lestari, D. A., & Susiloningtyas, D. (2022). Spatial Analysis of Social Vulnerability to Earthquake Hazard in Bengkulu City. *International Journal on Advanced Science, Engineering and Information Technology*, 12(5), 1989–1996. https://doi.org/10.18517/ijaseit.12.5.11889

Mase, L. Z. (2017). Liquefaction potential analysis along coastal area of Bengkulu province due to the 2007 Mw 8.6 Bengkulu earthquake. *Journal of Engineering and Technological Sciences*, 49(6), 721–736. https://doi.org/10.5614/j.eng.technol.sci.2017.49.6.2

Mase, L. Z., Amri, K., Farid, M., Rahmat, F., Fikri, M. N., Saputra, J., & Likitlersuang, S. (2022). Effect of Water Level Fluctuation on Riverbank Stability at the Estuary Area of Muaro Kualo Segment, Muara Bangkahulu River in Bengkulu, Indonesia. *Engineering Journal*, 26(3), 1–16. https://doi.org/10.4186/ej.2022.26.3.1

Mase, L. Z., Sugianto, N., & Refrizon. (2021). Seismic hazard microzonation of Bengkulu City, Indonesia. *Geoenvironmental Disasters*, 8(5), 1–

17. https://doi.org/10.1186/s40677-021-00178-y

Meng, Q., Li, Y., Wang, W., Chen, Y., & Wang, S. (2023). A Case Study Assessing the Liquefaction Hazards of Silt Sediments Based on the Horizontal-to-Vertical Spectral Ratio Method. *Journal of Marine Science and Engineering*, 11(1), 104. https://doi.org/10.3390/jmse11010104

Mohamed, A., El khateeb, S. O., Dosoky, W., & Abbas, M. A. (2021). Site Effect Estimation Using Microtremor Measurements at New Luxor City Proposed Site, South Egypt*. *Journal of Geoscience and Environment Protection*, 09(09), 131–149. https://doi.org/10.4236/gep.2021.99008

Moustafa, S. S. R., Abdalzaher, M. S., Naeem, M., & Fouda, M. M. (2022). Seismic Hazard and Site Suitability Evaluation Based on Multicriteria Decision Analysis. *IEEE Access*, 10(July), 69511–69530. https://doi.org/10.1109/ACCESS.2022.3186937

PASI. (2013). *HVSR data acquisition unit GEMINI-2 user manual*. Torino, Italy: PASI.

Ridwan, M., Yatini, Y., & Pramono, S. (2021). Mapping of Potential Damages Area in Lombok Island Base on Microtremor Data. *Jurnal Pendidikan Fisika Indonesia*, 17(1), 49–59. https://doi.org/10.15294/jpfi.v17i1.27028

Ryanto, T. A., Iswanto, E. R., Indrawati, Y., Setiaji, A. B., & Suntoko, H. (2020). Sediment Thickness Estimation in Serpong Experimental Power Reactor Site Using HVSR Method. *Jurnal Pengembangan Energi Nuklir*, 22(1), 29–37. https://doi.org/10.17146/jpen.2020.22.1.5949

Saputra, F. R. T., Rosid, M. S., Fachruddin, I., Ali, S., Huda, S., & Wiguna, I. P. A. P. (2022). Analysis of Soil Dynamics and Seismic Vulnerability in Kalibening District, Banjarnegara Using the HVSR Method. *Journal of Physics: Conference Series*, 2377(1), 012038. https://doi.org/10.1088/1742-6596/2377/1/012038

Silitonga, B. E., Suardi, I., Firmansyah, A., Hanif, M., Ramdhan, M., & Sembiring, A. S. (2023). Tectonic Structures of Northern Sumatra Region Based on Seismic Tomography of P and S Wave Velocity. *Eksplorium*, 44(1), 1–12.

ISSN: 2579-5821 (Print)
ISSN: 2579-5546 (Online)
URL address: http://journal.unhas.ac.id/index.php/geocelebes
DOI: 10.20956/geocelebes.v8i1.24638

Jurnal Geocelebes Vol. 8 No. 1, April 2024, 11 – 25

2D Marine Seismic data Analysis Using Comparison of Kirchhoff's Migration Method and Finite Difference Method (Case Study: Nias Basin, North Sumatera)

Cindy Fatika Nur Annisa[1]*, Muliadi[1], Okto Ivansyah[2], Subarsyah[3]

[1]Geophysics Study Program, Department of Physics, Tanjungpura University, Indonesia.
[2]Politeknik Negeri Pontianak, Indonesia.
[3]Marine Geological Survey and Mapping Center (BBSPGL), Indonesia.

*Corresponding author. Email: cindyfa13@student.untan.ac.id

Manuscript received: 20 December 2022; Received in revised form: 6 September 2023; Accepted: 25 October 2023

Abstract

Seismic migration is one of the important stages in seismic data processing which aims to map seismic events to their actual positions. The migration process used in this study is post-stack time migration in the time domain using the Kirchhoff migration technique and the finite difference method to determine the results of subsurface imaging from the two migration techniques and then compare them to determine the accuracy of selecting the appropriate migration for the L08 basin trajectory research area. Nias basin, North Sumatra. The processing steps are carried out according to the preprocessing to processing stages in the Promax 5000 software. Based on the results of the study, the optimum use of aperture migration in Kirchhoff migration will produce good subsurface cross-sectional imaging. The aperture value used is 3000 ms. In the finite difference migration, subsurface imaging is much more focused with a time step variation of 10 ms, whose function is to focus the hyperbolic diffraction energy on the migration data.

Keywords: finite difference; Kirchhoff migration; reflection seismic.

Citation: Annisa, C. F. N., Muliadi., Ivansyah, O., & Subarsyah. (2024). 2D Marine Seismic data Analysis Using Comparison of Kirchhoff's Migration Method and Finite Difference Method (Case Study: Nias Basin, North Sumatera). *Jurnal Geocelebes*, 8(1): 11–25, doi: 10.20956/geocelebes.v8i1.24638

Introduction

The need for oil and natural gas in Indonesia continues to increase yearly, so oil and gas energy exploration activities continue to be carried out. Bearing in mind that oil and natural gas are still the dominating energy in national energy use, efforts to increase oil and natural gas reserves are made regularly. One of them is expanding the scope of the search for new oil and gas reserves, especially in the high seas (marine). The National Energy Committee (KEN) provided recommendations regarding biogenic gas research in oil and gas basins in several locations in 2016 and provided recommendations regarding biogenic gas research in 10 Indonesian basins, one of which is the Nias basin, North Sumatra.

The method used in this study is the seismic method, especially the use of the seismic reflection method which utilizes reflected waves from the injection of wave sources which are generally in the form of explosions using dynamite as a source in the reflector field (rock coating boundary) (Permana et al., 2015).

The seismic method is one of the geophysical methods of geophysical method by utilizing seismic waves seismic waves to produce vibrations on the waves are generated from a source and then recorded source and then recorded then

recorded by the receiver. The farther distance between the source and the receiver, the longer the recording process (Nainggolan et al., 2019).

The seismic method has a wave source from dynamite and vibroseis (if the reflection is on land), air guns (if the reflection is at sea), and sledgehammers (if refraction) and has a receiver in the form of a geophone (if the survey is carried out on land) or hydrophone (if the survey is carried out at sea) so that the response from wave propagation can be received by the receiver or sensor. The influence of the reflector field when seismic waves bounce can cause one of them is the diffraction and smiling effect, both of which affect the results of the subsurface cross section during data processing. So, it is necessary to do a migration method which is a problem limitation in this study (Sea et al., 2017).

Migration is a process in seismic data processing that aims to improve the image of the subsurface cross section that has been processed from acquisition data that initially has reflectors that do not match the actual data (Sidiq et al., 2019). Migration aims to make seismic sections like the actual geological conditions based on the reflectivity of the earth's layers. The accuracy of the migration technique greatly affects the resulting seismic section (Nurlindah, 2017). The difference in amplitude anomalies seen between layers is due to the contrast in density of rocks in the subsurface and shows better reflectivity after migration (Asriani, 2020). Each method has its advantages and disadvantages and each has different sub-methods. All these migration methods have the same goal but with different approaches and processing steps according to the problems that exist in the data itself (Rasimeng, 2020).

The methods used in this study are the Kirchhoff migration method and the finite difference method. The working principle of each of these migration methods that produce the reflectivity image pattern will be considered. In Kirchhoff's migration, the problem is solved by using the sum of the amplitudes at the reflector points along the path at the actual location, and the range of the structure migrated by this method is wider, with the migrated angle reaching a maximum point of 90˚. The finite-difference migration method, on the other hand, is a migration that utilizes wave separation using the finite-difference numerical method. This method is often referred to as the wave equation method, seismic data processing looks for differential operators in the wave equation either explicitly or implicitly (Sheriff & Gerald, 1995) and has the advantage that it can be applied to data with a low signal-to-noise ratio (bad data).

Research related to seismic methods, specifically Kirchhof migration and Finite Difference data processing, has been conducted by several previous researchers. Sukmana et al. (2014), have conducted Finite Difference and Kirchhof migration studies on 2D reflection seismic data and can produce migration stack data showing the desired subsurface image. Chintia et al. (2017), have conducted research by analyzing the gap parameters in the predictive deconvolution stage, which works to reduce short-period multiples and increase the signal-to-noise ratio in marine 2D reflection seismic data processing. Anggary et al. (2015), has carried out a comparison between the post-stack time migration finite difference method and the Kirchhoff method with gap parameters deconvolution seismic data 2D line "SRDA". From the various studies conducted, the researcher realizes that migration with one method allows there to still be reflectors whose reflectivity pattern is not clear. Therefore, in this research, a comparison was made between the Kirchhoff migration method and the finite difference method in the Nias Basin research area, North Sumatra, to

complement each other and to know the advantages and disadvantages of each migration to obtain better subsurface cross-sectional imaging results.

Materials and Methods

The field data used in this study are the GM3-BIO-NIAS-L08 data, which is one of the 2D seismic line on the detailed Singkel line (Figure 2), which has 26 lines with a length of 767.03 km, obtained from seismic acquisitions conducted by the Marine Geological Survey and Mapping Center (BBSPGL) using the Geomarine III vessel, which was carried out from 20 June to 13 July 2018 in the Nias Basin, North Sumatra, using the SEG-D data format (BBSPGL, 2018).

Data processing was supported by the ProMAX 5000 2D software to successfully obtain the best seismic cross section by applying the Kirchhoff Post Stack Time Migration method and the Finite Difference method. Data processing begins in detail with the first stage being pre-processing, namely data input, geometry editing, filtering, and deconvolution (Figure 2). This data does not need to be reformatted, but the data used has not been added to the positional information and contains changes to it. The input data used in data processing are raw data in SEG-D format.

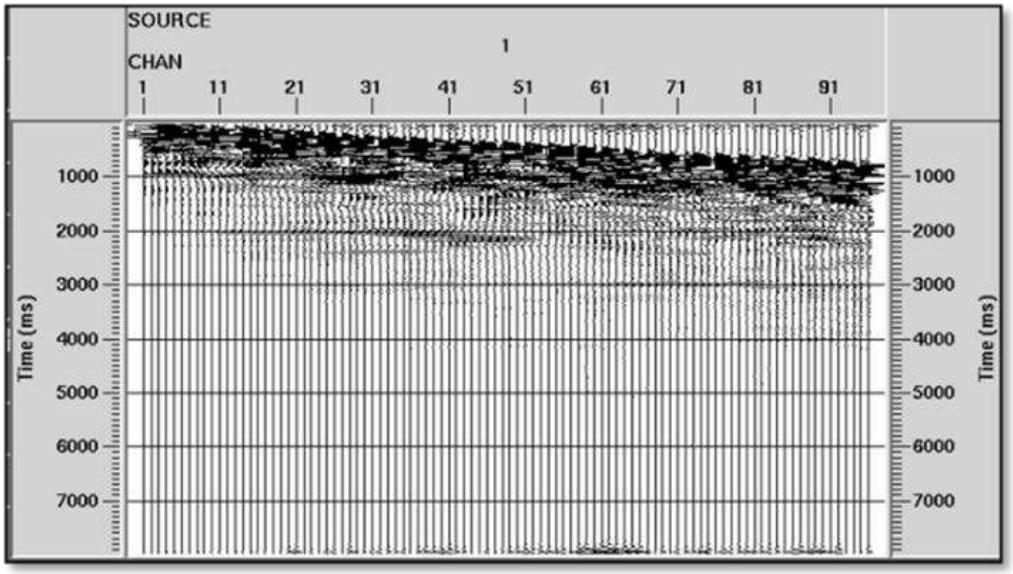

Figure 1. Shot gather with a bandpass filter.

Table 1. Table parameters

Configuration	off-end
Aktif Channel	96
Line Azimuth	345˚
Shot interval	25 m
Group Interval	12.5 m
Number of Shot	946
Near offset	50 m
Far offset	1137,5 m
Fold Maximum	24
Line Length	23,625 km
SR	2 ms
RL	8000 ms

Figure 1 shows an example of shot gather data with a bandpass filter applied. The shot gather is then combined with geometry parameters (Table 1) whose function is to match the survey geometry with the recorded seismic data, because the seismic data recorded in the field only contains SOU_SLOC data or station values, FFID which indicates the shot number and channel that is active in data acquisition. as the function of data acquisition in indicating hydrocarbon content in the subsurface, acquisition needs to be planned and calculated based on the target to be obtained based on what parameters are used (Banuboro et al., 2017). In addition, to facilitate data presentation in data processing, other acquisition parameters

need to be added such as shot point coordinates, receiver coordinates, CDP coordinates, CDP numbering, offsets, and others.

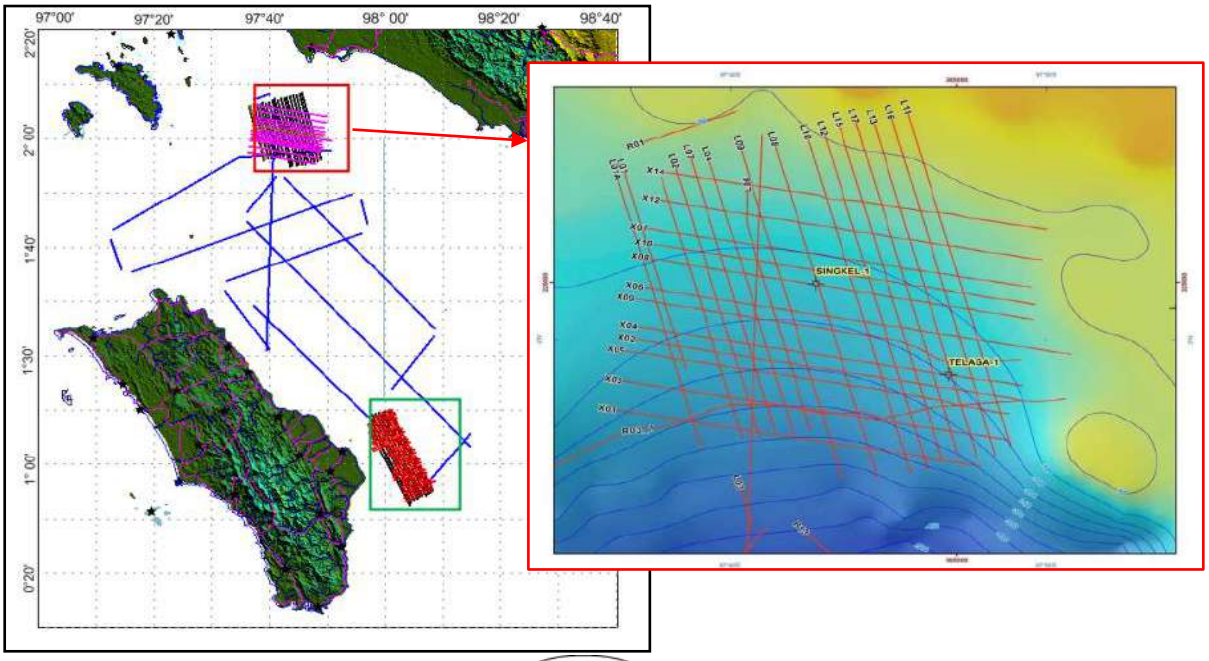

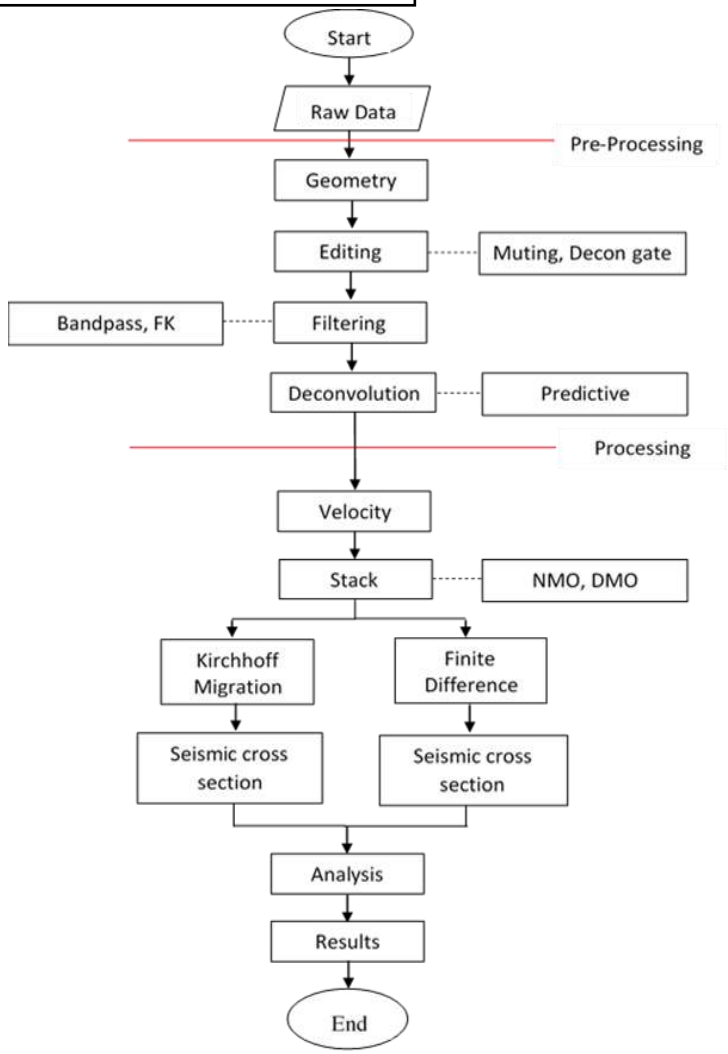

Figure 2. Research flowchart (below) and Location of the Nias Basin Biogenic Gas Survey, North Sumatra, with detailed research locations at the Singkel Site (red box) (BBSPGL, 2018) (left).

Geometry aims to match the file number (there is an observer report) to the file record of the seismic data recorded in 1 shot. Frequency filters such as bandpass and FK filters are applied to this data to separate the desired frequencies from the seismic waves and eliminate unwanted frequencies, so that the resulting image will be smoother and the layers are clearer (Permana et al., 2015). This process is enhanced by predictive deconvolution, which is used to predict the arrival of multiple reflection waves in the seismic traces by applying gap values, including the length of the gap and the length of the operator tested by the process, to the data. The selection of multiple gap values is also used to see how far the noise is reduced and the deflection width, which is the primary data, is still maintained. The gap value is reinforced by applying autocorrelation analysis to see how effectively predictive deconvolution is applied. This method can reduce multiple short period types of noise to increase the required signal-to-noise ratio (Chintia et al., 2017). The next stage is what is known as routine processing, which includes velocity analysis, stacking, NMO, DMO corrections and migration.

Velocity analysis uses the semblance method, where the velocity obtained is the root mean square (Vrms), which is the total velocity of the horizontal layering system in the form of square roots. The purpose of stacking the survey data is to increase the number of seismic traces in a CDP after NMO correction so that the signal-to-noise ratio (S/N) is higher because coherent signals enhance each other and incoherent noise cancels each other out. NMO and DMO corrections were performed to eliminate the effect of different offset distances for each receiver in the CDP format and to see the pattern of reflectivity at the zero-offset position of the CDP (Sukmana et al., 2014). Then, with the presence of complex geological structures that cause velocity variations with depth, causing problems in determining the position of the structure and problems at the time of the migration process. Therefore, velocity analysis is a very important process in the seismic data processing stage (Manrulu, 2016).

The stacking to migration stage can be referred to as the post-stacking stage, which aims to return the reflector to its true position. So that the migration stage has a function as eliminating the effects of diffraction at discontinuity points (faults) and moving the event layer obliquely in this position caused by oblique reflectors or faults. In a seismic cross section with zero offset, the waves received by the receiver are considered as a depiction of the shape of a layer directly below the source and receiver (Asrori & Santosa, 2015).

The cross section resulting from the migration process in the time domain called time migration can generally be applied to small to medium lateral velocity variations and the migration process in the time domain performed after the stack (post-stack time migration) is relatively faster and more efficient in processing seismic data (Anggary et al., 2015).

The migrations used are Kirchhoff and Finite Difference. The Kirchhoff migration process is carried out by adding the amplitude of a reflector point along a notch, which is the actual possible location in the form of a diffraction curve, while the finite difference migration uses a wave separation using the finite difference numerical method. An apple-to-apple analysis of the seismic section was then carried out on both methods to determine which migration gave the best results.

Results and Discussion

Preprocessing

The trace display shown in Figure 3 is a display of trace acquisition data that has been provided with geometry and bandpass filter information, and it is known that this

data has multiple, which indicates the presence of a seismic event that experiences more than one reflection from the position of the primary reflector. The multiple is included in the coherent noise found in the collected trace, so the filter frequency applied to this data really helps to eliminate the existing noise.

The filters used include bandpass and FK filters. Prior to filtering, a spectral analysis is performed to identify the frequency content of the data so that the frequency design to be used can be determined. The frequency used is usually above 3 dB, and in this processing the frequency 10-15-45-60 is used (Figure 4). When selecting this frequency, it is important to consider whether the data used needs to be bandpass filtered, as seismic data typically has a frequency range of 10 to 70 dB, and anything below a frequency of 10 or above a frequency of 70 will be clipped or eliminated.

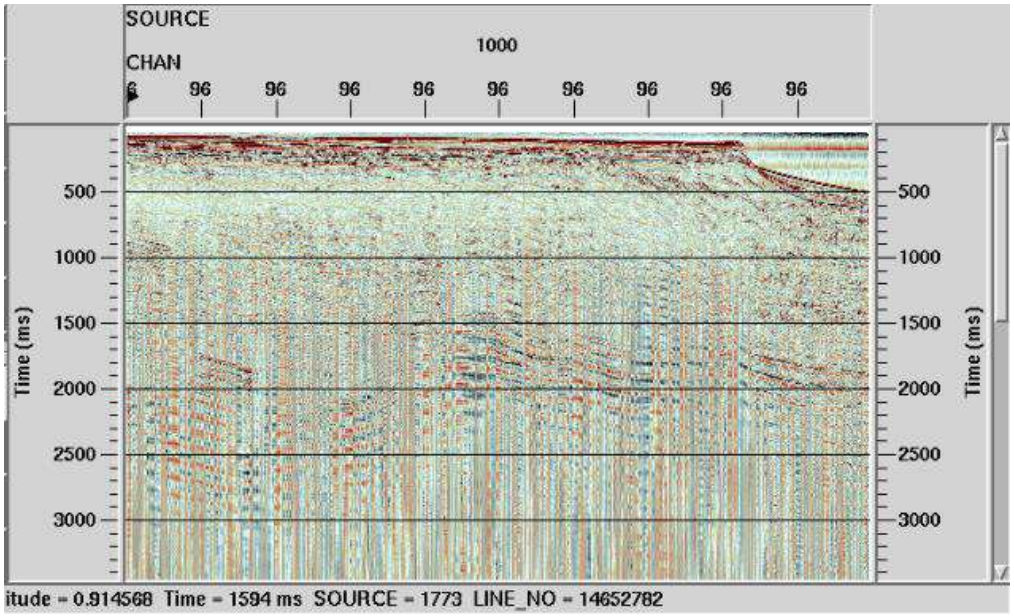

Figure 3. Brute-stack geometry.

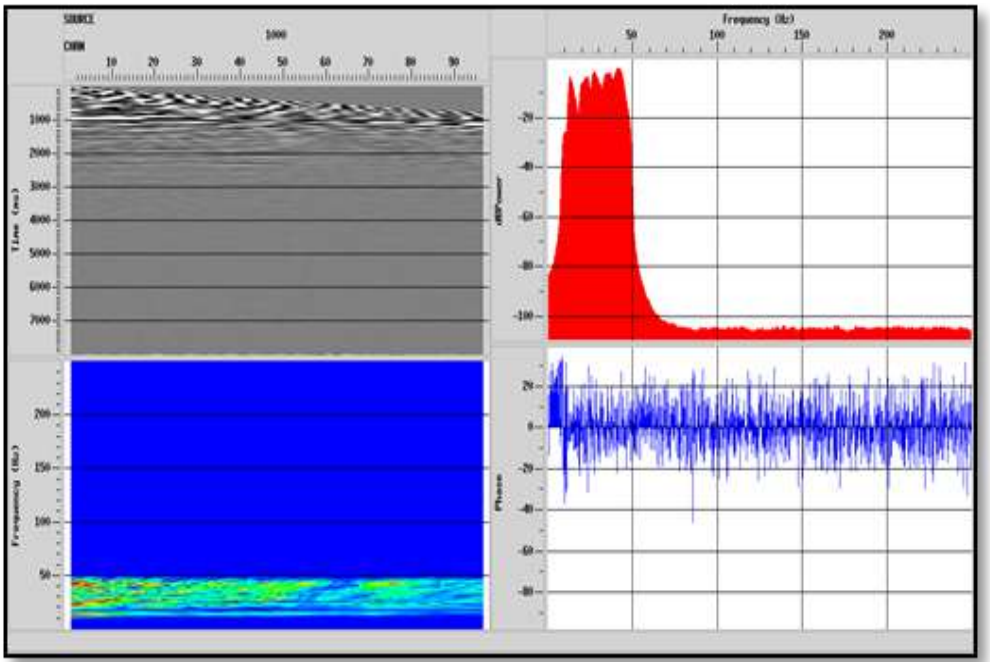

Figure 4. Interactive spectral bandpass 10-15-45-60.

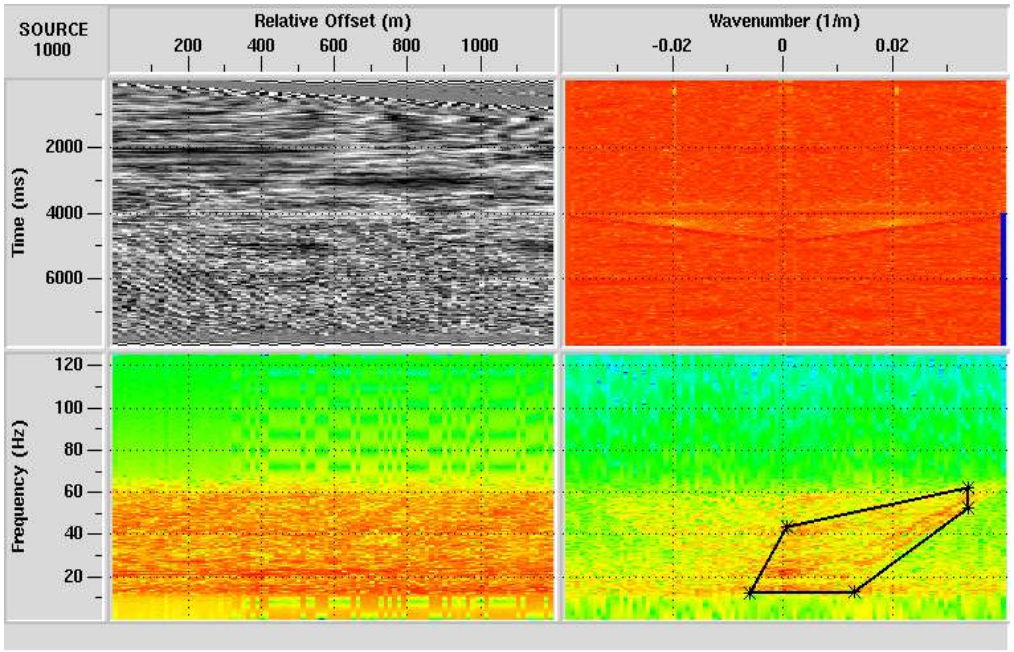

Figure 5. Picking results on FK analysis.

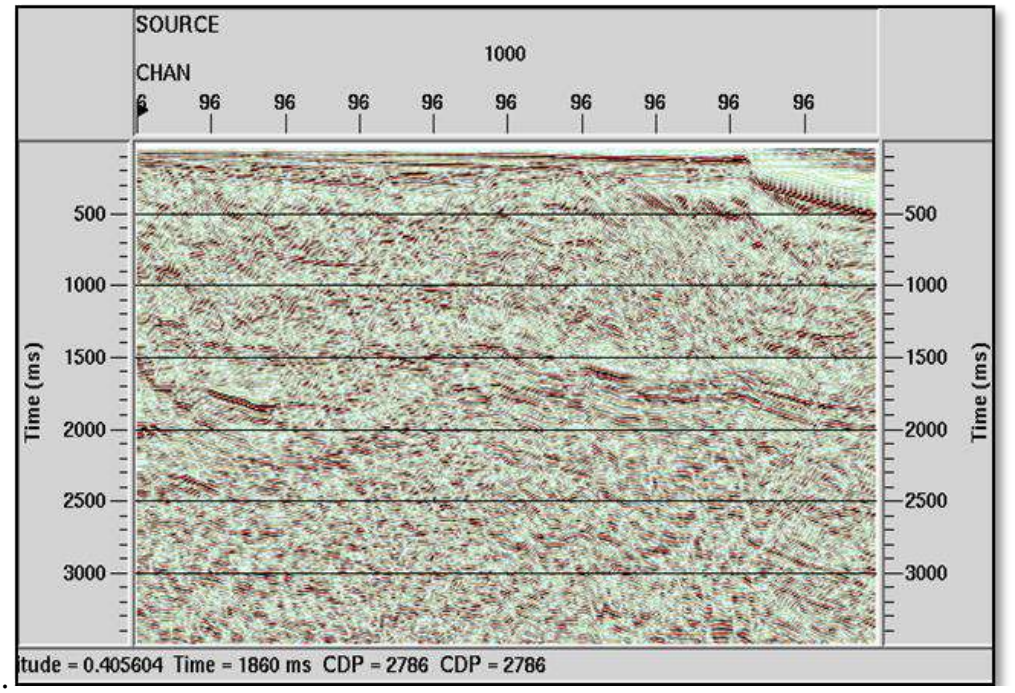

Figure 6. Brutestack after deconvolution.

The frequency filter used next is the FK filter, which functions as a linear coherence filter in the space-time domain wave equation (t-z), which is transformed into the wavenumber frequency domain due to the dip. The FK filter in this study is focused on the elimination of surface wave noise, direct waves, and bias waves that appear in the first reflection of seismic data. The modules used are F-K analysis and F-K filter. The selection results in the F-K analysis (Figure 5) correspond to the number selection with the noise data to be eliminated. Sub-sampling and automatic gain control are also applied to this data to display frequencies more clearly so that noise can be reduced. The noise to be reduced is the noise marked with a red bias (in the picking polygon in the figure), with the frequency domain and wavenumber

used so that the recorded double noise can be attenuated and the picking performed is expected to match the actual data. In research conducted by Rasidin et al. (2022), that the use of F-K Filter is very powerful in removing noise contained in seismic data. The frequency of seismic data is difficult to separate if it only relies on a bandpass filter, so the polygon selection in the F-K filter is based on polygon selection. Polygons in the F-K filter is because coherent noise such as ground rollers and multiples will have. The velocity and frequency differences with the actual reflected wave thus have different slopes on the frequency spectrum and wave number. As can be seen in the figure above (Figure 6), the multiple has been well reduced, but the reflector trace is still somewhat abstract at times between 1000 ms and 2500 ms and its structure is not clearly visible, although good reflector seismic events are visible on the trace surface.

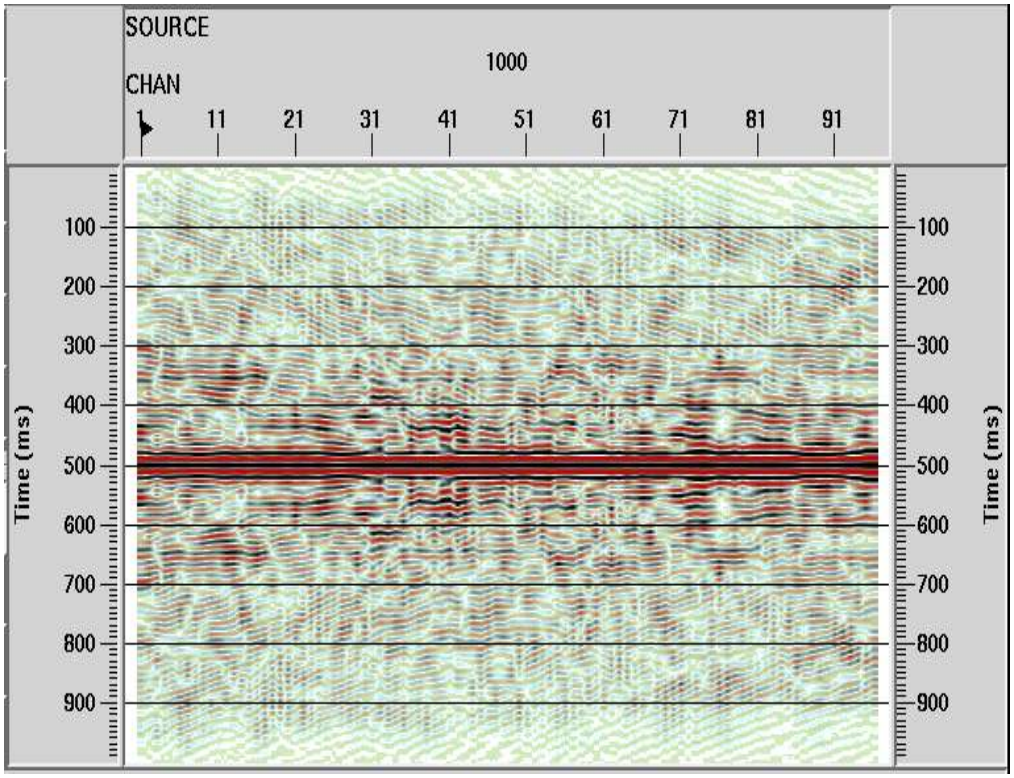

Figure 7. Autocorrelation gap 85-35 ms.

This process is enhanced by the selection of gaps in predictive deconvolution using the principle of a prediction error filter because multiples can always be predicted in seismic traces. The selection of this deconvolution is also based on research conducted by Romauli et al. (2016), that the spectral analysis of the predictive deconvolution is more effective at enhancing signal and suppressing noise than spiking deconvolution. Compared to spiking deconvolution. and of course, after try and error. This predictive deconvolution process uses a method of selecting several gap values to validate that the gap is close to the true value, characterized by reduced noise, and that the deflection width, which is the primary data, is still preserved (Figure 6). In autocorrelation, the width of the deflection indicates the presence of the primary data (black line), the rest is noise. So, in this study, a gap value of 85-35 ms (Figure 7) was chosen after trial and error in autocorrelation analysis, including using gap values of 80-12, 90-30 and 120-40.

Processing

The velocity analysis method used on this data is the velocity semblance method or

amplitude plot, which is a plot of velocity signal similarity versus two-way zero offset time (TWT). This method displays the Semblance and CDP gather sections simultaneously.

The semblance display is shown as color contours, generally with the maximum color coherence being red and the minimum coherence being blue, and when using semblance panels, it is usually chosen by ensuring that the signal amplitude does not differ from the offset. If the seismic amplitude is evenly distributed along the displacement curve, the horizontal semblance of the semblance will be maximized by the gather as the event progresses.

In the Figure 8, the retrieval speed starts at 1000 m/s and the retrieval should have increasing speed values as the TWT (Two Way Travel time) increases, thus avoiding retrieval at multiple speed values. The CDP collection shown has a range of 100 between other CDPs when picking and NMO has been applied. Picking is done on CDP as much as approximately 3358 data. but not all CDPs are picked, the rest that are not picked will be interpolated from the speed picking results on CDP. and the data created has been applied smoothing using the velocity manipulation module. this is also applied in research conducted by Jamaludin et al. (2020).

After the velocity analysis is obtained, the next step in this study is to divide the data into two treatments, namely the stack to which DMO correction is added and the stack to which DMO correction is not added. This is done with the aim of checking which data is close to the actual data to be sent to the migration stage, so that the final data is in accordance with the appearance of the desired subsurface image by looking at the seismic shaping reflectors in the data.

The subsurface section using the DMO data stack before migration shows a firmer structure (Figure 9b) compared to the results of the stack without DMO (Figure 9a). In this figure can be seen that the resulting section is not very good because the resulting geological conditions are not very clear, making it difficult to distinguish between seismic horizons, especially in complex areas such as those marked with a red circle in Figure 9. Also, this migration has not been applied to the data in the flow stack, so the signal position is not at the true position and the visible reflector is still affected by diffraction effects.

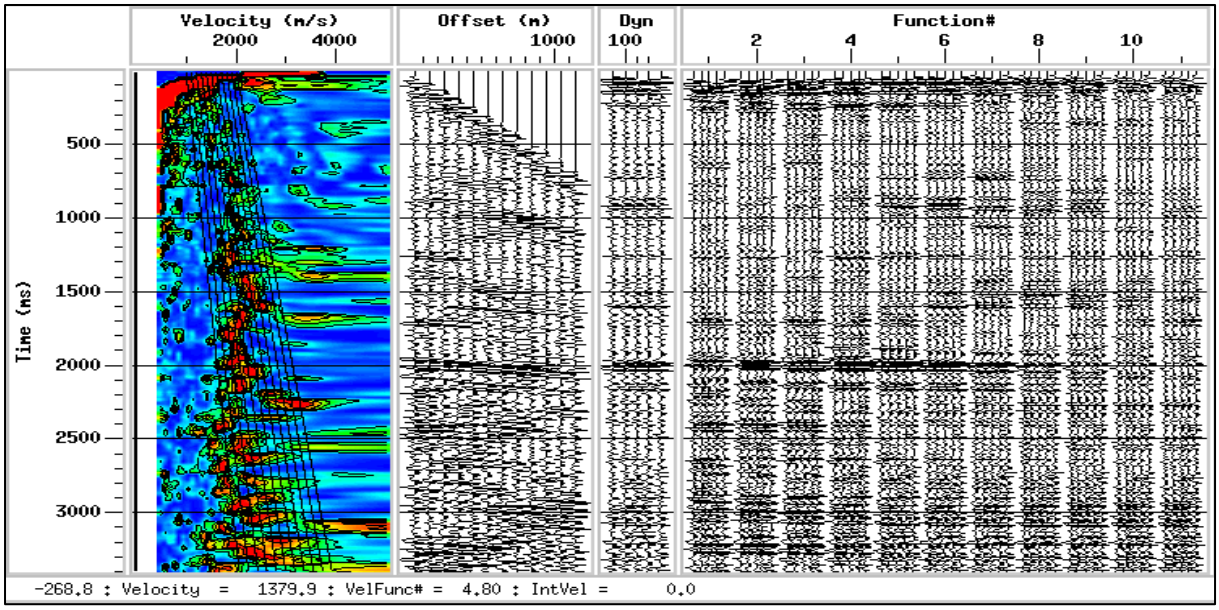

Figure 8. Picking velocity analysis on CDP 106.

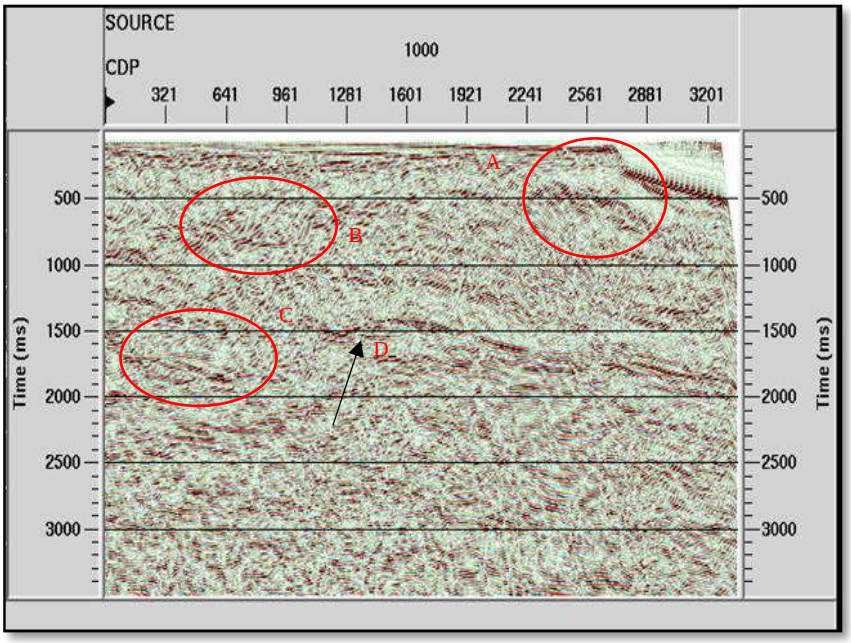

(a)

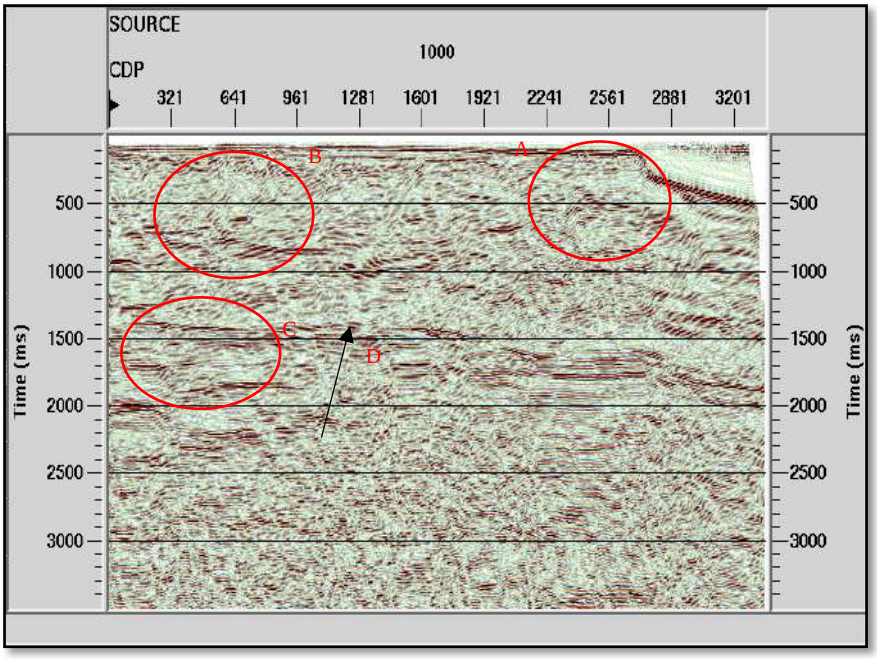

(b)

Figure 9. Brute Stack without DMO (a) and with DMO (b).

The two figures show a seismic cross section propagating in TWT (two-way travel time). In Figure 9a there are reflectors that are not continuous at points A, B, C and D. This is because the stack method used is based on a travel time parameter that is highly dependent on the velocity and trace model in the CDP survey, which must first be corrected by NMO to remove the effect of offset distance. While the results of the brute stack cross section with DMO (Figure 9b) show that the reflector has increased S/N, as indicated by more solid reflector lines, especially at points A, B, C and D, because the DMO stack uses more CDP gather, resulting in a better cross section. At 1500 ms or point D there is clear continuity, although it does not look good for imaging the seismic section.

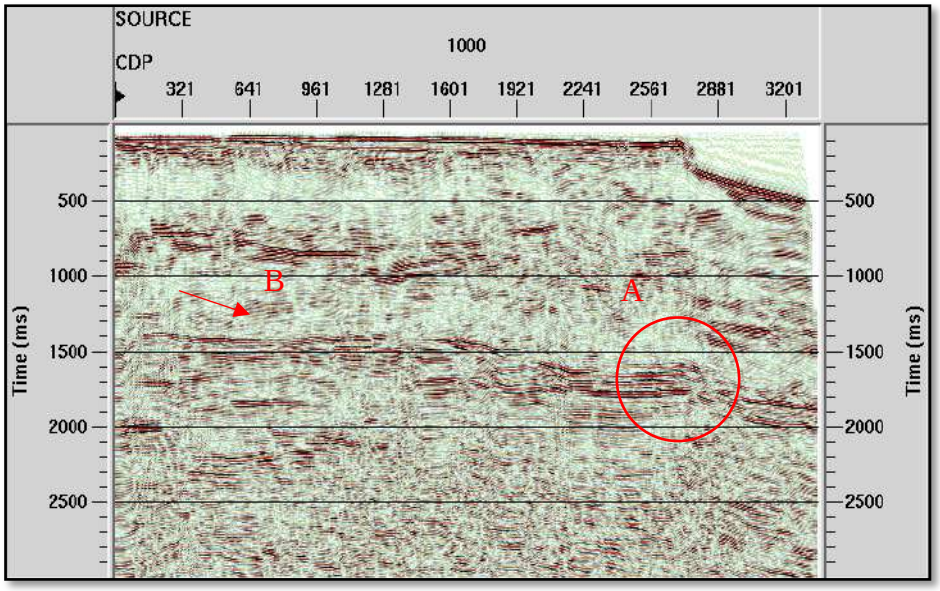

(a)

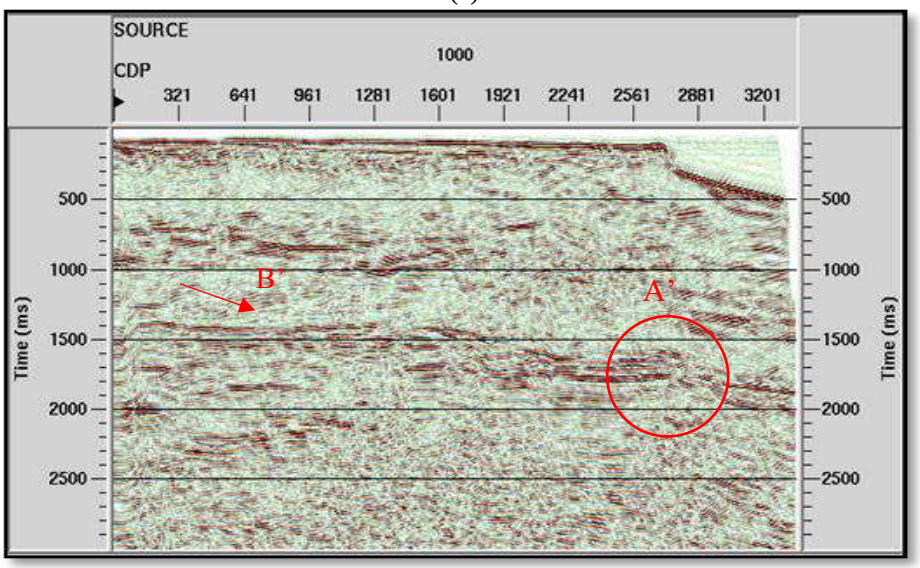

(b)

Figure 10. Kirchhoff migration results (a) and Finite Difference (b).

Migration result and final analysis

Based on the results of the stacking performed, the subsurface image used in the migration and final analysis is a data process corrected by NMO and enhanced by DMO correction, because NMO correction itself is only effective when used on a flat reflector, and if it is not flat then CDP point shifting or so-called reflector point smearing occurs. DMO takes the slope of the reflecting plane in the data, so that the dispersion of the reflected points disappears and the signal-to-noise ratio increases. This is because DMO modifies the results of the reflection point stack, which is at the zero-offset point of a reflector, and corrects for the sloped layer by creating the seismic trace within the CDP (Susanti et al., 2020).

The results of this research migration data have been operated with the optimum stack and have been attempted by providing NMO correction, CDP interval of 6.25 m, frequency 50 Hz, maximum dip 180 and Vrms in time migration, as well as providing sub-sampling trace display with f-k decon, dip scan stack and automatic gain control (agc) whose function is to

clarify the appearance of the cross-section reflector. Once the stacking results have been compiled, the migration results then apply the DMO correction up to the analysis stage.

Figure 10a shows the results of the Kirchhoff migration test with an aperture of 3000m using the DMO correction. The aperture used in the Kirchhoff migration is an important parameter to show its relationship with the noise generated. Previous tests have been carried out with apertures of 0 m, 1000 m, 3000 m and 6000 m, but for the data to be used for the migration, an aperture of 3000 m was chosen. This was chosen based on changes in aperture affecting the range and changes in angle can determine the level of tilt of the reflector, so that the more tilted the reflector value, the greater the angle value, this has also been proven by Handani et al. (2015) in their research. However, there are several things that need to be considered before choosing an aperture width, such as not using an aperture width that is too small, this will cause damage to tilt events and changes in amplitude that will vary and generate random noise, especially in deeper parts as the dominant event. Then, using an aperture that is too large can reduce the quality of the migration with a low signal to noise ratio and cause random noise in good shallow data.

The migration stack finite difference results (Figure 10b) appear to be no different from the Kirchhoff migration results, but at the migration horizon line the finite difference is not as clear as the Kirchhoff migration. And at the boundary of the strata, which is marked with a white line at 2000 ms to 2400 ms, seismic events can be seen that are more clearly continuous.

The finite difference migration applied to this data is conceptually physical, the method used is the same as Kirchhoff migration. This migration uses a maximum frequency of up to 80 Hz, with input data parameters in the form of final stack and time domain interval velocity. The method used in the finite difference migration itself is fast explicit Finite Difference (FD) time migration, which has previously been carried out FD migration data processing with the implicit FD algorithm with the parameters analyzed in this migration is the time step to be migrated before being compared with Kirchhoff migration. The time steps used are 5 ms, 10 ms, 20 ms, and 40 ms. The time step is used to concentrate the diffraction energy of the hyperbola. In this data, the time step used is 10 ms, when using 20 ms and 40 ms the seismic event on the imaging fades, this can occur because the hyperbola diffraction energy has begun to weaken. In contrast to Rahman et al. (2023) who in their research stated that the use of the Implicit FD Time algorithm is better, in this study Fast Explicit FD Time is better at processing data, this has also been proven by Jamaluddin et al. (2019) who stated that explicit finite difference migration succeeded in maintaining frequency data in accordance with the desired target. This can occur possibly due to the acquisition data model obtained or differences in reflectors and noise contained in the research data. Migration is performed in post-stack time migration. The post-stack time migration is performed in the time domain after the stacking process. The advantage of this technique is that it can produce high resolution subsurface sections on steep reflector planes. Based on the reflector analysis, it is shown that the continuity of the Kirchhoff migration results is clearer than the FD migration results.

The Kirchhoff migration in Figure 10a between CDP 2561 and 3000 at point A produces continuous reflector continuity and a clearer image. This also highlights the importance of the migration aperture parameter in Kirchhoff's migration, as selecting the correct aperture affects the resulting subsurface cross section. The Kirchhoff migration was able to minimize

the diffraction effect in the subsurface image data. While the finite difference migration in Figure 10b produces a better focus and a firmer reflector at its zero offset point than the Kirchhoff migration. However, the appearance at the same CDP, which is between 2561 and 3000 CDP at point A' of the reflector, is not very clear. And the seismic events shown at point B' are much weaker compared to the results of Kirchhoff's migration at point B.

The results of this migration are good for use with data that has a high signal-to-noise ratio and a steep slope, because the finite difference migration concept allows predictions to be made about possible reflectors, the slope constraint can avoid smoothing non-coherent data and amplifying noise, and the migration is relatively more accurate, although the handling of the slope of this migration is limited. Meanwhile, Kirchhoff migration can be used for a variety of steep slope data, but because of its general nature, it is possible that the reflector from data with high S/N will not focus too much on the reflection, is able to handle steep slopes, and break in when summing can work to suppress noise. However, this may have different results for other data types or when using other seismic data corrections such as SRME (Surface-Related Multiple Elimination) corrections and Radon transformation, as well as the pre-stack time migration method, whose function is to correct for NMO errors in the return traces. Seismic to zero offset position.

Conclusion

Based on the results of this study, it can be concluded that the use of optimum aperture migration in Kirchhoff migration produces subsurface cross sections with clearer reflector appearances and the use of time steps in finite difference migration. Kirchhoff. Therefore, the best subsurface imaging on GM3-BIO-NIAS-L08 Site Singkel data after migration analysis is performed using Finite Difference migration.

Acknowledgements

The author would like to thank all those who have helped in carrying out this writing so that it can be completed properly specially the Marine Geological Survey and Mapping Center (BBSPGL) Bandung, which provided the author with the opportunity to directly experience the internship process and final project supervision (TA) independently of COVID-19.

Author Contribution

Each author has a task in completing this research. Reference collection, data processing, and analysis were conducted by Cindy Fatika Nur Annisa and Subarsyah as field supervisors. The recorded discussion was guided by Muliadi and Okto Ivansyah. All authors reviewed the manuscript.

Conflict of Interest

In this research, all authors have no financial or personal relationships with other people or organizations, so the author can account for the research results.

References

Anggary, S. R. D., Danusaputro, H., & Harmoko, U. (2015). Perbandingan Post Stack Time Migration Metode Finite Difference dan Metode Kirchoff dengan Parameter Gap Dekonvolusi Data Seismik Darat 2D Lintasan "SRDA". *Youngster Physics Journal*, 4(1), 79–86. https://ejournal3.undip.ac.id/index.php/bfd/article/viewFile/8057/7837

Asriani. (2020). *Peningkatan Kualitas Penampang Seismik Menggunakan Travel Time Tomography Pada Area Shallow Gas*. Universitas Hasanuddin.

Asrori, A. D. H., & Santosa, B. J. (2015).

Migrasi Domain Kedalaman Menggunakan Model Kecepatan Interval dari Atribut Common Reflection Surface Studi Kasus pada Data Seismik Laut 2D. *Jurnal Sains dan Seni ITS*, 4(1), B32–B37. https://ejurnal.its.ac.id/index.php/sains_seni/article/view/9261

Balai Besar Survei dan Pemetaan Geologi Kelautan (BBSPGL). (2018). *Penelitian Gas Biogenik Cekungan Nias, Sumatera Utara* (Survei KR Geomarine III). Bandung.

Banuboro, A., Warnana, D. D., Syaufuddin, F., & Guntara, A. D. (2017). Analisa Parameter Desain Akuisisi Seismik 2D dengan Metode Dinamik pada Lingkungan Vulkanik, Studi Kasus: Cekungan Jawa Barat Bagian Utara. *Jurnal Teknik ITS*, 6(2), B227-B232. https://doi.org/10.12962/j23373539.v6i2.24094

Chintia, B., Ivansyah, O., & Sampurno, J. (2017). Analisis Parameter Gap Dalam Tahapan Dekonvolusi Prediktif Guna mereduksi Short Period Multiple dan Meningkatkan S/N Ratio pada Pengolahan Data Seismik Refleksi 2D Marine. *Positron*, 7(1), 25–33. https://dx.doi.org/10.26418/positron.v7i1.20783

Handani, R., Harmoko, U., Kusuma, A. I. (2015). Analisis Pengolahan Data Seismik Lapangan "R"dengan Metode CRS (Common Reflection Surface) Stack pada Data Cross Section Marine 2D. *Youngster Physics Journal*, 4(4), 327–334. https://ejournal3.undip.ac.id/index.php/bfd/article/view/9414

Jamaluddin., Sea, J. G., Djajadihardja, Y. S., Massinai, M. A., Aswad, S., & Maria. (2019). Analisis Frekuensi Data Seismik Hasil Migrasi Finite Difference. *Jurnal Geosaintek*, 5(3), 119–126. http://doi.org/10.12962/j25023659.v5i3.6033

Jamaluddin., Sea, J. G., Fitriani, F., & Maria, M. (2020). Pengolahan Data Seismik 2D Marine Menggunakan ProMAX di Area Tenggara Pulau Simeulue. *Petrogas*, 2(2), 26–43. https://doi.org/10.58267/petrogas.v2i2.42

Manrulu, R. H., Jambonada, N., Ashari, A., & Suasdin, J. (2016). Studi Pengolahan Data (Processing) Seismik dengan Menggunakan Program Promax. *Jurnal Fisika FLUX*, 13(2), 126–132. https://ppjp.ulm.ac.id/journal/index.php/f/article/view/3457

Nurlindah. (2017). *Analisis Data Seismik Marine 2D Dengan Menggunakan Metode Migrasi Kirchhoff (Studi Kasus: Perairan Waigeo, Papua Barat)*. Universitas Hasanudin.

Permana, U., Triyoso, K., & Sanjaya W.S., M. (2015). Pengolahan Data Seismik Refleksi 2D Untuk Memetakan Struktur Bawah Permukaan Lapangan "X" Prabumulih, Sumatera Selatan. *Alhazen Journal of Physics*, 2(1), 28–37. https://journal.uinsgd.ac.id/index.php/ahjop/article/view/308

Rahman, M. N. W., Sailah, S., & Nainggolan, T. B. (2023). Penerapan Metode Migrasi Beda Hingga Pada Data Seismik Post Stack di Utara Laut Bali Perairan Utara Bali. *Jurnal Ilmu dan Teknologi Kelautan Tropis*, 15(1), 85–97. https://doi.org/10.29244/jitkt.v15i1.41541

Rasidin, S. M., Nainggolan, T. B., Dewi, I. K., & Farid, F. (2022). Analisis Migrasi Seismik Laut 2D Metode Kirchhoff Pre-Stack Time Migration dan Post-Stack Time Migration Pada Wilayah Laut Seram. *Jurnal Teknik Kebumian*, 6(2), 30–37. https://online-journal.unja.ac.id/jtk/article/view/21181

Rasimeng, S., Ekarena, A. I., Mulyanto, B. S., Subarsyah., & Djaja, A. W. (2020). Optimalisasi Pencitraan Struktur Bawah Permukaan Menggunakan Metode Kirchhoff Pre-Stack Time

Migration pada Data Seismik Laut Wetar. *Jurnal Geofisika Eksplorasi*, 06(2), 101–112. https://doi.org/10.23960/jge.v6i2.67

Romauli, A., Manik, H. M., & Subarsyah, S. (2016). Penerapan Dekonvolusi Spiking dan Dekonvolusi Prediktif Pada Data Seismik Multichannel 2D di Laut Flores. *Jurnal Teknologi Perikanan dan Kelautan*, 7(2), 153–162. https://doi.org/10.24319/jtpk.7.153-162

Sea, J. G., Massinai, M. A., Aswad, S., & Djajadihardja, Y. S. (2017). Difraksi Dan Efek Smiling Pada Data Seismik. *Jurnal Geocelebes*, 1(1), 13–16. https://doi.org/10.20956/geocelebes.v1i1.1775

Sheriff, R. E., & Geldart, L. P. (1995). *Exploration Seismology* (2nd). Cambridge University Press.

Sidiq, A. P., Manik, H. M., & Nainggolan, T. B. (2019). Studi Komparasi Metode Migrasi Seismik Dalam Mengkarakterisasi Reservoir Migas di Blok Kangean, Laut Bali Menggunakan Inversi Impedansi Akustik Berbasis Model. *Jurnal Ilmu dan Teknologi Kelautan Tropis*, 11(1), 205–219. https://journal.ipb.ac.id/index.php/jurnalikt/article/view/23028

Sukmana, A., Kamallulah., & Ardi, N. D. (2014). Migrasi Finite Diffrence dan Kirchhoff pada Data Seismik Refleksi 2D. *Fibusi (Jurnal Online Fisika)*, 2(1), 1–9.

Susanti, W., Ivansyah, O., Muliadi, M., & Avianthara, B. (2020). Analisis Perbandingan Migrasi Kirchhoff dan Migrasi Fx pada Data Seismik 2D Darat. *Prisma Fisika*, 8(1), 21–25. https://dx.doi.org/10.26418/pf.v8i1.39927

ISSN: 2579-5821 (Print)
ISSN: 2579-5546 (Online)
URL address: http://journal.unhas.ac.id/index.php/geocelebes
DOI: 10.20956/geocelebes.v8i1.26521

Jurnal Geocelebes Vol. 8 No. 1, April 2024, 26 – 36

Genesis of Bauxite Ore in Toba Area Sanggau District, West Kalimantan Province

Ricka Aprillia[1]*, Wahdaniah Mukhtar[1], Septami Setiawati[1], Govira Christiadora Asbanu[2], Ibnu Munzir[3]

[1] Department of Mining Engineering, Tanjungpura University, 78124, Indonesia.
[2] Department of Environmental Engineering, Tanjungpura University, 78124, Indonesia.
[3] Institute of Geological Science, Jagiellonian University, 30387, Poland.

*Corresponding author. Email: rickaaprillia1990@gmail.com

Manuscript received: 27 April 2023; Received in revised form: 16 August 2023; Accepted: 12 January 2024

Abstract

Indonesia's largest bauxite reserves are in the province of West Kalimantan, which is 703 million tons Bauxite is formed from rocks with a high relative aluminum (Al) content, low iron (Fe) content, and small amount of quartz. The mineralogy and characteristics of lateritic bauxite deposits are closely related to several factors, one of which is the texture and composition of the bedrock such as color, mineral composition, and shape of the ore. This study discusses the genetic type of bauxite deposits based on mineralogy and geochemistry using mineragraphic, XRD, and XRF methods. The primary data from bauxite ore samples were collected from the stockpile of PT. Dinamika Sejahtera located in Toba area. The quantitative result of the geochemical analysis indicates a higher amount of alumina observed using the XRF method. Granodiorite bauxite, which is bauxite coming from granodiorite bedrock, generally has abundant geochemical elements, especially SiO_2 and Al_2O_3. The lateritic bauxite type in the Toba area is a product of granodiorite weathering from the Sepauk Tonalite formation is embedded within a clay matrix which exhibits a brownish to red color with coarse to boulder-size of concretion texture without relict. Some important elements in bauxite laterite deposits are Al, Fe, Si (Silicon), and Ti (Titanium). The comparison between Al and Si values is a benchmark for the economics of bauxite mines. Gibbsite is the major mineral in the bauxite ore, while hematite, goethite, kaolinite, and quartz are the accessory minerals. The deposit is recognized as Low-Fe bauxite due to comparing Al_2O_3, Fe_2O_3, and Si_2O_3 concentrations. The weathering process has altered the primary texture, remaining resistant and secondary minerals. The petrographic analysis shows the replacement of Gibbsite as bauxite ore which presents as kaolinite replacement and fills the mineral cracks. The result of this study is expected to be useful in determining the exploration method for the bauxite deposits.

Keywords: Al_2O_3; Bauxite; Fe_2O_3; Gibbsite; Si_2O_3; XRF methods.

Citation: Aprilia, R., Mukhtar, W. Setiawati, S., Asbanu, G. C., & Munzir, I. (2024). Genesis of Bauxite Ore in Toba Area Sanggau District, West Kalimantan Province. *Jurnal Geocelebes*, 8(1): 26–36, doi: 10.20956/geocelebes.v8i1.26521

Introduction

Laterite bauxite is a concretion layer rich in alumina and iron, reddish-brown in color due to contamination by iron oxide, porous, and found dominantly in tropical–subtropical areas (Toreno & Moe'tamar, 2012). To produce 1 ton of alumina, 2 to 3 tons of bauxite is required to extract alumina using a smelter to produce aluminum. Aluminum is most used in transportation, but it is also used in building and construction materials, machine tools, energy, packaging, durable goods, and other applications (Pusat Sumber Daya Mineral Batubara dan Panasbumi, 2022).

Indonesia has the sixth largest bauxite reserve in the world with approximately 1,200 million tons spread across the Riau

Islands, Bangka and Belitung, West Kalimantan, and a small portion is found in Central Kalimantan and Banten (Haryadi., 2016). In 2021, indicated resources and probable reserves dominated the bauxite resources and reserves. West Kalimantan has the highest bauxite resources in Indonesia, around 2.07 billion tons or 57.32% of all bauxite resources in Indonesia, with bauxite reserves total 0.84 billion tons, or 66.77% of total national mineral reserves. To increase the resilience of reserves, exploring new areas is required to increase the inferred resources, detailed exploration is also needed to improve the measured resources (Pusat Sumber Daya Mineral Batubara dan Panas bumi, 2022). Accordingly, the demand for bauxite ore has also increased and is estimated to reach 18,616,342 tons during 2020-2025 (Anggrahini et al., 2020).

Indonesia's largest bauxite reserves are in the province of West Kalimantan, which is 703 million tons (Haryadi., 2016). West Kalimantan is supported by felsic to intermediate bedrock (such as Sienite, Quartz Diorite, Granodiorite, and Nefelin). The characteristics of West Kalimantan, with the rainfall rate, tropical climate, and the mechanism of the weathering process so that lateritization processes occur in the formation of deposits and the characteristics of the resulting bauxite (Ramadhan et al., 2014).

Bauxite is formed from rocks with a relatively higher Aluminum (Al) and low iron (Fe) content with small amount of quartz (Jafar, 2017). The various mineralogy and characteristics of lateritic bauxite deposits are closely related to several factors, including the texture and composition of the bedrock. This study discusses the genetic type of bauxite deposits based on mineralogy and geochemistry using mineragraphic, XRD and XRF methods. Mineragraphic and XRD methods are used to determine the mineral content of bauxite ore, while the XRF method determines the elemental composition of bauxite deposits. It is versatile and able to evaluate up to eighty elements at different sensitivities, detecting concentrations ranging from 100% to a few parts per million (Winarno et al., 2023a). The percentage of minerals and elements in bauxite will determine the genetic type of bauxite deposits in the study area which will guide in selecting the appropriate exploration method. The research location was carried out in West Kalimantan because it is the largest bauxite producer in Indonesia.

Geological Setting

Regional stratigraphy

Based on regional conditions, the research area located in Sanggau Regency is included in the regional geological map of the Pontianak/ Nangataman sheet (Figure 1), where the research area is only composed of Tonalite Sepauk and Alluvial which was mapped by Sanyoto & Pieters (1993). While regionally, this area consists of various rock formations from old to young described by Sanyoto & Pieters (1993):

1. Pinoh metamorphic rocks

This formation consists of slate, hornstone, phyllite, quartzite, schist, amphibolite, gneiss, and migmatite (Sanyoto & Pieters, 1993), which also acts as the source rock for uranium mineralization in West Kalimantan (Tjokrokardono et al., 2004). These rocks are estimated to be Carboniferous to Triassic in age and are intruded by the Sepauk Tonalite of Lower Cretaceous to Upper Cretaceous age.

2. Sepauk Tonalite

Sepauk tonalite is widely distributed in the Pontianak/ Nangataman sheet, the formation is the bedrock and dominates the rocks in the study area. This formation is of Lower Cretaceous to Upper Cretaceous age and consists of granodiorite and biotite-

hornblende tonalite, quartz diorite, slightly diorite, and monzogranite (Sanyoto and Pieters, 1993), which intrude into the Pinoh metamorphic rock so that the metamorphic rock seems to be floating above the tonalite complex. The tonalite complex is medium to coarse-grained, homogeneous in texture, and with a quartz content of around 15-30%, while feldspar is around 40-50% (Tjokrokardono et al., 2004).

3. Laur Granite

This formation is aligned with the Sepauk Tonalite, which is Lower Cretaceous to Upper Cretaceous in age, composed of monzogranite biotite-hornblende rocks, a little biotite syenogranite and granodiorite hornblende-biotite (Sanyoto & Pieters, 1993).

4. Gabro Biwa

Gabro Biwa is estimated to be of Upper Cretaceous age and is not aligned with the Sepauk Tonalite and Laur Granite. This formation consists of gabbro, composed of hornblende-clinopyroxene minerals, sometimes with biotite, hypersthene, and olivine, and a little hornblende diorite with or without clinopyroxene. Some gabbro shows a layered texture (Sanyoto & Pieters, 1993).

5. Tebidah Formation

This formation is Lower Oligocene in age (Sanyoto and Pieters, 1993), composed of alternating wake lithos and green and red mudstones, a bit of siltstone withlternating layered sandstones and mudstones (Tjokrokardono et al., 2004).

6. Alluvium deposits, beaches, lakes, swamps, and terraces

This deposit consists of mud, sand, gravel, and plant residues of Quaternary age and covers the Sepauk Tonalite Formation unconformably (Sanyoto and Pieters, 1993).

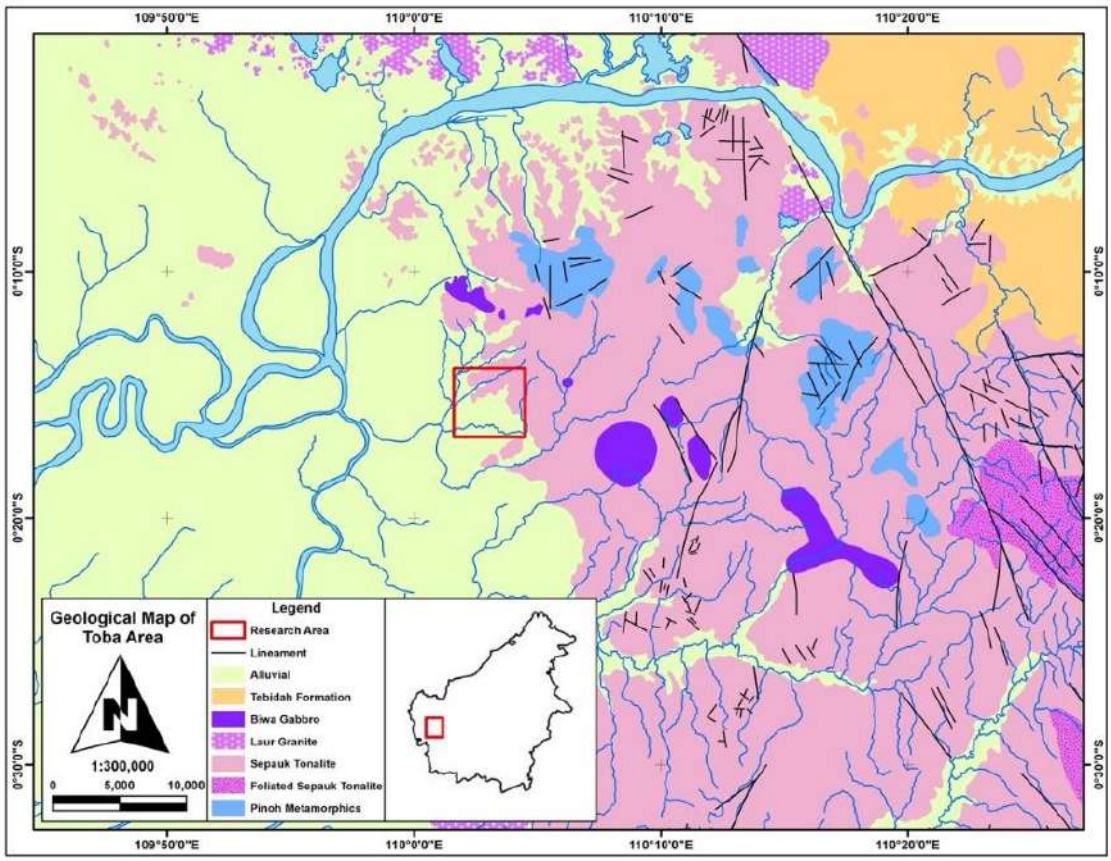

Figure 1. Geological map of research area in Pontianak/ Nangataman sheet after Sanyoto and Pieters (1993).

Bauxite deposits

Bauxite in Indonesia is produced by the supergene enrichment of the Cretaceous peralkaline and alkaline igneous rocks (Nugraheni et al., 2021). According to Economou-Eliopoulos & Kanellopoulos (2022), the most preferred global bauxitization period is the Cretaceous to Eocene. The lithology in the researched area consists of granodiorite, quartz diorite, biotite-hornblende granite, and tonalite. In comparison, the bauxite around the researched area in Tayan District, Sanggau Regency, West Kalimantan, is found in diorite, quartz monzodiorite, quartz diorite, and microdiorite pyroxene (Nugraheni et al., 2022). A previous study by Ramadhan et al. (2014) in the Kenco area, Landak Regency, West Kalimantan, showed that laterite bauxite in the area derived from weathering of Al-rich igneous rock including granodiorite, quartz diorite, and diorite.

Topography, Rainfall and Weathering

The topographical condition of Sanggau Regency is located at an altitude of 0 – 400 meters above sea level with flat landscapes to undulating hills with maximum daily rainfall for the last 10 years, which is from 2011 - 2020 of 1,231 mm/day (Gazhian et al., 2022), with slopes ranging from 0 - >21% (Purwanto & Paiman, 2014). Such topographical conditions will affect the process of rock weathering (Wakila et al., 2019). Rocks on steep slopes tend to be easily weathered compared to rocks on sloping places (Hasria et al., 2021) because rocks will be very easily eroded or weathered because they will directly meet the weather around them (Boinauw, 2017; Wang et al., 2023).

Materials and Methods

This study uses primary data from a sample unit of bauxite ore weighing 20 kg taken from the stockpile of PT. Dinamika Sejahtera located in Toba area. The 1 kg sample was then sent to the Hasanuddin University mineral geochemistry laboratory to prepare polish sections and manufacture bulk powders for petrographic analysis, X-ray Diffraction (XRD), and X-ray Fluorescence (XRF) analysis. Petrographic analysis used a Nikon polarizing microscope instrument Model: Eclipse Ci-L (Ci-L BF-BP), which aims to identify rock-forming minerals, secondary minerals, and the relationship between minerals or rock textures. Meanwhile, minerals that are very fine in size or glass-shaped minerals that cannot be identified by petrographic analysis are carried out using the XRD Shimadzu Model: XRD-7000L instrument. The Shimadzu XRF instrument Model: EDX720 was used to analyze the main chemical elements.

Results and Discussion

Results

1. Texture

The texture of the concretion megascopically is in the form of a hard-rounded material and is rich in aluminum hydroxide. According to Delvigne (1998), cement components in the form of iron oxide minerals and aluminum hydroxide minerals are possessed by the texture of concrete in thin sections. The source rock of bauxite in the study area comes from the granodiorite of Sepauk Tonalite. The megascopic appearance of the granodiorite bauxite sample is embedded within a clay matrix which exhibits a brownish to red color with coarse to boulder-size of concretion texture without relict (Figure 2).

Microscopically, the clay matrix is composed of kaolinite, goethite, gibbsite, and quartz. Silica in the bauxite predominantly appears in the form of kaolinite and quartz, while the other impurity minerals present as goethite and hematite. The appearance of a thin section shows the main role of the hematite as the cement, which occurs in very high amounts

in the sample, and the quartz mineral with a coarse crystal size. The texture of granodiorite bauxite has predominantly aluminum oxide, while quartz and iron oxide minerals are abundant. The iron oxide minerals are well-distributed in the sample when observed under the microscope in the thin section sample because the iron oxide minerals are the cement in the concretion texture. The iron oxide and quartz minerals show that the mobile minerals' dissolution stage in forming bauxite has not taken place effectively. A small amount of aluminum hydroxide indicates that water circulation in forming bauxite is not dominant.

Figure 2. (left) Megascopic appearance of concretion texture of bauxite sample. (right) Petrographic appearance of concretion texture in PPL (Plain Polarized Light).

2. Mineralogy

The granodiorite bauxite contains common minerals such as halloysite, illite, kaolinite, boehmite, diaspore, gibbsite, goethite, hematite, and quartz (Wulansari et al., 2016). Al is the most widely distributed metal in the environment, occurring naturally in the trivalent state (Al^{+3}) as silicates, oxides, and hydroxides, but may combine with other elements such as chlorine, sulfur, fluorine, and form complexes with organic matter (Igbokwe et al., 2019). The petrographic analysis of bauxite ore reveals that mineral content consists of gibbsite ($Al(OH)_3$) which is very dominant, kaolinite ($Al_2Si_2O_5(OH)_4$), hematite (Fe_2O_3), and goethite ($FeO(OH)$). Gibbsite is more common in a humid tropical climate, and boehmite is more common in a tropical climate with a long dry season. In addition, dehydrated minerals appear more often in the dry, upper parts of the profiles than in the lower, wetter parts close to the groundwater level. It is also well known that sedimentary bauxite deposits contain more gibbsite when they are porous and young but more boehmite and diaspore when they are old and compacted (Bárdossy, 1982). Gibbsite in the ore sample is present in granular subrounded nodules measuring 50-200µm, whereas some grains indicate the alteration of gibbsite from kaolinite (Dyussenova et al., 2022). Some grains show the exolution texture together with hematite measuring 10µm in granular shape, while the others are present in the matrix along with kaolinite and partially hematite. In the matrix, there are also traces of gibbsite which have been altered from kaolinite (Figure 3).

The kaolinite mostly occurs in a matrix and fills the space among grains where the kaolinite alteration by gibbsite is very clear under the microscope. Iron oxide minerals are dominated by hematite which presents as isolated minerals in sub-angular to sub-rounded shapes measuring 50-200 µm. Some are in the form of microcrystalline assemblages of fine-grained, rounded shapes altering the minerals that were formed before. It is also present in the matrix along with gibbsite and kaolinite. Generally, laterite bauxite from granodiorite bedrock still contains 10 to

30% quartz, there are also iron oxides (FeOx) such as goethite, hematite, and other clay minerals (Winarno et al., 2023b). The other iron oxide mineral is goethite in irregular texture and smooth acicular shapes around 10-50µm in size. Goethite resembles gibbsite and is associated with the gibbsite, particularly in the form of grains. Further, the XRD analysis shows the mineralogy of the bauxite sample composition quantitatively, including gibbsite (70,4 wt%), dickite (23,8 wt%), hematite (5,8 wt%), and other minerals (3,9 wt%).

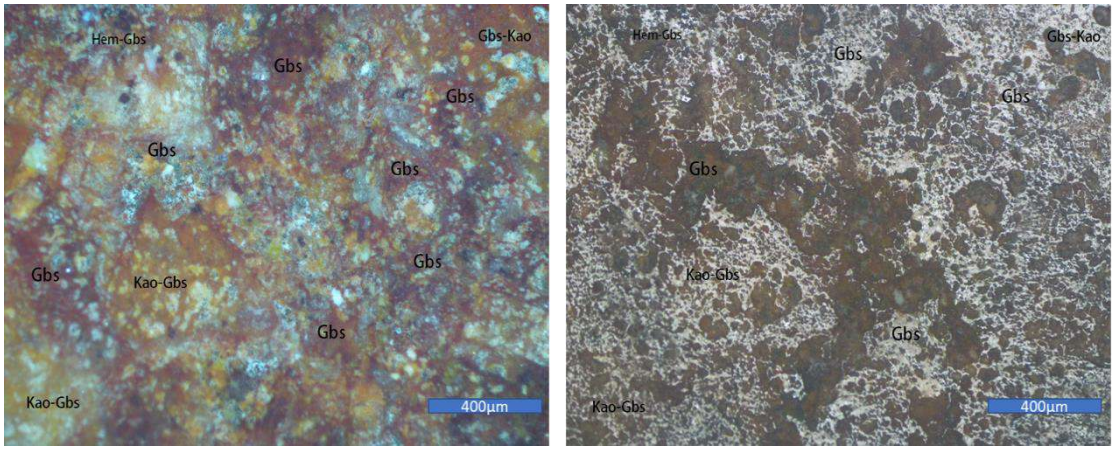

Figure 3. The petrographic appearance of the bauxite ore sample depicted the kaolinite alteration by gibbsite and hematite in XPL (Crossed Polarized Light) and PPL (Plain Polarized Light).

3. Geochemistry

The quantitative result of the geochemical analysis indicates a higher amount of alumina observed using the XRF method. Granodiorite bauxite generally has abundant geochemical elements, especially SiO_2 and Al_2O_3 (Wulansari et al., 2016). The abundance is influenced by the intermediate igneous bedrock, which is rich in Al_2O_3 and SiO_2 found in the lateritic bauxite as gibbsite and quartz respectively (Figure 4).

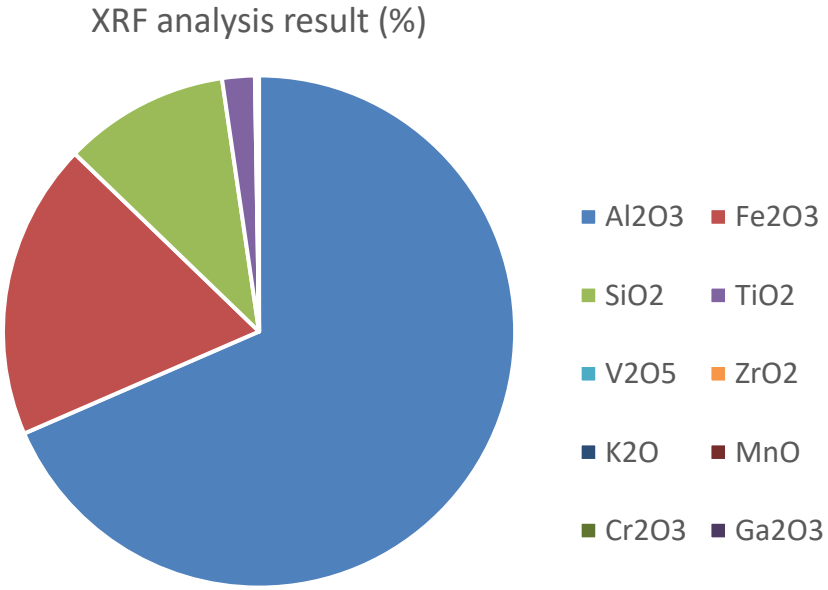

Figure 4. Mineral occurrence in the lateritic bauxite ore sample from XRF analysis.

Similar with Wulansari et al. (2016), the amount of aluminum oxide is relatively higher around 68.478%. Below the aluminum oxide, iron oxide, and silica oxide measuring 18,736 % and 10,467 % respectively. Lastly, titanium oxide is counted at around 2,061 % while V_2O_5, ZrO_2, K_2O, MnO, Cr_2O_3, and Ga_2O_3 are very low amounts, less than 1 %.

Discussion

Some important elements in bauxite laterite deposits are Al, Fe, Si, and Ti. The comparison between Al and Si values is a benchmark for the economics of bauxite mines. According to Ramadhan et al. (2014), the formation of lateritic bauxite deposits is controlled by several interrelated and influencing factors, but these factors can also change in forming deposits, such factors as Al-rich bedrock as the source, subtropical areas with relatively higher rainfall, Daily temperature above 200C, Undulating topography, old age river, and the formation above the permanent groundwater table. The compound elements considered are single-element enrichment bonds that react to water media and precipitate new compounds, in bauxite mining, these compounds are Aluminum trihydrate (Al_2O_3), Iron trihydrate (Fe_2O_3), Silicate oxide (SiO_2), Titanium oxide (TiO_2) and Total silicates (R-SiO_2). Studying the mineral composition of various genetic and lithological types has allowed us to solve one of the most important problems of forming the main rock-forming minerals of bauxite—gibbsite and boehmite—and trace their spatial and genetic relationships (Mamedov et al., 2022). Many believe that boehmite is formed due to the dehydration of gibbsite under the influence of elevated temperature due to the pressure of overlapping strata and the igneous intrusions, as well as metamorphisms (Bárdossy, 1982).

The ore sample from the lateritic bauxite deposit formed by the weathering of Sepauk tonalite as a bedrock contains a rich amount of aluminum hydroxide identified as gibbsite, while the dominant iron oxide was found as hematite. The weathering process has altered the primary texture, remained resistant and secondary minerals. The petrographic analysis shows the replacement of Gibbsite is known as bauxite ore which presents as kaolinite replacement and fills the mineral cracks (Mildan et al., 2021). The enrichment of the gibbsite indicates the significant influence of meteoric water circulation during chemical weathering. Al_2O_3 (68,478 wt.%) and Fe_2O_3 (18,736 wt.%) are the main oxides of the bauxite ore sample from the lateritic bauxite deposit while scarce contents of SiO_2 and TiO_2 occurred around 10,467 wt% and 2,061 wt% respectively. The other major elemental oxides (V_2O_5, ZrO_2, K_2O, MnO, Cr_2O_3, and Ga_2O_3) have concentrations that are systematically below 1 wt.%.

According to the bauxite classification of Bárdossy (1982), the bauxite deposit mainly consists of a Low-Fe bauxite, as suggested by the sample distribution in the Al_2O_3–SiO_2–Fe_2O_3 ternary diagram shown in Figure 5.

Binary plots among the major elemental oxides (Figure 6) indicate that, in the ore bauxite sample there is a positive correlation exists between Al_2O_3 and TiO_2, and between Al_2O_3 and Fe_2O_3, whereas negative correlations exist between Al_2O_3 and SiO_2 and Al_2O_3 and CaO. These correlations are typical of strongly weathered deposits where immobile elements accumulate and mobile elements are leached out (Putzolu et al., 2018). This is also confirmed by the low contents of alkali and alkali earth elements, which are highly mobile during chemical weathering (Gu et al., 2013; Zamaniana et al., 2016).

The intensive development of laterite in the wet tropics causes the formation of laterite soils. Generally, the lateritization process in

bauxite comprises several stages: dissolving, transporting, and re-depositing of minerals. The most important factors in dissolution are pH, solubility, and mineral stability. Factors affecting minerals' transport and re-deposition are climate, topography, morphology, and mobility of elements. Weathering results will be transported by groundwater or rainwater, then precipitated again. The process occurs well on a sloping land surface with a certain slope, morphological, and topographical conditions that tend to be undulating.

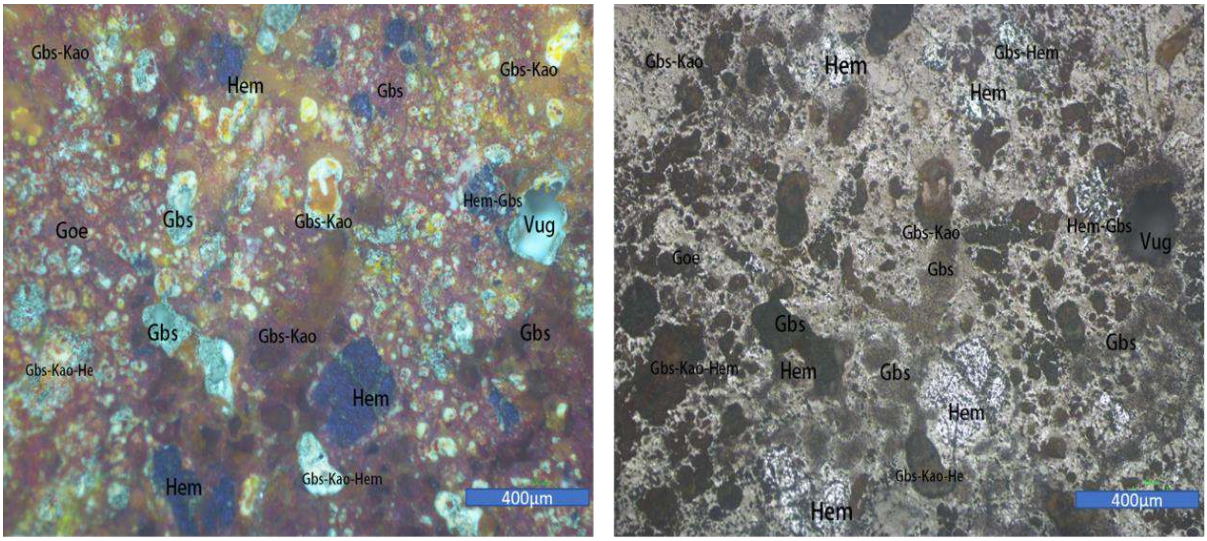

Figure 5. The petrographic appearance of the bauxite ore sample depicted occurrence of gibbsite as major mineral while hematite, goethite, and kaolinite are the accessory minerals in in XPL (Crossed Polarized Light) and PPL (Plain Polarized Light).

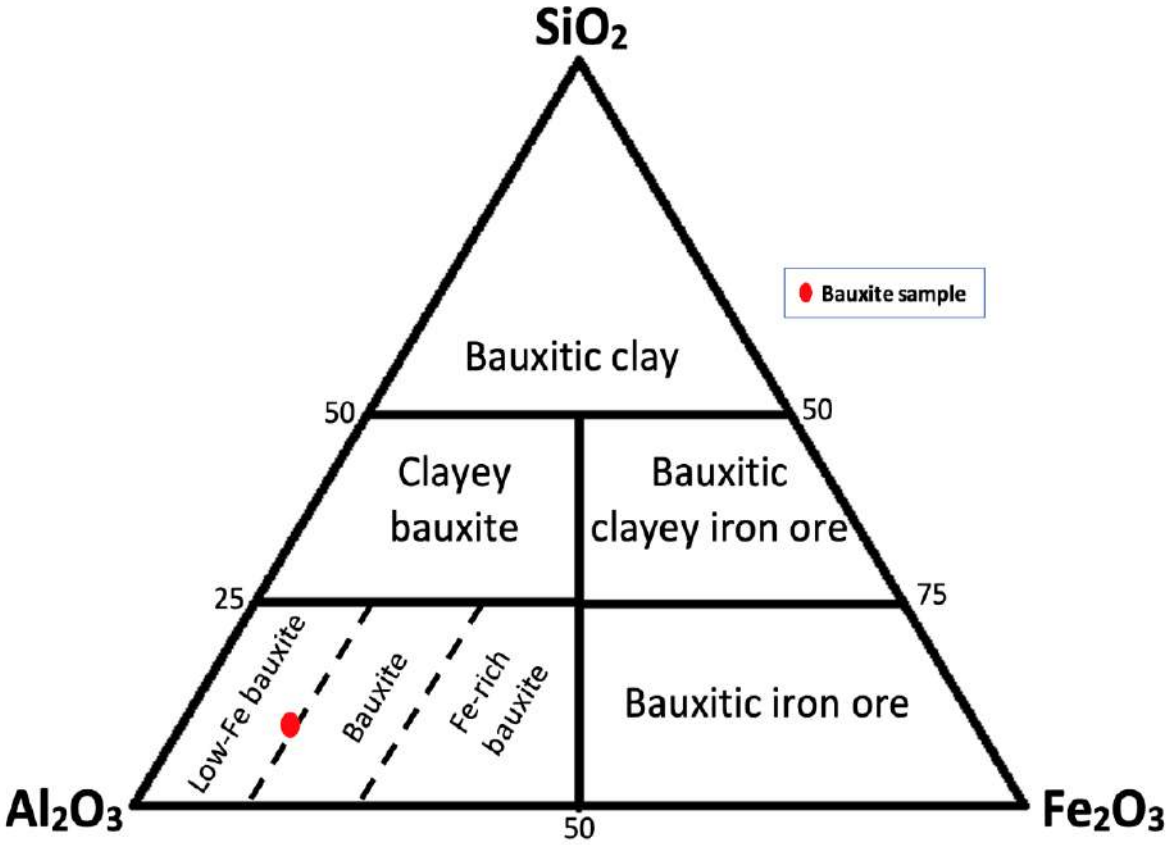

Figure 6. Al_2O_3–SiO_2–Fe_2O_3 classification diagram (modified from Bárdossy (1982), for the display of bauxite ore sample.

Conclusion

The conclusion of this study is the lateritic bauxite type in Toba area is a product of granodiorite weathering from Sepauk Tonalite formation. Gibbsite is the major mineral in the bauxite ore, while hematite, goethite, kaolinite and quartz are the accessory minerals. The deposit is recognized as Low-Fe bauxite due to comparing Al_2O_3, Fe_2O_3, and Si_2O_3 concentrations.

Acknowledgements

The entire process of data collection, data analysis and publication of the results of this study was funded by the DIPA of the Faculty of Engineering, Tanjungpura University. The authors thanks to Dr. Hasria Alang, M.Kes. who have provided many inputs in the process of writing this paper. Hopefully this paper can play a role in the development of science, especially regarding mineral resources exploration.

Author Contribution

This paper was completed thanks to the collaboration of all authors. The idea on this topic was first proposed by Ibnu Munzir and he also analyzed the results and made maps. Field surveys and sampling was done by Ricka Aprillia. Wahdaniah Mukhtar determines the method and analizes the problem. Septami Setiawati collected references and Govira Asbanu helped arranged the background and some editing. Hopefully this kind of collaboration will continue.

Conflict of Interest

This research was conducted independently without any financial support from any parties.

References

Anggrahini, A. H., Wibowo, A. P., & Rosyid, F. A. (2020). Peramalan Kebutuhan Bijih Bauksit Untuk Memenuhi Kebutuhan Aluminium Nasional Menggunakan Model ARDL dan VAR. *Prosiding TPT XXIX PERHAPI 2020*, 401–412. https://prosiding.perhapi.or.id/index.php/prosiding/article/view/170

Bárdossy, G. (1982). *Bauxite Deposits on Carbonate Rocks, Developments in Economic Geology*. Elsevier.

Boinauw, H. (2017). Pembelajaran Geologi: Kajian Pelapukan Geologi. *Jurnal Ilmiah Jendela Pengetahuan*, 10(22), 59–63. https://ejournal.unpatti.ac.id/ppr_iteminfo_lnk.php?id=1623

Delvigne, J. E. (1998). *Atlas of Micromorphology of Mineral Alteration and Weathering*. Mineralogical Association of Canada.

Dyussenova, S., Abdulvaliyev, R., Akcil, A., Gladyshev, S., & Ruzakhunova, G. (2022). Processing of Low-Quality Gibbsite-Kaolinite Bauxites. *Metals*, 12(6), 1030. https://doi.org/10.3390/met12061030

Economou-Eliopoulos, M., & Kanellopoulos, C. (2023). Abundance and Genetic Significance of Lithium in Bauxite Deposits: A Comparative Review. *Minerals*, 13(7), 962. https://doi.org/10.3390/min13070962

Gazhian, S. R., Nirmala, A., Aprillia, R., Sutrisno, H., & Meilasari, F. (2022). Tailing Pond Maintenance System PT. Dinamika Sejahtera Mandiri at The Teraju Site, Toba District, Sanggau Regency. *Jurnal Teknik Sipil*, 22(2), 122–126. https://dx.doi.org/10.26418/jtst.v22i2.59158

Gu, J., Huang, Z., Fan, H., Jin, Z., Yan, Z., & Zhang, J. (2013). Mineralogy, Geochemistry, and Genesis of Lateritic Bauxite Deposits in The Wuchuan-Zheng'an-Daozhenarea, Northern Guizhou Province, China. *Journal of Geochemical Exploration*, 130, 44–59.

https://doi.org/10.1016/j.gexplo.2013.03.003

Haryadi, H. (2016). Analisis Lost Opportunity (LO) Bauksit Indonesia. *Jurnal Teknologi Mineral dan Batubara*, 12(1), 45–57. https://doi.org/10.30556/jtmb.Vol12.No1.2016.230

Hasria, H., Asfar, S., Ngkoimani, L. O., Okto, A., Jaya, R. I. M. C., & Sepdiansar, R. (2021). Pengaruh Geomorfologi Terhadap Pola Distribusi Unsur Nikel Dan Besi Pada Endapan Nikel Laterit di Kabupaten Buton Tengah-Sulawesi Tenggara. *Jurnal Geosapta*, 7(2), 103–114. http://dx.doi.org/10.20527/jg.v7i2.10716

Igbokwe, I. O., Igwenagu, E., & Igbokwe, N.A. (2019). Aluminum Toxicosis: A Review of Toxic Actions and Effects. *Journal of Interdisciplinary Toxicology*, 12(2), 45–70. https://doi.org/10.2478/intox-2019-0007

Jafar, N. (2017). Analisis Unsur Endapan Bauksit Menggunakan X-Ray Fluorescence (XRF) PT. Antam Tbk. Unit Geomin Daerah Kenco Kabupaten Landak Provinsi Kalimantan Barat. *Journal of Chemical Process Engineering*, 2(1), 46–49. https://doi.org/10.33536/jcpe.v2i1.115

Mamedov, V., Boeva, N., Makarova, M., Shipilova, E., & Melnikov, P. (2022). The Problem of the Formation of Boehmite and Gibbsite in Bauxite-Bearing Lateritic Profiles. *Minerals*, 12, 389. https://doi.org/10.3390/min12030389

Mildan, D., Subandrio, A. S., Bangun, P., & Sunjaya, D. (2021). Contrasting Genesis of Lateritic Bauxite on Granodioritic and Andesitic Rocks of Mempawah Area, West Kalimantan. *IAGI Journal*, 1(2), 81–88. https://doi.org/10.51835/iagij.2021.1.2.33

Nugraheni, R. D., Riyandhani, C. P., Apriniyadi, M., & Sunjaya, D. (2021). Critical Raw Materials Enrichment in Bauxite Laterite: A Case Study of Diverse Parent Rock Types. *IOP Conference Series: Earth and Environmental Science*, 882, 012024. https://doi.org/10.1088/1755-1315/882/1/012024

Nugraheni, R. D., Sunjaya, D., Sutopo, B., Apriniyadi, M., Riyandhani, C. P., & Ronoatmojo, I. S. (2022). Spatial Simulation Model of Bauxite Grades Using R Data Analysis: Its Implication for Exploration Activity. *Indonesian Journal on Geoscience*, 9(3), 337–353. https://doi.org/10.17014/ijog.9.3.

Purwanto, A., & Paiman. (2014). Inventarisasi Karakteristik Lahan Lokasi Sumber Air Panas Untuk Pengembangan Pariwisata di Kecamatan Jangkang Kabupaten Sanggau. *Jurnal Edukasi*, 12(2), 179–192. https://journal.ikippgriptk.ac.id/index.php/edukasi/article/view/154

Pusat Sumber Daya Mineral Batubara dan Panasbumi. (2022). *Neraca Sumber Daya dan Cadangan Mineral Batubara dan Panas Bumi Tahun 2021*. Kepala Bagian Umum Sub Koordinator Perencanaan dan Keuangan.

Putzolu, F., Papa, A. P., Mondillo, N., Boni, M., Balassone, G., & Mormone, A. (2018). Geochemical Characterization of Bauxite Deposits from The Abruzzi Mining District (Italy). *Minerals*, 8(7), 298. https://doi.org/10.3390/min8070298

Ramadhan, F. R., Aribowo, Y., Widiarso, D. A., & Betraz, A. (2014). Geologi, Karakteristik dan Genesa Endapan Laterit Bauksit P.T. ANTAM (Persero) Tbk. Unit Geomin, Daerah Kenco, Kabupaten Landak, Provinsi Kalimantan Barat. *Geological Engineering E-Journal*, 6(1), 80–95. https://ejournal3.undip.ac.id/index.php/geologi/article/view/6754

Sanyoto, P., & Pieters, P. E. (1993). *Peta Geologi Lembar Pontianak/ Nangataman, Kalimantan Skala 1:250.000*. Pusat Penelitian dan Pengembangan Geologi. Bandung

Tjokrokardono, S., & Soetarno, D. (2004). Studi Geologi Regional dan Mineralisasi Uranium di Pegunungan Schwaner Kalimantan Barat dan Tengah. *Prosiding Seminar Geologi Nuklir dan Sumberdaya Tambang Tahun 2004*, 64–84. https://inis.iaea.org/collection/NCLCollectionStore/_Public/39/123/39123070.pdf

Toreno, E. Y., & Moe'tamar. (2012). Karakteristik Cebakan Bauksit Laterit di Daerah Sepiluk – Senaning, Kabupaten Sintang, Kalimantan Barat. *Buletin Sumber Daya Geologi*, 7(2), 45–56. https://doi.org/10.47599/bsdg.v7i2.102

Wang, W., Feng, J., & Qui, M. (2023). Mineral Weathering and Element Migration in Granite Weathering Pits (Gnammas): A Case Study in Eastern China. *Minerals*, 13(1), 70. https://doi.org/10.3390/min13010070

Wakila, M. H., Heriansyah, A. F., Firdaus, F., & Nurhawaisyah, S. R. (2019). Pengaruh Tingkat Pelapukan Terhadap Kadar Nikel Laterit Pada Daerah Ussu, Kec. Malili Kab. Luwu Timur Prov. Sulawesi Selatan. *Jurnal Geomine*, 7(1), 30–35.

Winarno, T., Sendjaja, P., & Wibowo, F. R. (2023a). The Relationship Between Geological and Environmental Aspects with the Anomalies of Track Elements and Heavy Metal Elements in the Volcanic Area of the Muria Peninsula. *E3S Web of Conferences*, 448, 03067. https://doi.org/10.1051/e3sconf/202344803067

Winarno, T., Ali, R. K., Simangunsong, H., & Almiftahurrizqi, (2023b). Characteristics and Genesis of Laterite Bauxite in Sompak District and Surrounding Areas, Landak Regency, West Kalimantan. *Indonesian Journal on Geoscience*, 10(1), 37–49. https://ijog.geologi.esdm.go.id/index.php/IJOG/article/view/857

Wulansari, D., Setijadji, L. D., & Warmada, I. W. (2016). Karakterisasi Kandungan Mineral Dalam Bauksit Dengan Metode Xrd Semi-Kuantitatif Di Kawasan Tambang Tayan, Kalimantan Barat. Proceeding, Seminar Nasional Kebumian Ke-9, 612–623.

Zamaniana, H., Ahmadnejad, F., & Zarasvandi, A. (2016). Mineralogical And Geochemical Investigations of The Mombi Bauxite Deposit, Zagros Mountains, Iran. Geochemistry, 76(1), 13–37. https://doi.org/10.1016/j.chemer.2015.10.001

ISSN: 2579-5821 (Print)
ISSN: 2579-5546 (Online)
URL address: http://journal.unhas.ac.id/index.php/geocelebes
DOI: 10.20956/geocelebes.v8i1.28303

Jurnal Geocelebes Vol. 8 No. 1, April 2024, 37 – 50

Subsurface Interpretation of the Panjang Fault Area, Lampung, Based on Geomagnetic Method

Syamsurijal Rasimeng[1], Fahruddin[2], Ferdio Valentin[1]*, Theressia Githa Aurora[1], Jesica Nurlaili[1]

[1]Department of Geophysical Engineering, Faculty of Engineering, Lampung University, Lampung 35141, Indonesia.
[2]Department of Physics, Faculty of Mathematics and Natural Sciences, Lambung Mangkurat University, Banjarmasin 70123, Indonesia.

*Corresponding author. Email: ferdiovalentin02@gmail.com

Manuscript received: 14 August 2023; Received in revised form: 4 January 2024; Accepted: 22 January 2024

Abstract

Research on the area along the Panjang Fault - Lampung, the area from the Teluk Betung to Tanjung Karang Barat area using the 19-T GSM PPM tool with base rover acquisition on 2 tracks 2 kilometers apart obtained 40 acquisition points with a spacing of 0.3 kilometers. This study aims to determine the type of lithology and subsurface rock structure by utilizing the susceptibility value of rocks from magnetic anomalies. In the process of processing magnetic anomaly data, upward continuation is carried out as high as 350 m which is intended to reduce the total anomaly with the upward anomaly results so that a residual anomaly is obtained. Next, make a 2D subsurface model on the incision A - B in the residual anomaly map. Based on the results of qualitative interpretation, the total magnetic anomaly of the research area illustrates positive to negative anomaly values with a tighter contour pattern that indicates the presence of a fault structure. While based on quantitative interpretation, the 2D modeling in incision A - B shows a susceptibility value of 0.100 cgs which can be identified as breccia tuff rock, a susceptibility value of 0.0391 cgs is thought to be rhyolitic tuff rock, pumice tuff rock, and sandstone tuff, and a susceptibility value of 0.150 cgs is a rock from the intrusion of Mount Betung in the form of andesite-basalt lava. In addition, rocks with a susceptibility value of 0.0024 cgs are metamorphic rocks. The correlation between 2D modeling and regional geology is seen in the research area, which is in the Tarahan Formation (Tpot), which is suspected to be a fault structure in the Bumi Waras area with a strike direction of NW - SE which is the course of geothermal manifestations or minerals.

Keywords: local magnetic anomaly; magnetic susceptibility; Panjang Fault.

Citation: Rasimeng, S., Fahruddin, F., Valentin, F., Aurora, T. G., & Nurlaili, J. (2024). Subsurface Interpretation of the Panjang Fault Area, Lampung, Based on Geomagnetic Method. *Jurnal Geocelebes*, 8(1): 37–50, doi: 10.20956/geocelebes.v8i1.28303

Introduction

Faults are areas of interest for mineral, geothermal and oil and gas exploration, because they are the pathway for hydrothermal fluids to the surface, and the pathway for oil and gas migration to the reservoir. Bandar Lampung City is a densely populated area located at the southern tip of Sumatra Island (Mangga et al., 1993). Based on the geological map of Tanjungkarang Sheet, Bandar Lampung City is affected by several active faults. One of them is the Lampung Fault with a northwest-southeast direction, which is one of the faults located in the Bandar Lampung area in Panjang District, Bandar Lampung City to Natar District, South Lampung Regency. Lampung Fault also divides Bandar Lampung City with morphology along the fault in the form of slopes to steep hills.

The magnetic method is a geophysical method that works to utilize the magnetic properties of rocks and materials under the earth's surface. The data measured in this method is the value of the magnetic field in each area. Through IGRF correction and daily variation correction, anomalous magnetic field values will be obtained. This anomalous magnetic field value is then mapped in the magnetic anomaly contour. From the mapping results, the geological structure of the survey area can be identified (Fashihullisan et al., 2014). Therefore, based on this, the fault structure in the Bandar Lampung area can be identified by the magnetic method. For many years, magnetic prospecting has been used to investigate the subsurface structures associated with mineral deposits (Ben et al., 2021).

Magnetic method is a geophysical method based on the measurement of magnetic field intensity variations (Abdullah & Sunaryo, 2014). Magnetic surveying is a geophysical technique that can provide valuable insight into the Earth's crust by detecting differences in magnetization (Nicolosi et al., 2016). The source of the earth's magnetic field is generally divided into, (i) the intensity of the earth's main magnetic field (main field); (ii) the intensity of the external magnetic field (external field) and (iii) the intensity of the anomaly magnetic field (Nuha ABA et al., 2014; Rasimeng et al., 2020).

The magnetic anomalies are always superposition of potential fields from sources of different depths and scales. The potential fields can be decomposed in the spatial or frequency domain to give more specific geological interpretations, and this process is generally termed as the potential field separation (Yang & Li, 2023). The source of the magnetic anomaly is a dipole field that produces positive and negative anomaly pairs. The reduction process to the polar direction refers to changes in the magnetic field in the vertical direction, as seen from the North Pole of the Earth to facilitate qualitative interpretation (Setiadi et al., 2016). So, the author uses this method to produce more accurate modeling of subsurface structures and can show the rock layers as well. The total magnetic field anomaly data at the measurement location is still in the form of magnetic dipoles. Therefore, it is necessary to make a reduction correction to the pole. This dipole anomaly is transformed to the earth's magnetic north pole by changing the direction of the anomalous magnetic field slope to 90˚. After reduction to the poles, the total magnetic field anomaly value becomes monopole (Hiden et al., 2023). Prominent magnetic field anomalies are often referred to as local magnetic fields (crustal fields) because these magnetic fields are generated from rocks with strong magnetic mineral content in the earth's crust (Heningtyas et al., 2020).

Magnetic anomaly characteristics, such as direction of maximum extension and gradient, can reveal information about the direction, dip, and strike of tectonic structures, such as faults and dike swarms (Hinze et al., 2013; De Ritis & Chiappini, 2023). In addition, magnetic anomalies can also reveal the location, extent, and depth of crustal volumes with very low or fully demagnetized magnetization (Bouligand et al., 2014; Tontini et al., 2019). The magnetic anomalies obtained still contain two regional and residual anomalies, so they need to be separated (Ilapadila et al., 2019). Regional – residual anomaly separation is a very important step. Therefore, an appropriate data filter is needed to obtain accurate data results for better interpretation. There are several methods used to separate the two anomalies. However, the most used method is the upward continuation method. Previous research using the upward continuation method such as Hiskiawan (2016) and Nurdin et al. (2017).

Based on research conducted by Heningtyas et al. (2017), it states that knowing the arrangement of rock formations around the fault line and knowing the fault line based on geomagnetic modeling of magnetic field anomaly distribution patterns. Furthermore, research by Sulandari et al. (2023) conducted in the Lampung - Panjang Fault can be identified using magnetic methods with the separation of regional and residual anomalies and the Filter Horizontal Derivative (FHD) process for the interpretation process. Then the Bandar Lampung area is categorized as a landslide-prone area because the constituent rocks have many fractures that make the slope unstable. The Bandar Lampung area also has many faults that cause many hills with steep morphology (Agustina et al., 2020). Based on the results of the research that has been done before, this research uses geomagnetic method which aims to determine the variation of magnetic field and subsurface interpretation in Lampung Fault area, especially around Teluk Betung to Tanjung Karang Barat, Bandar Lampung City. By utilizing the physical properties of rocks in the form of susceptibility values, to find out types of lithology or rocks are under the surface of the Lampung Fault area. Geophysical data from the results of research using magnetic methods in the form of rock susceptibility anomaly values that can be a target object to determine what types of minerals are in the subsurface and can determine the structure or lithology below the surface of the research area.

Materials and Methods

Geographical Location

Geographically, the research location is in the Bandar Lampung area between 50º20'-50º30' N and 105º28'-105º37' E, precisely in Teluk Betung District to Tanjung Karang Barat District, Bandar Lampung, Lampung Province.

Geological Setting

Geologically, the research location generally has rock outcrops along the Lampung fault area in the form of andesitic-basaltic rocks shown in Figure 1.

The lithological contact of rock units and formations exposed on the surface along the Lampung fault consists of the Tarahan Formation (Tpot), Campang Formation (Tpoc), Waygalih schist rock unit (Pzgs), Young Volcanic deposits of G. Betung (Qhv(b)) and Lampung Formation (QTl). While the lithology of each formation or rock unit is; Lampung Formation (QTI) in the form of stony tuff, rhyolitic tuff, solid tuff, tuffaceous claystone, and tuffaceous sandstone; G. Betung Young Volcano Unit (Qhv(b)) in the form of lava (andesite-basalt), breccia and tuff; Alluvium (Qa) in the form of crusts, pebbles, sand, clay, and peat. Tertiary rocks are composed of volcanic products and intrusive rocks. It consists of the Campang Formation (Tpoc) with the lower part being a mixture of mudstone, shale and compact tuff, the upper part is a breccia of various materials with sandstone and siltstone inserts; Tarahan Formation (Tpot) in the form of compact tuff, breccia with lentil inserts; Pre-Tertiary rocks are composed of bedrock in the form of metamorphic rocks of the Inseparable Kasih Mountain Complex (Pzg) in the form of Pelitan schist and a little gneiss; and the Waygalih Schist rock unit (Pzgs) in the form of green amphibole schist, diorite orthogenes amphibolite (Mangga et al., 1993; Mulyasari et al., 2018).

Data Acquisition

Acquisition with a line system where magnetic field measurements at each location on the surface consist of two tracks with about 300 meters between each measurement point, and the number of measurement data is 40 measurement points (Figure 2).

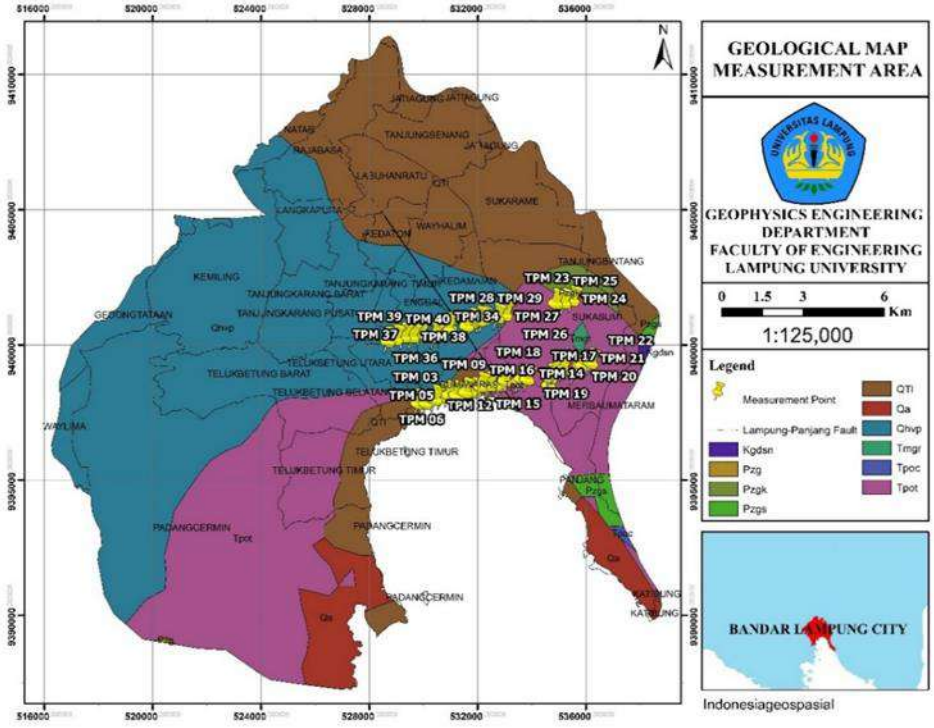

Figure 1. Geologic map of Bandar Lampung and surrounding areas (modified form Mangga et al., 1993; Mulyasari et al., 2018).

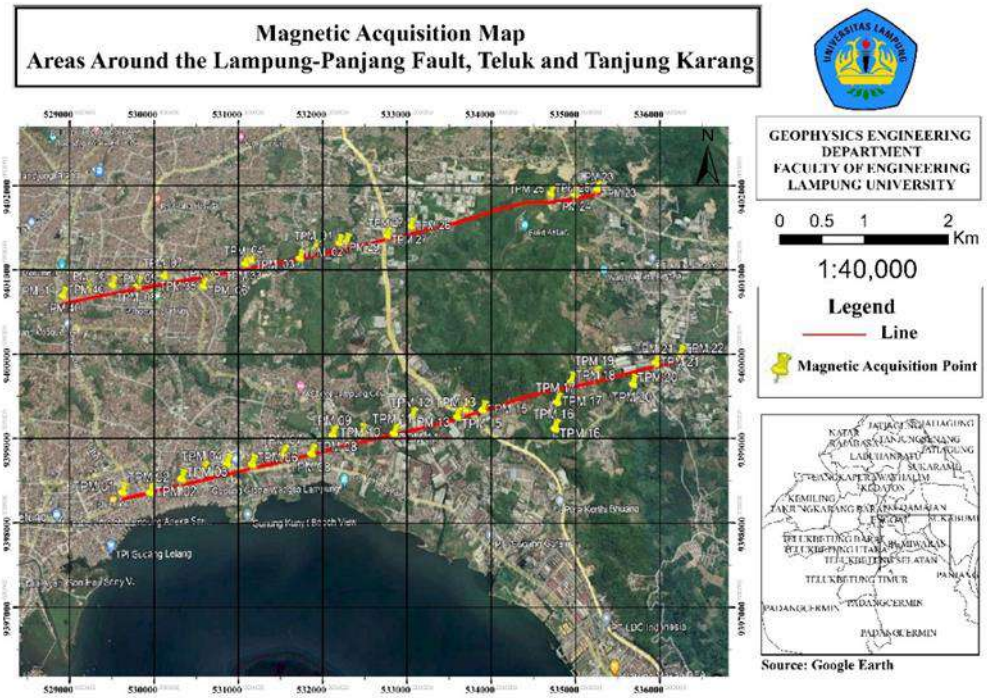

Figure 2. Location map of measurement points.

The line-type acquisition system will get data that has a regular and fixed distance. Magnetic field measurements use the GSM-19T Proton Precession Magnetometer (PPM) tool for the rover and base station respectively. Base station data measurements are placed in a noise-free area to get the optimal tool reading value. While the rover measurement data is carried out mobile in accordance with the acquisition design that has been made as shown in the magnetic acquisition map. The reading value of the tool obtained from

the acquisition in the field is then calculated to obtain the magnetic anomaly value.

Data Processing and Analysis

Data processing in this study goes through several stages, the first of which is making IGRF (International Geomagnetic References Field) through the BMKG website https://www.bmkg.go.id/geofisika-potensial/kalkulator-magnet-bumi.bmkg and correction of daily variations. The second stage calculates magnetic anomalies from total magnetic field data in the research area. With the following equation:

$$HA = H_{total} - H_{IGRF} \pm \Delta H_{\text{diurnal}} \quad (1)$$

Description:

HA : Magnetic Anomaly
$\Delta H_{diurnal}$: Diurnal Variation Value
H_{total} : Total Magnetic Field Value
H_{IGRF} : IGRF Value

The next stage is the upward continuation process where this process is carried out to eliminate residual anomalies by looking at the tendency of the contour pattern of the continuation results (Fikar et al., 2019). Continuation is carried out as high as 350 m which is used to eliminate local magnetic effects and can facilitate the interpretation process if a separation is made between regional and residual anomalies (Regita et al., 2022). To get the residual anomaly using the following equation:

$$\text{Res} = T_{Anomaly} - T_{Upward} \quad (2)$$

Description:

Res : Residual Anomaly
$T_{Anomaly}$: Total Anomaly
T_{Upward} : Anomaly of Upward Result

Then the Reduce to Pole process localizes the residual anomaly results which are transformed from dipole to monopole form for further analysis of magnetic patterns using 2-dimensional modeling. This modeling is seen based on the high-low value of magnetic anomalies in the study area so that areas with anomalies with drastic high-low changes can be seen to determine fault and intrusive areas (Fashihullisan et al., 2014). Based on the magnetic field anomaly contours, quantitative interpretation can be done using 2D modeling, by matching the residual anomaly curve based on the trajectory data selected from the residuals. magnetic field anomaly map with the model curve which is done iteratively (Efendi et al., 2016). This processing stage can be seen through the following flowchart: (Figure 3).

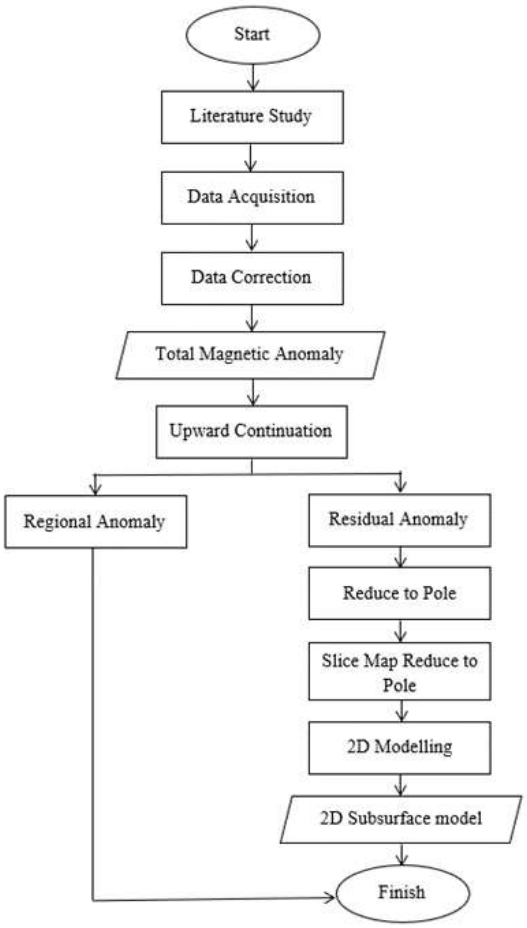

Figure 3. Research flowchart.

Results and Discussion

This study began with an acquisition in the Bandar Lampung area, Lampung. Magnetic acquisition was carried out with the help of PPM (Proton Precession Magnetometer) GSM-19 T Magnetometer tool and assisted with Garmin GPS tool to determine and plot the acquisition point. Acquisition points were made as many as 40 points with

line acquisition technique, this acquisition area stretches from Teluk to Tanjung Karang which cuts the Panjang Fault area - Lampung.

Data processing after the acquisition process is carried out by finding the value of the magnetic field anomaly by carrying out the correction process of the magnetic data obtained. However, before that, it is necessary to correct the daily variation using the time interpolation method from the rover and base station where the base measurements are made with a time interval of 900 seconds or 15 minutes. So that the results of the magnetic field can be seen in Figure 4.

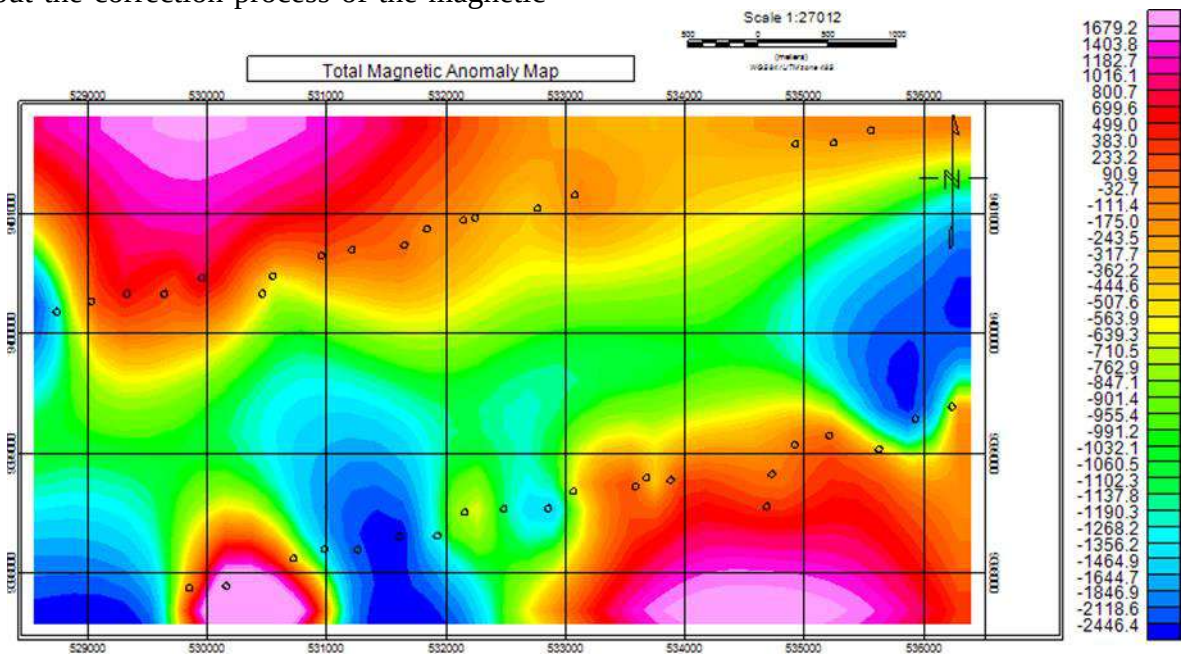

Figure 4. Contour map of the total magnetic field anomaly of the study area.

The magnetic field anomaly map made is lifted by the upward continuation method as high as 350 meters with the help of the Ms Fortran PS 4.0 program by entering the script that has been made, but before that changes are made to the nodes on the magnetic field anomaly map which n2 for the Fortran program to be used, n2 is made on the nodes which is 64x64 grids and the data obtained is 4,096 nodes on the anomaly map so that the level of accuracy on the map increases and the X space used is 119.015 and the Y space is 60.730, then a magnetic field anomaly map will be obtained that has been lifted at an altitude of 350 meters from the height of the starting point of measurement which can be seen in Figure 5.

In the upward continuation transformation process transformation process causes anomalous sources with short wavelength responses will experience significant attenuation compared to the length of anomalous sources with large wavelengths (Blakely, 1996). Upward continuation is done to remove residual or local effects from the measurement area which will then only leave local effects because it is lifted 350 m high. However, lifting with the upward continuation method is done to create local or residual magnetic field anomalies which will be used to make subtractions or differences to obtain local anomalies.

The upward continuation filter operation allows transformation of data measured at one surface to several higher surfaces (Amigun et al., 2012) and tends to smooth the original data by attenuating anomalous short wavelengths relative to the wavelengths of their counterpart. The upward anomaly results are included in the

regional anomaly so that regional effects are obtained and require residual effects for further processing. The processing to get the residual anomaly effect is done by entering both maps and then doing math to subtract and will get a residual or local anomaly map like Figure 6 below.

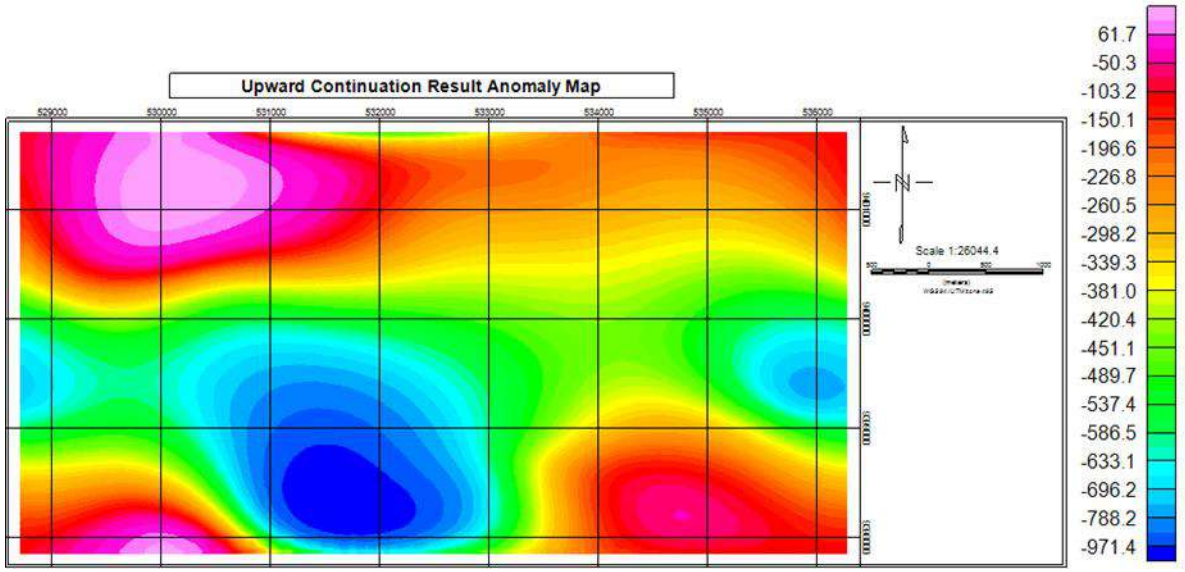

Figure 5. Contour map of total magnetic field anomaly upward continuation 350 m height.

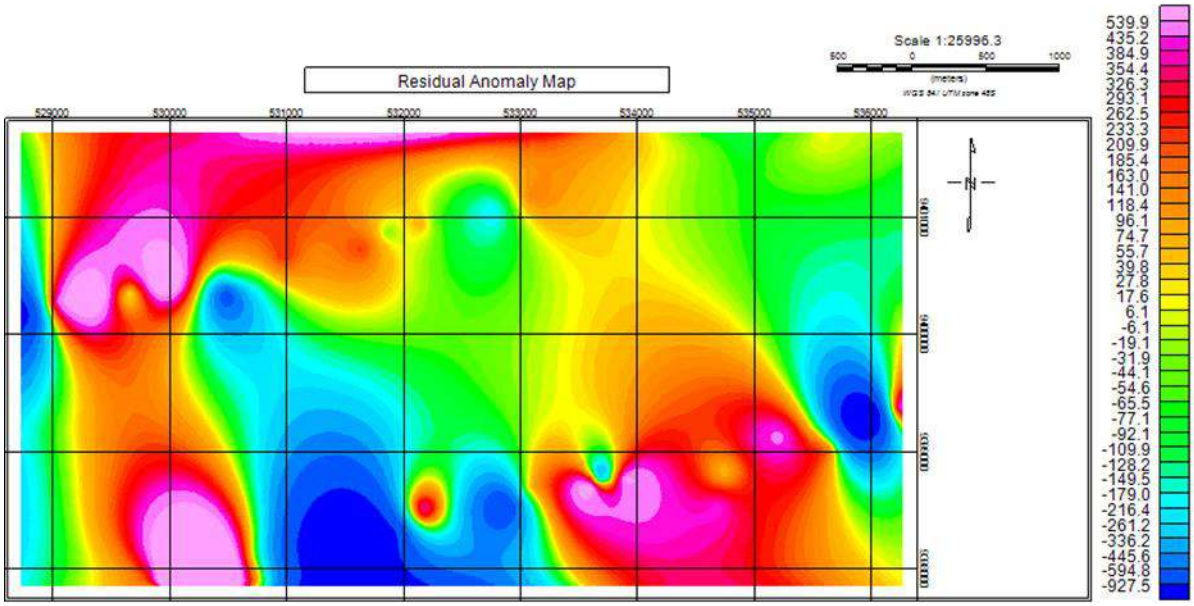

Figure 6. Total magnetic field residual anomaly contour map.

The residual anomalies obtained are still under the influence of the dipole effect or two poles. The north and south poles of the subsurface object, so that for the purposes of a more definite and clear interpretation, a transformation is carried out to change the dipole effect to monopole. The transformation carried out is RTP (Reduce to magnetic pole) which will result in the assumption that the anomalous object is below the surface right with the highest anomalous value.

The result of the RTP transformation is shown in Figure 7 below. To produce higher resolution magnetic maps the downward continuation method of Tran & Nguyen (2020) has been applied to the magnetic data. Small amplitude anomalies are shown more clearly on the continuation map (Abdelrahman et al., 2024).

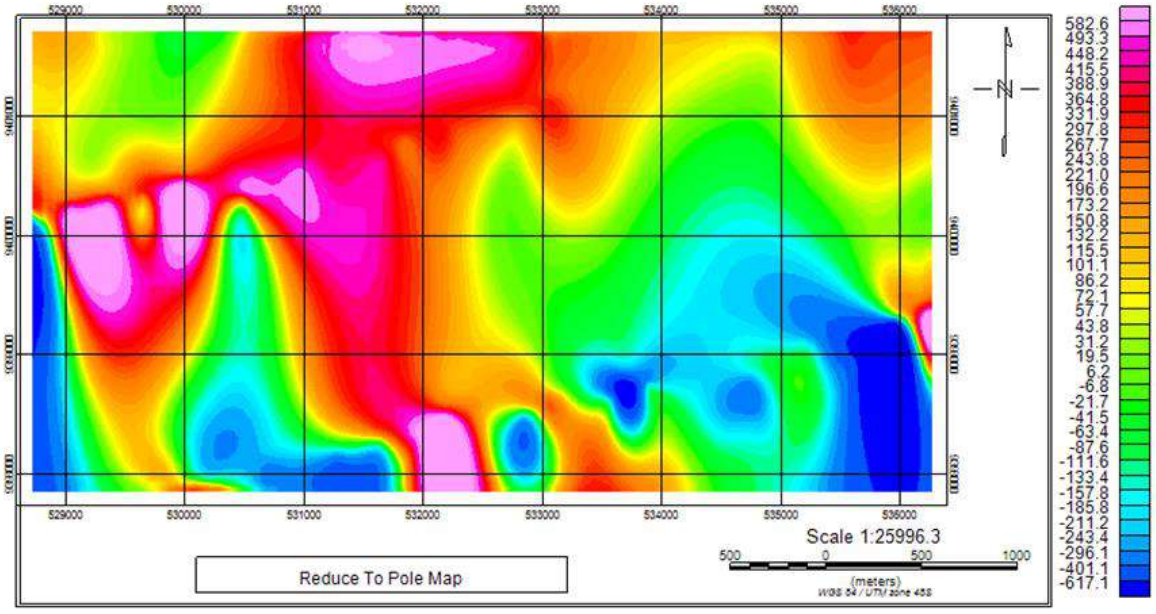

Figure 7. Contour map of total magnetic field anomaly reduce to the pole.

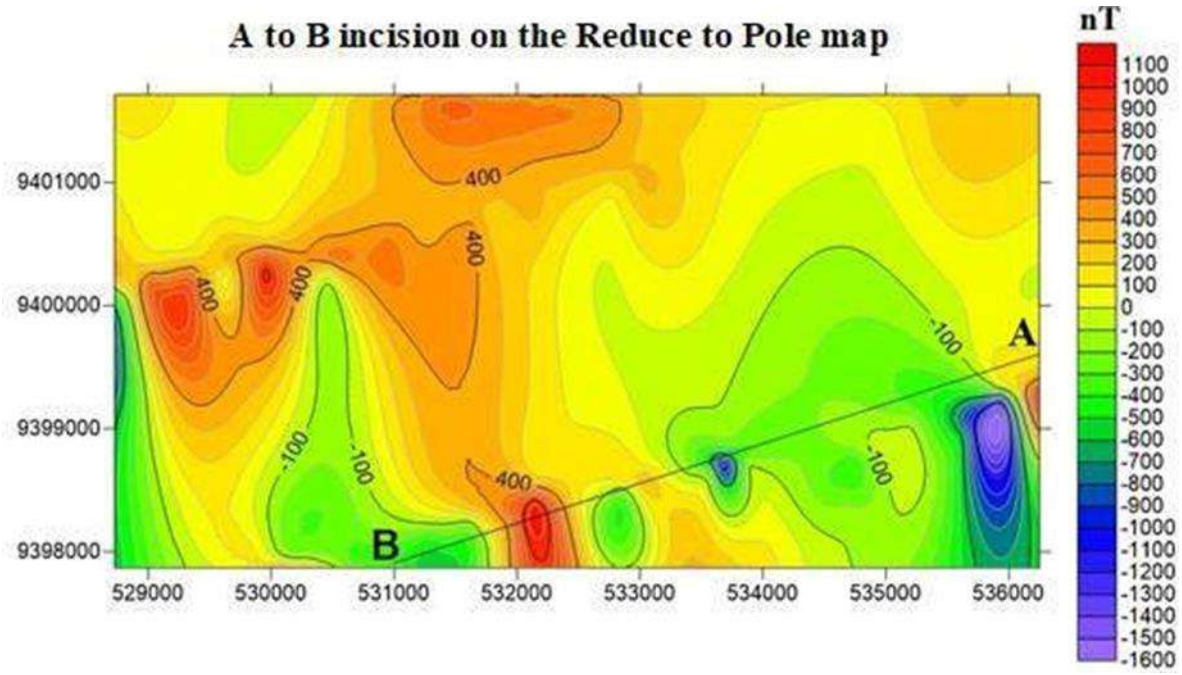

Figure 8. Incision AB on the contour map of magnet total field anomaly reduce to the pole.

The transformed anomaly map can be interpreted with the assumption that the anomalous object is in the area with the highest susceptibility anomaly value, but to interpret it, an incision or slice must be made to clarify and carry out further processing.

The slice was done with an incision line or slice from A to B cutting the Panjang Fault area - Lampung which is the target area in the study. The incision made on the RTP map from A to B can be seen in Figure 8.

After the incision or slice is made, further modeling is carried out using the help of Mag2DC software. This modeling process is known as forward modeling, where this modeling already has a susceptibility value graph from the incision results that have been read files in the software so that it only needs to make a model that produces the

same line (fit) with the line of the incision results. The modeling carried out must adjust to the formation on the geological map and see the cross section of the incision results on the geological map and for the susceptibility value in the rock adjusts to the type of rock that exists in the geological formation of the measurement area and refers to the rock susceptibility table according to experts and research that has been done before.

Qualitative Interpretation

Qualitative interpretation is based on the contours of the total magnetic field anomaly resulting from upward continuation by analyzing the anomaly pattern correlated with geological conditions such as rock structure and susceptibility variations below the earth's surface. In the interpretation, a reduction map to the pole is needed to determine the pole pair. Because qualitatively the anomaly map describes the distribution of contour pairs, the tendency of the grid direction of each closed pattern contour pair and those that appear to have a sharper anomaly gradient than the surrounding area is the basis for determining the polar pair.
The total magnetic anomaly in the study area can be divided into several magnetic anomaly clusters. The first group of high positive total magnetic anomalies at values of +500 nT to +1100 nT. Second, moderate positive total magnetic anomalies at values of +500 nT to 0 (zero) nT. Then the low total magnetic anomaly group with values of -800 nT to 0 nT and finally the very low total magnetic anomaly group which has values of -800 nT to -1600 nT. The study area illustrates positive to negative magnetic anomalies. Negative and positive anomaly values and contour patterns appear close together, indicating the presence of fault structures in the area, because fault structures are characterized by anomalous lines, contour density, bending anomalies, and twin anomalies (negative and positive) (Titi, 2016; Aufia et al., 2019). Geologically, it is a manifestation that subsurface there are non-magnetic rocks which are interpreted to be a manifestation that subsurface there are rocks that have been strongly to weakly altered. According to Aktaş et al. (2023), geophysical and geological data can display the tectonic structure of the bay. an area with depth estimation analysis applied to magnetic data to identify anomalies caused by geological structures, and the boundaries or edges of subsurface resources. caused by geological structures, and the boundaries or edges of the subsurface resources. resources. These methods include reduction to polar (RTP), slope derivative, source edge detection (SED), SF, and slope derivative of the total field horizontal gradient magnitude filter (TAHG). and the Euler deconvolution method to determine depth and boundaries.

Quantitative Interpretation

Quantitative interpretation is done by creating a geomagnetic model using Mag2DC software by entering data on the earth's magnetic field parameters in the study area. Numerical modeling requires IGRF parameters, declination angle, inclination angle, and maximum depth needed in the analysis of the research area as shown in Table 1.

Table 1. Earth magnetic field parameters of the research area.

No	Parameters	Value
1	IGRF	44326.3 nT
2	Declination	0.411286^{o}
3	Inclination	-27.8929^{o}
4	Maximum depth	500 m

In addition to the parameters of the earth's magnetic field, the modeling process requires additional data in the form of stratigraphic maps and geological maps of the research area. With the help of geological information, modeling of anomaly-causing objects is carried out. Qualitative interpretation uses the results of qualitative interpretation incisions.

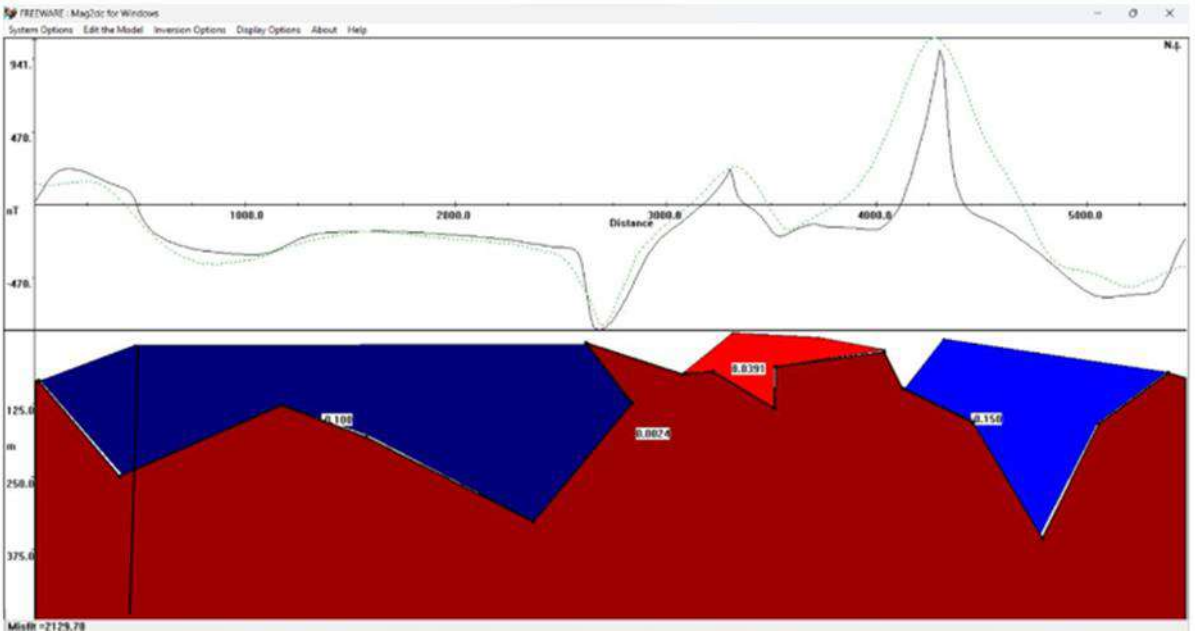

Figure 9. Modeling of the A-B incision.

The incision will show a subsurface cross section to explain the existing rock structure. The results of the A-B incision modeled in Mag2DC different susceptibility contrasts with the surrounding rocks so that it can be interpreted that there are 4 anomaly-forming rocks in the model as shown in Figure below. In the A-B profile modeling based on the reference susceptibility value of Telford et al. (1990) shows a susceptibility value of 0.100 cgs for the first body (dark blue color) estimated to be a tuff breccia rock covering the southern layer with a thickness of 25 meters to 300 meters from the surface.

At a susceptibility value of 0.0391 cgs for the second body (red color) with a depth of between 5 meters to 120 meters from the earth's surface, it is estimated to be rhyolitic tuff, claystone tuff and sandstone tuff. In the third body (blue color) with a susceptibility value of -0.150 cgs and with a depth of 15 meters to 350 meters from the earth's surface then bedrock depths to more than 300 meters are estimated to be andesite - basalt lava from the intrusion of Mount Betung. The fourth body (dark red color) and a susceptibility value of 0.0024 cgs with a north-south direction is a metamorf schist rock.

In modeling cross-section A – B (Figure 9) is tolerated with the geological conditions and surface appearance in the study area. Based on the regional stratigraphic column, there are three layers of Tertiary to Quaternary age and the fourth layer is Paleozoic aged schist malachite rock. The three layers near the surface are Tarahan Formation (Tpot) in the form of solid tuff, breccia with lentil inserts, Lampung Formation (QTi) in the form of stony tuff, rhyolitic tuff, solid tuff tuff, tuffaceous claystone, and tuffaceous sandstone then Young Volcano Formation (Qhv) in the form of lava (andesite-basalt), breccia and tuff and the lower layer is malleable rock as the base or parent rock. The fault structure is estimated to exist in Bumi Waras area with strike direction NW - SE (Northwest - Southeast) in Tarahan Formation. The fault is thought to be the course of geothermal or mineral manifestations.

Conclusion

From the results of magnetic anomaly data modeling, high positive (+500 nT to +1100 nT), medium positive (+500 nT to 0 nT),

and low negative (-800 nT to -1600 nT) magnetic anomalies were identified, indicating the presence of fault structures in the area. The positive and negative anomaly values of contour density in the study area are suspected to be fault structures with coordinates 5º26' 0.819" S -111º19' 25.863" W and depth 25 meter until 500 meter. Based on the regional geology, the study area tracks through three formations, among others: Tarahan Formation (Tpot), Lampung Formation (QTi), and Young Volcano Formation (Qhv), so that from the magnetic anomaly value, it is known that the lithology of the research area with a susceptibility value of 0.100 cgs is breccia tuff rock, a susceptibility value of 0.0391 cgs rhyolite tuff rock, a susceptibility value of -0.150 cgs intrusive rock (andesite-basalt), and a susceptibility value of 0.0024 is metamorphic rock.

Acknowledgements

Thanks to the Department of Geophysical Engineering, University of Lampung, especially the Exploration Laboratory, which has given permission to use geophysical equipment for acquisition purposes, so that the survey in this study can be carried out.

Author Contribution

Rasimeng, S. and Rafied, F. conducted a literature study and created a research survey design. Then the authors Valentin, F., Aurora, T.G., and Nurlaili, J. carried out acquisition, data processing and 2D modeling, as well as analysis and interpretation of the results.

Conflict of Interest

The authors declare no conflict of interest.

References

Abdelrahman, K., Nguyen, D. V., Prasad, K. N. D., Vo, Q. T., Le, D. V., Pham, L. T., Gomez-Ortiz, D., Fnais, M. S., & Eldosouky, A. M. (2024). Structural mapping of the west central Arabian Shield (Saudi Arabia) using downward continued magnetic data. *Journal of King Saud University-Science*, 36(2), 103039. https://doi.org/10.1016/j.jksus.2023.103039

Abdullah, M. F., & Sunaryo, S. (2014). Pendugaan Jenis Batuan Bawah Permukaan Daerah Bendungan Karangkates Menggunakan Metode Geomagnetik. *Physics Student Journal*, 2(1), 741–744.

Agustina, L. K., Harbowo, D. G., & Al Farishi, B. (2020). Identifikasi Kawasan Rawan Longsor Berdasarkan Karakteristik Batuan Penyusun di Kota Bandar Lampung. *Elipsoida: Jurnal Geodesi dan Geomatika*, 3(01), 30–37. https://doi.org/10.14710/elipsoida.2020.7769

Aktaş, G., Hisarlı, Z. M., & Demirel, A. S. (2023). Interpretation of the tectonic structure of Gemlik Bay using magnetic data. *Tectonophysics*, 863, 230021. https://doi.org/10.1016/j.tecto.2023.230021

Amigun, J. O., Afolabi, O., & Ako, B. D. (2012). Application of airborne magnetic data to mineral exploration in the Okene Iron Ore Province of Nigeria. *International Research Journal of Geology and Mining*, 2(6), 132–140. https://www.interesjournals.org/articles/Application-of-airborne-magnetic-data-to-mineral-exploration-in-the-okene-iron-ore-province-of-nigeria.pdf

Aufia, Y. F., Karyanto. K., Rustadi, R. (2019). Pendugaan Patahan Daerah "Y" Berdasarkan Anomali Gayaberat Dengan Analisis Derivative. *Jurnal Geofisika Eksplorasi*, 5(1), 75–88.

Ben, U. C., Akpan, A. E., Mbonu, C. C., Ebong, E. D. (2021). Novel

Methodology for Interpretation of Magnetic Anomalies Due to Two-Dimensional Dipping Dikes Using the Manta Ray Foraging Optimization. *Journal of Applied Geophysics*, 192, 104405. https://doi.org/10.1016/j.jappgeo.2021.104405

Blakely, R. J. (1996), *Potential Theory in Gravity and Magnetic Applications*, Cambridge University Press, Cambridge.

Bouligand, C., Glen, J. M. G., & Blakely, R. J. (2014). Distribution of buried hydrothermal alteration deduced from high-resolution magnetic surveys in Yellowstone National Park. *Journal of Geophysical Research: Solid Earth*, 119(4), 2595–2630. https://doi.org/10.1002/2013JB010802

Tontini, F. C., Tivey, M. A., de Ronde, C. E. J., & Humphris, S. E. (2019). Heat flow and near-seafloor magnetic anomalies highlight hydrothermal circulation at Brothers volcano caldera, southern Kermadec arc, New Zealand. *Geophysical Research Letters*, 46(14), 8252–8260. https://doi.org/10.1029/2019GL083517

Chiappini, M. (2021). Aeromagnetism. In Alberton, D., & Elias, A. S., Encyclopedia of Geology (Second Ed., 675–688). Elsevier. https://doi.org/10.1016/B978-0-08-102908-4.00131-4

De Ritis, R., & Chiappini, M. (2023). High resolution magnetic anomalies, volcanism and tectonics of the active "La Fossa" vulcanic system (Vulcano island) and Lipari Island (South Italy). *Journal of Volcanology and Geothermal Research*, 438, 107823. https://doi.org/10.1016/j.jvolgeores.2023.107823

Efendi, R., Lamangkona, F., & Sandra, S. (2016). Pemodelan 2D Reservoar Geotermal Menggunakan Metode Geomagnet di Desa Kasimbar Barat. *Gravitasi*, 15(1), 1–7. https://bestjournal.untad.ac.id/index.php/GravitasiFisika/article/view/7896/6235

Fashihullisan, A. L., Susilo, A., & Jam'an, A. F. (2014). Identifikasi Daerah Sesar dan Intrusi Berdasarkan Perbandingan Antara Filter (RTP, Upward, Downward, dan Aniltic Signal) Data Mapping Regional Magnetik Daerah Garut, Jawa Barat. *Physics Student Journal*, 2(1).

Fikar, M., Hamimu, L., Manan, A., & Suyanto, I. (2019). Pemodelan 2D Data Magnetik Menggunakan Transformasi RTP untuk Pendugaan Sesar di Daerah Kasihan, Pacitan, Jawa Timur. *Jurnal Rekayasa Geofisika Indonesia*, 01(02), 33–42. https://ojs.uho.ac.id/index.php/jrgi/article/view/8721/7850

Heningtyas, H., Wibowo, N. B., & Darmawan, D. (2020). Pemodelan 2D dan 3D Metode Geomagnet untuk Interpretasi Litologi dan Analisis Patahan di Jalur Sesar Oyo. *Jurnal Lingkungan dan Bencana Geologi*, 10(3), 115–126. http://dx.doi.org/10.34126/jlbg.v10i3.157

Heningtyas, H., Wibowo, N. B., & Darmawan, D. (2017). Interpretasi Struktur Bawah Permukaan dengan Metode Geomagnet di Jalur Sesar Oyo. *Jurnal Ilmu Fisika dan Terapannya*, 6(2), 138–148. https://journal.student.uny.ac.id/ojs/index.php/fisika/article/view/6909/6646

Hiden, H., Azhari, S., Alaa, S., & Yudianto, D. (2023). Identification of the distribution of golf mineral carrier rocks using the geomagnetic method in Pujut Lombok. *Gravitasi*, 22(1), 16–22. https://bestjournal.untad.ac.id/index.php/GravitasiFisika/article/view/16103/11875

Hiskiawan, P. (2016). Pengaruh Pola Kontur Hasil Kontinuasi Atas pada Data Geomagnetik Intepretasi

Reduksi Kutub. *Saintifika*, 18(1), 18–26. https://jurnal.unej.ac.id/index.php/STF/article/view/2760

Hinze, W. J., von Frese, R. R. B., & Saad, A. H. (2013). *Gravity and Magnetic Exploration: Principles, Practices, and Applications*. Cambridge University Press. https://doi.org/10.1017/CBO9780511843129

Ilapadila. I, Harimei, B., Maria, M. (2019). Analysis of Regional Anomaly on Magnetic Data Using the Upward Continuation Method. *IOP Conference Series: Earth and Environmental Science*, 279(012037). https://doi.org/10.1088/1755-1315/279/1/012037

Mangga, S. A., Amirudin, A., Suwarti, T., Gafoer, S., & Sidarto, S. (1993). *Peta Geologi Lembar Tanjungkarang, Sumatera*. Pusat Penelitian dan Pengembangan Geologi.

Mulyasari, R., Haerudin, N., Karyanto, K., Darmawan, I. G. B., & Arifianti, Y. (2018). Zonasi Area Potensi Gerakan Massa di Sepanjang Sesar Lampung-Panjang Kota Bandar Lampung. *Prosiding Semnas SINTA FT UNILA*, 1, 190–197. http://repository.lppm.unila.ac.id/11569/3/CR-1-34.pdf

Nicolosi, I., D'Ajello Caracciolo, F., Branca, S., Ferlito, C., Chiappini, M. (2016). The earliest open conduit eruptive center of the Etnean region: evidence from aeromagnetic, geophysical, and geological data. *Bulletin of Volcanology*, 78(50), 1–11. https://doi.org/10.1007/s00445-016-1042-3

Nuha ABA., M. U., Yulianto, T., & Harmoko, U. (2014). Interpretasi Bawah Permukaan Daerah Sumber Air Panas Diwak-Derekan Berdasarkan Data Magnetik. *Youngster Physics Journal*, 3(2), 129–134. https://ejournal3.undip.ac.id/index.php/bfd/article/view/5285

Nurdin, N. H., Massinai, M. A., & Aswad, S. (2017). Identifikasi Pola Sebaran Intrusi Batuan Bawah Permukaan Menggunakan Metode Geomagnet di Sungai Jenelata Kabupaten Gowa. *Jurnal Geocelebes*, 1(1), 17–22. https://doi.org/10.20956/geocelebes.v1i1.1776

Rasimeng, S., Tarigan. J. L., Ferucha, I., & Robbani, M. A. (2020). Identification of geothermal reservoar based on 3D modeling of data anomaly magnetic residual reduction to pole in the region of geothermal prospect Villamasin East Oku. *SEG Technical Program Expanded Abstracts 2020*. https://doi.org/10.1190/segam2020-3412730.1

Regita, E., Arman, Y., & Zulfian, Z. (2022). Interpretasi Kualitatif Sebaran Batuan di Kabupaten Belu dan Sekitarnya Berdasarkan Data Anomali Magnetik. *Prisma Fisika*, 10(2), 151–154. https://dx.doi.org/10.26418/pf.v10i2.55586

Setiadi, I., Darmawan, A., & Marjiyono, M. (2016). Pendugaan Struktur Geologi Bawah Permukaan Daerah Terdampak Lumpur Sidoarjo (Lusi) Berdasarkan Analisis Data Geomagnet. Jurnal *Lingkungan dan Bencana Geologi*, 7(3), 125–134.

Sulandari, B., Suteja, A., Hadibroto, H., Nurmaliah, N., Setyanta, B., & Garniwa, A. (2023). Deliniasi Struktur Sesar Lampung-Panjang dan Identifikasi Potensi Sumberdaya Alam Berdasarkan Anomali Magnet Daerah Bandar Lampung. *Jurnal Geologi dan Sumberdaya Mineral*, 24(4), 195–203. https://doi.org/10.33332/jgsm.geologi.v24i4.721

Telford, W., Geldart, L., & Sheriff, R. (1990). *Applied Geophysics*. Cambridge University Press.

Titi, Y. L. A. (2016). *Pemodelan 3-D Struktur Bawah Permukaan Pulau Flores dan Zona Sesar Belakang Busur Berdasarkan Analisis Data*

Gravitasi. Institut Teknologi Sepuluh Nopember Surabaya.

Tran, K. V., & Nguyen, T. N. (2020). A novel method for computing the vertical gradients of the potential field: application to downward continuation. *Geophysical Journal International*, 220(2), 1316–1329. https://doi.org/10.1093/gji/ggz524

Yang, Y., & Li, Y. (2023). Ore-controlling structures of the Qingchengzi Pb-Zn-Au-Ag orefield, northeastern China and significance for deep ore prospecting: Revealed from gravity and magnetic anomalies. *Ore Geology Reviews*, 156, 105376. https://doi.org/10.1016/j.oregeorev.2023.105376

ISSN: 2579-5821 (Print)
ISSN: 2579-5546 (Online)
URL address:http://journal.unhas.ac.id/index.php/geocelebes
DOI: 10.20956/geocelebes.v8i1.32853

Jurnal Geocelebes Vol. 8 No. 1, April 2024, 51 – 61

Analysis of Ground Vibration Levels Due to the Blasting Process at PT. Bumi Suksesindo

Nofry Hence Tarumasely, Novandri Kusuma Wardana, Rizqi Prastowo*

Mining Engineering Program, Institut Teknologi Nasional Yogyakatya, 55281, Indonesia.

* Corresponding author. E-mail: rizqi@itny.ac.id

Manuscript received: 23 January 2024; Received in revised form: 2 April 2024; Accepted: 3 April 2024

Abstract

Ground vibration is one of the effects of the blasting process; when the ground vibration reaches the highest level, it will disturb comfort and even cause damage to the surrounding building structure. This research aims to determine the magnitude of ground vibrations in Pit A and Pit C, as well as determine the relationship between Peak Particle Velocity (PPV) and scaled Distance, and determine the maximum explosive charge weight per delay based on the SNI 7571: 2010 reference. Actual ground vibration measurement data during research based on PPV theory and the actual PPV power regression relationship with scaled distance was used to obtain a ground vibration prediction formula to be a reference for determining the amount of explosive filling per delay. The ground vibration produced in the blasting process is hoped not to exceed the safe threshold. Prediction of the ground vibration formula at 100 m to 1500 m according to the US Bureau of Mines where the Mean Squared Error (MSE) value is 0.54, the MSE value from the Langefors-Kihlstrom equation is 1.85 while the MSE value from the Ambersays-Hendorn equation is 0.31 with the slightest deviation is very good to use as a reference for predicting ground vibrations with the predicted PPV formula. Hence, the maximum explosive charge with a PPV limit of 2 mm/s is 2.452 kg, a PPV limit of 3 mm/s is 11.332 kg, and a PPV limit of 5 mm/s is 23.040 kg. The factors that influence ground vibration are the Distance from the blasting location to the measurement location and the maximum number of explosives per delay, so the results taken from this research are that blasting in Pit A and Pit C is still categorized as safe for infrastructure and community housing.

Keywords: Blasting Ground Vibration; Scaled Distance (SD); Peak Particle Velocity (PPV); Power Regression.

Citations: Tarumasely, N. H., Wardana, N. K., & Prastowo, R. (2024). Analysis of Ground Vibration Levels Due to the Blasting Process at PT. Bumi Suksesindo. *Jurnal Geocelebes*, 8(1): 51–61, doi: 10.20956/geocelebes.v8i1.32853

Introduction

PT Bumi Suksesindo (BSI) implemented an open-pit mining system (surface mining) using the open-pit mining method. Gold and copper mining activities consist of unloading, loading, and transportation. One of PT Bumi Suksesindo's activities is rock demolition using drilling and blasting methods.

The blasting process in mining activities destroys rock and propagates seismic waves on the earth's surface, which can cause vibrations in the rock mass or surrounding material (Bui et al., 2021). The vibration level in a blast varies depending on the blast design used (Roy et al., 2016).

Ground vibration at a certain level, if it exceeds the threshold, can cause damage to the surrounding environment (Yin et al., 2018). Pit A and Pit C are active pits at BSI is located close to residential areas and temples, which are places of worship for Hindus. The Distance from Pit A and Pit C to residential areas and temples is 1,300 meters. Because the distance is close, more attention must be paid to the effects on the environment from blasting activities so that

they do not disturb the comfort and safety of the community (Fadhly et al., 2014; Halimah & Octova, 2018; Himanshu et al., 2018).

This research aims to determine the amount of ground vibration produced by each blast in Pit A and Pit C BSI and its impact on infrastructure and settlements in the surrounding community. The research also aims to determine the relationship between Peak Particle Velocity (PPV) and Scaled Distance (SD) and determine the maximum explosive charge weight with a safe distance in blasting activities based on the SNI 7571: 2010 reference (Ma'rief et al., 2020a). Research to reduce the impact of vibrations has also been carried out at PT Bukit Asam. This research concludes that the PPV value is <3 mm/s with a measurement distance of 1000 meters from the employee housing location, stuffing is needed (Tohirin et al., 2022).

Research Methods

Primary data consists of the mass of the blast hole filling, blasting geometry, field coordinates, distance from the blast source to the recording device, and ground vibrations. Blasting geometry consists of Burden (B), spacing (S), hole diameter (D), and hole height (H). Meanwhile, secondary data includes explosives, reference blasting standards, and patterns. Ground vibration measurements were carried out using the Blastmate III tool, with an accuracy of 0.5 mm/s (Instantel, 2020). Field data collection is in the form of actual field wave velocity or Peak Particle Sum (PVS) (Lawal & Kwon, 2021). PVS is the sum of the peak wave velocities in vertical (V), longitudinal (L), and transverse (T) waves, obtained using Equation 1.

$$PVS = (V^2 + L^2 + T^2)^{0,5} \quad (1)$$

Research Sites

This research was conducted at BSI in Sumberagung Village, Pesanggaran District, Banyuwangi Regency, East Java Province (Figure 1). The main activity is BSI focuses on the gold and copper production business unit at Tujuh Bukit Operation, better known as Tumpang Pitu. It has a Production Operation Mining Business Permit covering an area of 4,998 ha.

Explosion Concept

The blasting method aims to dismantle or separate a rock from its parent rock. In dispersing rock using the drilling and blasting method, the rock fragmentation resulting from blasting is a significant factor, where the rock fragmentation size is expected to follow the needs of subsequent mining activities (Roy, 2021). A blasting operation is declared successful in mining activities if the production target is met (Nateghi, 2012; Putra, 2023). The use of explosives is efficient, which is expressed in the amount of rock that is successfully dismantled per kilogram of explosives called (powder factor); evenly sized fragmentation is obtained with a few chunks less than 15% of the Number of rocks exposed per blast (Herdy et al., 2015; Moomivand & Vandyousefi, 2020).

Ground Vibration

Blasting activities can cause several risks; there are three types of damage can be caused by blasting: ground vibrations, fly rock, and air blast or sound (Nuñez et al., 2022). Ground vibrations are particle movements that occur due to the propagation of seismic waves. When detonation occurs, the residual energy will produce seismic waves, which cause movement in the ground. The movement in the ground affects the rock mass and propagates in the form of compressive waves (Nguyen et al., 2020). When the magnitude of the compressive wave is greater than the tensile strength of the rock, it will cause a crushed zone (Ma'rief et al., 2020b).

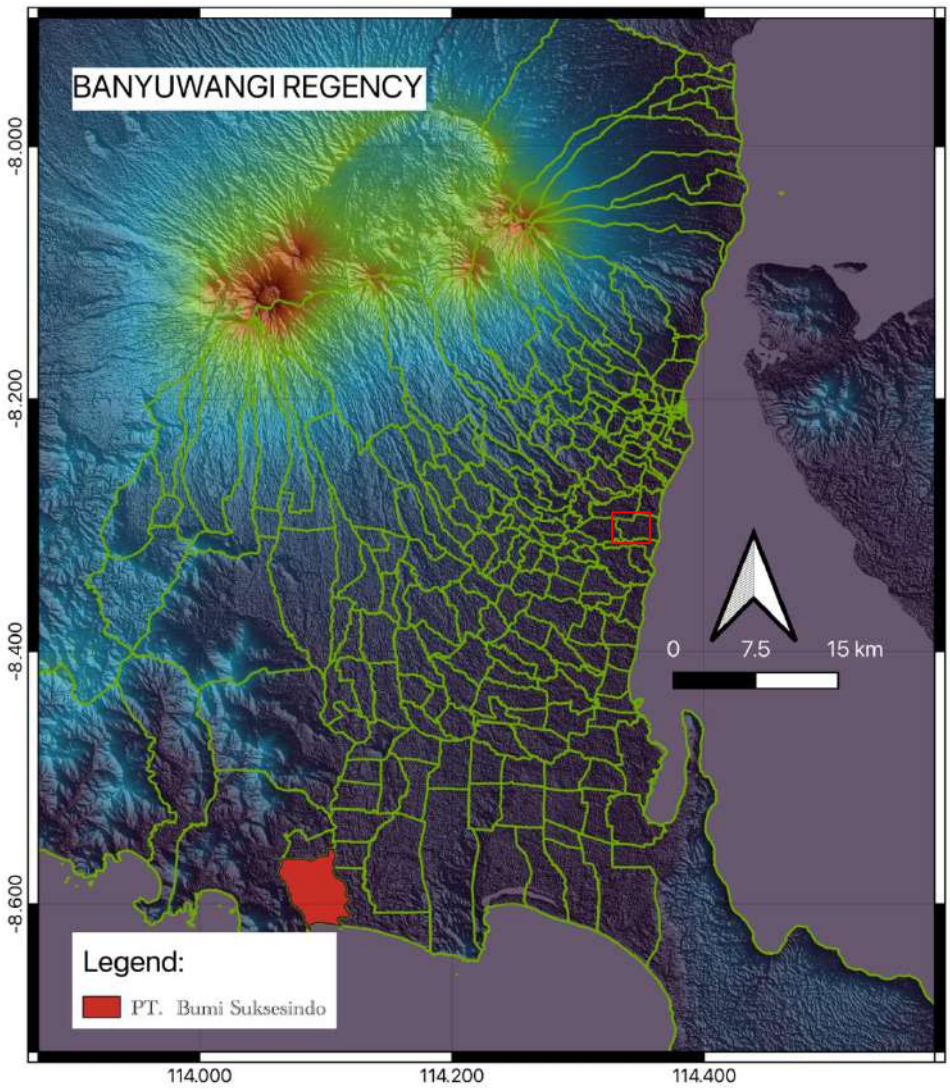

Figure 1. Research location on red square.

Seismic waves are elastic waves that propagate on the earth's surface, representing energy transmission due to explosions. Seismic waves are divided into two large classes: Body and Surface (Kumar & Mishra, 2020). In blasting activities, the rock response to compressive waves is the formation of two body waves and one surface wave (Nuñez et al., 2022). The body waves formed are Primary Waves (P-waves) and Secondary Waves (S-waves). P-waves have a more incredible speed than S-waves. Meanwhile, the surface waves formed are Rayleigh waves (R-wave) (Amiri et al., 2020). Rayleigh waves have a smaller velocity than both body waves.

Peak Particle Velocity (PPV)

Several researchers have conducted investigations and put forth various conventional vibration predictors to predict PPV. These predictors are outlined and summarized in Table 1.

Table 1. The conventional formula used for predicting PPV.

Name	Formula
United State Bureau of Mines (Duvall and Petkof, 1959)	$PPV = K\left[\frac{D}{\sqrt{Q_{max}}}\right]^{-B}$
Langefors – Kihlstrom (Langefors and Kihlstrom, 1963)	$PPV = K\left[\sqrt{\left(\frac{Q_{max}}{D^{2/3}}\right)}\right]^{-B}$
Ambraseys – Hendron (Ambraseys and Hendron, 1968)	$PPV = K\left[\frac{D}{Q_{max}{}^{1/3}}\right]^{-B}$

Table 1 is a compilation of standard vibration prediction equations proposed by a range of scholars, scientists, researchers, and field engineers. The equation for calculating PPV was established by the United States Bureau of Mines (USBM) as follows:

$$PPV = K\left[\sqrt{\frac{D}{Q_{max}}}\right]^{-B} \text{ or } PPV = K[SD]^{-B} \quad (2)$$

Where PPV is the Peak Particle Velocity, SD is the scaled distance, and K and B are site constants. The site constants K and B were determined by plotting graph between PPV and different SD. The general equation of straight line is

$$y = mx + C \quad (3)$$

This implies that the PPV and SD data should demonstrate a linear relationship when plotted on a logarithmic scale graph paper. consequently, y = PPV, x = SD, intercept C = k, and slope −B = m.

Results and Discussion

Blasting activities were carried out using an Epiroc PowerROC T-50 drill using the rotary percussive method. The diameter of the blast hole varies depending on the location to be blasted (Supratman et al., 2017; Moomivand & Vandyousefi, 2020). The diameters used is 115 mm with a staggered drilling pattern. Data of geometry of blasting shown in Table 2 below.

Table 2. Actual blasting geometry.

Location	n	B (m)	S (m)	D (m)	*Stemming* (m)	PC (m)
Pit A	567	3.25	3.18	8.41	2.5	5.91
Pit A	752	3.19	3.63	8.26	2.5	5.76
Pit A	351	2.80	3.40	8.39	2.5	5.89
Pit A	345	3.32	3.90	8.69	2.5	6.19
Pit C	584	3.38	3.90	8.22	2.5	5.72
Pit A	495	2.90	3.49	7.94	2.5	5.44
Pit A	922	2.56	3.15	8.44	2.5	5.94
Pit A	1098	3.39	3.55	8.56	2.5	6.06
Pit A	948	3.56	4.27	8.36	2.5	5.86
Pit C	466	3.56	3.69	8.41	2.5	5.91

Where n is number of holes, B is burden, S is Spacing, D is depth.

Ground Vibration Measurement

Ground vibration measurements in the field aim to determine PPV due to blasting. Ten measurements of ground vibrations from Pit A and Pit C blasting were carried out using a micromate with a measurement location inside the mine. Data ground vibration shown in Table 3 below.

Table 3 Actual ground vibration measurement results.

No	PPV (mm/s)			PVS (mm/s)	Distance (m)	Explosives (kg)
	Transverse	Vertical	Longitudinal			
1	1.09	1.06	1.04	1.3	547	29567
2	1.94	0.90	1.88	2.0	644	58552
3	1.33	1.33	1.40	1.6	584	21793
4	1.79	1.47	2.10	2.5	515	21794
5	0.54	0.52	1.26	1.3	787	38507
6	1.92	0.59	1.03	1.9	505	29478
7	1.14	0.65	0.95	1.5	678	51922
8	1.21	0.69	1.55	1.6	767	67218
9	1.58	1.03	1.10	1.8	624	46497
10	7.77	6.98	11.60	12.9	193	17240

Vibration standards resulting from blasting applied by BSI is by SNI Standard 7571:2010. PPV data obtained from ground vibration measurements and SD calculation

results were then carried out power regression analysis from the USBM (US Bureau of Mines) equation, the Ambersay – Hendorn (AH) equation, and the Lagefors – equation. Kihlstrom (LK), to obtain a similar relationship between peak particle velocity (PPV) and scaled Distance (SD) (Yilmaz, 2023).

The results of the power regression analysis will obtain the constant values K and n, which are site factors, and the coefficient of determination (R^2), which measures the strength of the relationship between variables (Jalbout & Simser, 2014; Rusmawarni et al., 2017; Rezaeineshat et al., 2020).

In Table 4 below are the results of scaled distance calculations during field research according to the USBM equation, which regresses Power with actual PPV to get the predicted PPV formula, which is PPV= $8024{,}6 \times (SD)^{-2{,}671}$.

Table 4. Calculation of USBM scaled distance values.

No	Distance (m)	Product Charger per Delay (kg)	Scale Distance ($m^{½}/kg^{¾}$)	PPV measured (mm/s)	PPV Predicted (mm/s)
1	547	536	23.62	1,307	1.72
2	644	761	23.34	2,042	1.78
3	584	551	24.86	1,554	1.50
4	515	740	18.92	2,453	3.12
5	787	742	28.89	1,297	1.01
6	505	475	23.15	1,983	1.82
7	678	876	22.91	1,496	1.87
8	767	905	25.49	1,586	1.41
9	624	773	22.44	1,828	1.98
10	193	264	11.87	12.93	10.83

Table 5. Calculation of Ambersay – Hendorn Distance scale values.

No	Distance (m)	Product Charger per Delay (kg)	Scale Distance ($m^{½}/kg^{¾}$)	PPV measured (mm/s)	PPV Predicted (mm/s)
1	547	536	83.01	1,307	1.91
2	644	761	87.98	2,042	1.68
3	584	551	87.85	1,554	1.69
4	515	740	70.92	2,453	2.68
5	787	742	108.35	1,297	1.07
6	505	475	79.42	1,983	2.10
7	678	876	88.81	1,496	1.65
8	767	905	99.46	1,586	1.29
9	624	773	84.86	1,828	1.82
10	193	264	36.22	12,93	11.40

Figure 4 explains that comparing the PPV predicted and PPV measured, the coefficient of determination (R^2) is 0.9857. This value states that the strength of the relationship in the variable value obtained using the USBM equation is 98%.

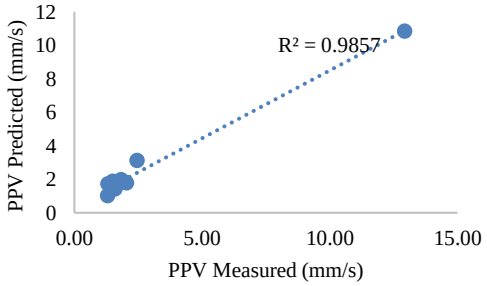

Figure 4 Comparison graph of predicted PPV and actual PPV of USBM.

In Table 5 above are the results of scaled distance calculations during field research according to the equation Ambersay – Hendorn (AH), which is regressed by Power with the actual PPV to get the predicted PPV formula, which is PPV.= $26184 \times (SD)^{-2.156}$.

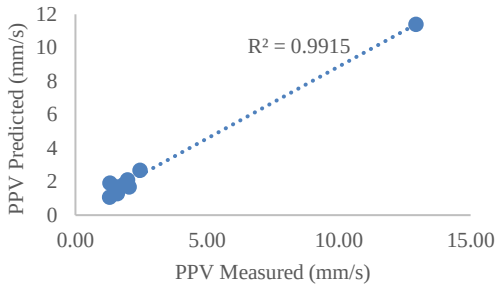

Figure 5 Comparison Chart of Actual PPV and Predicted PPV Ambersay – Hendorn

Figure 5 above explains where the comparison graph of predicted PPV (AH) and actual PPV gets a coefficient of determination value (R^2) is 0.9916. This value states that the strength of the relationship in the variable values obtained using the Ambersay – Hendorn (AH) equation is robust, with a value of 99%.

In Table 6 below are the results of scaled distance calculations during field research according to the Lagefors – Kiehlstrom equation (LK), which is regressed on Power with the actual PPV to get the predicted PPV formula, which is PPV= $1029{,}7 \times (SD)^{-4{,}1}$.

Table 6 Calculation of Lagefors – Kiehlstrom distance scale values.

No	Distance (m)	Product Charger per Delay (kg)	Scale Distance ($m^{½}/kg^{¾}$)	PPV measured (mm/s)	PPV Predicted (mm/s)
1	547	536	4.89	1.31	1.54
2	644	761	4.63	2.04	1.92
3	584	551	5.06	1.55	1.34
4	515	740	3.97	2.45	3.60
5	787	742	5.46	1.30	0.98
6	505	475	4.88	1.98	1.54
7	678	876	4.49	1.50	2.18
8	767	905	4.84	1.59	1.60
9	624	773	4.49	1.83	2.18
10	193	264	3.18	12.93	8.91

Figure 6 below explains where the comparison graph of predicted PPV Lagefors – Kiehlstrom (LK) and actual PPV gets a coefficient of determination value (R^2) is 0.9441. This value states that the strength of the relationship in the variable values obtained using the LK equation is strong, with a value of 94%.

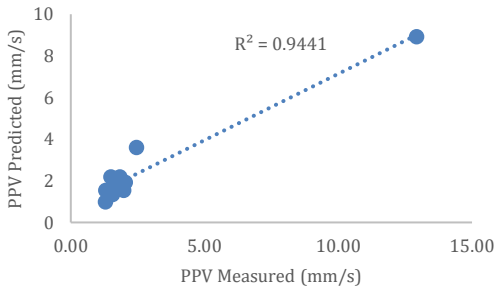

Figure 6 Comparison Chart of Predicted PPV and Actual PPV Lagefors – Kiehlstrom.

From the calculation of the predicted peak particle velocity value based on the equation (USBM, Ambersays-Hendorn, and Langefors-Kiehlstrom), the average Mean Squared Error value compared to the actual (Jianhua et al., 2022). The peak particle velocity deviation value from the actual PPV is obtained, namely using the USBM theory with an MSE value of 0.54, the MSE value from the Ambersays-Hendorn (AH) equation is 0.31, and the MSE value from the Langefors-Kiehlstrom equation (LK) which is 1.85.

The conclusion is that the Ambersays-Hendorn, with an MSE value of 0.31 from the actual, which gives the slightest deviation, is more appropriate for

determining PPV predictions based on deviations from the actual PPV (Duvall & Petkof, 1959; Nateghi, 2012). Research on Ground Vibration Levels in Bedrock Blasting Operations in Sorowako East and West Areas of Pt Vale Indonesia Tbk, Sorowako, Nuha District, East Luwu Regency, South Sulawesi Province also shows that the coefficient of determination of Ambersays-Hendorn. The largest compared to USBM and LK is 0.7027 (Yudha et al., 2022).

Recommended Maximum Explosive Charge per Delay

Recommendations for the maximum explosive charge per delay are made because of the BSI blasting location is very close to residential areas, so the effects of ground vibrations resulting from blasting activities need to reach a threshold that could damage buildings belonging to communities around the mine. The location of blasting and residential areas shows in Figure 7 below.

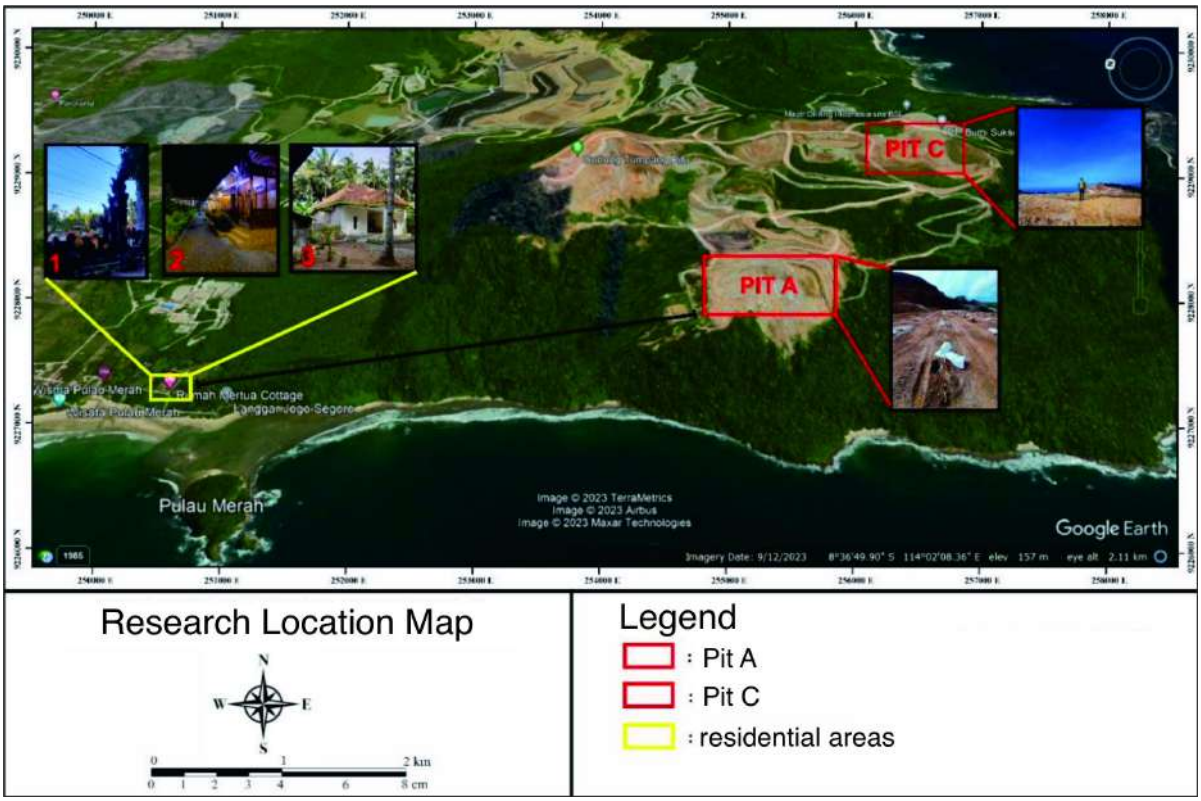

Figure 7. Location of blasting and residential areas.

Table 8 Analysis of the Biggest Explosion Effects on Residential Settlements

PPV Limit	Measured		Prediction	
	Distance (m)	Explosives (Kg)	Distance (m)	Explosives (Kg)
2 mm/s	193	17.240	193	13.745
3 mm/s				24.140
5 mm/s				49.078
12.93 mm/s				183.667

To maximize the blasting process to increase BSI recommended maximum explosive filling per delay from 100 m – 1500 m with a predicted PPV of 2 mm/s, 3 mm/s, and 5 mm/s according to the reference standard SNI 7571: 2010. The equation used to predict the filling explosives per delay, which is the PPV predicted by the Ambersays-Hendorn theory, is described as follows:

$$\text{PPV predictions} = 26184 \times \left(\frac{R}{Q^{1/3}}\right)^{-2.156} \quad (5)$$

The most significant vibration level analysis can be seen in Table 8, which explains the effect of blasting on residential areas. The results obtained are not by measurements in the field because predictably, at 193 m with a PPV limit of 2 mm/s, there are 13.745 kg of explosives, a PPV of 3 mm /s, as much as 24.140 kg of explosives, PPV 5 mm/s as much as 49.078 kg, and PPV 12.93 mm/s as much as 183.667 kg.

Predictively, at the same distance of 193 m with a PPV of 12.93 mm/s, the actual number of explosives is still relatively small, which is 17.240 kg compared to the predicted number of explosives of 183,667 kg. The conclusion obtained from this analysis of the most considerable vibration levels is that the closer the measurements are made in the field, the greater the PPV value obtained, and the farther distance between the vibration measurements carried out in the field, the smaller the PPV level.

Conclusion

The results of ground vibrations during blasting in Pit A, which were carried out 8 times, and the results of ground vibrations during blasting in Pit C, which was carried out 2 times, there was one blast that exceeded the vibration threshold set by PT. Bumi Suksesindo, on April 30, 2023, blasting occurred in Pit C with the most significant ground vibration, which is 12.93 mm/s at a measuring distance of 193 m with actual explosive material of 17,240 kg. However, in analysis, the number of explosives used at the same distance of 193 m with a PPV of 12.93 mm/s, the actual number of explosives is still relatively small compared to the predicted number of explosives with the Amount of 183,667 kg. Therefore, the conclusion that can be drawn is that blasting in Pit A and Pit C is still categorized as safe for infrastructure and community settlements. Factors that influence ground vibration in the field are the distance from the blasting location to the measurement location and the maximum number of explosives per delay. The peak particle velocity deviation using the Ambersays-Hendorn theory gets the smallest deviation value, which is 0.31, so the Ambersays-Hendorn theory is more appropriate for determining the maximum number of explosives at a safe distance during detonation. With the PPV prediction formula= $26184(SD)^{-2,156}$.

The recommended charge/ delay with a PPV value of 2 mm/s during the research is at 100 meters, a maximum charge/delay of 1.912 kg, at a distance of 200 meters, a maximum charge/delay of 15.296 kg, at a distance of 300 meters, a maximum charge/delay of 51.623 kg, at a distance of 400 meters, a maximum charge/delay of 122.365 kg, at a distance of 500 meters, a maximum charge/delay of 238.995 kg, at a distance of 600 meters, a maximum charge/delay of 412.983 kg, at a distance of 700 meters, a maximum charge/ delay of 655.802 kg.

Acknowledgments

Thanks to the supervisor and all crew members of PT Bumi Suksesindo who have provided data to complete this research.

Author Contribution

During the development of this research journal, multiple authors made contributions to various aspects. Nofry Hence Tarumasely was responsible for data processing and library resources, while Novandri Kusuma Wardana contributed to journal compilation. Additionally, Rizqi Prastowo served as an observer and supervisor in the compilation of this journal.

Conflict of Interest

This study did not involve any funds or finances issued between the authors or the

parties engaged in the investigation. for the author to comply with the regulations outlined in the Jurnal Geocelebes.

References

Ambraseys, N. N., & Hendron, A. J. (1968). *Dynamic Behaviour of Rock Masses*. J. Wiley & Sons.

Amiri, M., Hasanipanah, M., & Amnieh, H. B. (2020). Predicting ground vibration induced by rock blasting using a novel hybrid of neural network and itemset mining. *Neural Computing and Applications*, 32(18), 14681–14699. https://doi.org/10.1007/s00521-020-04822-w

Bui, X. N., Nguyen, H., Tran, Q. H., Nguyen, D. A., & Bui, H. B. (2021). Predicting Ground Vibrations Due to Mine Blasting Using a Novel Artificial Neural Network-Based Cuckoo Search Optimization. *Natural Resources Research*, 30(3), 2663–2685. https://doi.org/10.1007/s11053-021-09823-7

Duvall, W. I., & Petkof, B. (1959) *Spherical propagation of explosion-generated strain pulses in rock*. Washington DC: US Bureau of Mines.

Fadhly, F., Yulhendra, D., & Anaperta, Y. M. (2014). *Analisis Ground Vibration pada Kegiatan Peledakan dengan Metoda Peak Particle Velocity Beserta Pengaruhnya Terhadap Bangunan di PT. Pamapersada Nusantara Distrik MTBI Job Site Tanjung Enim*. https://www.researchgate.net/publication/283515623_ANALISIS_GROUND_VIBRATION_PADA_KEGIATAN_PELEDAKAN_DENGAN_METODA_PEAK_PARTICLE_VELOCITY_BESERTA_PENGARUHNYA_TERHADAP_BANGUNAN_DI_PT_PAMAPERSADA_NUSANTARA_DISTRIK_MTBU_JOB_SITE_TANJUNG_ENIM

Halimah, H., & Octova, A. (2018). Analisis Ground Vibration Untuk Mendesain Lereng Yang Stabil Pada Penambangan Batu Gamping CV Tekad Jaya Halaban Kabupaten 50 Kota Sumatera Barat. *Jurnal Bina Tambang*, 3(4), 1784–1792. https://ejournal.unp.ac.id/index.php/mining/article/view/102303/0

Herdy, A. S., Widodo, S., & Nurwaskito, A. (2015). Analisis Pengaruh Powder Factor terhadap Hasil Fragmentasi Peledakan pada PT. Semen Bosowa Maros Provinsi Sulawesi Selatan. *Jurnal Geomine*, 3(1), 154–158. https://doi.org/10.33536/jg.v3i1.17

Himanshu, V. K., Roy, M. P., Mishra, A. K., Paswan, R. K., Panda, D., & Singh, P. K. (2018). Multivariate statistical analysis approach for prediction of blast-induced ground vibration. Arabian Journal of Geosciences, 11(16), 460. https://doi.org/10.1007/s12517-018-3796-8

Instantel. (2020). *8-Channel Blastmate IIITMand Minimate PlusTMMulti-sensor Vibration and Overpressure Monitors*. https://cdn.thomasnet.com/ccp/10019814/103446.pdf

Jalbout, A., & Simser, B. (2014). Rock mechanics tools for mining in high stress ground conditions at Nickel Rim South Mine. *Deep Mining 2014: Proceedings of the Seventh International Conference on Deep and High Stress Mining*, 189–208. https://doi.org/10.36487/ACG_rep/1410_11_Jalbout

Jianhua, Y., Jiyong, C., Chi, Y., Xiaobo, Z., & Liansheng, L. (2022). Discussion on blasting vibration monitoring for rock damage control in rock slope excavation. *Earthquake Engineering and Engineering Vibration*, 21, 53–65. https://doi.org/10.1007/s11803-021-2071-2

Kumar, S., & Mishra, A. K. (2020). Reduction of blast-induced ground vibration and utilization of explosive energy using low-density explosives

for environmentally sensitive areas. *Arabian Journal of Geosciences*, 13(14), 655. https://doi.org/10.1007/s12517-020-05645-8

Langefors, U., & Kihlstrom, B. (1963) *The modern technique of rock blasting*. Wiley.

Ma'rief, A. A., Qadri, A., Okviyani, N., & Mahyuni, E. T. (2020a). Analisis Pengaruh Jumlah Bahan Peledak Terhadap Ground Vibration Akibat Ledakan Pada Area Pit SM-A Tambang Batubara Di PT. Sims Jaya Kaltim Jobsite PT. Kideco Jaya Agung Kabupaten Paser Provinsi Kalimantan Timur. *Jurnal Geomine*, 7(2), 74–79. https://doi.org/10.33536/jg.v8i1.578

Ma'rief, A. A. F., & Miranda, M. (2020b). Analisis Ground Vibration Akibat Ledakan Pada Tambang Nikel Di PT. Vale Indonesia, Tbk. *Jurnal Geocelebes*, 4(2), 129–133. https://doi.org/10.20956/geocelebes.v4i2.11084

Moomivand, H., & Vandyousefi, H. (2020). Development of a new empirical fragmentation model using rock mass properties, blasthole parameters, and powder factor. *Arabian Journal of Geosciences*, 13(22), 1173. https://doi.org/10.1007/s12517-020-06110-2

Nateghi, R. (2012). Evaluation of blast induced ground vibration for minimizing negative effects on surrounding structures. *Soil Dynamics and Earthquake Engineering*, 43, 133–138. https://doi.org/10.1016/j.soildyn.2012.07.009

Nguyen, H., Drebenstedt, C., Bui, X. N., & Bui, D. T. (2020). Prediction of Blast-Induced Ground Vibration in an Open-Pit Mine by a Novel Hybrid Model Based on Clustering and Artificial Neural Network. *Natural Resources Research*, 29(2), 691–709. https://doi.org/10.1007/s11053-019-09470-z

Nuñez, A. E. C., Ortiz, C. E. A, & Silva, J. M. (2022). Effect of Dynamic Stress Produced by Rock Blasting on the Optimal Dimensioning of Room and Pillars in Horizontal Layers. *Advances in Materials Science and Engineering*, 7826557, 1–13. https://doi.org/10.1155/2022/7826557

Putra, S. A. P. (2023). *Optimasi Powder Factor Terhadap Fragmentasi Batuan Hasil Peledakan Dan Digging Time Di Pit C Tambang Emas, PT. Bumi Suksesindo, Kab. Banyuwangi, Provinsi Jawa Timur*. UPN Veteran.

Rezaeineshat, A., Monjezi, M., Mehrdanesh, A., & Khandelwal, M. (2020). Optimization of blasting design in open pit limestone mines with the aim of reducing ground vibration using robust techniques. *Geomechanics and Geophysics for Geo-Energy and Geo-Resources*, 6(40), 1–14. https://doi.org/10.1007/s40948-020-00164-y

Roy, M. P., Singh, P. K., Sarim, M., & Shekhawat, L. S. (2016). Blast design and vibration control at an underground metal mine for the safety of surface structures. *International Journal of Rock Mechanics and Mining Sciences*, 83, 107-115. https://doi.org/10.1016/j.ijrmms.2016.01.003

Roy, P. P. (2021). Emerging trends in drilling and blasting technology: concerns and commitments. *Arabian Journal of Geosciences*, 14(7), 652. https://doi.org/10.1007/s12517-021-06949-z

Rusmawarni, R., Nurhakim, N., Riswan, R., & Ferdinandus, F. (2017). Evaluasi Isian Bahan Peledak Berdasarkan Ground Vibration Hasil Peledakan Overburden Pada PT Bina Sarana Sukses Kecamatan Sungai Raya Kabupaten Hulu Sungai Selatan Provinsi Kalimantan Selatan. *Jurnal*

Fisika Flux: Jurnal Ilmiah Fisika Fmipa Universitas Lambung Mangkurat, 14(1), 8–13. http://dx.doi.org/10.20527/flux.v14i1.3583

Supratman, S., Anshariah, A., & Bakri, B. (2017). Produktivitas Kinerja Mesin Bor Dalam Pembuatan Lubang Ledak Di Quarry Batugamping B6 Kabupaten Pangkep Propinsi Sulawesi Selatan. *Jurnal Geomine*, 5(2), 59–62. https://doi.org/10.33536/jg.v5i2.127

Tohirin, T., Wijaya, A. E., & Prastowo, R. (2022). Analisis Getaran Tanah untuk Mengurangi Kerusakan Akibat Peledakan pada Tambang Terbuka. *Jurnal Geocelebes*, 6(2), 203–211. https://journal.unhas.ac.id/index.php/geocelebes/article/view/19831

Yilmaz, O. (2023). Drilling and blasting designs for parallel hole cut and V-cut method in excavation of underground coal mine galleries. *Scientific Reports*, 13(1), 2449. https://doi.org/10.1038/s41598-023-29803-6

Yin, Z. Q., Hu, Z. X., Wei, Z. Di, Zhao, G. M., Hai-Feng, M., Zhang, Z., & Feng, R. M. (2018). Assessment of Blasting-Induced Ground Vibration in an Open-Pit Mine under Different Rock Properties. *Advances in Civil Engineering*, 4603687, 1–10. https://doi.org/10.1155/2018/4603687

Yudha, A. W., Hariyanto, R., Siri, H. T., Gunawan, K., & Siwidiani, I. L. (2022). Kajian Teknis Pengontrolan Ground Vibration Level Pada Operasi Peledakan Bedrock Sorowako East Dan West Area PT Vale Indonesia Tbk, Sorowako Kecamatan Nuha Kabupaten Luwu Timur Provinsi Sulawesi Selatan. *Jurnal Teknologi Pertambangan*, 8(1), 26–41. https://doi.org/10.31315/jtp.v8i1.9129

ISSN: 2579-5821 (Print)
ISSN: 2579-5546 (Online)
URL address: http://journal.unhas.ac.id/index.php/geocelebes
DOI: 10.20956/geocelebes.v8i1.32159

Jurnal Geocelebes Vol. 8 No. 1, April 2024, 62 – 70

Application of Seismic Refraction Tomography in Determining the Soil Hardness Level in IKN Nusantara Area

Andi Alamsyah, Piter Lepong, Wahidah*, Rahmiati

Geophysics Study Program, Mulawarman University, 75242, Indonesia.

*Corresponding author. Email: wahidah@fmipa.unmul.ac.id

Manuscript received: 5 December 2023; Received in revised form: 10 March 2024; Accepted: 27 April 2024

Abstract

Numerous studies supporting infrastructure construction are currently underway in the New Capital Territory of Nusantara (IKN Nusantara). A geophysical method known as Seismic Refraction Tomography (SRT) has been employed within the IKN Nusantara to identify hard and soft layers based on the P-wave velocity (Vp). The data acquisition involved 24 channels of geophone spaced at intervals 3 and 4 meters. Measurements were conducted alongfour trajectories of 69 and 92 meters, reaching penetration depths of 12 – 20 meters. P-wave velocity values ranging between 200 – 3500 m/s were recorded. Additionally, the Unconfined Compressive Strength (UCS) value was determined using an empirical equation tailored for mudrock-shale lithology, establishing the correlation between Vp and UCS. In the shallow depths of 0 – 3 meters, UCS values indicated levels below 20 MPa, classifying the materials as having low to medium hardness. However, at depths greater than 3 meters, this layer transitioned to material with high hardness levels, as evidenced by UCS rate exceeding 20 MPa across all trajectories. This suggest that the IKN Nusantara is conducive to infrastructure development.

Keywords: Infrastructure; New Capital Territory of Nusantara (IKN Nusantara); Seismic Refraction Tomography (SRT); Vp.

Citation: Alamsyah, A., Lepong, P., Wahidah, W., & Rahmiati, R. (2024). Application of Seismic Refraction Tomography in Determining the Soil Hardness Level in IKN Nusantara Area. *Jurnal Geocelebes*, 8(1): 62 – 70, doi: 10.20956/geocelebes.v8i1.32159

Introduction

East Kalimantan is the province where the capital of the new state (IKN Nusantara), exhibits diverse geological formations that fundamentally shape soil characteristics. These variations in the soil characteristics and geological structures significantly impact geotechnical properties, encompassing strength, consolidation, and drainability (Efendi, 2023). A comprehensive comprehension of these geotechnical aspects is imperative for the strategic planning of secure, sustainable development and the effective mitigation of potential disasters stemming from natural conditions natural conditions.

Bachtiar (2022) highlighted the prevalent geological structure in the IKN area, primarily characterized by NE-SW faults, as illustrated in Figure 1. Ezrahayu and Supriyanto (2021) also stated that the location of the prospective new national capital has structures in the form of anticlines, synclines, and is thought to contain thrust faults and normal faults. However, there is a lack of in-depth analysis and detailed studies on this aspect. Generally, regions with such fault structures are considered prone to landslide, a critical factor that demands thorough consideration during the construction-of future infrastructures for the area's development.

Seismic Refraction Tomography (SRT) has become a common method for exploring the geotechnical properties of soil (Asamoah et al., 2018; Whiteley et al.,

2018; Oladotun et al., 2019; Adewoyin et al., 2021; Shin et al., 2022; Opemipo et al., 2022; El Hameedy et al., 2023). According to Jabrane et al. (2023) and Abudeif et al. (2023), this technique relies on the principle of seismic wave retardation, which is dispersed by layers of rocks beneath the surface. This dispersion produces a representation of the variation in compressional wave velocity (P-wave velocity – Vp) within the earth.

This study focuses on assessing the hardness level of the soil beneath the IKN to support infrastructure development using the mentioned geophysical method.

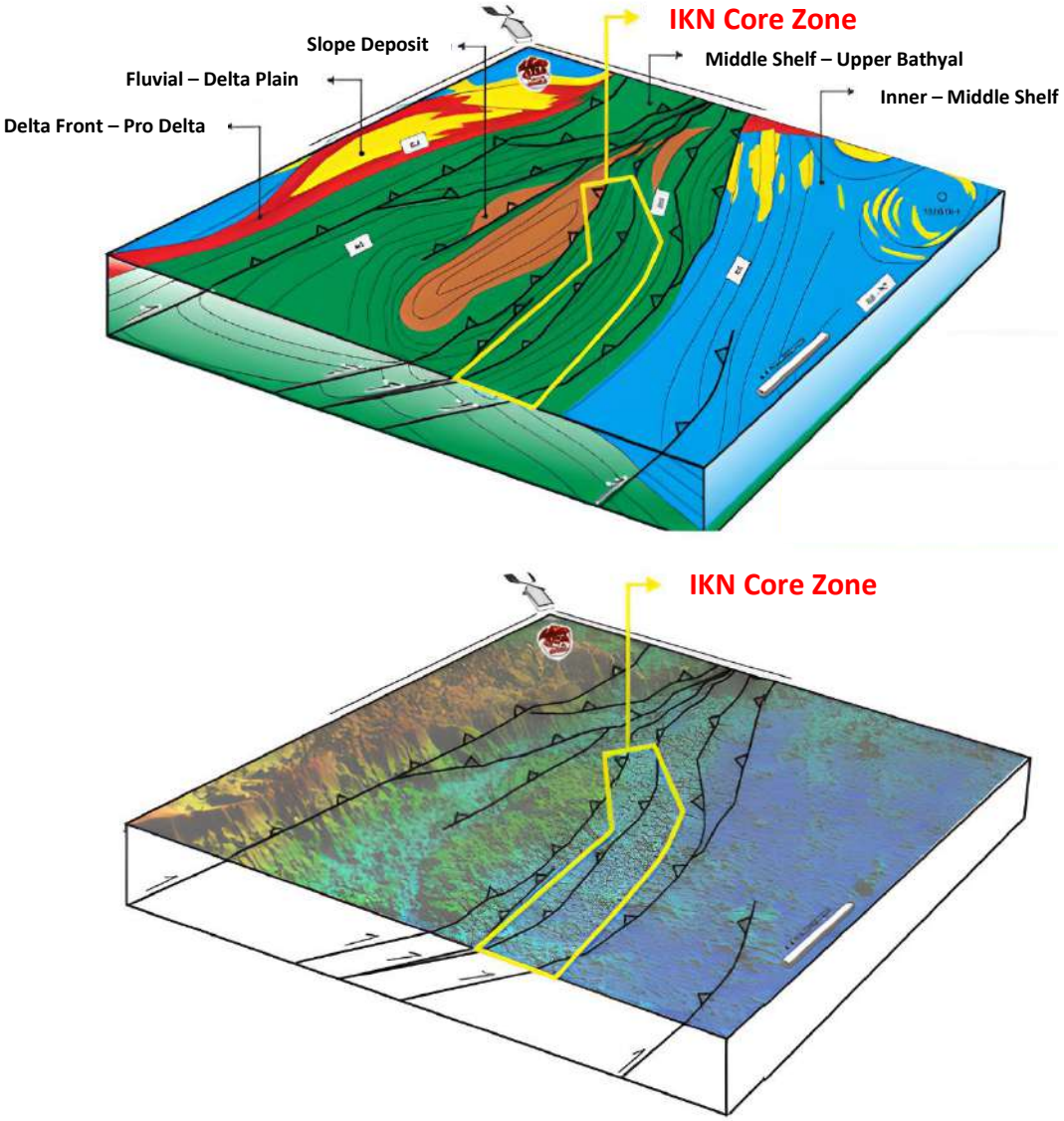

Figure 1. Fault interpretation in the facies of IKN area (Bachtiar, 2022).

Geological Background

Geologically, the location of this survey is included in the geological sheet of Balikpapan (Supriatna et al., 1995). The top formations consist of quartz brass with inserts of sludge, scraps, pebbles, and fine-layer oleic stones. Quartz brass is the main rock in this formation, which has a color range of green, gray, to brownish, fine to moderate grains. The Pamaluan Formation is the lowest rock found in the Samarinda sheet, and the upper part of the formation relates to the Bebulu Formation.

Stratigraphically, according to Bachtiar (2022), the geological composition of the study area is characterized by marine sediments attributed to the late Tertiary-Oligocene Pamaluan Formation, representing a middle shelf facies. This is illustrated in the stratigraphic column in Figure 2, with the IKN area highlighted by red boxes.

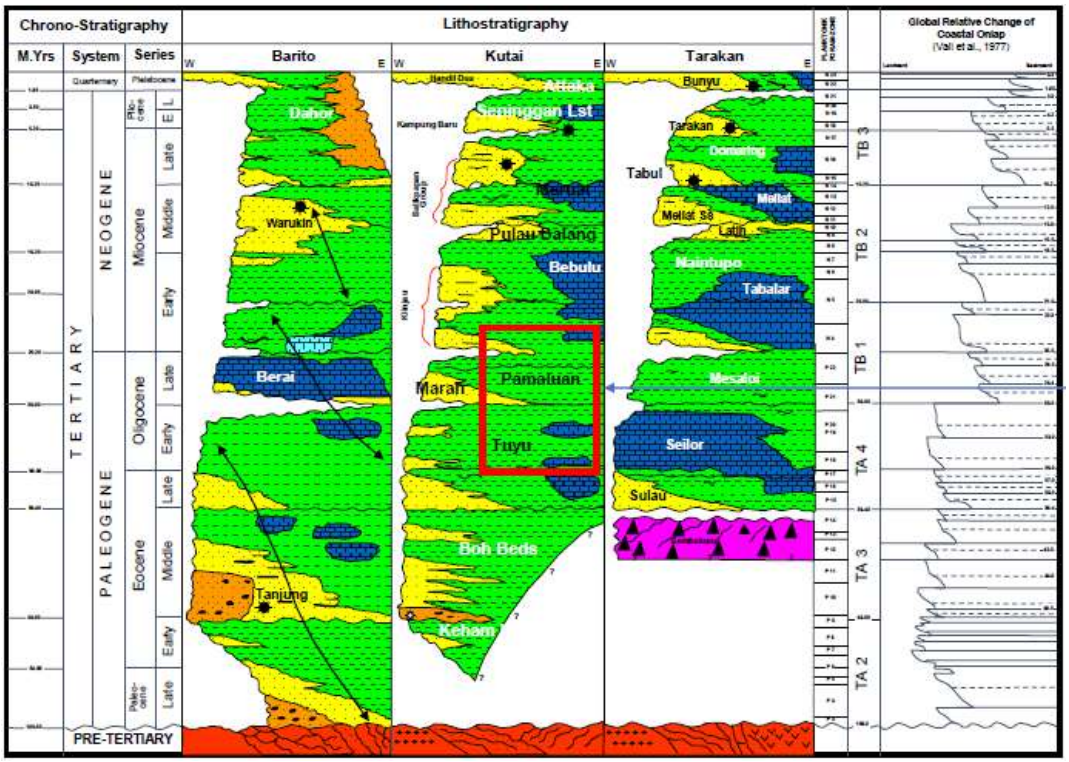

Figure 2. Stratigraphic chart of the regional geology of area (Bachtiar, 2022).

In particular, the research area is situated in the Sepaku District, Penajam North Paser Regency, East Kalimantan Province, precisely where the new state capital of Indonesia (IKN Nusantara area) is being developed, as illustrated in Figure 3.

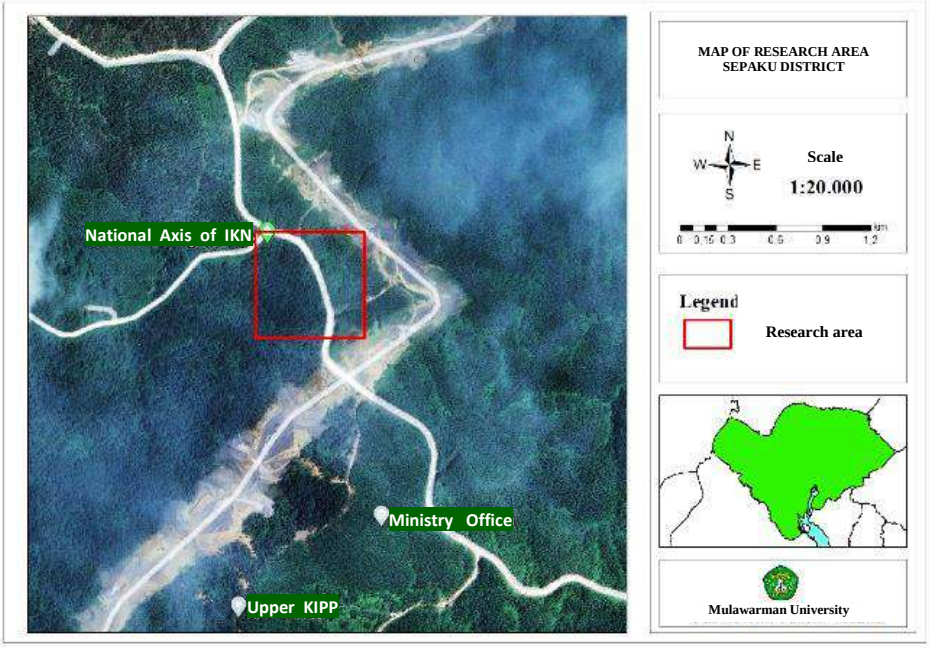

Figure 3. The map of the research area.

The study encompassed seismic refraction data acquisition, subsequent data processing, and interpretation. The acquisition phase utilized a DAQLink III seismograph equipped with 24 channels and a 9 kg hammer sledge serving as the wave source. A total of four seismic refraction surveys were carried out, with one track oriented NE-SW (parallel to the strike direction) and the remaining three tracks oriented relatively NW-SE (perpendicular to the strike). Track details are presented in Table 1 below.

Table 1. Track details.

Tracks	Geophone spacing (m)	Track length (m)
1 *(parallel to the strike)*	4	9
2	3	6
3	3	69
4	3	69

A simplified flow chart of this study is shown in the following Figure 4.

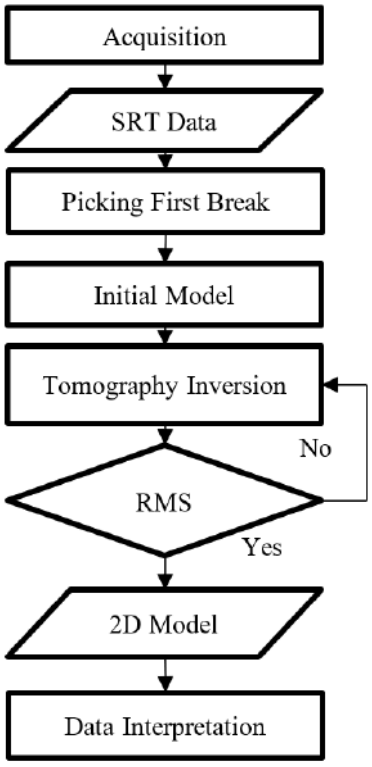

Figure 4. The map of the research area

1. **Picking First Break**. The timing of the wave is established by identifying the position of the first break on the refractive seismic record. The selection of the first break involves a subjective assessment to determine its position.
2. **Inversion Tomography**. This step involves generating a two-dimensional model of Vp intersections to illustrate subsurface conditions.
3. **Interpretation and 2D Model of Vp.** The Vp 2D model is scrutinized and interpreted by comparing the primary wave velocity (Vp) values with reference tables or previous research. Additionally, an analysis is conducted to assess the concordance of the interpreted primary wave velocity results with the geological conditions at the research site, enhancing the accuracy of the findings. Subsequently, the Vp values are incorporated into Equation 1.

$$UCS = 12.746 * Vp^{1.194} \quad (1)$$

This equation is an empirical relationship applicable to mudrock–shale rocks and siltstone or flax rocks (Poulos, 2021). The calculated results are employed to ascertain the hardness level or provide geotechnical descriptions, as outlined in Table 2.

Table 2. Relationship between Vp dan UCS (Poulos, 2021)

Vp (km/s)	Geotechnical Desc.	UCS (MPa)
< 2.0	Low strength rock	< 10
2.0 – 2.5	Medium strength rock	10 – 20
2.5 – 3.5	High strength rock; stratified, jointed	20 – 60
– 7.0	Very high strength rock	> 60

Results and Discussion

Seismic Refraction Tomography (SRT) cross-section on Track 1, Track 2, Track 3, and Track 4 are shown in Figure 5. The color bar in the figure represents the value

of the Vp, where the blue to red color shows the Vp from low to high.

Cross-section of Track 1, as depicted in Figure 5a, indicates the presence of two lithologies: soil and clay shale. Lithology 1 represents soil with a P-wave velocity ranging from approximately 700 to 1000 m/s and an average thickness of 2 meters. The soil near the surface is categorized as soft soil with a Vp around 700 to 800 m/s and a thickness of approximately 1 meter.

The undulation Vp contour lines indicate the heterogeneous presence of soil-containing material close to the surface. Between 50 and 80 meters, there is a change in the relative descent of the contour pattern, interpreted as subsidence or a decrease in seismic profiles.

In general, higher Vp values correspond to materials with greater geotechnical strength due to increased density, while porosity, weathering, and fracturing decrease. The Vp values can be utilized to calculate the Ultimate Compressive Strength (UCS). In Track 1, the predominant lithology falls into the high-strength rock category, with a calculated UCS ranging from 22 to 51 MPa. Conversely, the soil near the surface is classified as low to medium strength rock, with a UCS value less than 15.85 MPa.

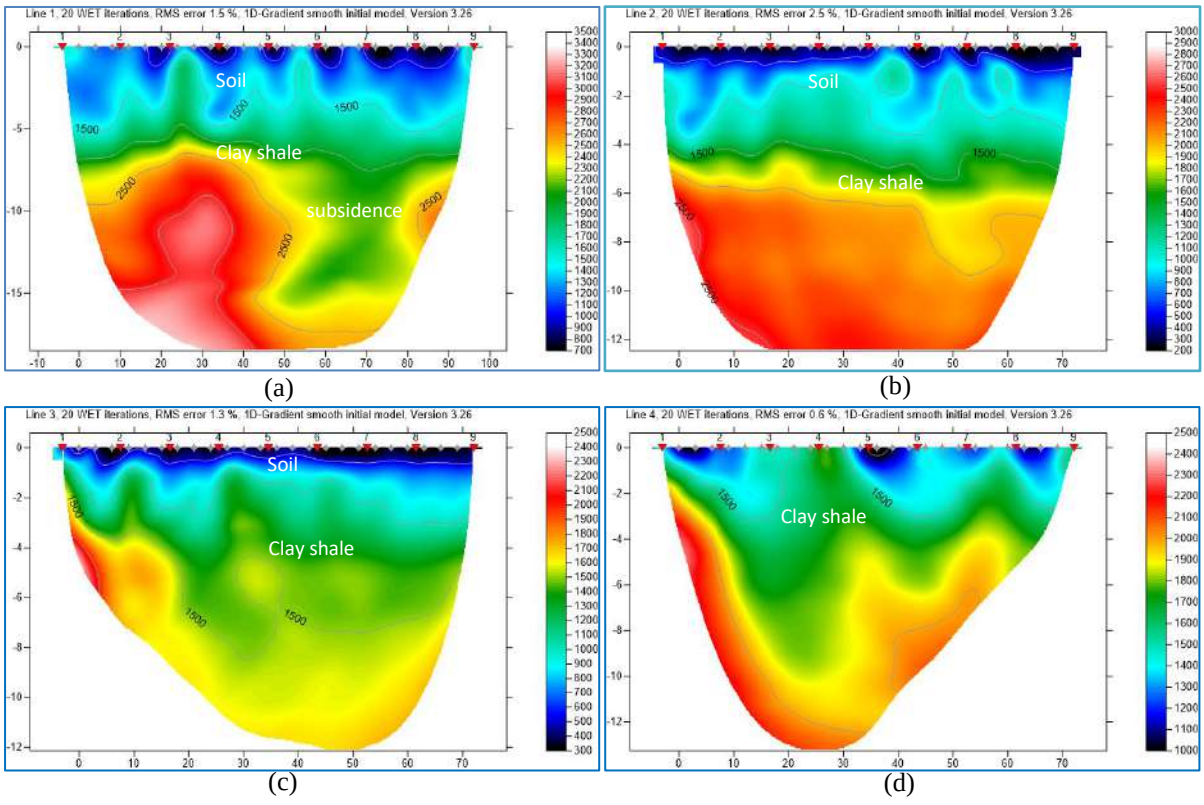

Figure 5. SRT (Vp) section of (a) Track 1; (b) Track 2; (c) Track 3; (d) Track 4.

Track 2, oriented perpendicular to the strike (NW-SE), exhibits two distinguishable lithologies: soil and clay shale. The soil layer is characterized by a Vp ranging from approximately 200 to 1000 m/s, with an average thickness of 3 meters.

The surface soil, with a Vp of around 200 to 800 m/s, is interpreted as soft soil and has a thickness of approximately 1 meter. Additionally, lithology 2 is identified as clay shale, featuring a Vp between 1000 and 3500 m/s and located at a depth of 3 to 12 meters.

In Figure 5b, the undulation Vp contour lines indicate the presence of inhomogeneous material, particularly soil

close to the surface. At a depth greater than 4 meters, where Vp exceeds 1500 m/s, the clay shale layering pattern appears relatively uniform. This is interpreted as a relatively stable stratum without structural features such as fractures or faults.

The cross-section of Track 2 is predominantly classified as medium-high strength rock category with UCS calculation resulting in a range of (19-38) MPa. The surface soil falls into the low strength rock category, with a UCS value of less than 6 MPa.

Moreover, track 3 exhibits a lithology pattern similar to the preceding tracks. The soil layer has a Vp ranging from approximately 300 to 1000 m/s with an average thickness of 2 meters. The surface soil, with a Vp of around 200 to 800 m/s, is interpreted as soft soil with a thickness of approximately 1 meter. The second lithology is identified as clay shale, featuring a Vp between 1000 and 3500 m/s, located at a depth of 3 to 12 meters. The depth of the clay shale layer on this track is roughly the same as the one found on Track 2.

The undulation of the Vp contour lines reveals in homogeneous especially soil close to the surface. At depths exceeding8 meters with Vp >1500m/s, it is observed that the clay shale bedding pattern is relatively deeper compared to other tracks. These results, suggest that the clay shale is relatively tilted to the west.

Overall, the dominant section of Track 3 falls into the high-strength rock category, with UCS calculation results ranging from (20-22) MPa. The surface soil is categorized as low-strength rock, with a UCS value of less than 10 MPa. In Track 4, which is aligned with the dip direction, only one lithology has been identified, which is clay shale, as illustrated in Figure 5d. The topsoil layer was not discernible as it had been removed in this area. The clay shale layer on this track exhibits a Vp ranging from approximately 1000 to 2500 m/s, extending from the surface to a depth of 12 meters. The undulating Vp contour lines indicate the presence of material inhomogeneity, particularly soil close to the surface. The undulating velocity contour pattern is attributed not only to the inhomogeneity of the clay shale material but also to the influence of noise generated by the vibrational activity of heavy equipment actively operating in the survey area.

On the other hand, the cross-section of Track 4 is predominantly classified as high-strength rock, with UCS calculation results ranging from (24-31) MPa. The surface soil falls into the medium-strength rock category, with a UCS value of less than 18 MPa. The UCS calculation results using Equation 1 are presented in Table 3, which also provides a geotechnical description based on the correlation results of Vp with UCS.

Generally, the P wave velocity values from the results of seismic refraction tomography (SRT) measurements on the four tracks show two lithologies, namely soil with a Vp value of around 200 m/s - 1000 m/s and clay shale with a Vp value of around 1000 m/s - 3500 m/s, except for Track 4, only the clay shale layer was identified and exposed on the surface. In civil construction terms, clay shale is classified as an intermediate rock containing montmorillonite clay (Ohlmacher, 2000; Akisanmi 2022).

Its presence poses a challenge because of its low durability making it susceptible to weathering (Pratama et al., 2015). Therefore, special attention is needed in civil construction planning to overcome this factor.

Even though the research area is dominated by clay shale lithology, the level of rock strength also needs to be considered to determine whether construction is feasible in the area. Based on Table 3, the average

UCS value of the four tracks is greater than 20 MPa which is categorized as high strength rock geotechnical material, except for soil material close to the surface to a depth of around 3 meters which is categorized as low to medium strength rock.

Tanjung et al. (2023) and Amran and Pradana (2023) claim that properly compacted clay soil will have increased shear strength. The mineral content of the material determines how stable its swelling-shrinking characteristics are.

This is supported by the results of research by Susilawati (2022) which states that measuring the strength of soil and rock by cone penetration test shows the presence of a hard layer (Qc >150 kg/cm^2) range between 2.0 – 4.0 m below the ground surface and locally can reaches 5.8 m.

Table 3. UCS calculation results with geotechnical description.

Track	Depth (m)	Vp (m/s)	UCS (MPa)	Geotechnical Description
1	0 – 2.5	1200	15.8	Medium Strength Rock
	2.5 - 6	1600	22.3	High Strength Rock
	6 – 10.5	2200	32.7	High Strength Rock
	10.5 - 16	2800	43.6	High Strength Rock
	16 -20	3200	51.1	High Strength Rock
2	0 – 2.5	500	5.6	Low Strength Rock
	2.5 - 6	1400	19.0	Medium Strength Rock
	6 – 10.5	2250	33.6	High Strength Rock
	10.5 - 12	2500	38.1	High Strength Rock
3	0 – 3	800	9.8	Low Strength Rock
	3 – 7.5	1500	20.7	High Strength Rock
	7.5 - 12	1600	22.3	High Strength Rock
4	0 – 2.5	1300	17.4	Medium Strength Rock
	2.5 - 6	1700	24.0	High Strength Rock
	6 – 10.5	1950	28.3	High Strength Rock
	10.5 - 13	2150	31.8	High Strength Rock

Table 3 shows a correlation between the P wave velocity value and the UCS value. According to Awang et al. (2017) and Kessler et al. (2017), it is now simpler to determine UCS value without the necessity for physical testing on samples or borehole and sample collection processes because this empirical link has been acknowledged. We are able to recognize that the compressive strength index value is crucial for the design factor because of the seismic test that yields the P-wave velocity value when conducted on the ground surface. One of the most crucial factors in rock engineering qualities is the UCS value.

In civil construction terms, clay shale is classified as an intermediate rock containing montmorillonite clay that has low durability due to weathering. Hence, special attention is required in civil construction planning to address this factor. However, the average UCS value of clay lithology at a depth of more than 3 meters is still considered suitable for construction because it is still greater than 20 MPa which is categorized as high strength rock geotechnical material. To be more convincing, it is necessary to carry out a MASW (Multichannel Analysis Surface Wave) survey to analyze the level of rock stiffness and other geotechnical parameters.

Conclusion

The Seismic Refraction Tomography (SRT) measurements reveal that the predominant compression seismic wave velocity (Vp) exceeds 1500 m/s interpreted as clay shale which is under the soil layer.

Acknowledgements

The authors acknowledged the Head of Geophysics Laboratory for supporting the SRT tools and FMIPA UNMUL for funding this research.

Author Contribution

Field acquisitions were carried by Piter Lepong and Team. All authors discussed, interpreted and wrote the manuscripts which were leading by Andi Alamsyah.

Conflict of Interest

The authors declare no conflict of interest.

References

Abudeif, A. M., Aal, G. Z. A., Abdelbaky, N. F., Gowad, A. M. A., & Mohammed, M. A. (2023). Evaluation of Engineering Site and Subsurface Structures Using Seismic Refraction Tomography: A Case Study of Abydos Site, Sohag Governorate, Egypt. *Applied Sciences*, 13(4), 2745. https://doi.org/10.3390/app13042745

Adewoyin, O. O., Joshua, E. O., Akinyemi, M. L., Omeje, M., & Adagunodo, T. A. (2021). Evaluation of Geotechnical Parameters of Reclaimed Land from Near-Surface Seismic Refraction Method. Heliyon, 7(4), E06765. https://doi.org/10.1016/j.heliyon.2021.e06765

Akisanmi, P. (2022). Classification of Clay Minerals. *Mineralogy* (M. René (ed.); p. Ch. 12). IntechOpen. https://doi.org/10.5772/intechopen.103841

Amran, Y., & Pradana, D. Y. (2023). Parameter Nilai Kuat Tekan Bebas Tanah terhadap Tingkat Kepadatan Tanah Lempung Ekspansif. *Teknologi Aplikasi Konstruksi (TAPAK)*, 12(2), 166–178. http://dx.doi.org/10.24127/tp.v12i2.2595

Asamoah, K. N., Seidu, J., Ewusi, A., & Ansah, E. (2018). Geotechnical Investigation at Sanzule Beach, Ghana, Using Seismic Refraction Tomography. *IJISET-International Journal of Innovative Science, Engineering & Technology*, 5(2), 45–53. https://ijiset.com/vol5/v5s2/IJISET_V5_I02_05.pdf

Awang, H., Rashidi, N.R.A., Yusof, M., & Muhammad, K. (2017). Correlation Between P-wave Velocity and Strength Index for Shale to Predict Uniaxial Compressive Strength Value. *MATEC Web of Conferences* 103, 07017. https://doi.org/10.1051/matecconf/201710307017

Bachtiar, A. (2022). *Aspek geologi untuk mitigasi bencana Ibu Kota Nusantara*. National Webinar. https://www.its.ac.id/tgeofisika/wp-content/uploads/sites/33/2022/11/Materi-Dr-Andang-Bachtiar.pdf

Efendi, A. W. (2023). Pemodelan Penurunan Tanah Di Ibu Kota Negara Nusantara Menggunakan Analisis Numerik Metode Elemen Hingga Lisa V.8. *Paduraksa: Jurnal Teknik Sipil Universitas Warmadewa*, 12(1), 21–29. https://doi.org/10.22225/pd.12.1.5643.21-29

El Hameedy, M. A., Mabrouk, W. M., Dahroug, S., Youssef, M. S., & Metwally, A. M. (2023). Role of Seismic Refraction Tomography (SRT) in bedrock mapping; case study from industrial zone, Ain-Sokhna area, Egypt. *Contributions to Geophysics and Geodesy*, 53(2), 111–128. https://doi.org/10.31577/congeo.2023.53.2.2

Ezrahayu, P. & Supriyanto, S. (2021). Identifikasi Sesar di Bawah Permukaan yang Dapat Menyebabkan Gempa Berdasarkan Metode First Horizontal Derivative dan Second Vertical Derivative di Kabupaten Penajam Paser Utara, Kalimantan Timur. *Jurnal Geosains Terapan* 4(1), 15–22. https://geosainsterapan.id/index.php/id/issue/download/6/6

Jabrane, O., Martinez-Pagan, P., Martinez-Segura, M. A., Alcala, F. J., El Azzab,

D., Vásconez-Maza, M. D., & Charroud, M. (2023). Integration of Electrical Resistivity Tomography and Seismic Refraction Tomography to Investigate Subsiding Sinkholes in Karst Areas. *Water*. 15(12), 2192. https://doi.org/10.3390/w15122192

Kessler, J. A., Schmitt, D.R., Chen, X., Evans, J. P., & Shervains, J. W.. (2017). Predicting Uniaxial Compressive Strength from Empirical Relationships between Ultrasonic P wave Velocities, Porosity, and Core Measurements in a Potential Geothermal Reservoir, Snake River Plain, Idaho. *American Rock Mechanics Association (ARMA)*, 17-391. https://www.osti.gov/servlets/purl/1749943

Ohlmacher, G. C. (2000). The Relationship Between Geology and Landslide Hazards of Atchison, Kansas, and Vicinity. *Current Research in Earth Science,* 244, 1–16. https://doi.org/10.17161/cres.v0i244.11833

Oladotun, A. O., Oluwagbemi, J. E., Lola, A. M., Maxwell, O., & Sayo, A. (2019). Predicting Dynamic Geotechnical Parameters in Near-Surface Coastal Environment. *Cogent Engineering*, 6(1), 1588081. https://doi.org/10.1080/23311916.2019.1588081

Opemipo, O. D., Moroff, O., Sunday, O., Victor, O., & Christopher, B. (2022). Subgrade Soil Evaluation Using Integrated Seismic Refraction Tomography and Geotechnical Studies: A Case of Ajaokuta-Anyigba Federal Highway, North-Central Nigeria. *NRIAG Journal of Astronomy and Geophysics*, 11(1), 293–305. https://doi.org/10.1080/20909977.2022.2094530

Pratama, A. W., Iswan, I., & Jafri, M. (2015). Korelasi Kuat Tekan dengan Kuat Geser pada Tanah Lempung yang Didistribusi dengan Variasi Campuran Pasir. *Journal Rekayasa Sipil Dan Desain (JRSDD)*, 3(1), 157–170. https://journal.eng.unila.ac.id/index.php/jrsdd/article/view/434

Poulos, H. G. (2021). Use of shear wave velocity for foundation design. *Geotechnical and Geological Engineering*, 40(2), 1921–1938. https://doi.org/10.1007/s10706-021-02000-w

Shin, B.-S., Wientgens, L., Schaab, M., & Shutin, D. (2022). Near-Surface Seismic Measurements in Gravel Pit, over Highway Tunnel and Underground Tubes with Ground Truth Information as an Open Data Set. *Sensors*, 22(17), 6687. https://doi.org/10.3390/s22176687

Supriatna, S. Sukardi, R, & R. Rustandi. (1995). *Peta Geologi Bersistem, Lembar Samarinda, Kalimantan skala 1:250.000*. Pusat Penelitian dan Pengembangan Geologi.

Susilawati, R. (2022). *Kajian geologi dalam rencana pembangunan IKN nusantara*. Diskusi IAGI "Menyongsong IKN Nusantara dari Perspektif Kebumian". https://www.iagi.or.id/web/digital/43/Hasil-Kajian-Geologi-dalam-Rencana-Pembangunan-IKN-Nusantara-(1).pdf

Tanjung, D., Sarifah, J., & Ardian, J. P. (2023). Pengaruh Nilai Kuat Tekan Bebas terhadap Penambahan Abu Sekam Padi pada Tanah Lempung. *Jurnal Teknik Sipil*. 2(1), 68–77. https://jurnal.uisu.ac.id/index.php/JTSIP/article/view/7662

Whiteley, J. S., Chambers, J. E., Uhlemann, S., Wilkinson, P. B., & Kendall, J. M. (2018). Geophysical Monitoring of Moisture-Induced Landslides: A Review. *Review of Geophysics*, 57(1), 106–145. https://doi.org/10.1029/2018RG000603

ISSN: 2579-5821 (Print)
ISSN: 2579-5546 (Online)
URL address: http://journal.unhas.ac.id/index.php/geocelebes
DOI: 10.20956/geocelebes.v8i1.33969

Jurnal Geocelebes Vol. 8 No. 1, April 2024, 71 – 82

1D Audio Magnetotelluric Modelling for Deep Aquifer Identification in the Lava Fan Area of Haruman Peak, Malabar Mountains

Nabilah Rahmawati[1], Nabila Putri Kusuma[1], Shofie Dzakia Hanifah[1], G.M. Lucki Junursyah[2], Asep Harja[1]*

[1]Department of Geophysics, Padjadjaran University, Jl. Raya Bandung-Sumedang KM. 21, Jatinangor, Sumedang, West Java, 45363
[2]Center for Geological Survey, Geological Agency, Ministry of Energy and Mineral Resources, Bandung, Indonesia

*Corresponding author. Email: asep.harja@geophys.unpad.ac.id

Manuscript received: 14 March 2024; Received in revised form: 20 April 2024; Accepted: 28 April 2024

Abstract

The Malabar Mountains area acts as a catchment and infiltration zone for rainwater. Haruman Peak is the location of one of these areas. Information on the well-preserved depth of the shallow aquifer at 40 meters reinforces this. This research reviews the results of subsurface 1D resistivity structures from AMT data to obtain information on the depth of deep aquifers on the western slope of the Haruman Peak Lava Fan, Haruman Mountains. 1D modelling shows an aquifer at depth of 140.56-2080.07 meters with resistivity ranging from 5.25-68.08 Ωm. At depths of 453.32 m (HR02), 530.8 m (HR03), 1464.97 m (HR01), and 2080.07 m (HR02), interbedded tuff-andesite with minor pumice identifies the deep aquifer. In addition, a depth of 140.56 m (HR02) with a resistivity value of 68.08 Ωm indicates a shallow aquifer. Looking at the elevation of the Bandung Basin, water from aquifers located at elevations > 700 meters above sea level will flow into the Bandung Basin.

Keywords: 1D; audio magnetotelluric; deep aquifer; Haruman peak; subsurface resistivity structure.

Citation: Rahmawati, N., Kusuma, N. P., Hanifah, S. D., Junursyah, G. M. L., & Harja, A. (2024). 1D Audio Magnetotelluric Modelling for Deep Aquifer Identification in the Lava Fan Area of Haruman Peak, Malabar Mountains. *Jurnal Geocelebes*, 8(1): 71–82, doi: 10.20956/geocelebes.v8i1.33969

Introduction

Mount Malabar is a type B volcano located south of Bandung and forms the boundary between the Bandung plateau (700 m) to the north and the Pangalengan plateau (1400 m) to the south. The Malabar Mountain complex is a crucial catchment and rainwater infiltration zone. Haruman Peak is one of the main infiltration zones of the Bandung–Soreang Groundwater Basin located on the western side of the Malabar Mountain range (Harja et al., 2021). The mountain slopes that lead into the Bandung Basin support this claim, as stated by Suhari and Siebenhüner (1993). Furthermore, recent studies by Harja et al. (2021, 2023) have provided clear and precise information on the depth of shallow aquifers at 40 meters, which are still well-preserved.

Information on the existence of deeper aquifers is not yet clearly known. Therefore, a deep investigation of geophysical measurement is needed, one of which uses the Audio Magnetotelluric (AMT) method that can detect resistivity variations from tens of meters to tens of kilometers (Gomo, 2023). This method utilizes lightning activity in the ionosphere as its source with a frequency range from 0.1 Hz–10 kHz (Constable, 2016), which is both environmentally friendly and easy to use. The AMT method is used in hydrology to determine aquifer thickness and depth, to define the deepest geological strata, and to characterize groundwater migration (Li et

al, 2021; Montahaei, 2022; Tripathi et al., 2019; Xu et al., 2020; 2023; Zaher et al., 2021). The expected result of using AMT method in this research is to determine the presence of deeper aquifers based on the contrast of rock resistivity values modelled in 1D.

Geology of the research area

The research was focused on the western slope of Haruman Peak, Malabar Mountains, West Java, with three points including HR01 (7°8'20.10"S and 107°34'48.36"E), HR02 (7°8'24.78"S and 107°34'51.48"E), and HR03 (7°8'28.98"S and 107°34'50.14"E) (Figure 1). The description of stratigraphy and lithology in the research area is based on the Geological Map of Garut and Pameungpeuk Quadrangle, Java (Alzwar et al., 1992). The geology of the measuring region is separated into volcanic rock units and surface sediment units, with Tertiary volcanic rocks overlain by Quaternary volcanic rocks that deposit surface sediment units. The rock units exposed around the AMT research area are Miocene to Holocene age rocks, including the Beser Formation (Tmb), with a thickness of about 500–1000 m consisting of tuffaceous breccia and lavas of andesitic to basaltic composition and containing pumice fragments; and the Waringin-Bedil Andesite, Old Malabar (Qwb), with a thickness of about 600 m consisting alternation of lavas, breccia, and tuffs.

The Beser Formation (Tmb) is a Late Miocene rock unit spread northwest of the Garut and Pameungpeuk Quadrangle. It is overlapped unconformity by the Pliocene Tufaan Breksi Formation (Tpv), consisting of breccia, tuff, and sandstone, and has a thickness of about 600–700 m. Furthermore, there is the Old Undecomposed Volcanic Rock Formation (Qtv) with a thickness of 500–800 m, Plio-Pleistocene age, which overlaps the Tufaan Breccia Formation (Tpv) and overlaps incongruously with Old Quaternary Volcanic Rocks. The Qtv Formation products are assumed to be the product of eruptions with undecomposable sources, including fine to coarse tuff, pumice tuff breccia, and andesite lava.

Above the Qtv formation settled the Pleistocene-aged Waringin Bedil Andesite unit, Old Malabar (Qwb). Then, the rock unit is overlain by the Undifferentiated Efflata Deposits of Old Volcanics (Qopu), with a thickness of about 400 m consisting of fine to coarse tuff, tuffaceous breccia, and old laharic deposits, and formed in the Pleistocene era. The products of the formation filled the valley of the Old Malabar volcanic depression and formed the Pangalengan plateau. After that, there was a deposition of Pleistocene rocks with a thickness of 1400 m above it, which is the Malabar-Tilu Volcano Rock Unit (Qmt) consisting of tuff, laharic breccia containing minor of pumice, and lavas. The unit is overlapped by the Tilu Lava Formation (Qtl) and its constituent rocks come from G. Malabar I/Ipis, G. Malabar II/Puncakbesar, and G. Tilu. Lastly, the Tilu Lava Formation (Qtl) that appears to the southwest of the Old Malabar volcanic depression is composed by andesitic lava and basaltic andesite formed in the Pleistocene epoch.

Based on Garut and Pameungpeuk Quadrangle, the research area located south of a northwest-southeast trending fault. Faults can be an outlet or entry of surface water into the aquifer layer below the surface and can withstand the direction of water flow that should be (Keegan-Treloar et al., 2022; Kurniawan et al., 2022).

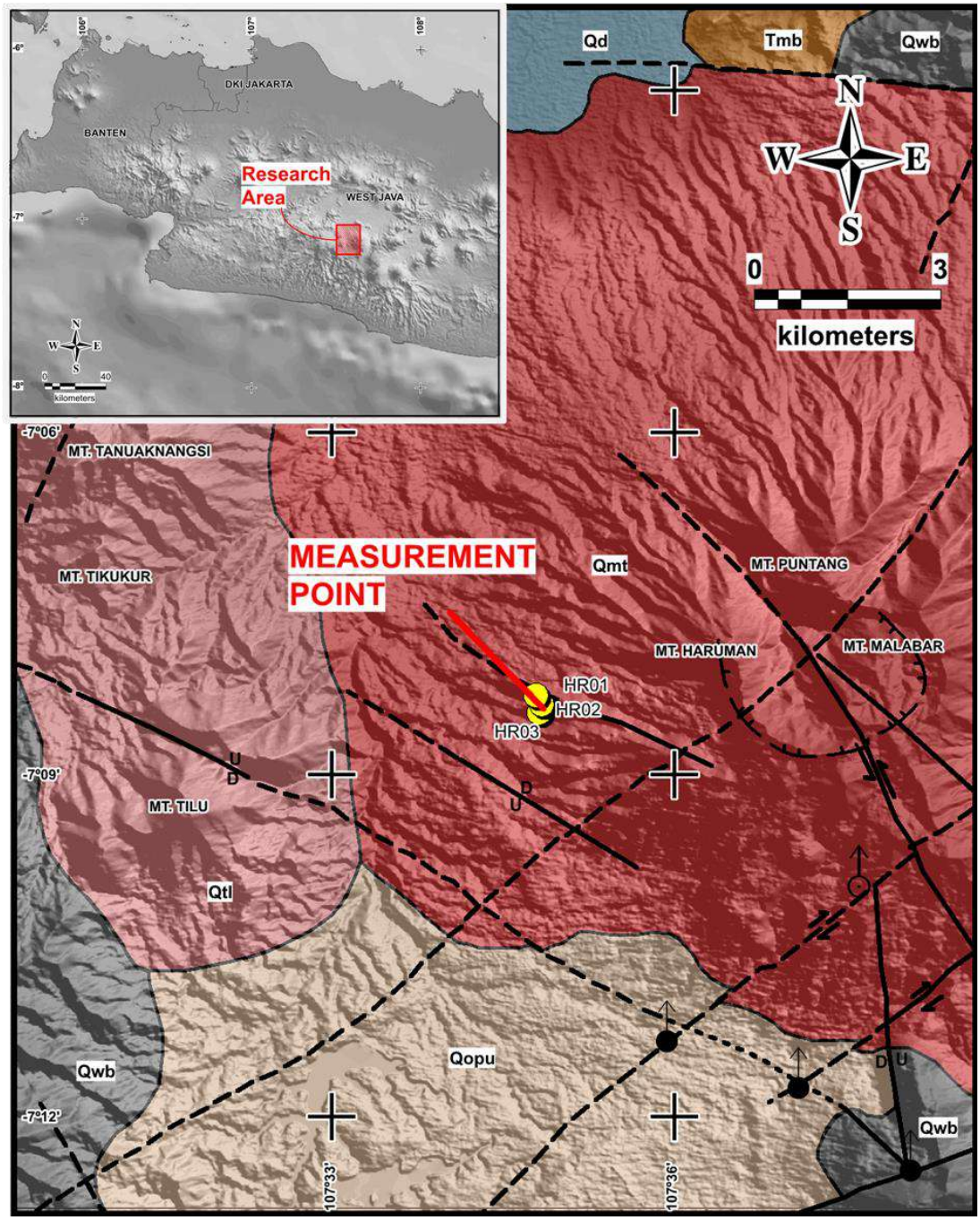

Figure 1. Geologic Map of Research Area (modification of Garut and Pameungpeuk Map, Java by Alzwar et al., 1992).

Research Methods

AMT method measurements with the recorder main unit MTU-5A were carried out at three points on the western slope of the Malabar Mountains, precisely in Warjabakti Village, Cimaung District, Bandung Regency, West Java. The distance between HR01 and HR02 is about 175 meters, while the distance between HR02 and HR03 is about 135 meters. The data generated from the AMT acquisition is in the form of magnetic and electric field intensity variation data in the time domain (Hidayat et al., 2021). Each point is measured using vector measurement mode for 30 minutes. The length of the AMT measurement makes the data obtained in the frequency range of 0.35 Hz to 10400 Hz (Wu et al., 2023). The data is then processed to obtain an apparent resistivity curve, which is calculated based on the ratio

of the size of the electric field (E) and the magnetic field (H) (Figure 2). The comparison is called the Cagniard equation (Equation 1) (Cagniard, 1953).

$$\rho_a = \frac{1}{5f}\left|\frac{E_x}{H_y}\right|^2 \quad (1)$$

The steps of the procedure are Fast Fourier Transform, Robust Processing, and cross-power selection (XPR) (Kurniawan et al., 2019). Fast Fourier Transform is a method used to transform data from the time domain to the frequency domain. The next step is robust processing, which tries to detect, eliminate, and decrease outliers. This step performs iterative weighting of residuals to lower the weight of outliers. The robust process considers the coherence of each robust parameter's results. Coherence is a real number with a dimension ranging from 0 to 1, where 1 indicates a perfectly coherent transmission. The robust process has three types of cross-power parameters, such as No Weight—doing the same weighting at each frequency, Rho Variance—doing high weighting on the type resistance that has as many snippets as the desired cross-power value, and Ordinary Coherence—doing high weighting at frequencies with good coherence between the H and E components (Junursyah et al., 2020). The Ordinary Coherence parameter has the highest coherence value among the three cross-power parameters, with coherence greater than 70%. The apparent resistivity and phase curves generated in the robust process usually have random patterns due to noise in the recorded data, therefore XPR is carried out to smoothen the curve. The XPR is carried out by selecting high-weight XPR data and eliminating low-weight XPR data (Figures 2, 3, and 4).

Curve trend analysis is the next step that removes data far from the curve trend (outliers). The deviant curve data is affected by noise in the initial data, robust results, and XPR. The maximum depth is then calculated based on the skin depth using Equation 2.

$$\delta = 503\sqrt{\frac{\rho}{f}} \quad (2)$$

After the curve trend analysis, the data is modeled in 1D with Occam inversion to calculate the maximum depth based on resistivity variation. The Occam inversion serves to minimize the roughness level of the resulting model. The results from the inversion calculation of the model will be smoother, establishing the fitting process of field data (Constable et al., 1987).

Furthermore, the data is analyzed to determine the dimensionality of the subsurface resistivity structure, known as skewness analysis. This analysis to determine if there are deviations or distortions in the impedance tensor in magnetotelluric data (Junursyah, 2022). There are two techniques for skewness analysis: Swift skew and Bahr skew. Swift skew is the ratio between the diagonal components (Z_{xx} and Z_{yy}) and the non-diagonal components (Z_{xy} and Z_{yx}) of the impedance tensor (Equation 3). If the $skew_{Swift}$ value > 0.3 implies 3D or noise. If the $skew_{Swift}$ value < 0.3, it suggests 1D or 2D (Pranata et al., 2017). Swift skew is a one-dimensional data analysis for determining whether the underlying electrical structure is distorted or not. The skewness value will look deviated if the impedance tensor has telluric distortion (Xiao et al., 2011; Tripathi et al., 2019).

$$Skew_{Swift} = \left|\frac{Z_{xx} + Z_{yy}}{Z_{xy} - Z_{yx}}\right| \quad (3)$$

Bahr skew is a calculation developed on the value of phase sensitivity skewness (η) or regional skew by considering telluric distortion in the impedance tensor (Bahr, 1991). The phase sensitivity slope can be determined using Equation (4).

$$\eta = \frac{\sqrt{2\left|ReZ_{xx}\cdot ImZ_{yx} - ReZ_{yy}\cdot ImZ_{xy} + ReZ_{xy}\cdot ImZ_{yy} - ReZ_{yx}\cdot ImZ_{xx}\right|}}{|Z_{xy} - Z_{yx}|} \quad (4)$$

Re represents the real part of a complex number, while Im represents the imaginary

part. If the value of $\eta > 0.3$, it suggests 3D inductive effect, while $\eta = 0$ suggests an ideal values of 1D-2D electrical structure. A value of $\eta < 0.3$ implies the response of 2D structure (Xiao et al., 2011). A value of less than 0.3 indicates a regionally 2D structure, but it is not sufficient (Tripathi et al., 2019). In this research, the technique used in dimensionality analysis is Bahr skew to clarify the subsurface structure. Research flow chart can be seen in Figure 6.

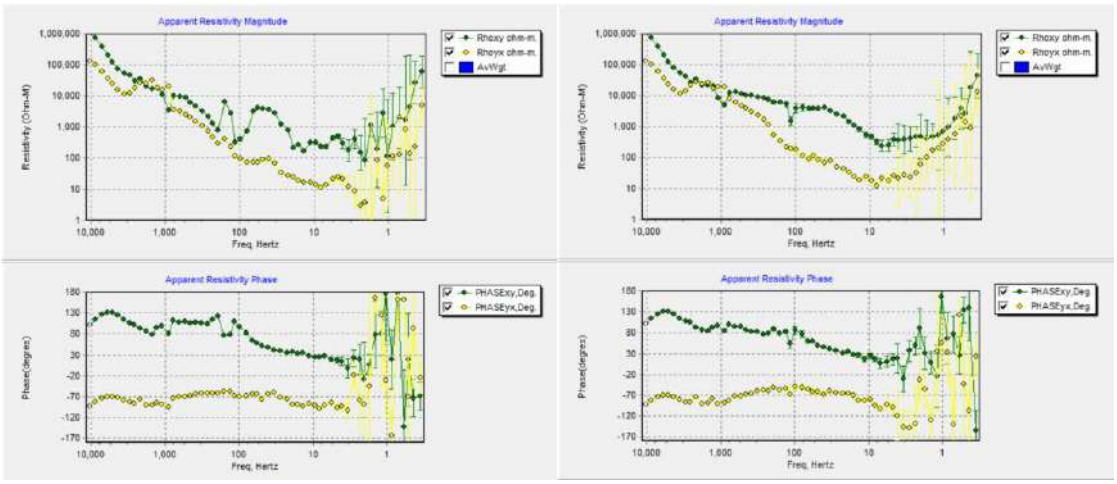

Figure 2. Comparison of the apparent resistivity curve and phase at HR01 before (left) and after XPR (right).

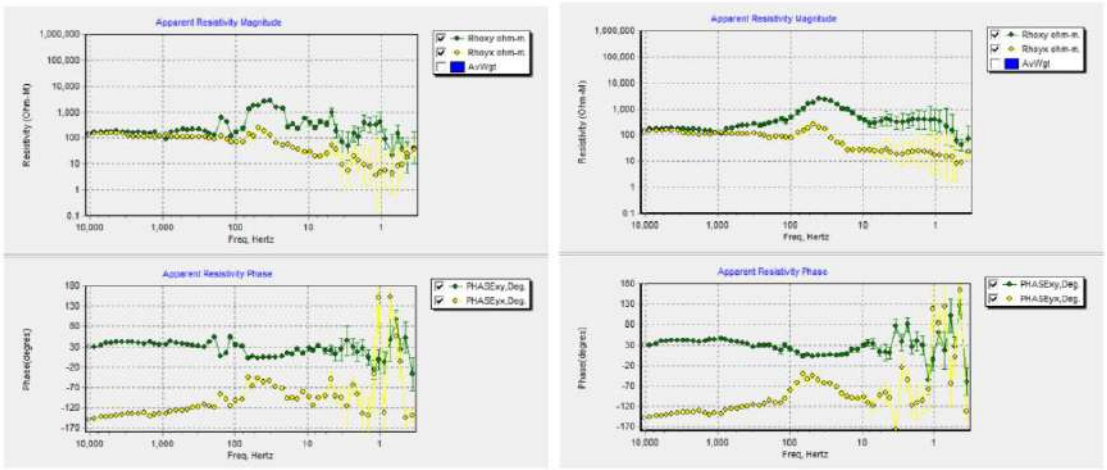

Figure 3. Comparison of the apparent resistivity curve and phase at HR02 before (left) and after XPR (right).

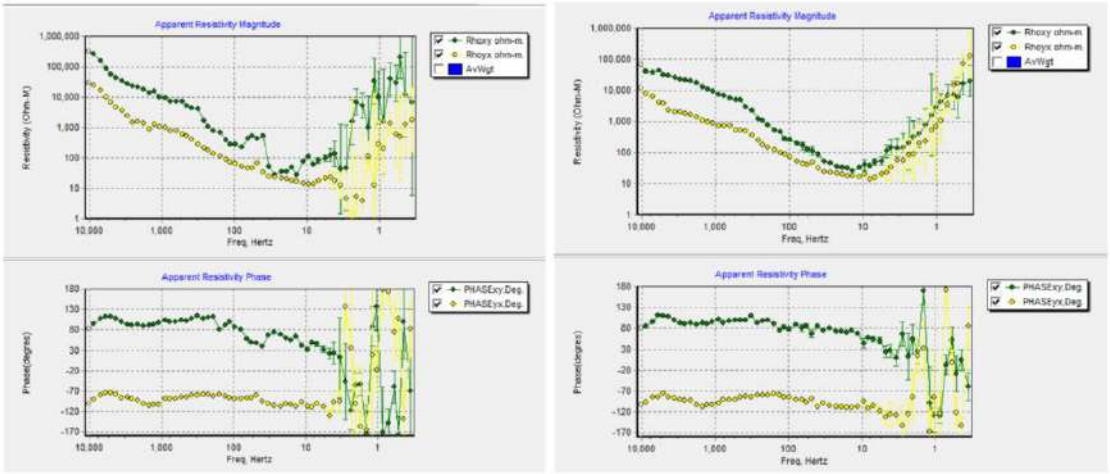

Figure 4. Comparison of the apparent resistivity curve and phase at HR03 before (left) and after XPR (right).

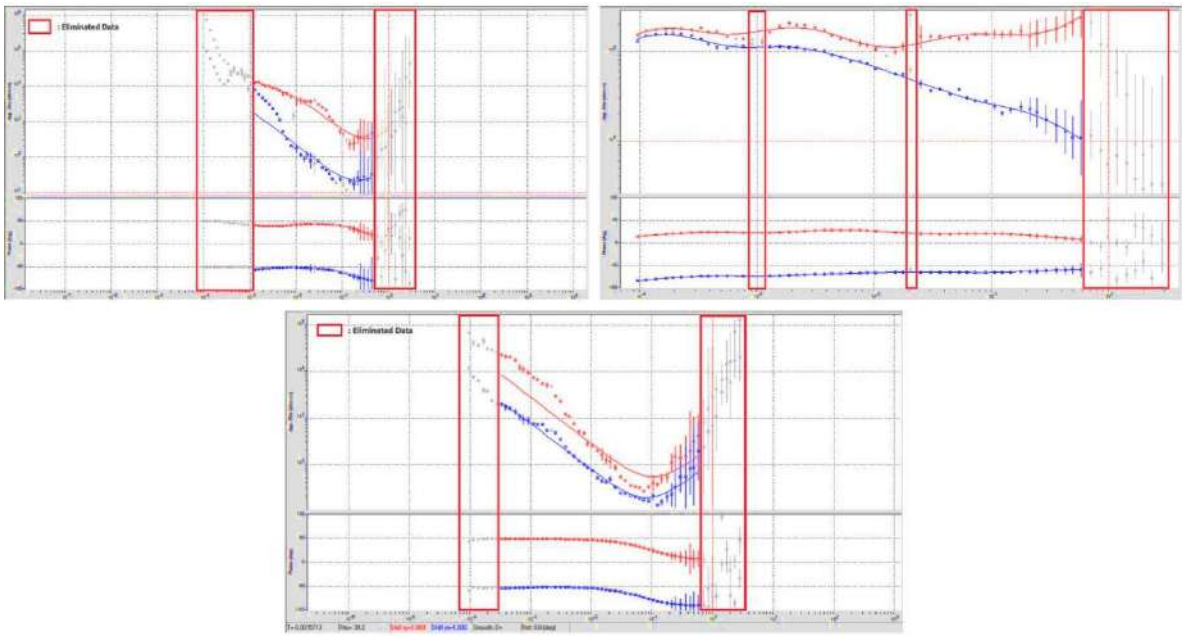

Figure 5. The apparent resistivity and phase curves over period at HR01 (a), HR02 (b) and HR03 (c) showing the elimination of outliers based on curve trend analysis.

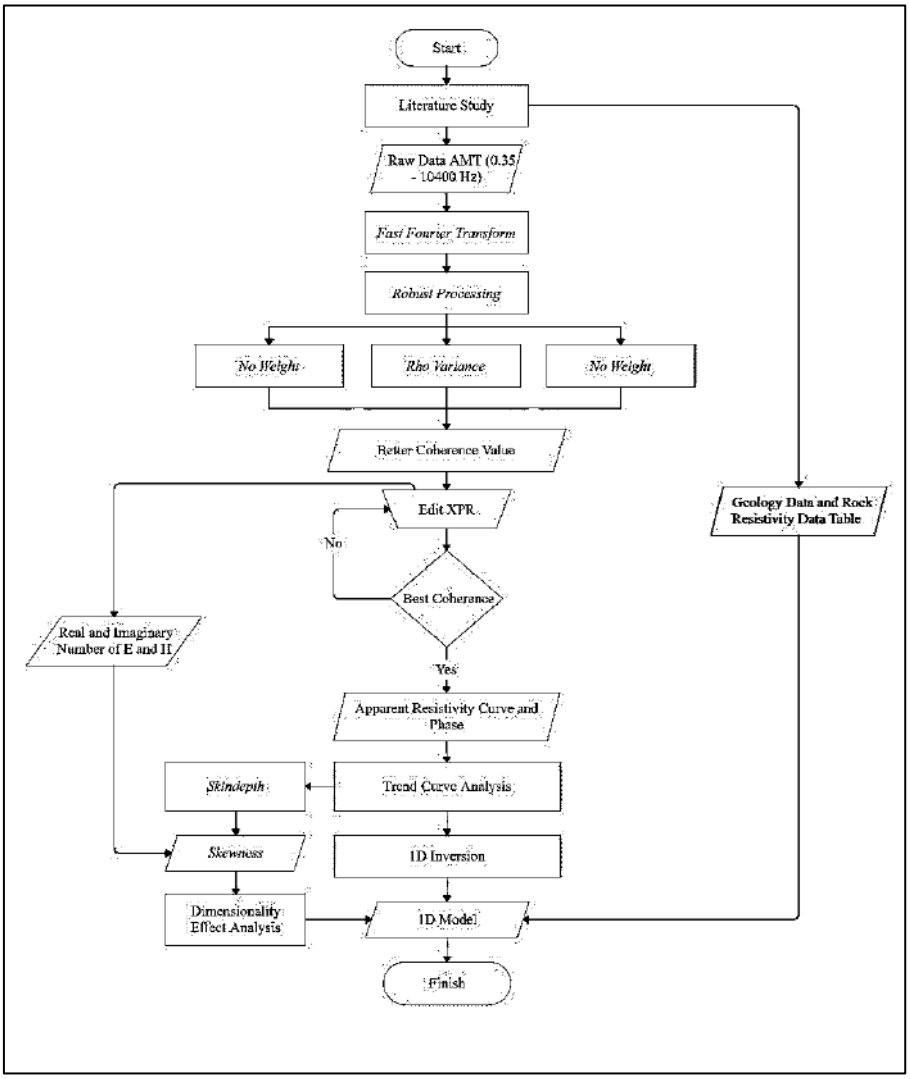

Figure 6. Flow chart from process, data analysis, to 1D modelling (modification from Junursyah et al., 2021; 2023).

Results and Discussion

Data was processed in 1D inversion modelling (Figure 7) using invariant mode (combined mode TE and TM). The analysis and interpretation of 1D modelling results will be correlated with stratigraphic models (Figure 8) regarding the relationship between rock resistivity values in general (Figure 9) and formation unit information on the Geological Map of Garut and Pameungpeuk Quadrangle, Java. According to Figure 8, the increase or decrease in resistivity values as depth increases shows the presence of different lithological formations or arrangements.

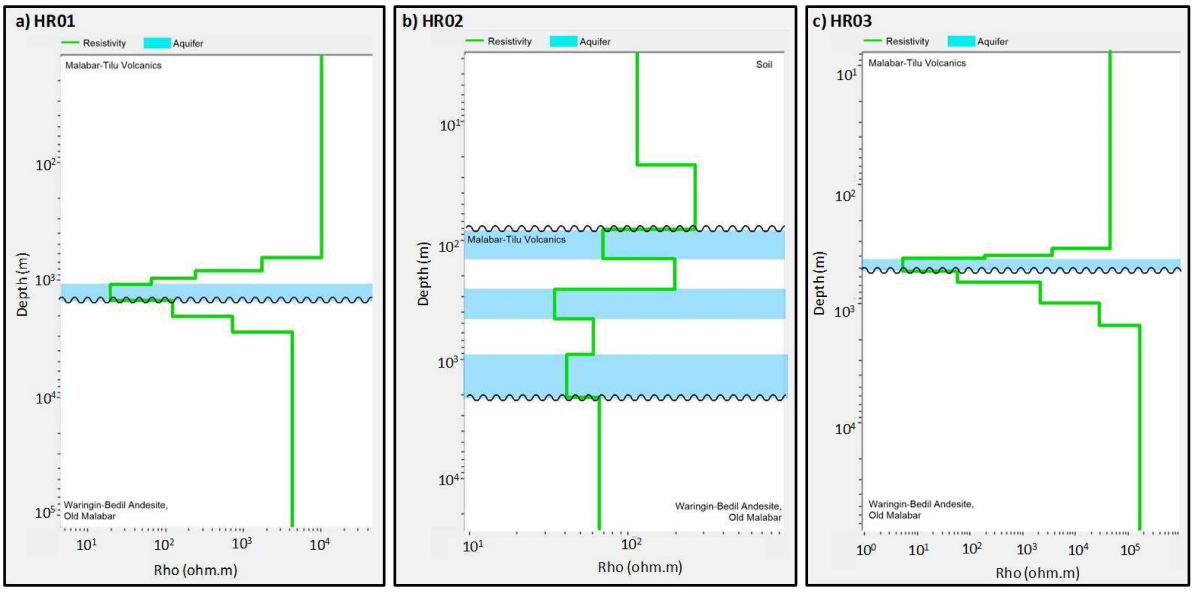

Figure 7. Results of 1D inversion of AMT data at a) HR01, b) HR02, and c) HR03.

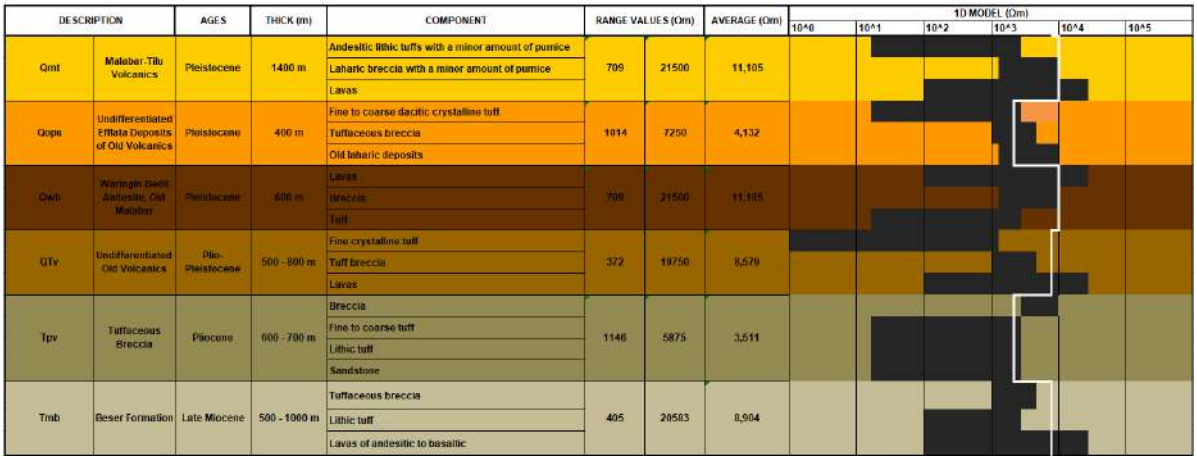

Figure 8. Stratigraphic Model of Haruman Peak, Malabar Mountains Area and Its Surroundings Based on the Range of Rock Resistivity Values in Figure 9 and Formation Information on the Geological Map of Garut and Pameungpeuk Quadrangle, Java.

The results of modelling the 1D resistivity structure shown in Figure 7a., obtained a depth of up to 2704.98 meters with a variation in resistivity values of 19.1 Ωm to 10103.77 Ωm. Layers 1 to 5 decreased resistivity values from 10103.77 Ωm to 19.10 Ωm at a depth of 1464.97 meters. In layers 6-8, the resistivity value reaches 4160.19 Ωm at a depth of >2704.8 meters. When viewed from the change in resistivity value and depth, layers 1 to 5 are predicted as Malabar Tilu Volcanic Rock (Qmt), which overlies the unconformity of Waringin-Bedil Andesite Unit, Old Malabar (Qwb) in layers 6 to 8. Layer 5 has a lower resistivity value and is thought to be

filled with fluid, whereas layers 1-4 and 6-8 have impermeable qualities, as shown by a higher resistivity value than layer 5. The higher the resistivity value, the more massive or dense the rock. Hence, layer 5, at the HR01 has the potential to be an aquifer comprised of tuff-andesite and a minor of pumice. When viewed from the lithological properties and types of water-carrying layers (Kodoatie, 2021), the aquifer at the HR01 is identified as confined aquifer with impermeable upper and lower layers.

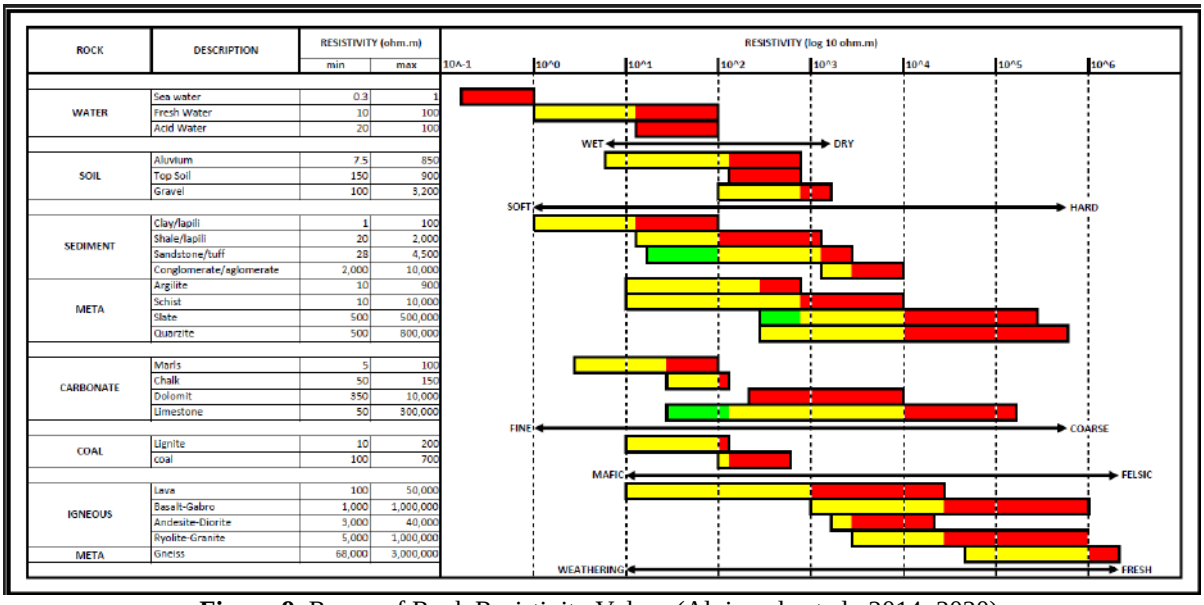

ROCK	DESCRIPTION	RESISTIVITY (ohm.m) min	max
WATER	Sea water	0.3	1
	Fresh Water	10	100
	Acid Water	20	100
SOIL	Aluvium	7.5	850
	Top Soil	150	900
	Gravel	100	3,200
SEDIMENT	Clay/lapili	1	100
	Shale/lapili	20	2,000
	Sandstone/tuff	28	4,500
	Conglomerate/aglomerate	2,000	10,000
META	Argilite	10	900
	Schist	10	10,000
	Slate	500	500,000
	Quarzite	500	800,000
CARBONATE	Marls	5	100
	Chalk	50	150
	Dolomit	350	10,000
	Limestone	50	300,000
COAL	Lignite	10	200
	coal	100	700
IGNEOUS	Lava	100	50,000
	Basalt-Gabro	1,000	1,000,000
	Andesite-Diorite	3,000	40,000
	Ryolite-Granite	5,000	1,000,000
META	Gneiss	68,000	3,000,000

Figure 9. Range of Rock Resistivity Values (Alviyanda et al., 2014; 2020).

Based on Figure 7b., 1D inversion modelling obtained depths of up to 2080.07 meters with variations in resistivity values of 34.2 to 259.31 Ωm. The resistivity value in layers 1 and 2 increased from 114.82 Ωm to 259.31 Ωm at a depth of 80.32 meters. When viewed from the correlation of resistivity values and depth in Figure 8, layers 1 and 2 can be predicted as soil layers formed due to the physical-chemical weathering process of rocks, biological activities of organisms, and a long-term climate (Kalev & Toor, 2018). Different things happen in layers 3 to 8, where resistivity values fluctuate as depth increases. The resistivity value in layer 3 reaches 68.08 Ωm, increases significantly to 195.06 Ωm in layer 4, and decreases sharply to 34.2 Ωm in layer 5. Furthermore, resistivity rises again in layer 6 with a value of 59.94 Ωm but falls back in layer 7 to 40.65 Ωm before finally reaching 65.44 Ωm in layer 8. The resistivity value of rocks that fluctuate with increasing depth illustrates the complexity of the constituent rocks and other contents in each layer. Based on Figure 8, layers 3 to 7 reaching a depth of 2080.07 meters can be predicted as the Malabar-Tilu Volcano Rock Unit (Qmt), which overlies the unconformity Waringin-Bedil Andesite Unit, Old Malabar (Qwb) in layer 8. If there is a drop in resistivity value in layers 3, 5, and 7, this may indicate the possibility of other content, such as fluid, in these layers. Hence, layers 3, 5, and 7 at the HR02 can be said to have the potential to be aquifers composed of tuff-andesite with a minor pumice content. Based on lithological properties and types of water-carrying layers (Kodoatie, 2021), aquifers in layer 3 include *unconfined aquifers*, which have only one watertight boundary layer at the bottom and only groundwater levels at the top (*soil*). The aquifers in layers 5 and 7 are identified as confined aquifers, where the upper and lower layers are impermeable.

The results of modelling the 1D resistivity structure shown in Figure 7c., obtained a depth of up to 1488.83 meters with a variation in resistivity values between 5.25 to 157470 Ωm. Based on the correlation of resistivity and depth values in Figure 8, layers 1–4 are predicted as Malabar Tilu Volcano Rock Unit (Qmt) based on the correlation of resistivity and depth data in Figure 8. These comprised andesitic lithic tuffs with a minor amount of pumice, breccia, and lavas. In addition, layers 5-8 are predicted as Waringin-Bedil Andesite Units, an Old Malabar (Qwb) formation comprised of lavas, breccia, and tuff rocks. Layer 4 has a low resistivity (5.25 Ωm) compared to other layers, indicating it is an aquifer layer comprised of tuff-andesite rock with a minor pumice content. When viewed from the lithological properties and types of water-carrying layers (Kodoatie, 2021), the aquifer at the HR03 is a type of *confined aquifer*.

According to Oktariadi et al. (2021), the Bandung Basin is located between 650 and 700 meters above sea level. Thus, water from aquifers at 140.56 m (HR02), 453.32 m (HR02), and 530.8 m (HR03) are predicted to flow into the Bandung Basin.

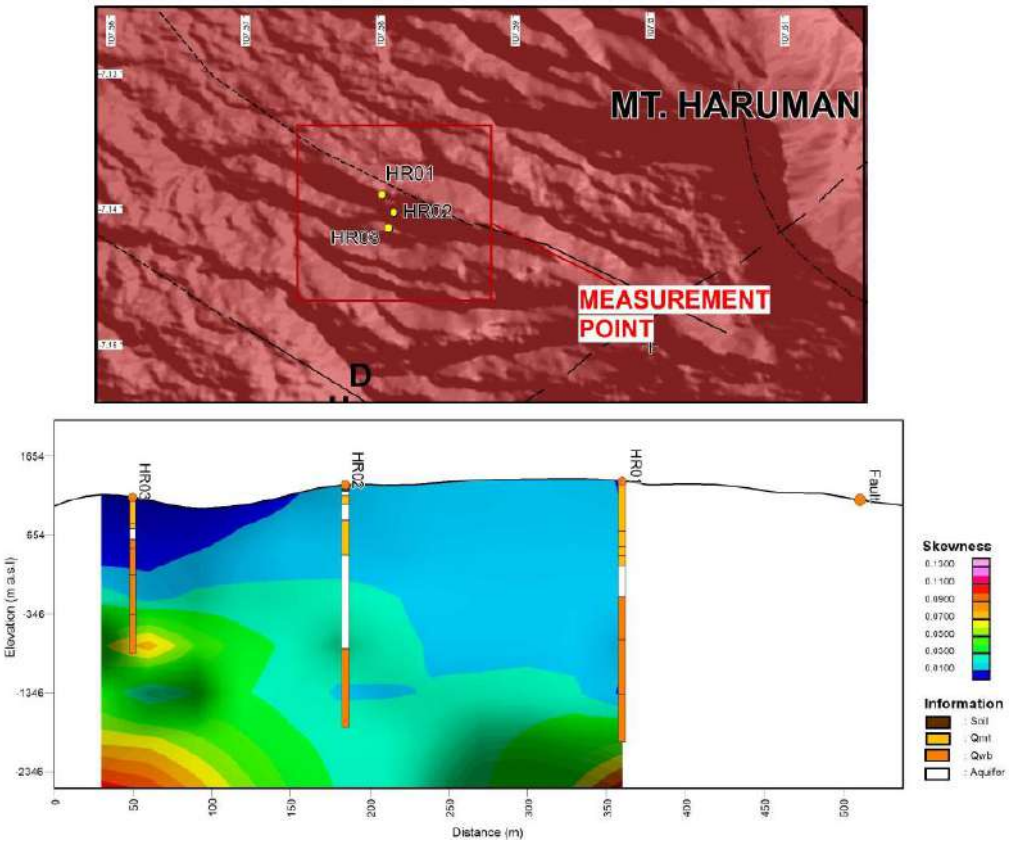

Figure 10. Bahr Skewness Cross-section.

Another step is dimensionality analysis, which aims to clarify the subsurface resistivity structure under research. Based on the results of the dimensionality analysis of AMT data, the Bahr Skew has value variation of 0.01 - 0.13 (Figure 10). The skewness value of the aquifer layer at HR01 ranges from 0.01 - 0.02 (light blue), the aquifer layer at HR02 has two skewness values ranging from 0.01 - 0.02 (light blue) and 0.02 - 0.03 (light green), and the skewness value of the aquifer layer at HR03 ranges from 0 to 0.01 (dark blue). The effect of 3D dimensionality on data is defined by a skewness value (η) > 0.3, while $\eta < 0.3$ implies the 2D dimensionality effect. The ideal condition of 1D-2D *electrical structure* is indicated by $\eta = 0$ (Xiao, 2011). Hence, the aquifer layer in the 1D model interpretation indicates that it is

unaffected by the dimensionality effect. In the skewness cross-section, there is a slight dimensionality effect in the subsurface of measuring points HR01 and HR03. Geological features are thought to be the cause of this; however, it does not affect the surrounding aquifers.

Conclusion

Deep aquifer (confined aquifers) with resistivity values of 5.25 - 40.65 Ωm were identified at depths of 453.32 m (HR02), 530.8 m (HR03), 1464.97 m (HR01), and 2080.07 m (HR02) with lithology in the form of andesite-tuff with minor of pumice. In addition, an unconfined aquifer was also identified at the HR02 point at a depth of 140.56 m with a resistivity value of 68.08 Ωm. Bandung Basin is located between 650 and 700 meters above sea level (m.a.s.l.), and water from aquifers that have an altitude >700 meters above sea level is expected to flow into the Bandung Basin. Water from aquifers located at depths of 140.56 m (HR02), 453.32 m (HR02), and 530.8 m (HR03) has the potential to flow into the Bandung Basin.

Acknowledgements

The author expresses his gratitude to the Geological Survey Center for its role and facilities in the process of acquiring AMT data in Haruman, to M. Riyan Maulana and colleagues for their assistance in completing this research, as well as to the Academic Leadership Grant (ALG) and Unpad Lecturer Competency Research (RKDU) for their support of this research.

Author Contribution

The acquisition process was carried out by all authors with the assistance of the Geological Survey Center and Asep Harja. Data processing was carried out by Nabilah R. and G. M. Lucki Junursyah. All authors discussed, interpreted, and wrote the manuscript.

Conflict of Interest

The authors declare no conflict of interest.

References

Alviyanda, Junursyah, G. M. L, Gumilar, I. S., & Mardiana, U. (2014). Interpretation of Subsurface Structure in Tertiary Sediment Based on Magnetotelluric Data, South Buton area. *Proceedings of the Indonesian Petroleum Association, 38th Annual Convention and Exhibition*, Jakarta.

Alviyanda, Junursyah, G. M. L., & Sumintadireja, P. (2020). Stratigraphic Model of East Biak Based on Magnetotelluric Data. *Journal of Mathematical & Fundamental Sciences*, 52(2), 232–249. https://doi.org/10.5614/j.math.fund.sci.2020.52.2.7

Alzwar, M., Akbar, N., & Bachri, S. (1992). *Peta Geologi Lembar Garut dan Pameungpeuk, Jawa, Skala 1:100.000*. Pusat Penelitian dan Pengembangan Geologi.

Bahr, K. (1991). Geological Noise in Magnetotelluric Data: A Classification of Distortion Types. *Physics of the Earth and Planetary Interiors*, 66(1-2), 24–38. https://doi.org/10.1016/0031-9201(91)90101-M

Cagniard, L. (1953). Basic Theory of the Magneto-Telluric Method of Geophysical Prospecting. *Geophysics*, 18(3), 605–635. https://doi.org/10.1190/1.1437915

Constable, S. C., Parker, R. L., & Constable, C. G. (1987). Occam's Inversion: A Practical Algorithm for Generating Smooth Models from Electromagnetic Sounding Data. *Geophysics*, 52(3), 289–300. https://doi.org/10.1190/1.1442303

Constable, C. (2016). Earth's Electromagnetic Environment. *Surveys in Geophysics*, 37, 27–45.

https://doi.org/10.1007/s10712-015-9351-1

Gomo, M. (2023). Use of Electric Potential Difference in Audio Magnetotelluric (AMT) Geophysics for Groundwater Exploration. *Groundwater for Sustainable Development*, 20, 100864. https://doi.org/10.1016/j.gsd.2022.100864

Harja, A., Ma'arif M., F. R., Nanda, M. D., Duvanovsky, D. A., Tangke, R., Shafa, Z. I., Fillsani, S., Gunawan, I., & Susanto, K. (2021). Studi Hidrogeofisika Gunung Malabar Sebagai Gunung Tertinggi pada Sistem Hidrologi Cekungan Bandung. *Jurnal Geologi dan Sumberdaya Mineral*, 22(4), 223–230. https://doi.org/10.33332/jgsm.geologi.v22i4.654

Harja, A., Aprilia, B. A., Susanto, K., & Fitriani, D. (2023). Identifikasi Zona Akuifer Menggunakan Metode Resistivitas-DC di Daerah Kipas Lava Pegunungan Malabar Kabupaten Bandung Jawa-Barat. *JIIF (Jurnal Ilmu dan Inovasi Fisika)*, 7(1), 49–57. https://doi.org/10.24198/jiif.v7i1.43216

Hidayat, H. Setiawan, J. J., Ibrahim, A., Marjiyono, M., & Junursyah, G. M. L. (2021). Studi Magnetotelurik (MT) Untuk Mendelineasi Potensi Regional Gas Serpih bawah Permukaan Berdasarkan properti Tahanan Jenis di Cekungan Kutai, Kalimantan Timur. *Jurnal Geologi Dan Sumberdaya Mineral*, 22(2), 107–114. https://doi.org/10.33332/jgsm.geologi.v22i2.571

Junursyah, G. M. L., Prabowo, A., & Hidayat, W. (2020). Analisis Kualitas Data Magnetotelurik Berdasarkan Parameter Koherensi Studi Kasus: Data Magnetotelurik Di Daerah Bandung, Jawa Barat. *Jurnal Mineral Energi dan Lingkungan*, 4(2). 78–83. https://doi.org/10.31315/jmel.v4i2.3679

Junursyah, G. M. L., Amalia, T. D. A., Hidayat., Rizkika, O., Marjiyono, M., & Handyarso, A. (2021). Optimasi Kualitas Data Magnetotelurik di Daerah Singkawang dan Sekitarnya Berdasarkan Analisis Koherensi. *Publikasi Khusus Geosains Laboratorium dan Sarana Penyelidikan*, 69–86.

Junursyah, G. M. L., Parlindungan, E., Hidayat, H., & Harja, A. (2022). Reduksi Efek Dimensionalitas 3D pada Data Magnetotelurik Menggunakan Analisis Koherensi, Tren Kurva, dan Skin Depth: Studi Kasus di Pulau Yapen Bagian Selatan dan Sekitarnya, Papua. *Jurnal Geologi dan Sumberdaya Mineral*, 23(4), 247–255. https://doi.org/10.33332/jgsm.geologi.v23i4.712

Junursyah, G. M. L, Fauzhy, M. A., Hidayat, & Harja, A. (2023). Reduksi Efek Dimensionalitas 3D Berdasarkan Analisis Koherensi Pada Data Magnetotelurik Di Daerah Bandung Bagian Timur. *Publikasi Laboratorium dan Sarana Penyelidikan*, 49–60.

Kalev, S. D., & Toor, G. S. (2018). The composition of soils and sediments. *Green Chemistry* (pp. 339–357). Elsevier. https://doi.org/10.1016/B978-0-12-809270-5.00014-5

Keegan-Treloar, R., Irvine, D. J., Solórzano-Rivas, S. C., Werner, A. D., Banks, E. W., & Currell, M. J. (2022). Fault-controlled springs: A review. *Earth-Science Reviews*, 230, 104058. https://doi.org/10.1016/j.earscirev.2022.104058

Kodoatie, R. J. (2021). *Tata Ruang Air Tanah.* Penerbit Andi.

Kurniawan, O., Surya, R. D., & Wargaliyasa, G. (2022). Analisis Fault Fracture Density pada Potensi Panas Bumi NonVulkanik untuk Menentukan Recharge Area; Studi Kasus di Wilayah Lore Lindu, Sulawesi Tengah. *Jurnal Ilmiah*

Geomatika, 2(2), 45–53. https://doi.org/10.31315/imagi.v2i2.9417

Kurniawan, R., Ardi, N. D., & Hidayat, H. (2019). Analisis Penampang Resistivitas 2D Metode Magnetotellurik dan Audio-magnetotellurik Untuk Mengetahui Sistem Petroleum Pada Cekungan Singkawang. *Wahana Fisika*, 4(2), 81–88. https://doi.org/10.17509/wafi.v4i2.21869

Li, J., Wang, W., Cheng, D., Li, Y., Wu, P., & Huang, X. (2021). Hydrogeological Structure Modelling Based on An Integrated Approach Using Multi-Source Data. *Journal of Hydrology*, 600, 126435. https://doi.org/10.1016/j.jhydrol.2021.126435

Montahaei, M. (2022). Audio-Magnetotelluric Modeling for 2D Characterization of Shallow Sedimentary Basins and Groundwater System in Central Zagros, Iran. *Pure and Applied Geophysics*, 179(12), 4567–4594. https://doi.org/10.1007/s00024-022-03181-y

Oktariadi, O., Kasbani, K., & Memed, M. W. (2021). *Geologi Lingkungan Cekungan Bandung*. Badan Geologi.

Pranata, E., Irawati, S. M., & Niasari, S. W. (2017). Magnetotelluric Data Analysis using Swift Skew, Bahr Skew, Polar Diagram, and Phase Tensor: A Case Study in Yellowstone, US. *Proceedings of the Pakistan Academy of Sciences*, 54(3), 311–317. https://www.paspk.org/wp-content/uploads/2017/09/Magnetotelluric-Data-Analysis.pdf

Suhari, S., & Siebenhüner, M. (1993). Environmental geology for land use and regional planning in the Bandung Basin, West Java, Indonesia. *Journal of Southeast Asian Earth Sciences*, 8(1–4), 557–566. https://doi.org/10.1016/0743-9547(93)90053-R

Tripathi, A., Shalivahan, S. S., Bage, A. K., Singh, S., & Yadav, P. K. (2019). Audio-Magnetotelluric Investigation of Bakreswar Geothermal Province, Eastern India. *Journal of Earth System Science*, 128, 102. https://doi.org/10.1007/s12040-019-1115-8

Wu, Q., Li, Y.-B, Mi, H.-Z, Wang, G., & Zhang, Z.-Y. (2023). Simulation and Observations of Audio Magnetotelluric Measurements over Water-Covered Areas. *Minerals*, 13(8), 990. https://doi.org/10.3390/min13080990

Xiao, Q., Cai, X., Liang, G., Xu, X., & Zhang, B. (2011). Application of 2D Magnetotelluric Methods in a Geological Complex Area, Xinjiang, China. *Journal of Applied Geophysics*, 75, 19–30. https://doi.org/10.1016/j.jappgeo.2011.06.007

Xu, Z., Li, G., Xin, H., Tang, J., & Lv, F. (2020). Hydrogeological Prospecting in the Da Qaidam Area of the Qaidam Basin Using the Audio-Frequency Magnetotelluric Method. *Journal of Applied Geophysics*, 182, 104179. https://doi.org/10.1016/j.jappgeo.2020.104179

Xu, Z., Xin, H., Weng, Y., & Li, G. (2023). Hydrogeological Study in Tongchuan City Using the Audio-Frequency Magnetotelluric Method. *Magnetochemistry*, 9(1), 32. https://doi.org/10.3390/magnetochemistry9010032

Zaher, M. A., Younis, A., Shaaban, H., & Mohamaden, M. I. I. (2021). Integration of Geophysical Methods for Groundwater Exploration: A Case Study of El Sheikh Marzouq Area, Farafra Oasis, Egypt. *The Egyptian Journal of Aquatic Research*, 47(2), 239–244. https://doi.org/10.1016/j.ejar.2021.03.001

ISSN: 2579-5821 (Print)
ISSN: 2579-5546 (Online)
URL address: http://journal.unhas.ac.id/index.php/geocelebes
DOI: 10.20956/geocelebes.v8i1.33887

Jurnal Geocelebes Vol. 8 No. 1, April 2024, 83 – 97

Regional Lineament Pattern and Morphotectonic Analysis: The Investigation of Geological Structures and Present-Time Relative Tectonic Activity in the Tin Granite Area of Belitung Island, Indonesia

Harnanti Y. Hutami[1]*, Nur Ayu Anas[2], Erlangga I. Fattah[1]

[1]Geophysical Engineering Department, Faculty of Industry and Technology, Institut Teknologi Sumatera 35365, Indonesia
[2]Geological Engineering Department, Universitas Cendrawasih, Papua, Indonesia

*Corresponding author. Email: harnanti.hutami@tg.itera.ac.id

Manuscript received: 14 March 2024; Received in revised form: 24 April 2024; Accepted: 28 April 2024

Abstract

Belitung Island is located on the East Coast of Sumatra and is the southernmost extension of the Southeast Asian granite belt. Despite the flat terrain of the island, numerous granite outcrops provide insight into the past tectonic activities that caused the uplift in the region. This study analyzes the current state of Belitung's tectonic activity by examining its morphotectonic index and lineament pattern. A National Digital Elevation Model (DEMNAS) dataset with a resolution of up to 8.1 m will be used to assess the geological patterns and relative tectonic activity from the surface. The relationship between the regional lineament system and morphotectonic quantification throughout the landforms of Belitung Island will also be considered. The modified Segmented Tracing Algorithm (m-STA) technique extracted the lineament features. The Index of Relative Active Tectonic (IATR) was calculated by averaging several morphotectonic indices, such as asymmetry factors (AF), stream-length index (SL), mountain-front sinuosity (Smf), and valley floor width-height ratio (VF) factors, to quantify the relative tectonic activity of the area. The combination of the two methods shows that Belitung is currently experiencing relatively weak tectonic activity compared to the past. This is supported by the surface appearance, which is mainly composed of lowlands. Several granite outcrops and highlands are aligned along the NW-SE and NE-SW directions, corresponding to the main geological structures in the area.

Keywords: lineament; morphotectonic index; relative tectonic activity; structural geology.

Citation: Hutami, H. Y., Anas, N. A., and Fattah, E. I. (2024). Regional Lineament Pattern and Morphotectonic Analysis: The Investigation of Geological Structures and Present-Time Relative Tectonic Activity in the Tin Granite Area of Belitung Island, Indonesia. *Jurnal Geocelebes*, 8(1): 83–97, doi: 10.20956/geocelebes.v8i1.33887

Introduction

Earth's surface morphology reflects the interaction between the rock and its geomorphological processes (Bishop, 2007). This concept has been one of the early targets for a better understanding of topographic features at the Earth's surface geological processes (Goudie, 2004). The attributes upon the Earth's surface have all the profound significance of their present and earlier chapters' conditions. A reciprocal relationship between tectonic activity and the geomorphological response of Earth's surface allows us to evaluate current deformation processes due to the geological structures within the region (Goudie, 2004; Laake, 2022).

The interpretation of remote sensing data helps evaluate the geometry and landform variation of the earth's surface, which implies the structural, depositional, and erosional aspects (Laake, 2022). The continuously modified landforms are quantified using a set of geomorphic indices and are directly related to the active tectonic deformation (Zhazhalayi & Surdashy, 2022).

Despite the thickness of the sedimentary cover, lineaments are initially described as significant lines in the earth's face and later concluded as lines in the landscape that reveal the hidden architecture of the deep layers of rocks (Florinsky, 2016). The concept delineates geological lineaments, such as lithological boundaries, faults, fractures, and joints, caused by tectonic activities and geomorphological processes in terms of topographical lineaments (Ahmadi & Pekkan, 2021).

Belitung is located on the East Coast of Sumatra and is recognized as the southernmost continuation of the Southeast Asian granite belt through which the Bentong-Raub suture extends from Peninsular Malaysia. However, the extent of the suture extension is still not identified in this area due to a lack of supporting data (Wang et al., 2021; Zhang et al., 2023). Zhang et al. (2023) conducted a study on the correlation of the Bentong-Raub suture in the Bangka-Belitung Islands using information on granitic rocks and their ages to investigate this. Wang et al. (2021) estimated the types of granite distributed along the suture line, including Bangka and Belitung. They obtained their results using U-Pb geochronological, petrologic, elemental, and Sr-Nd-Pb-Hf isotopic studies. The findings indicate that the granite types found in the Bangka Belitung Islands belong to the Main Range Granite Province. Some granitoid formations on Belitung Island include Tanjungpandan Granite, Baginda Adamelite, Burungmand Granodiorite, and Batubesi Granite. Each of these formations is believed to have formed during different tectonic phases based on the mineral elements present in them (Lehmann & Harmanto, 1990).

A comprehensive investigation was conducted to unveil the tectonic evolution of Belitung Island. The study relied on the analysis of geochemical and petrographic data. The findings revealed that the Tanjungpandan and Batubesi granites were formed during the syn-collision period between the Sibumasu and Indochina plates in the Late Triassic era. Conversely, the Baginda Adamelite and Burungmandi Granodiorite were formed during the post-collision tectonic phase that persisted until the Early Cretaceous period (Baharuddin & Sidarto, 1995). The Tanjungpandan granite outcrop area features a distinctive terrain shaped by morphotectonics, influenced by the underlying geological structure and tectonic movements. The lofty hills and scattered boulders within the formation offer evidence for this phenomenon. Concerning geomorphology analysis in granitic zones, a quantitative morphometric and morphotectonic analysis was carried out on river drains within moderately elevated granitic terrain and low-lying alluvium country. This revealed that the type of lithology and rock resistance affects the deformation of granitic terrain, as sedimentary rocks are more deformed than granitic rocks (Bhatt et al., 2020; Manjare, 2020).

Belitung Island is commonly classified as part of Sumatra Island, which has a history of tectonic activity due to the Sumatran Fault Systems and the closure of the Paleotethys Sea that led to the formation of the Bentong-Raub suture. Despite the island's relatively flat terrain, numerous granite outcrops offer a fascinating glimpse into the past tectonic activities that caused the granitoid uplift in the region. Additionally, the geological structures associated with the Sumatran faults system and Bentong-Raub suture may have intersected with the region, resulting in landform variations. As depicted in Figure 1, the area's higher terrain aligns with the main structures' NW-SE and NE-SW trends.

The area's geological formations and recent tectonic movements have yet to be analyzed in-depth. Although surface traces are not well-preserved, we believe past geological structures and tectonic episodes are

responsible for landform variation. The shrinkage of granite and the elevated topographic section at the center of the area are significant indicators of these changes. It is vital to develop approaches that can provide an initial estimate of potential geological structures that influence the landform changes up to the present time. This study aims to delve into the current state of Belitung's tectonic activity, analyzing its morphotectonic index and lineament pattern to gain insights into the related structural geology. The results of this analysis will provide valuable information to better understand the area's geological structures and landform changes.

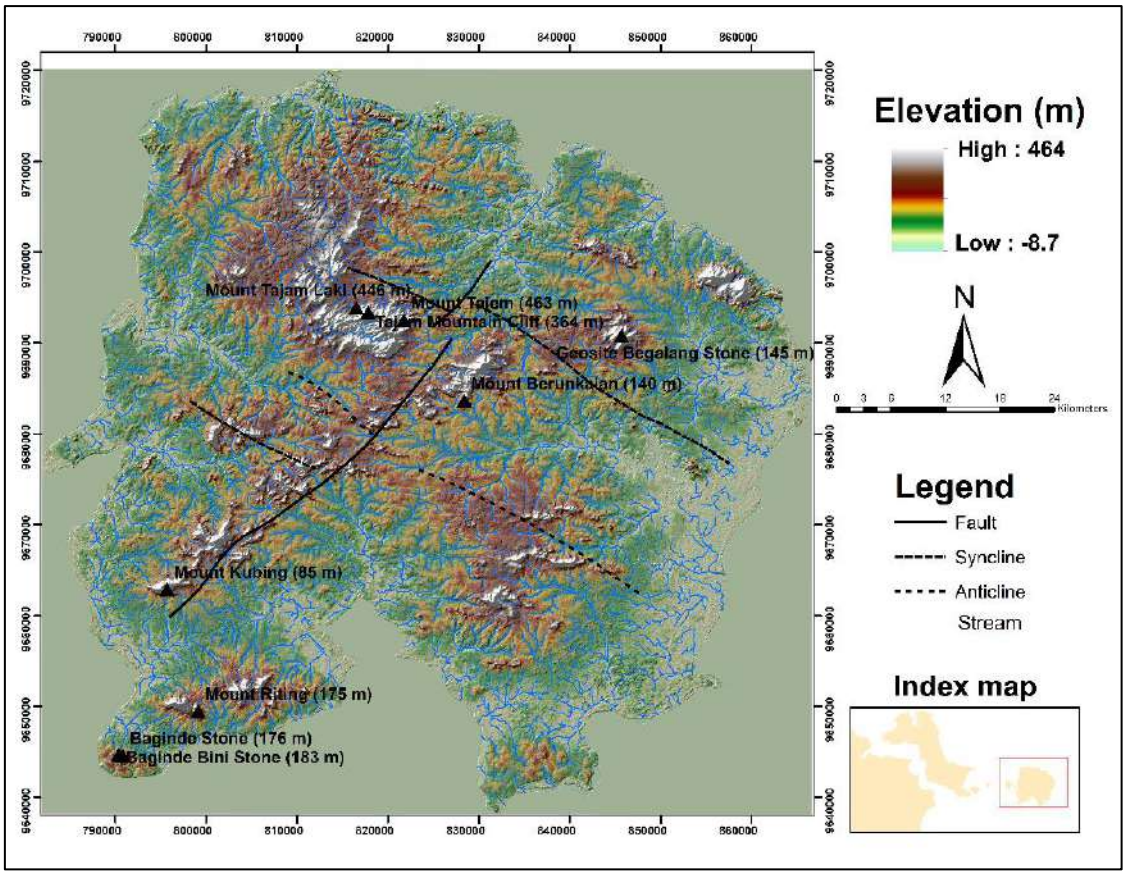

Figure 1. The map shows the variations of topographic levels in the study area.

Geology summary of the study area

Previous investigations have shown that the tectonic evolution of the Bangka-Belitung islands, to which Belitung belongs, has been influenced by the movement of the continental crust of the Sunda Shelf during oroclinal bending. Belitung Island's tectonic activity has significantly shaped its current morphological conditions (Zahirovic et al., 2014). In the Middle Triassic - Early Jurassic, magmatism formed granitoid spread along the western part of the Bukit Barisan and the Tin Islands (Bangka-Belitung Islands). The granitoid originated had an absolute age of around 250 - 143 million years with an average age of approximately 220 million years with the formation of the tectonic order, including post-collision (Cobbing et al., 1986). The peak of magmatism in Peninsular Malaysia and the Tin Islands is at 220 million years, with the emergence of older granitoid in the Tin Islands (Barber & Crow, 2009; Cobbing et al., 1986; Lehmann & Harmanto, 1990).

The tectonic process on Belitung Island began with flysch sedimentary deposits from the Kelapakampit Formation (PCKs)

and the collision that formed the Siantu Formation (PCsv) in the form of alkaline igneous rock (lava) and breccias during the Permian-Carbonaferous periods. The main magmatism activity occurred during the Triassic-Cenozoic periods. The formation of horst and graben parallel to the orogenic axis within this period happened due to a collision between the Sibumasu-Gondwana and Indochina blocks. This extensional tectonic arrangement led to the formation of the granite Main Range Province and Eastern Province in the Southeast Asian granite belt (Ng et al., 2017; Usman, 2016).

The recorded magmatism processes on Belitung Island are associated with the appearance of the Tanjung Pandan Granite Formation (Trtg), which contains primary cassiterite in the Triassic. The Tanjung Pandan granites in the northwest corner of Belitung Island is the largest igneous intrusion outcropped area consisting mainly of biotite granite, with a separate, minor quartz syenite sub-unit (Lehmann & Harmanto, 1990). The granite intrusion episodes had succeeded in breaking through sedimentary rocks, producing fractures in granite. In the Early Jurassic, the magmatic process was still ongoing and made the Adamelite Baginda (Jma) intrusion, which did not contain cassiterite.

The last magmatic process occurred in the Late Cretaceous, marked by diorite of Batubesi Formation (Kbd) and granodiorite of Burungmandi Formation (Kbg) intrusion. In the Late Cretaceous to the Quaternary, the dominant methods are erosion and deposition, which produce sand-carbonate deposits (Qpk) and alluvium (Qa) (Baharuddin & Sidarto, 1995). Structures that occurred in this area are folds, faults, joints, and lineaments. The direction of axial folds is NW-SE, and the faults are trending NE-SW (Baharuddin and Sidarto, 1995).

Materials and Methods

We aim to employ a National Digital Elevation Model (DEMNAS) dataset with a resolution of up to 8,1 m to assess the geological patterns and relative tectonic activity from the surface while considering the relationship of the regional lineament system and morphotectonic quantification throughout the entire landforms of the Belitung Island.

Linear features extraction

We utilized remotely sensed data from the National Digital Elevation Model (DEMNAS) and geological maps of Belitung Island (1:250,000) to analyse the tectonic impacts and structural trends of the nineteen sub-watersheds of the interest area.

This study employed a modified Segmented Tracing Algorithm (m-STA) to extract geological linear features more accurately and efficiently. The m-STA is a highly sensitive and effective tool that leverages SAR backscattering intensity images to detect lines from pixels read as vector elements by analyzing local variations in the gray level of digital numbers (Army & Saepuloh, 2020; Saepuloh et al., 2018). The main objective of this approach was to identify surface geological structures by taking advantage of the dual orbit mode of Sentinel-1. To this end, backscattering intensity images of Phased Array type-L Synthetic Aperture Radar (PALSAR) from the Advanced Land Observing Satellite (ALOS) were also utilized, as detailed in Table 1. The dual orbit mode, comprising the ascending and descending modes, is illustrated in Figure 2.

Table 1. Information of data utilized for lineament extraction.

Orbital Modes	Data	Acquired Time	Polarisation
Ascending	ALOS PALSAR	6 November 2010	HH/HV
Descending	Sentinel 1-A	7 November 2022	VV/VH

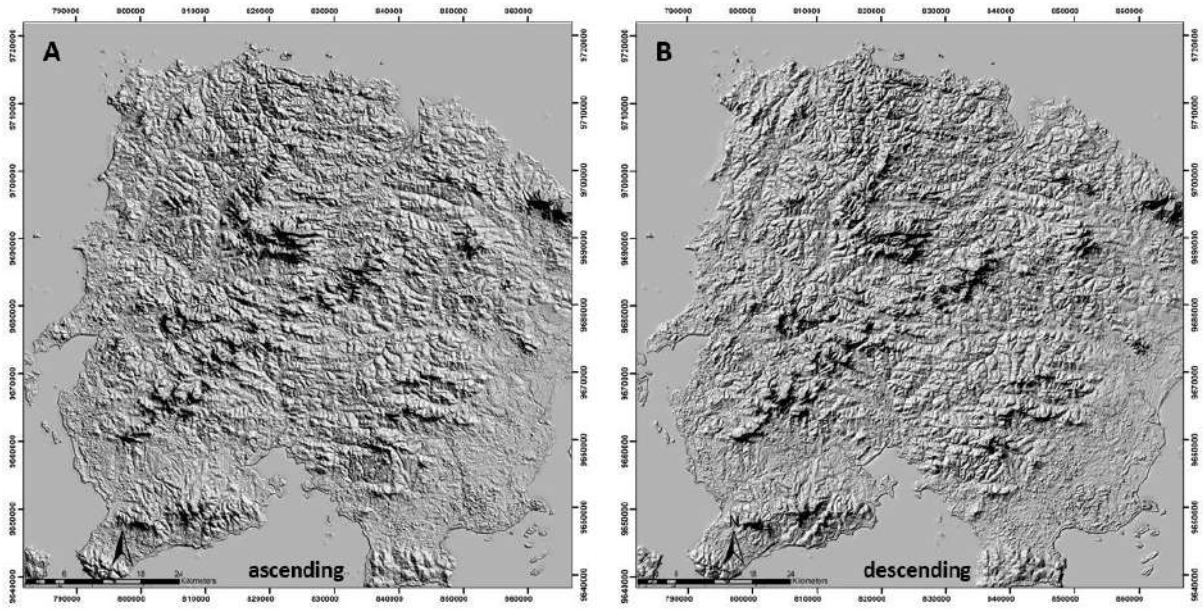

Figure 2. The dual orbital mode of ascending (A) and descending (B) for the study area with the detailed information listed in Table 1.

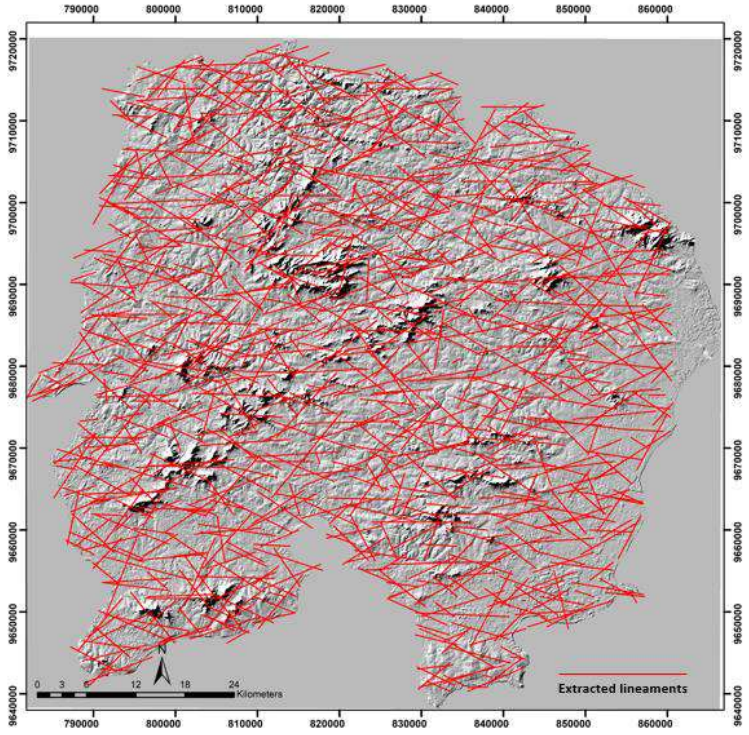

Figure 3. The extracted lineaments for the combined dual orbital modes of the study area.

This study used an automated process to extract lineaments from ascending and descending images, according to Saepuloh et al. (2018). The process had two main steps. The first step involved preparing the images through three stages: multi-looking, speckle filtering, and geometric correction. Multi-looking helped to increase the focus without sacrificing resolution, speckle filtering minimized noise from surrounding objects, and geometric correction corrected any distortions caused by topographic variations or radar inclination. These steps were crucial for the m-STA application.

The second step involved identifying line elements by examining local variation along 16 directions, with 11.25° intervals within a small 11 x 11 pixels window size. This was done by following the principle of STA. The segments were then transformed into a lineament by selecting a search ellipsoid window along a target segment whose start and middle points were inside the window with angle differences from the segment less than 11.25°. Segments that only had endpoints inside the window were excluded. The window size was determined by considering the agreement of the lineaments and major fault lengths in the study area.

Finally, one line was defined as a lineament by approximating the coordinates of the start and end points of the selected segments using the least squares method. The lineaments from the ascending and descending mode images were merged, and the overlaps were grouped into one line using the least square method, as shown in Figure 3.

Morphotectonic index quantification

The morphotectonic variables were calculated using each equation in Table 2, and our geomorphological analysis was grouped into two categories: drainage basin-based and mountain front-based: the drainage basin-based analysis calculated asymmetry factors (AF) and stream-length index (SL). In contrast, the mountain front-based analysis included mountain-front sinuosity (Smf) and valley floor width-height ratio (VF) factors.

The Asymmetry Factor (AF) Index is used to assess whether there is tectonic tilting at the scale of a drainage basin. The index values are most effective when applied to drainage basins with the same underlying rock type if neither lithologic controls nor localized climate affects the level of asymmetry (Green, 1997), which was calculated using Equation 2.

The SL index is calculated (Equation 3) to analyze the relationship between episodes of tectonic activity, which relatively changes the slope gradient and length of streams, rock resistance to erosion processes, and thus the study area's surface topography (Kumar et al., 2022).

The VF index differentiates between the broader-floored canyons of U-shaped valleys with higher VF and the relatively lower values of VF, which indicates the V-shaped valleys. The U-shaped valleys are associated with slower tectonic and uplift activities so that the streams may cut broad the valley floors. Low VF values reflect the more profound valleys with streams actively incising and commonly associated with the uplift. Each VF value throughout the segmented sub-watersheds is calculated using Equation 4 from Table 2 to get detailed values of VF.

Tectonic activity, which is mainly horizontal crustal movement, causes deformation in the Earth's surface, resulting in the formation of mountains. The shape of a mountain face can indicate the type of tectonic activity occurring in a particular area. For instance, mountain faces in regions with primarily compressive tectonic activity tend to be relatively straight. Conversely, mountain faces are often more winding or curved in areas with extensional tectonic activity. This is because extensional activity leads to the formation of valleys and depressions between mountain ranges, which can result in undulating or tortuous mountain faces (Eleni et al., 2015; Partabian et al., 2016).

Mountain Front Sinuosity (Smf) is an index used in morphotectonics to understand the geomorphological processes that lead to the formation of mountain faces. The index is a ratio of the mountain front length along the mountain's foot (Lmf) to the straight-line distance of the mountain front (Ls). The lower values of Smf, associated with the active tectonic and uplift, are shown as

straight mountain fronts. If this uplift rate ceases, the erosional processes tend to be more dominant and carve irregular mountain fronts, presented by the relatively higher value of Smf.

These indices have been proven to be effective tools in examining landform processes due to tectonic implications (Andrifa et al., 2021; Eleni et al., 2015; Gentana et al., 2018; Gupta et al., 2022; Shiran et al., 2020).

Table 2. The morphotectonic parameters to evaluate the relative tectonics of Belitung Island, Indonesia.

Morphotectonic indicators	Mathematical expression	Class ranges adopted in the study	References
Asymmetry factor (AF)	$AF = \left({}^{Ar}/_{At}\right) \times 100$ **(1)**	**Class 1** (high tilting): AF>65 or AF<35 **Class 2** (moderate tilting): 57<AF<65 or 35<AF<43 **Class 3** (low tilting): 43<AF<57	(Eleni et al., 2015; Green, 1997; Luirei et al., 2021; Partabian et al., 2016)
Stream-length gradient index (SL)	$SL = \left({}^{\Delta h}/_{\Delta l}\right) \times L$ **(2)**	**Class 1** (high active tectonic): SL > 500 **Class 2** (moderately active tectonic): 300 < SL < 500 **Class 3** (low active tectonic): SL < 300	
Mountain-front sinuosity (Smf)	$Smf = {}^{Lmf}/_{Ls}$ **(3)**	**Class 1** (active tectonic): Smf 1.2-1.6 **Class 2** (intermediate-to-low active tectonic): Smf 1.8-3.4 **Class 3** (tectonic inactive): Smf 2.0-7.0	
Valley floor width-height ratio (VF)	$Vf = \frac{(2 \times V_{fw})}{[(E_{ld} - E_{sc}) + (E_{rd} - E_{sc})]}$ **(4)**	**Class 1** (highly uplifted with V-shaped valley): Vf < 0,5 **Class 2** (moderately uplifted): Vf 0.5-1 **Class 3** (lowly uplifted with a U-shaped valley): Vf >1	

Results

Geological lineament pattern

The depicted rosette diagram in Figure 4 shows that linear surface features in the study area have at least three preferred orientations: NW-SE, NE-SW, and relatively E-W and ESE-WNW. The first two trends agreed with the direction of existing faults and folds mapped in the same direction, indicating synthetic and antithetic strike-slip faults developed within the study area (Baharuddin & Sidarto, 1995). However, the WSW-ENE axis pattern obtained from this study hypothetically informs us of a new pattern in the island region, which is presumed to be related to the extension of the Bentong-Raub suture.

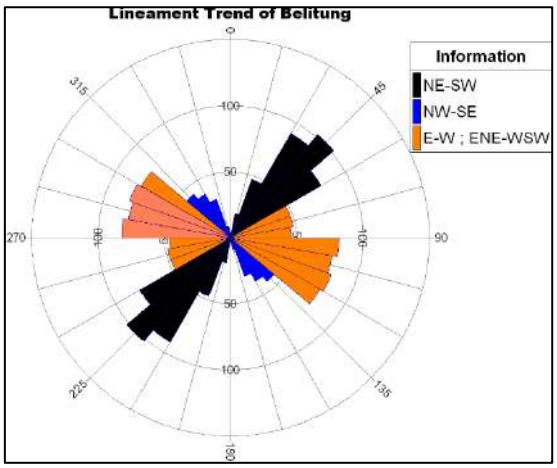

Figure 4. Rosette diagram showing linear surface trends of geological features identified from the lineament extraction.

Response of the morphological indicators regarding tectonic activity

According to the Smf values calculated for the 19 sub-watersheds (as seen in Figure 5), Belitung falls under the category of "Inactive Tectonics" with values ranging from 2–7, while the remaining sub-watersheds indicating lower-to-moderate category with values ranging from 1.8 – 3.4. Additionally, the Asymmetry Factor (AF) was calculated to determine the degree of slope or asymmetry of geological features, and it revealed that each correlated formation in Belitung falls under a different class. The higher tectonic class category is represented by sub-watersheds (1), (5), (16), and (18), with AF values ranging from 30-55. In contrast, other sub-watersheds have been classified under moderate and lower tectonic classes, represented by classes 2 and 3, respectively. The overall results of the AF and Smf value calculations are presented in Table 3.

The stream length gradient (SL) index is another factor when assessing tectonic activity. It examines the relationship between the geological structure and the shape of the drainage network. Generally, higher SL values in an area indicate an uplift marked by steeper slopes and faster river flow. Conversely, lower SL values suggest a more stable landscape with slower water transport. Belitung's SL values for 15 sub-watersheds fall into class 2, including sub-watersheds (1), (2), (3), (7), (8), (10), (16), (17), (18), and (19), while the other five belong to tectonic class 3 (Figure 6A).

The VF factor is crucial for identifying active tectonic activity in each area. This is based on the type and amount of tectonic activity. Figure 6B provided the VF value for each sub-watershed segment, and the spatial distribution shows the average result. The VF values in the Belitung area fall into three intervals: 2,286-17,175 (interval 1), 17,176-32,066 (interval 2), and 32,006-46,957 (interval 3). According to the reference, Belitung has a low uplift level (class 3), with a predominantly U-shaped valley.

Next up for analysis is averaging the Smf, AF, VF, and SL values for all sub-watersheds, which is the Index of Active Tectonic Relative (IATR). This index represents a summary and average of the given geomorphic indices which are used in the study and can be obtained using the equation:

$$IATR = S/N \quad (5)$$

S represents the sum of previous indices, and N represents the number of selected indices. This IATR quantified the active tectonic relative throughout the study area in terms of their classifications (Mahmood & Gloaguen, 2012). The values of the index were divided into four classes to define the degree of active tectonics: Class 1—very high ($1.0 \leq IATR < 1.5$); Class 2—high ($1.5 \leq IATR < 2.0$); Class 3—moderate ($2.0 \leq IATR < 2.5$); and Class 4—low ($2.5 \leq IATR$) (Gentana et al., 2018; Green, 1997).

This technique has been applied to several objectives, such as identifying the geomorphic indices changes within the fault system with the most seismic and motional potential (Eynoddin et al., 2017), the tectonic activity along the uplifted anticline zones that has resulted in various surface landforms (Othman & Omar, 2023; Partabian et al., 2016), and from the regional Indonesia area was the assessment for developing geological disaster-based area in Karangsambung geopark (Hidayat et al., 2023). These resulted in proper analysis that higher IATR corresponded to the higher impacted tectonic activity or most changed landforms, such as uplifted land, fault/ fracture traces, etc., in the study area (Figure 7).

Table 4 provides the IATR values for each sub-watershed in Belitung, which falls into the tectonic class 3 and 4 categories, suggesting a relatively low to medium level of tectonic activity in the present time.

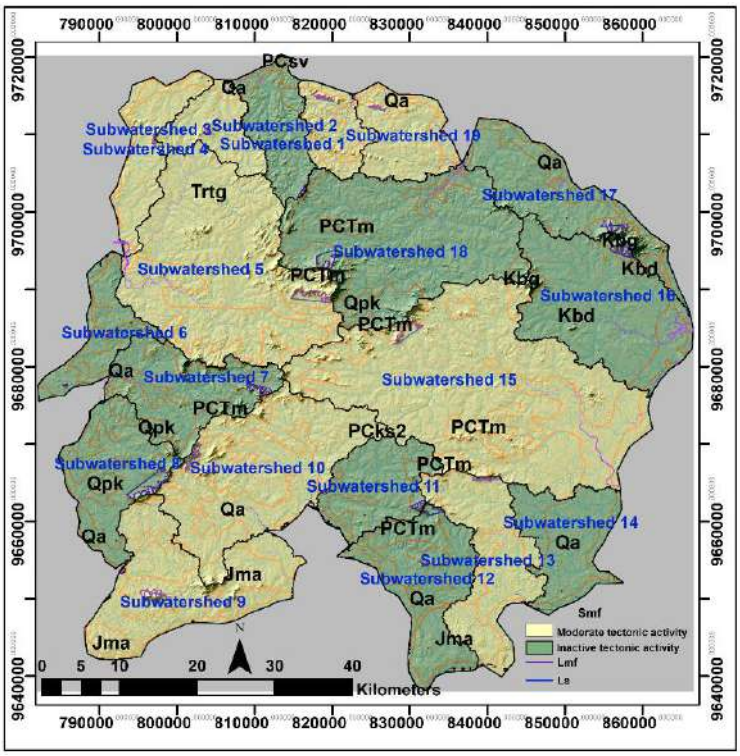

Figure 5. Map showing the spatial distribution of the Smf index regarding their calculated values.

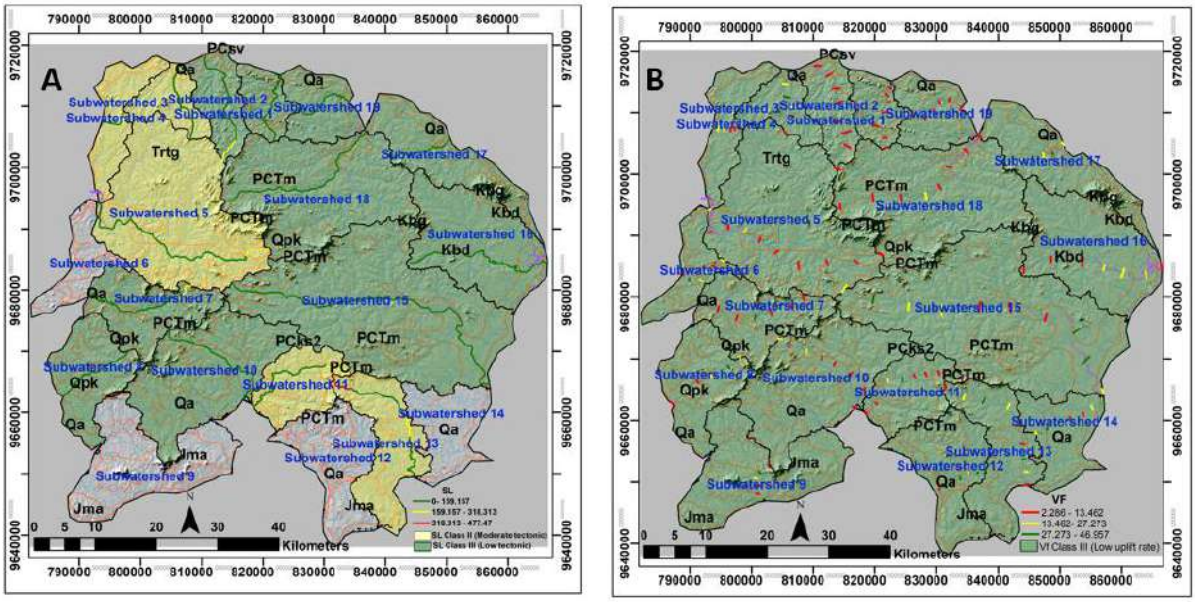

Figure 6. The spatial distribution of SL (A) and VF (B) regarding their classification.

Discussion

Over the years, Belitung Island has undergone significant tectonic activity, giving rise to various rock formations such as the Kelapakampit Formation, Siantu Formation, Tanjungpandan Granite outcrops, Baginda Adamelit, Burungmandi Granodiorite, and Batubesi Granite.

Through analysis of the morphotectonic index, Belitung falls within a very low tectonic classification. This is due to the prevailing effects of erosion and denudation in the region, which limit the range of surface elevation needed to calculate key indices like Smf, AF, VF, and HI.

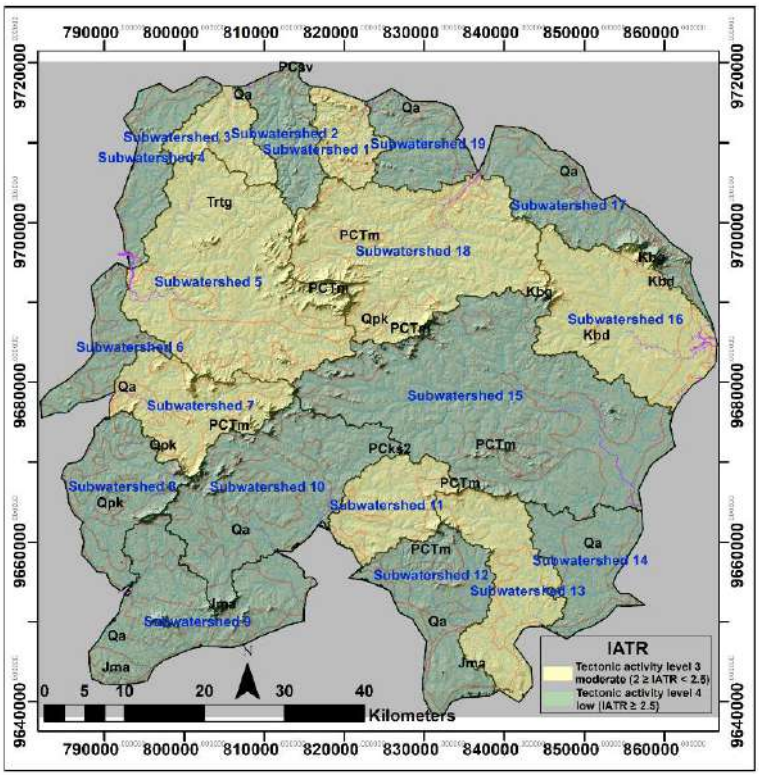

Figure 7. Map showing the spatial distribution of IATR in Belitung Island, Indonesia.

However, Sub-watersheds (1) and (5) in Belitung Island's northern region, where granitic intrusions from the Tanjungpandan Formation are present, exhibit higher AF values than other regions. Likewise, sub-watersheds (16) and (18) have AF values linked to the Kalapa Kampit Formation (PCKs) in the form of Flysch sediments weakly to moderately folded. These AF values represent the higher variation of these sub-watersheds asymmetry/ tilting slope and correlate to the higher tectonic level.

Moreover, analysis of the SL and VF indices reveals tectonic classes ranging from weak to medium. SL values were derived solely from 15 sub-watersheds located in Belitung, utilizing their primary drainages. The SL index highlights a notable value discrepancy between sub-watersheds 11 and 13, distinguished by their steeper river slopes. It can be inferred that the study area exhibits low-to-moderate tectonic activity based on the average values of AF, Smf, SL, and VF. These results brought our analysis to the path that, as per Baharuddin and Sidarto (1995), different types of tectonic activities began approximately 300 million years ago during the Permo-Carbon Age, forming flysch sedimentary deposits and the fold system of the Kelapakampit Formation.

The tectonic activity of the study area continued with magmatic activity that produced the Tanjungpandan Granite in the Triassic period. The granite intrusion phenomenon succeeded in breaking through sedimentary rocks, which also produced fractures in the granite.
In the Early Jurassic period, magmatic activity continued and caused the breakthrough of the Baginda Adamelite rocks, which ended in the Late Cretaceous by producing diorite and granodiorite breakthroughs. The erosion and deposition occurred in the aftermath, producing carbonaceous sand deposits and alluvium. These granitoid types then underwent uplift or were exposed to the surface due to intensive erosion events that caused the granite cover layer to erode. As a result, granite rocks were exposed on the surface

during the Cenozoic period (Tertiary quarter). However, erosion and deposition during the Tertiary-Quaternary period have left their mark, exposing the island's granite rocks. Denudation and deposition in valleys have resulted in a nearly level plain.

The geomorphic indices spatial distribution shows that the quantified area along the main streams analyzed corresponds to the orientation of the main structure within the islands, so our investigation continues to trace geologic features from lineaments to delineate the potential traces of structures.

The lineament pattern suggests a similar orientation to that of the main fault system of Sumatra in the NW-SE and NE-SW directions. In the granite outcrop areas (sub-watersheds 1,2,3 and 4), lineaments may correspond to zones of differential weathering and fracturing within the granite, which can further influence the hill terrain. Additionally, minor lineament orientation in the ENE-WSE and E-W directions are believed to be related to the collision process between the East Malaya continental terrane and Sibumasu, forming a suture known as Raub-Bentong. This suture extends north-south and turns southeast into Indonesia, including Belitung Island (Lehmann & Harmanto, 1990; Zhang et al., 2023). During this period, a subduction event also produced the Siantu Formation of basic igneous rocks (lava) and breccia.

Conclusion

The lineament analysis identified the dominantly NW-SE and NE-SW trending fault and fold, respectively. These two orientations have a strong correlation with the tectonic processes of Sumatra and the formation of the Sumatra Main Fault in the same direction. The other minor directions obtained are interpreted as part of the Bentong-Raub suture that passes through Belitung and is presumed to continue westward toward Kalimantan Island.

The quantitative geomorphology indices assessment combined with the lineament analysis from the satellite imagery indicate that Belitung Island is in a state of relatively low tectonic activity, with the more uplifted landform concentrated along the Tanjung pandan granitoid outcrop that was produced in the Triassic period during the magmatic activity and Kalapakampit folded system. The analysis is supported by a class 1 high AF value of less than 35.

Finally, the IATR shows that relatively low-to-moderate tectonic activity is distributed to the northwest and mostly concentrated in the southeast region, corresponding to the fault and fold systems of the island, respectively.

Acknowledgments

We thank Institut Teknologi Sumatra for supporting the study. Gratitude was also sent to this manuscript's reviewer, and everyone involved in the discussion informally.

Author Contribution

Harnanti Y. Hutami worked on the concept of the text and whole data analysis. Nur Ayu Anas contributed to morphotectonic data interpretation and provided good figures. Erlangga I. Fattah interpreted the lineament features in the study area.

Conflict of Interest

The authors declare that they have no known competing financial interests or personal relationships that could have appeared to influence the work reported in this paper article.

Table 3. The results of the asymmetry factor and sinuosity mountain front of the study area.

Sub-watersheds	Asymmetry Factor (AF)			AF Class	Sinuosity Mountain Front (Smf)			Smf Class
	Ar	At	AF		Lmf	Ls	Smf	
1	24,54	81,23	30,21	1	6,044	2,669	2,26	2
2	47,87	114,93	41,65	2	4,333	1,613	2,69	3
3	39,17	89,88	43,58	3	2,846	1,405	2,03	2
4	65,40	120,82	54,13	3	3,154	1,553	2,03	2
5	148,79	527,05	28,23	1	10,711	4,747	2,26	2
6	50,83	99,65	51,00	3	1,428	0,377	3,79	3
7	69,61	188,20	36,99	2	10,836	3,146	3,44	3
8	91,64	180,30	50,83	3	16,126	4,909	3,28	3
9	109,23	287,50	37,99	2	9,593	3,900	2,46	2
10	133,95	370,40	36,16	2	9,031	4,170	2,17	2
11	49,01	137,95	35,53	2	5,229	1,591	3,29	3
12	80,11	207,10	38,68	2	5,664	2,010	2,82	3
13	75,65	204,20	37,05	2	6,993	3,096	2,26	2
14	57,56	148,25	38,83	2	1,712	0,433	3,95	3
15	366,21	746,36	49,07	3	8,625	4,138	2,08	2
16	102,23	317,48	32,20	1	12,314	2,725	4,52	3
17	111,25	198,50	56,04	3	10,112	3,53	2,86	3
18	153,40	459,14	33,41	1	8,092	2,445	3,31	3
19	67,76	122,39	55,36	3	4,311	2,15	2,01	2

Table 4. Results of *IATR* Index Calculation according to geomorphic indices averaging values.

Sub-watersheds	Smf	AF	Vf	SL	IATR	Class
1	2	1	3	3	2.25	3
2	3	2	3	3	2.67	4
3	2	3	3	2	2.50	3
4	2	3	3	2	2.50	4
5	2	1	3	2	2.00	3
6	3	3	3	*	3.00	4
7	3	2	3	3	2.75	3
8	3	3	3	3	3.00	4
9	2	2	3	*	2.50	4
10	2	2	3	3	2.67	4
11	3	2	3	2	2.33	3
12	3	2	3	*	2.50	4
13	2	2	3	2	2.33	3
14	3	2	3	*	2.50	4
15	2	3	3	2	2.67	4
16	3	1	3	3	2.33	3
17	3	3	3	3	3.00	4
18	3	1	3	3	2.33	3
19	2	3	3	3	3.00	4

(*) means no calculated values in this sub-watershed.

References

Ahmadi, H., & Pekkan, E. (2021). Fault-based geological lineaments extraction using remote sensing and GIS—A review. *Geosciences (Switzerland)*, 11(5), 183. https://doi.org/10.3390/geosciences11050183

Andrifa, J., Sulaksana, N., Gentana, D., & Sulastri, M. (2021). Geological Lineament Pattern and Geomorphic Indices Characteristic Related To Geothermal Manifestation Appearance: A Case Study from Gunung Talang District and Its Surroundings, Solok Regency, West Sumatra Province, Indonesia. *International Journal of Scientific*

Research in Science and Technology, 8(3), 323–336. https://doi.org/10.32628/ijsrst218358

Army, E. K., & Saepuloh, A. (2020). Field Verifications of Geological Structures Related to SAR Detected Lineaments. *IOP Conference Series: Earth and Environmental Science*, 417(1), 012012. https://doi.org/10.1088/1755-1315/417/1/012012

Baharuddin, & Sidarto. (1995). *Peta Geologi Lembar Belitung, Sumatera (1:250,000)*. Puslitbang Geologi, Indonesia. https://geologi.esdm.go.id/geomap/pages/preview/peta-geologi-lembar-belitung-sumatera

Barber, A. J., & Crow, M. J. (2009). Structure of Sumatra and its implications for the tectonic assembly of Southeast Asia and the destruction of Paleotethys. *Island Arc*, 18(1), 3–20. https://doi.org/10.1111/j.1440-1738.2008.00631.x

Bhatt, S. C., Singh, R., Ansari, M. A., & Bhatt, S. (2020). Quantitative Morphometric and Morphotectonic Analysis of Pahuj Catchment Basin, Central India. *Journal of the Geological Society of India*, 96(5), 513–520. https://doi.org/10.1007/s12594-020-1590-1

Bishop, P. (2007). Long-term landscape evolution: linking tectonics and surface processes. *Earth Surface Processes and Landforms*, 32, 329–365. https://doi.org/10.1002/esp.1493

Cobbing, E. J., Mallick, D. I. J., Pitfield, P. E. J., & Teoh, L. H. (1986). The granites of the Southeast Asian Tin Belt. *Journal of the Geological Society*, 143(3), 537–550. https://doi.org/10.1144/gsjgs.143.3.0537

Eleni, K., Skilodimou Hariklia, D., Bathrellos George, D., Assimina, A., & Evangelos, K. (2015). Morphotectonic analysis, structural evolution/pattern of a contractional ridge: Giouchtas Mt., Central Crete, Greece. *Journal of Earth System Science*, 124(3), 587–602. https://doi.org/10.1007/s12040-015-0551-3

Eynoddin, E. H., Solgi, A., Pourkermani, M., Matkan, A., & Arian, M. (2017). Assessment of Relative Active Tectonics in the Bozgoush Basin (SW of Caspian Sea). *Open Journal of Marine Science*, 07(02), 211–237. https://doi.org/10.4236/ojms.2017.72016

Florinsky, I. V. (2016). Lineaments and Faults. *Digital Terrain Analysis in Soil Science and Geology*, 353–376. https://doi.org/10.1016/b978-0-12-804632-6.00014-6

Gentana, D., Sulaksana, N., Sukiyah, E., & Yuningsih, E. T. (2018). Index of active tectonic assessment: Quantitative-based geomorphometric and morphotectonic analysis at Way Belu Drainage Basin, Lampung Province, Indonesia. *International Journal on Advanced Science, Engineering and Information Technology*, 8(6), 2460–2471. https://doi.org/10.18517/ijaseit.8.6.6089

Goudie, A. S. (2004). Encyclopedia of Geomorphology. In *Encylopedia of Geomorphology* (eBook). Taylor & Francis.

Green, D. J. (1997). Active Tectonics Earthquakes, Uplift, and Landscape. *Environmental & Engineering Geoscience*, III(3), 463–464. https://doi.org/10.2113/gseegeosci.iii.3.463

Gupta, L., Agrawal, N., Dixit, J., & Dutta, S. (2022). A GIS-based assessment of active tectonics from morphometric parameters and geomorphic indices of Assam Region, India. *Journal of Asian Earth Sciences: X*, 8, 100115. https://doi.org/10.1016/j.jaesx.2022.100115

Hidayat, E., Muslim, D., Zakaria, Z., Permana, H., & Wibowo, D. A.

(2023). Index active tectonic relative of Karangsambung geopark area, Central Java, Indonesia: assessment for developing geological disaster-based areas. *IOP Conference Series: Earth and Environmental Science*, 1173, 012014. https://doi.org/10.1088/1755-1315/1173/1/012014

Kumar, N., Dumka, R. K., Mohan, K., & Chopra, S. (2022). Relative active tectonics evaluation using geomorphic and drainage indices, in Dadra and Nagar Haveli, western India. *Geodesy and Geodynamics*, 13(3), 219–229. https://doi.org/10.1016/j.geog.2022.01.001

Laake, A. (2022). *Remote Sensing for Hydrocarbon Exploration* (Springer R). Springer. https://doi.org/10.1007/978-3-030-73319-3

Lehmann, B., & Harmanto. (1990). Large-scale tin depletion in the Tanjungpandan tin granite, Belitung Island, Indonesia. *Economic Geology*, 85(1), 99–111. https://doi.org/10.2113/gsecongeo.85.1.99

Luirei, K., Bhakuni, S. S., Longkumer, L., Kumar, V., & Jamir, I. (2021). Geomorphic assessment of the factors contributing to the evolution of landforms in Ukhaldhunga area, Kosi River valley, Kumaun Himalaya, Uttarakhand. *Geosciences Journal*, 25(4), 465–478. https://doi.org/10.1007/s12303-020-0034-7

Mahmood, S. A., & Gloaguen, R. (2012). Appraisal of active tectonics in Hindu Kush: Insights from DEM derived geomorphic indices and drainage analysis. *Geoscience Frontiers*, 3(4), 407–428. https://doi.org/10.1016/j.gsf.2011.12.002

Manjare, B. S. (2020). Morphotectonic Analysis of Upper Tapi River Sub-basin, Madhya Pradesh. *Journal of Geoscience Research*, 1(1), 81–88. https://www.gondwanags.org.in/wp-content/uploads/2021/11/10-JGSR-Vol-1-1-Abstracts-Manajare.pdf

Ng, S. W.-P., Whitehouse, M. J., Roselee, M. H., Teschner, C., Murtadha, S., Oliver, G. J. H., Ghani, A. A., & Chang, S. C. (2017). Late Triassic granites from Bangka, Indonesia: A continuation of the Main Range granite province of the South-East Asian Tin Belt. *Journal of Asian Earth Sciences*, *138*, 548–561. https://doi.org/10.1016/j.jseaes.2017.03.002

Othman, A. T., & Omar, A. A. (2023). Evaluation of relative active tectonics by using geomorphic indices of the Bamo anticline, Zagros Fold-Thrust Belt, Kurdistan Region of Iraq. *Heliyon*, 9(7), e17970. https://doi.org/10.1016/j.heliyon.2023.e17970

Partabian, A., Nourbakhsh, A., & Ameri, S. (2016). GIS-based evaluation of geomorphic response to tectonic activity in Makran Mountain Range, SE of Iran. *Geosciences Journal*, 20(6), 921–934. https://doi.org/10.1007/s12303-016-0106-x

Saepuloh, A., Haeruddin, H., Heriawan, M. N., Kubo, T., Koike, K., & Malik, D. (2018). Application of lineament density extracted from dual orbit of synthetic aperture radar (SAR) images to detecting fluids paths in the Wayang Windu geothermal field (West Java, Indonesia). *Geothermics*, 72, 145–155. https://doi.org/10.1016/j.geothermics.2017.11.010

Shiran, M., Asadi, M. A. Z., Mozzi, P., Adab, H., & Amirahmadi, A. (2020). Detection of surface anomalies through fractal analysis and their relation to morphotectonics (High Zagros belt, Iran). *Geosciences Journal*, 24(5), 597–613.

https://doi.org/10.1007/s12303-019-0042-7

Usman, E. (2016). the Geochemical Characteristic of Major Element of Granitoid of Natuna, Singkep, Bangka and Sibolga. *Bulletin of the Marine Geology*, 30(1), 45–54. https://doi.org/10.32693/bomg.30.1.2015.74

Wang, Y., Qian, X., Zhang, Y., Gan, C., Zhang, A., Zhang, F., Feng, Q., Cawood, P. A., & Zhang, P. (2021). Southern extension of the Paleotethyan zone in SE Asia: Evidence from the Permo-Triassic granitoids in Malaysia and West Indonesia. *Lithos*, 398–399, 106336. https://doi.org/10.1016/j.lithos.2021.106336

Zahirovic, S., Seton, M., & Müller, R. D. (2014). The Cretaceous and Cenozoic tectonic evolution of Southeast Asia. *Solid Earth*, 5(1), 227–273. https://doi.org/10.5194/se-5-227-2014

Zhang, Y., Yu, X., Wang, Y., Qian, X., Gan, C., Ghani, A. A., Yu, Y., & Xu, C. (2023). Reconstructing the East Palaeo-Tethyan assemblage boundary in west Indonesia: constraints from Triassic granitoids in the Bangka and Belitung islands. *Geological Society, London, Special Publication*, 531, 265–286. https://doi.org/10.1144/SP531-2022-144

Zhazhalayi, P. K., & Surdashy, A. (2022). Neo-tectonism and quantitative morphotectonic analysis of Roste Valley at imbricated-suture zones, Kurdistan Region, Iraq. *Iraqi Geological Journal*, 55(2E), 35–58. https://doi.org/10.46717/igj.55.2E.3ms-2022-11-17

ISSN: 2579-5821 (Print)
ISSN: 2579-5546 (Online)
URL address:http://journal.unhas.ac.id/index.php/geocelebes
DOI: 10.20956/geocelebes.v8i1.27319

Jurnal Geocelebes Vol. 8 No. 1, April 2024, 98 – 107

Andesite Quality based on Compressive Strength Tests in the Ulujadi area, Palu City and the Banawa Area, Donggala Regency

Fauziah Alimuddin*, Asri Jaya, Haerany Sirajuddin

Department of Geology, Faculty of Engineering, Hasanuddin University, Makassar, 92171 Indonesia.

*Corresponding author. Email: fauziahalimuddin94@gmail.com

Manuscript received: 21 June 2023; Received in revised form: 24 March 2024; Accepted: 31 March 2024

Abstract

The research location is located in the Ulujadi area, Palu City, Central Sulawesi Province, which is one of the areas that has abundant andesite mineral content. This research aims to optimizing use of andesite rocks in the Ulujadi area of Palu City. The research was carried out using qualitative and quantitative methods in the form of rock sampling and laboratory analysis, namely compressive strength test analysis to determine the technical properties of rocks and petrographic analysis to determine the quality of andesite based on the minerals that make up it. The results of petrographic analysis show that the andesite rocks in the study area are composed of minerals that have a good level of resistance. ST 07 has a mineral composition of plagioclase (38%), pyroxene (5%), biotite (5%), hornblende (7%), and soil mass (45%), and has a compressive strength test of 123 MPa, included in the classification *strong*, and is used as a foundation for light to medium buildings (SNI 03-0394-1989). ST 08 has a mineral composition of plagioclase (32%), ground mass (50%), opaque minerals (5%), orthoclase (5%), quartz (4%), and hornblende (4%), with a compressive strength test value of 97MPa, including in the strong classification, and can be used as a foundation for light to medium buildings. Meanwhile, ST 09 has a mineral composition of plagioclase (30%), hornblende (12%), quartz (3%), biotite (3%), orthoclase (7%), pyroxene (5%), and soil mass (40%).), it is included in the weak category due to the relatively high degree of weathering, and can only be used as an ornamental stone.

Keywords: andesite; building materials; Ulujadi area; compressive strength; petrography.

Citation: Alimuddin, F., Jaya, A., & Sirajuddin, H. (2024). Andesite Quality based on Compressive Strength Tests in the Ulujadi area, Palu City and the Banawa Area, Donggala Regency. *Jurnal Geocelebes*, 8(1): 98–107, doi: 10.20956/geocelebes.v8i1.27319

Introduction

Indonesia is known as an archipelagic country that has conditions The most complex geology in the world. The uniqueness and complexity of geological conditions in the Indonesian archipelago is very interesting to study and study, because the products of these geological processes have the potential to be utilized and used to support development in Indonesia (Wisonir et al., 2018).

The Central Sulawesi region is one of the regions in the world that experiences active geological processes, and this area is included in the Geological Mandala area of Central Sulawesi which has positive and negative impacts. One of the positive things mentioned was the discovery of natural resources in the form of various kinds of minerals and rocks which have quite large potential, such as rock minerals which are useful in the fields of science and engineering, especially in the construction sector. One of the rocks which is a mineral with great potential is andesite.

The use of class C minerals, especially andesite, in the industrial world and construction sector has a very important role in supporting a development project (Alkhabsi et al., 2020). The rapid development of Indonesia has caused an

increase in the need for mining materials such as andesite which meets certain criteria (Adjie et al., 2020).

Andesite is a common type of volcanic rock, composed primarily of plagioclase feldspar and amphibole minerals. Its identification and characterization are essential for geological and environmental studies, as well as resource exploration (Sidik et al., 2023).

The increasing need for building materials is marked by an increase in demand for basic raw materials, including andesite stone. This has caused many companies to increase their efforts to increase andesite stone production, either in the form of developing activities to search for new sources in areas that have never been touched to search for main sources or increasing existing production capacity (Ilmi et al., 2018).

The volume of mining production of minerals tends to decline, for this reason, efforts are needed to increase the production of minerals, especially andesite which is the basic material for road construction (Setiawan et al., 2023).

Andesite lava igneous rock has a porphyritic texture and has a sheeting joint, massive and vesicular structure and has a mineral composition of plagioclase and pyroxene (Soviati et al., 2017). Andesite rock must meet the requirements and quality of natural stone for building materials in accordance with the Indonesian Industrial Standard (SII0378-80) (Karim & Suriadi 2019).

Petrographic analysis is used to see the composition of the minerals in rocks. Composition This is done by entering the mineral percentage so that the rock type is obtained. Petrographic analysis can analyze the genesis of its formation something rock. Observations through rock incisions were madeto classify mineralsmainand secondary rock constituent (Yani et al., 2019).

Based on petrography, andesite rocks are composed of several materials and minerals that have microscopic properties that can only be seen with the help of a microscope. These materials include (1) silica (SiO_2) with an amount between 52 – 63%, (2) quartz with an amount of around 20%, (3) biotite, (4) basalt, (5) felsic, (6) plagioclase feldspar, (7) pyroxene (clinopyroxene and orthopyroxene), and (8) hornblende with a very small percentage (Imron et al., 2019).

There are many studies regarding the quality of andesite developed, one of which is in the Batujajar East area, West Bandung Regency. According to Ridwan et al. (2018) andesite in this area can be utilized as road covering material, sidewalks, and decorative stone.

Andesite rock is one of the promising natural resource potentials in Central Sulawesi because it is a raw material for infrastructure development activities. One area in Central Sulawesi that has relatively abundant mineral content is the Ulujadi area, Palu City and is a rock sampling area (Figure 1).

In the research area, the distribution of andesite stone is quite wide, so it is important to provide information about the quality of andesite stone and its use. One way to determine the quality of andesite stone is to determine the mechanical properties of the rock, which is testing carried out by crushing the rock or (destructive testing). For construction needs, it is very important to know the mechanical properties of rock as a benchmark for the quality of the materials used. (Andika & Purnawan, 2020). Noor (2021) states the compressive strength test as one technical property, it is important to know the rock's crushing point against maximum pressure application.

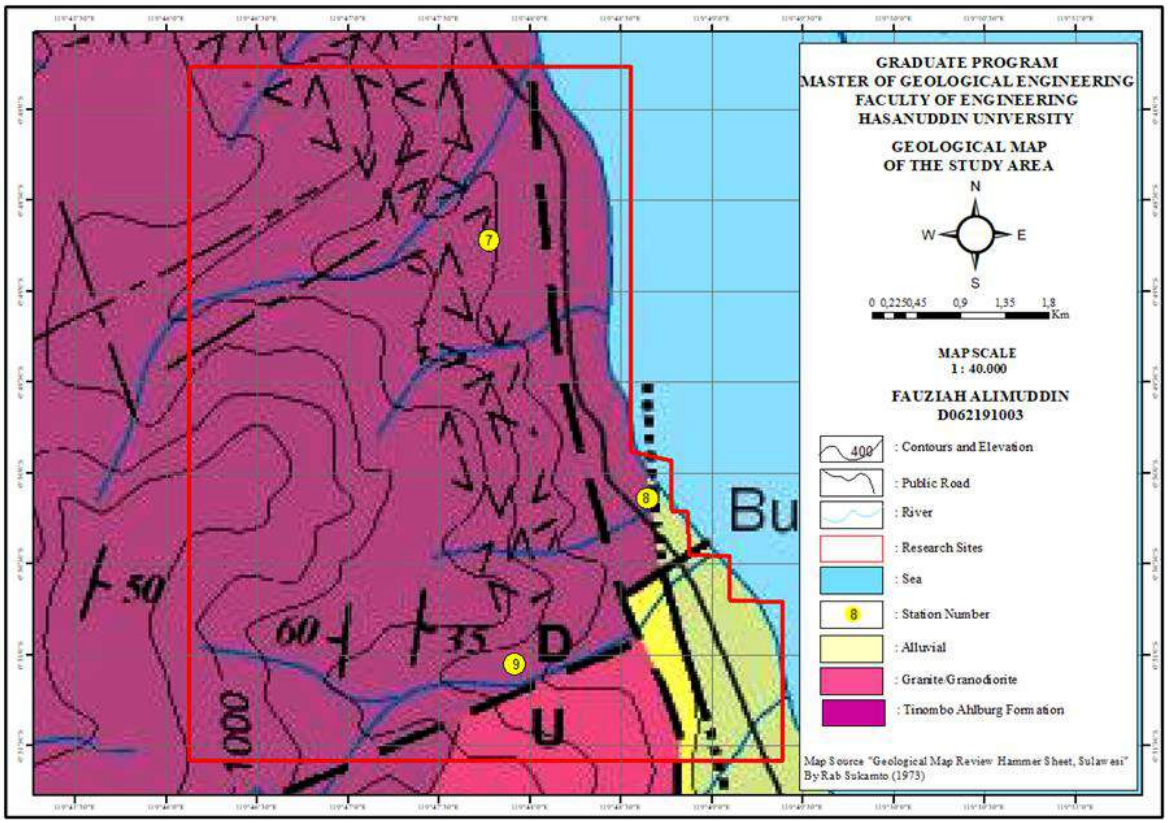

Figure 1. Geological map of research location (Sukamto, 1973).

The uniaxial compressive strength test is one of the important tests in rock mechanics. This compressive strength test is carried out to measure the uniaxial compressive strength of a block-shaped rock sample in one direction (uniaxial). The main purpose of this test is to classify rock strength and compact rock characteristics. This test produces several information, such as stress-strain curve, Poisson's ratio, uniaxial compressive strength, fracture energy, and specific fracture energy (Leba et al., 2020).

Uniaxial Compressive Strength carried out to determine the suitability of andesite stone as a basic material for highway construction. The uniaxial compressive strength of various types of rock varies greatly. Uniaxial compressive strength of intact rock is influenced by its physical properties (Melati, 2019).

The use of rocks is closely related to the physical properties of the rock itself. SNI 03-0394-1989 is generally used to determine the physical and mechanical properties of rocks, and is used as a quality requirement for natural materials for building materials. Table 1 – 3 are used as a reference to determine the quality of a rock based on the results of the compressive strength test.

Rock compressive strength measurements were carried out on each intact rock in the research area. The rock compressive strength test is one of the laboratory tests using a point load test, then the final value is converted into a UCS value in Table 1 (Asupyani, 2020).
Ariyanto et al. (2020) stated that the UCS test is a comparison between the pressure exerted on a rock sample and the surface area of the rock sample under pressure. This compressive strength is calculated when each rock sample experiences failure with the load (P) acting at the time the failure occurs. In the stress-strain curve, the uniaxial compressive strength of each rock sample is at the peak.

Table 1. Strength of Materials (Bienawski, 1989).

Qualitative Description	UCS (MPa)	MORE (MPa)	Rank
Very strong (very strong)	>250	>10	15
Very strong (very strong)	100-250	4-10	12
Strong	50-100	2-4	7
Medium (average)	25-50	1-2	4
Weak	5-25	The use of UCS	2
Very weak	4-5	was continued	1
Very weak (very weak)	1	further	0

UCS: Uniaxial Compressive Strength

Table 2. Quality Requirements for Natural Stone Building Materials (SNI. 03-0394-1989).

	Property	Natural Stone For					
		Foundation Building			Historical Milestones and Roadside Stones	Covering the Floor or Sidewalk	Decorative Stone or Paste
		Heavy	Medium	Light			
1	Press the minimum average strength (Kg/cm^2)	1500	1000	800	500	600	200
2	Rudel off crush resistance a. Index, minimum b. Chapter. Penetrate 2 mm max %	-16	-24	-30	-	-	-
3	Los Angeles shear resistance, through section 1.7 mm, max%	27	40	50			
4	friction wear resistance with Bauschinger, mm/ min, max	-	-	-			
5	Maximum water absorption %	5	5	8	5	5	5* 12**
6	Form immortality with						
	a. Destroyed, maximum %	12	12	12	12	12	12
	B. Cracked/ broken/ deformed	No cracks and no defects			No cracks and no defects		

Table 3. Utilization of andesite stone in the research area based on SII 0378-80.

No	Testing	Quar Press Stone/ Mineral Minimum Kg/cm^2
1	Foundation Building	
	a. Building Pressure Axles Heavy > 7,000 Kg	1500
	b. Building Under Axles Heavy < 7,000 Kg	1000
	c. Building Pressure Axles Heavy > 7,000 Kg	8000
2	Heavy Class	
	a. Class III Heavy Concrete Construction	1200
	b. Class II Heavy Concrete Construction	800
	c. Class I Heavy Concrete Construction	600
3	New Roadside Milestone	500
4	Covering Floor Pavements	400
5	Decorative Stone or Stick Stone	200

The aim of this research is to determine the characteristics of andesite stone based on its constituent minerals and the presentation of chemical elements, as well as to determine the quality of andesite stone in the Ulujadi area, Palu City based on the results of compressive strength tests.

Materials and Methods

In this research, the author used 2 methods, which are qualitative methods and quantitative methods. The qualitative method is the result of data collection in the field, while the quantitative method is the

result of petrographic analysis of rocks and the results of laboratory tests on compressive strength which are then adjusted to the quality requirements of natural stone for building materials (SNI 03-0394-1989).

Figure 2. Andesite rocks on the surface.

Figure 3. Rock example cut to size 4x4x4 cm.

Research is carried out by observing andesite rock outcrops on the surface at 3 points (Figure 2). Before the compressive strength test is carried out, rock samples were cut to size 4x4x4 cm (Figure 3), Next a compressive strength test is carried out by applying a one-way load using a uniaxial compressive strength testing machine. The load applied to the sample will increase every second until the sample reaches its elastic limit which is marked by the rock sample breaking.

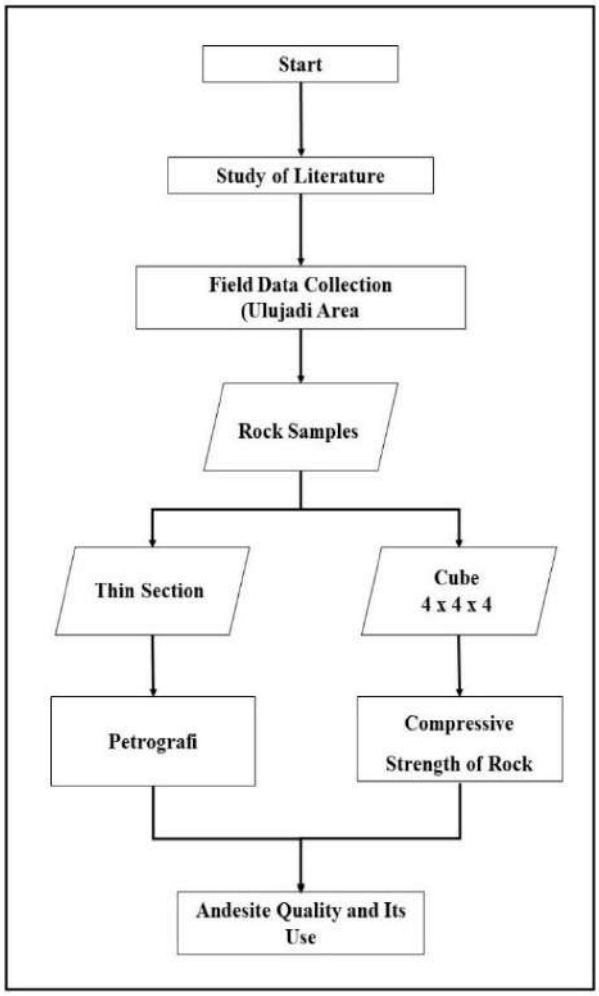

Figure 4. Flow diagram.

Petrographic analysis is needed to prove that the sample taken is indeed andesite rock, and this step includes making a thin incision and then observing the incision under a polarizing microscope to determine the color, texture, structure, and presentation of the mineral composition.

After obtaining the results of the compressive strength test and petrographic analysis, the two were correlated to obtain the type of andesite stone with its compressive strength value. The assessment obtained will determine the quality of the andesite stone and its optimal use. The use of andesite stone refers to the quality requirements of natural stone for building materials based on SNI 03-0394-1989. The research flow diagram can be seen in Figure 4.

Results and Discussion

Rock Compressive Strength Test

Testing the mechanical properties of andesite rock at the research location by analyzing the compressive strength of the rock at several observation locations. Each observation location produces different values (Table 3).

Based on classification Bienawski (1989), very significant differences were found, which are samples ST 07 = 123 MPa, ST 08 = 97 MPa and ST 09 = 17 MPa. Differences in compressive strength are influenced by several internal factors such as rock composition and external factors such as weathering. The average compressive strength value is 79 MPa. Based on the average compressive strength value, the rock unit is included in the strength classification (Table 1).

The differences in the variations in each value in the research area are of course influenced by several factors, such as the mineral composition where the minerals that make up the rock have experienced weathering so that they are less resistant and affect the compressive strength value of the rock. The level of intensive weathering is influenced by weather conditions, if it rains frequently then weathering takes place intensively, as well as the geological conditions of the research area which are greatly influenced by the structure of the Palu Koro so that the rocks are easily fractured and become weathered.

Petrographic Analysis

The results of petrographic analysis using thin section media show that the rocks at the observation location are porphyry andesite rocks. Apart from that, petrographic analysis is also carried out to determine weathering of rocks. The weathering value affects the compressive strength value (Table 4).

Table 4. Compressive Strength Test Data.

No	No. Station	Weight (g)	Size			Content Weight (gr/cm^3)	Cross-sectional area (mm^2)	Maximum Load (N)	Compressive Strength (MPa)
			Length (cm)	Width (cm)	Height (cm)				
1	ST 07	185.7	4.1	4.1	4.1	2.65	1701.00	209.842	123
2	ST 08	150.8	3.6	3.7	3.5	3.23	1332.00	129.862	97
3	ST 09	129.5	3.5	3.6	3.5	2.94	1260.00	21.096	17

Table 5. Results of petrographic observations.

No	Sample code	Matter	Md	Opq	Or	Qz	Hbd	Pixels	Bt	Stone Name
1	ST 07	38	45	-	-	-	7	5	5	porphyry andesite
2	ST 08	32	50	5	5	4	4	-	-	porphyry andesite
3	ST 09	30	40	-	7	3	12	5	-	porphyry andesite

Minerals formed in the study area are plagioclase, orthoclase, quartz, hornblende, opaque, pyroxene, biotite, and groundmass (Table 5). Table 5 discusses the presentation of the constituent minerals and the naming of rock types based on the composition of the minerals contained therein. In addition, there are photos of the incision and the special texture that forms in the incision. Cross-sections of parallel nicol and cross nicol in samples ST 07, ST 08 and ST 9 can be seen in Figure 5 – 7.

The results of microscopic observations of thin sections with sample code ST 07 show the appearance of a yellowish white absorption color, blackish gray interference color, the texture consists of holocrystalline crystallite, aphanitic porphyry granularity, inequigranular relations, mineral size 0.03 mm - 24 mm. The mineral composition consists of plagioclase (38%), hornblende (7%), pyroxene (5%), biotite (5%), and basal mass (45%) with the name Porphyry Andesite (Travis, 1955).

The results of microscopic observations of thin sections with sample code ST 08 show the appearance of a yellowish white absorption color, blackish gray interference color, the texture consists of holocrystalline crystallite, aphanitic porphyry granularity, inequigranular relations, mineral size 0.03 – 22 mm. The mineral composition consists of plagioclase (andesine) (32%), hornblende (4%), quartz (4%), opaque (5%), orthoclase (5%), and glass base mass (50%) with the name Porphyry Andesite. (Travis, 1955).

The results of microscopic observations of thin sections with sample code ST 09 show the appearance of a yellowish white absorption color, a blackish gray interference color, the texture consists of holocrystalline crystallite, aphanitic porphyry granularity, inequigranular relations, subhedral-anhedral mineral shape, mineral size 0.05 mm - 12mm. The mineral composition consists of plagioclase (30%), quartz (3%), hornblende (12%), pyroxene (5%), orthoclase (7%), and glass base mass (40%) with the name Porphyry Andesite (Travis, 1955).

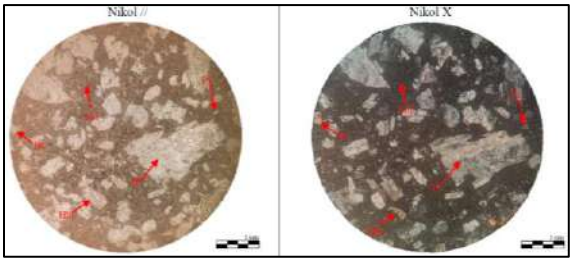

Figure 5. Thin section of andesite stone at ST 07.

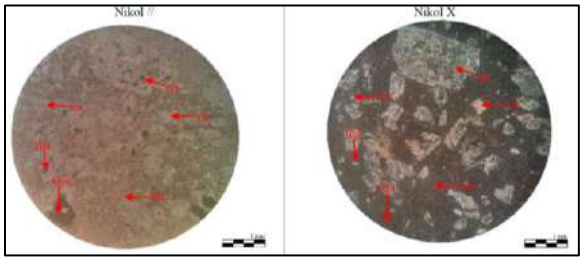

Figure 6. Thin section of andesite stone at ST 08.

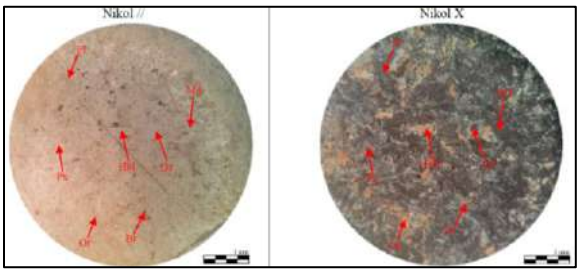

Figure 7. Thin section of andesite stone at ST 09.

Based on the petrographic analysis above, it can be concluded that this rock is an intermediate type of igneous rock with the name Porphyry Andesite (Travis, 1955).

Correlation analysis and recommendations for its use

The research area is porphyry andesite rock, where texture and mineral composition are the dominant factors that influence the compressive strength value. Based on the quality requirements for natural stone for building materials, the compressive strength test results of andesite rocks in the research area (ST 07 and ST 08) meet the qualification standards as rocks that have the potential to be used in the light sector medium building foundations, while

ST 09 has the potential to be used as decorative stone or plaster stone.

Then, based on the specifications issued by the Ministry of Public Works (Indonesian Industrial Standard (SII) 0378-80), andesite stone in the research area can be used as building materials (ST 07 and ST 08), which is for light to medium construction.

Conclusion

Analyzed results of petrographic observations related with the compressive strength of andesite rocks in the research area. The compressive strength values obtained at the research location were ST 07 = 123 MPa, ST 08 = 97 MPa, both of which are included in the strong and very strong specifications, while ST 09 = 17 Mpa including in the weak category because the level of weathering is quite high compared to the two other locations.

Based on the quality requirements for natural stone for building materials (SNI 03-0394-1989), andesite rocks at ST 07 and ST 08 stations can be used as building foundation material, while ST 09 is only intended as decorative stone or plaster stone. Then, based on SII 0378-80, andesite rocks in the ST 07 and ST 08 research areas can also be used as road construction concrete, while ST 09 can only be used as decorative stone or plaster.

Acknowledgements

Thanks to laboratory geological engineering and civil engineering at Tadulako University for allowing me to carry out this research in their laboratory, as well as to all parties who have helped and give enthusiasm for this research.

Author Contributions

Fauziah Alimuddin designed and performed all experiments and wrote the manuscript. All authors have read and approved the final manuscript.

Conflict of interest

The authors declare no conflict of interest.

References

Adjie, M., Sukartono, S., & Trianda, O. (2020). Kualitas Batu Andesit Berdasarkan Analisis Kuat Tekan Daerah Sumberejo Dan Sekitarnya, Kecamatan Durenan Kabupaten Trenggalek, Provinsi Jawa Timur. *GEODA Jurnal Mahasiswa Teknik Geologi*, 1(1), 87–94. https://journal.itny.ac.id/index.php/geoda/article/view/1780

Alkhabsi, G. A., Sukartono, S., & Trianda, O. (2020). Geologi dan Potensi Andesit sebagai Bahan Bangunan berdasarkan Kuat Tekan Daerah Pule dan Sekitarnya, Trenggalek, Jawa Timur. *GEODA Jurnal Mahasiswa Teknik Geologi*, 1(1), 9–15. https://journal.itny.ac.id/index.php/geoda/article/view/1824

Andika, B., & Purnawan, A. (2020). Studi Sifat Fisik dan Sifat Mekanik untuk Mengetahui Karakteristik Batupasir Formasi Balikpapan pada Lereng Penambangan Batupasir, Samarinda. *Prosiding Seminar Teknologi Kebumian dan Kelautan (SEMITAN)*, 2(1), 67–70. https://ejurnal.itats.ac.id/semitan/article/view/1058/861

Ariyanto, K. D., Rabin, S., Saleky, D. B., Titirloloby, A., & Cahyono, Y. D. G. (2020). Analisis Pengaruh Porositas Terhadap Uji Kuat Tekan Unikasial Pada Batu Gamping. *Prosiding Seminar Teknologi Kebumian dan Kelautan (SEMITAN)*, 2(1), 467–471. https://ejurnal.itats.ac.id/semitan/article/view/1058/861

Asupyani, H., Zakaria, Z., Sophian, R. I., & Pratama, R. (2020). Analisis Kekuatan Masa Batuan Pada Tunnel Gudang Handak Berdasarkan Metode Rock Mass Rating (RMR) Bieniawski 1989 PT Aneka Tambang

UBPE Pongkor. *Padjadjaran Geoscience Journal*, 4(4), 365–375. https://jurnal.unpad.ac.id/geoscience/article/view/32177

Bieniawski, Z. T. (1989). *Engineering Rock Mass Classifications, A Complete Manual for Engineering and Geologists in Mining, Civil, and Petroleum Engineering*. The Pennsylvania State University.

Ilmi, I., Taufan, Y. A., Denis, M., Nur, A.A., & Syafri, I. (2018). Identifikasi Prospek Andesit Menggunakan Metode Geolistrik di Kecamatan Cilaku, Kabupaten Cianjur, Jawa Barat. *Bulletin of Scientific Contribution: Geology*, 16(3), 229–236. https://jurnal.unpad.ac.id/bsc/article/view/19927/pdf

Imron, T., Nazli, R. S. S., & Raharja, S. (2019). Strategi Pengembangan Pemasaran Batu Andesit (Studi Kasus pada PT Duta Keluarga Imfaco, Bogor Jawa Barat). *MANAJEMEN IKM: Jurnal Manajemen Pengembangan Industri Kecil Menengah*, 13(2), 127–136. https://doi.org/10.29244/mikm.13.2.127-136

Karim, R., & Suriadi, S. (2019). Kajian Karakteristik Batuan Beku Andesit Sebagai Bahan Bangunan di Daerah Sulamadaha Kecamatan Ternatebarat Kota Ternate. *Dintek*, 12(2), 1–9. https://jurnal.ummu.ac.id/index.php/dintek/article/view/157/181

Leba, E. P., Erong, F. N. O., Marasabesy, Z., & Cahyono, Y. D. G. (2020). Analisis Pengaruh Kuat Tekan Batu Andesit Terhadap Model Dan Arah Rekahan. *Prosiding Seminar Teknologi Kebumian dan Kelautan (SEMITAN)*, 2(1), 417–421. https://ejurnal.itats.ac.id/semitan/article/view/1046/872

Melati, S. (2019). Studi Karakteristik Relasi Parameter Sifat Fisik dan Kuat Tekan Uniaksial pada Contoh Batulempung, Andesit, dan Beton. *Jurnal Geosapta*, 5(2), 133–139. http://doi.org/10.20527/jg.v5i2.6808

Noor, D. (2021). *Kualitas Batuan Andesit Gunung Cipinang, Desa Mekarsari Kecamatan Cikalong Kulon - Kabupaten Cianjur - Jawa Barat Sebagai Bahan Baku Kontruksi Dasar*. Teknik Geologi, Universitas Pakuan.

Ridwan, P., Arfiansyah, K., Kusuma, A. P., Amrullah, F., & Gani, R. M. G. (2018). Identifikasi Karakteristik dan Kualitas Andesit sebagai Bahan Bangunan Daerah Batujajar, Kecamatan Batujajar Timur, Kabupaten Bandung Barat. *Padjadjaran Geoscience Journal*, 2(3), 193–200. https://jurnal.unpad.ac.id/geoscience/article/view/17262/8238

Setiawan, D., Antosia, R. M., & Nugraha, P. (2023). Identifikasi Persebaran Batuan Andesit Sebagai Bahan Utama Agregat Menggunakan Metode Geolistrik Profiling Konfigurasi Wenner-Alpha. *Jurnal Geosaintek*, 9(2), 62–69. http://doi.org/10.12962/j25023659.v9i2.16986

Sidik, F. B., Nurawi, R. W., Muhlisin, H., Giamboro, W. S., & Hidayat, W. (2023). Identification of Andesite Rocks Using Dipole-Dipole Geoelectric Method in Batursari Subdistrict, Pekalongan Regency, Central Java. East Asian Jurnal of *Multidisciplinary Research (EAJMR)*, 2(10), 4149–4160. https://doi.org/10.55927/eajmr.v2i10.6459

SII 0378-80. (1980). *Standar Industri Indonesia No. 0378 – 80, Mutu dan Cara Uji Batu Alam Untuk bahan Bangunan*. Kementerian Pekerjaan Umum.

SNI 03-0349-1989. (1970) *SNI 03-0349-1989 Batu alam untuk bahan bangunan, Mutu dan cara uji*. Badan Standar Nasional (BSN).

Soviati, A. E., Syafri, I., & Patonah, A. (2017). Petrogenesis Batuan Andesit Bukit Cangkring, Daerah Jelekong, Kecamatan Baleendah, Kabupaten Bandung, Jawa Barat. *Padjadjaran Geoscience Journal*, 1 (2), 98–105. https://jurnal.unpad.ac.id/geoscience/article/view/14309/6912

Sukamto, R. (1973). *Peta Geologi Tinjau Lembar Palu, Sulawesi*. Puslitbang Geologi.

Travis, R. B. (1955). *Classification of Rocks*. Colorado School of Mines Quarterly.

Wisonir, W., Anugrah, D., Kusuma, D., Oka, P., Refiyanti, D., Mukti, R. G., & Trisnaning, P. T. (2018). Studi Karakteristiik Andesit Berdasarkan Analisis Petrografi Dan Sifat Keteknikan Batuan Sebagai Bahan Bangunan Di Daerah Mayang, Kecamatan Cisalak, Kabupaten Subang, Jawa Barat. *Geoweek 2018 Proceeding Seminar Nasional Kebumian Ke-11*, 65-73.

Yani, Y., Susilo, B. K., & Falisa, F. (2019). Perbandingan Kualitas Andesit Daerah Gunung Geblegan dan Pondokrasa, Kabupaten Lebak, Provinsi Banten Melalui Metode Kuat Uji Tekan Batuan dan Petrografi. *Proceeding Seminar AVOER XI 2019*.

ISSN: 2579-5821 (Print)
ISSN: 2579-5546 (Online)
URL address: http://journal.unhas.ac.id/index.php/geocelebes
DOI: 10.20956/geocelebes.v8i1.30785

Jurnal Geocelebes Vol. 8 No. 1, April 2024, 108 – 122

Stochastic Inversion in Determining the Distribution of Petroleum Carrying Sandstones in the "JS" Field of the South Sumatra Basin

Johannes Kurni Bintang Awan Situmorang[1]*, Gindo Tampubolon[2], Juventa[1], Muhammad Suhban[3]

[1]Teknik Geofisika, Universitas Jambi, Jl. Jambi – Muara Bulian Km. 15 36361, Jambi, Indonesia.
[2]Agroekoteknologi, Universitas Jambi, Jl. Jambi – Muara Bulian Km. 15 36361, Jambi, Indonesia.
[3]PT Pertamina Hulu Rokan Zona 1 – Jl. Raden Pamuk No.20-22 Kota Jambi, 3614, Jambi, Indonesia

*Corresponding author. Email: johannescitumorang@gmail.com

Manuscript received: 25 September 2023; Received in revised form: 20 April 2024; Accepted: 30 April 2024

Abstract

The "JS" field is a field located in the South Sumatra Basin, where the field has good prospects for the distribution of petroleum-bearing sandstone. The target of this research is the Air Benakat formation. This research uses the stochastic seismic inversion method to determine the probability of finding petroleum in sandstone. Stochastic seismic inversion has the advantage that it can overcome thin layers and can reduce existing data misalignments. So stochastic inversion can overcome the shortcomings of other seismic inversions, especially model-based seismic inversion which is the initial model for stochastic seismic inversion. Stochastic seismic inversion produces several realizations by showing uncertainty so as to get results that are close to the actual situation. Probability map of oil-bearing sandstones located in the north and east of the study area. with the slice results obtained for the acoustic impedance range of 8517-9051(m/s)*(g/cc) and oil sand probability with a value range of 0.61-0.78%.

Keywords: Petroleum; South Sumatra Basin; Stochastic Inversion.

Citation: Situmorang, J. K. B. A., Tampubolon, G., Juventa, J., & Suhban, M. (2024). Stochastic Inversion in Determining the Distribution of Petroleum Carrying Sandstones in the "Js" Field of the South Sumatra Basin. *Jurnal Geocelebes*, 8(1): 108–122, doi: 10.20956/geocelebes.v8i1.30785

Introduction

The "JS" field in this research is in the South Sumatra basin, where the South Sumatra basin is one of the back arc basins that has hydrocarbon potential in Indonesia. One of the formations in the South Sumatra Basin that produces hydrocarbons in the form of oil is the air bekanat formation. The basin is bounded by the mountain range in the southwest and the Sunda Shelf in the northeast. This basin has been proven to produce hydrocarbons with types of hydrocarbon traps that develop in the form of structural traps, stratigraphic traps, and a combination of the two traps (Prasetiyohadi et al., 2022).

The South Sumatra Basin is one of the basins that was formed because of tectonic movement between the Indo-Australia plate and Eurasia. The South Sumatra Basin began to form during the extension between the two plates which trended East-West at the end of the Pre-Tertiary – early Tertiary. Geologically, this basin is a foreland basin or back arc basin type (Gahana et al., 2019).

Stratigraphy

South Sumatra Basin is a basin where geological structures play a very active role in sediment deposition, good geological structures that occur during phases pre-rift, syn-rift, and post-rift (Gaol, 2016).

According to Rahmadani et al. (2020), structural development and basin evolution since the Tertiary are the result of the interaction of the three main structural directions (Figure 1). These include, the northeast-southwest direction or called the Jambi Pattern, the northwest-southeast direction or called the Sumatra Pattern, and the north-south direction or called the Sunda Pattern. This is what makes the geological structure in the South Sumatra Basin area more complex than other basins on the island of Sumatra. The northeast-southwest trending geological structure or Jambi Pattern is very clearly observed in the Jambi Sub-Basin.

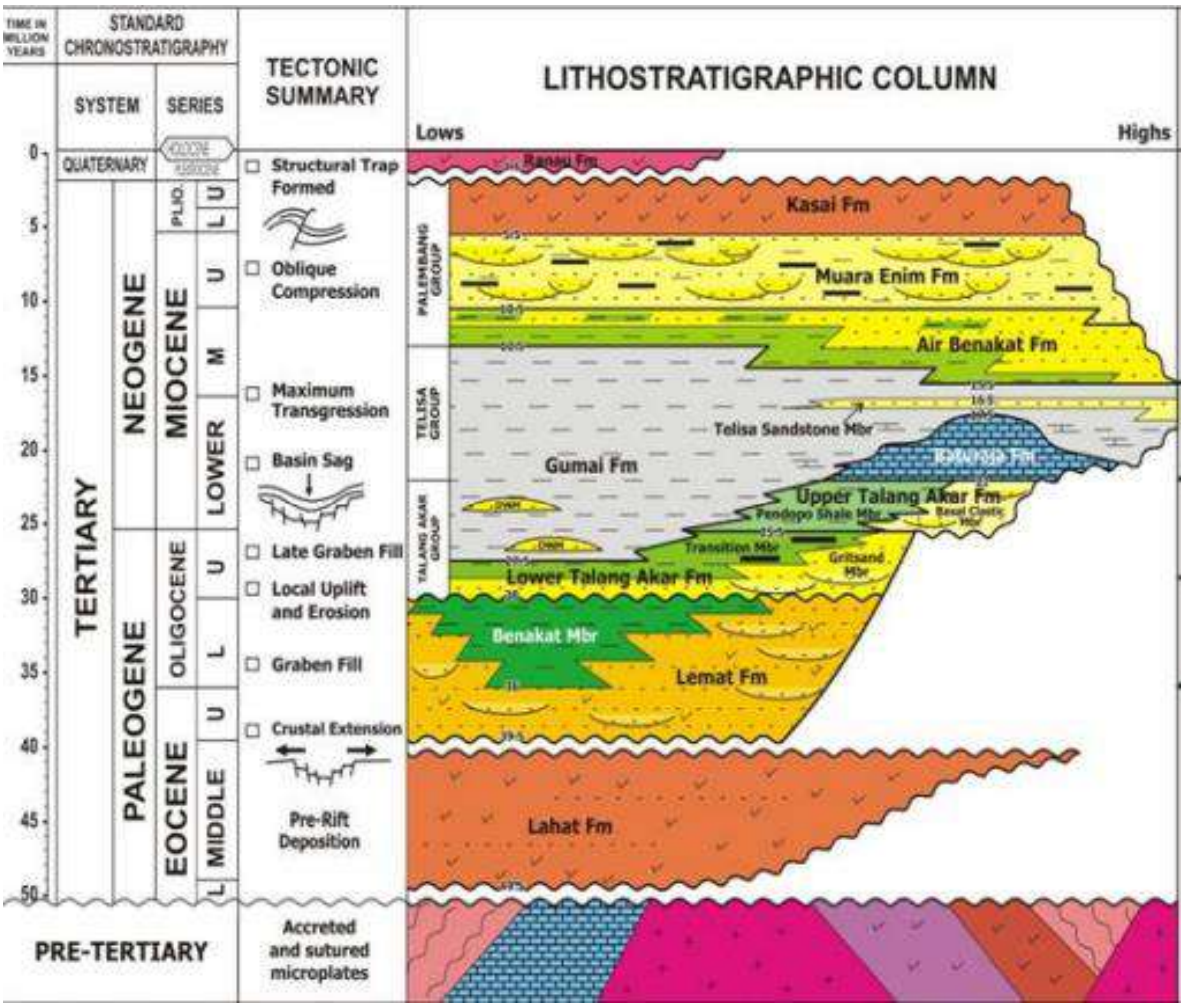

Figure 1. Stratigraphy of the South Sumatra Basin (Lukman et al., 2019).

Seismic Reflection

Seismic reflection is one of the geophysical methods used in exploration, especially hydrocarbons, using elastic waves as an interpretation medium. In principle, this method uses reflection principle from source to receiver. Seismic waves carry information about lithology and subsurface fluids in the form of travel time, reflection amplitude and phase variations (Dani & Sule, 2021). Supported by developments in computerized technology, seismic data processing, as well as interpretation techniques, seismic data in can be analyzed to delineate the physical (acoustic) properties of rocks and determine lithology, porosity, pore fluid, and so on.

Seismic Inversion

Seismic inversion is a technique for creating subsurface geological models using seismic data as input and well data as a control (Srivastava & Sen, 2009).

Seismic inversion serves as a crucial tool for estimating subsurface parameters in reservoir geophysics, playing a significant role in lithology prediction and geofluid discrimination. The seismic inversion method is one of method to describe and estimate the lower physical parameters surface in the form of acoustic impedance values using seismic data as input the data and well data as well the control. Acoustic impedance inversion is one of the seismic inversion methods after the stack (Prastika et al., 2018; Li et al., 2019). Deterministic inversion and stochastic inversion are inversion techniques that can be used. Deterministic inversion produces the inversion models with low frequency, so stochastic inversion is needed to reduce the problem of ambiguity and high uncertainty. So, it can find out the thin reservoir layer.

Stochastic Seismic

Stochastic seismic inversion is an inversion technique whose basic principle is to use a random simulation algorithm and produce more than one acoustic impedance model that meets the observed seismic data. More than one solution can overcome the problem of non-uniqueness and uncertainty in deterministic inversion, especially in the case of thin layers. (Fernandes et al., 2023). A stochastic inversion method is proposed for seismic reservoir characterization, aiming to provide models of facies and reservoir properties. This iterative optimization process is achieved through the probability perturbation method based on conditional simulation with multi-point geostatistics. Additionally, it incorporates a quantum annealing algorithm to enhance the accuracy of the inverted reservoir properties (Liu et al., 2018). Another advantage is that this method does not depend on the bandwidth of the seismic data used but on the block size when simulating the impedance model so that the results of this stochastic inversion are less smooth than the results of deterministic inversion. And by using this inversion you can capture small variables so that the resulting data is more accurate.

Materials and Methods

Data

The data source for this research comes from PT Pertamina Hulu Rokan Zone 1 which is located in Jambi City, Jambi. In its implementation, CGG HRS 10.6 and Petrel 2018 software were used. 3D Post Stack Migration (PSTM) seismic data was used and 3 wells data (Figure 2) with logs for each well were gamma ray, neutron porosity, density, caliper, resistivity, sonic, marker and checkshot (Table 1).

Table 1. Well data availability.

Log/well	J2	J5	J6
GR	√	√	√
NPHI	√	√	√
RHOB	√	√	√
PHIE	√		
DT	√	√	√
CALI	√	√	√
SP	√		√
Checkshot Marker	√	√	√

Data processing

Overall data processing is carried out on well data and seismic data. The number of well data used is 3, including; J1, J5, and J6, where a well sensitivity analysis will be carried out to determine the existence of the desired target. After obtaining the desired target, the well is tied to seismic so that there is alignment between the well target and the seismic data (Figure 3). Meanwhile, in processing seismic data, several stages are carried out, including horizons interpretation and faults to determine the continuity of the target layer so that the presence of the target is known in the seismic data, then doing time to depth to change the presence of the target from time domain to depth domain. After determining the presence of the target, a model-based seismic inversion was carried out (Figure 4) which became the initial model for stochastic seismic inversion and

obtained cross sections resulting from the inversion that has been carried out so that the presence of sandstone containing petroleum can be analyzed based on the inversion impedance and porosity values.

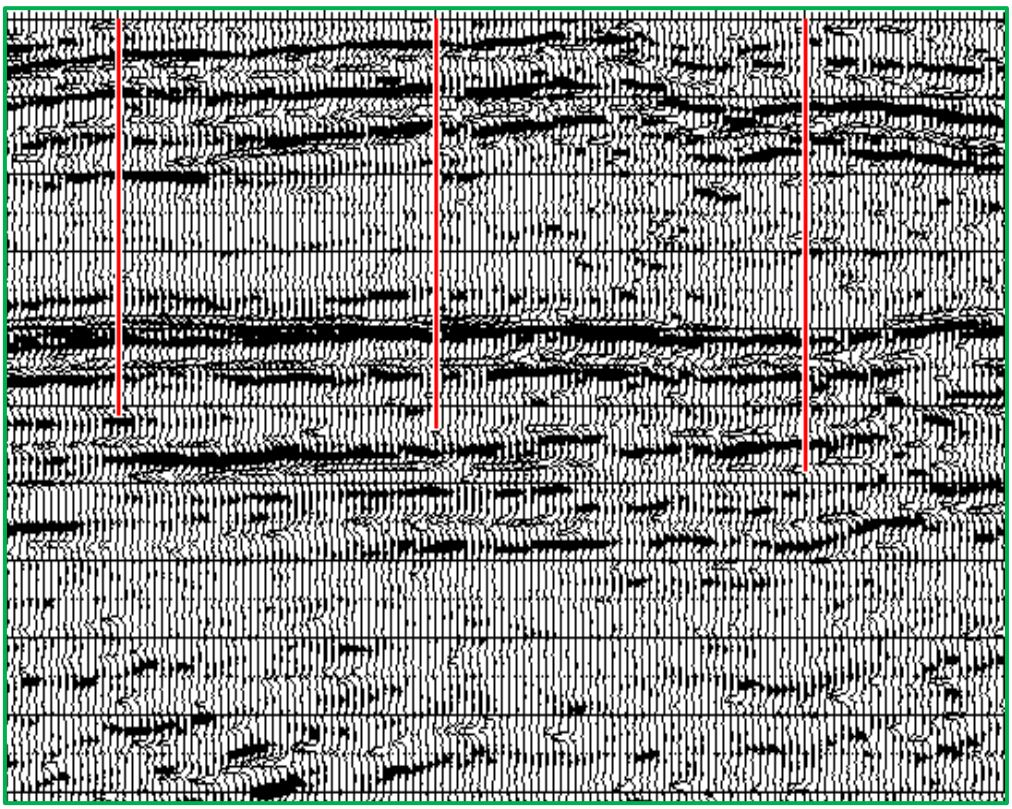

Figure 2. Seismic section of the "JS" field.

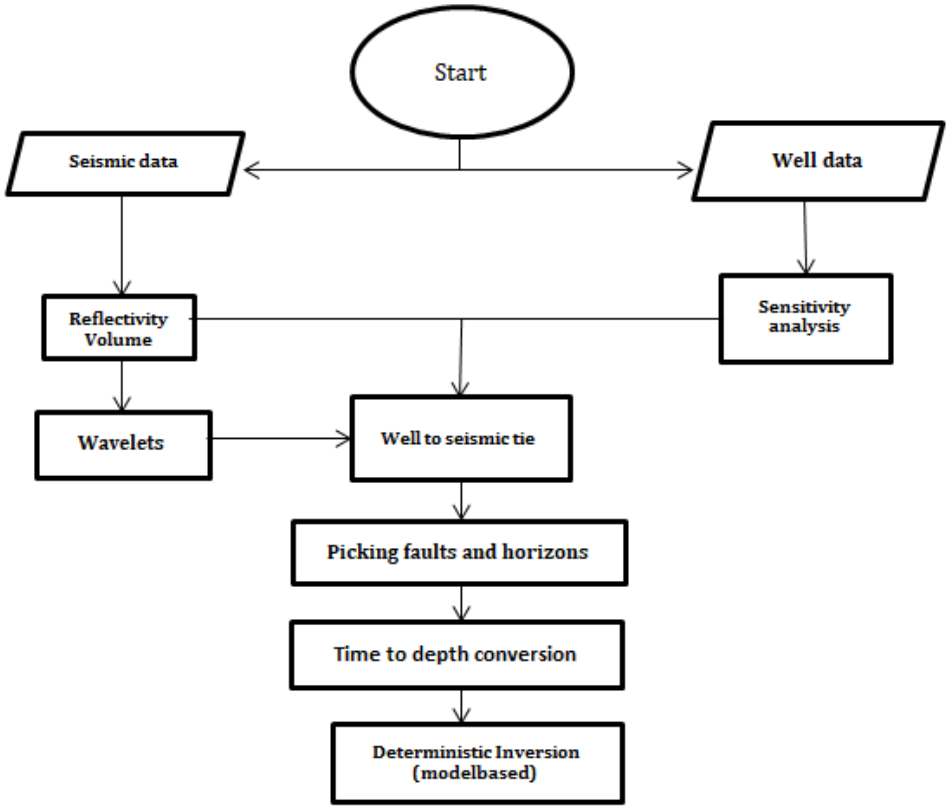

Figure 3. Model-based inversion flow diagram.

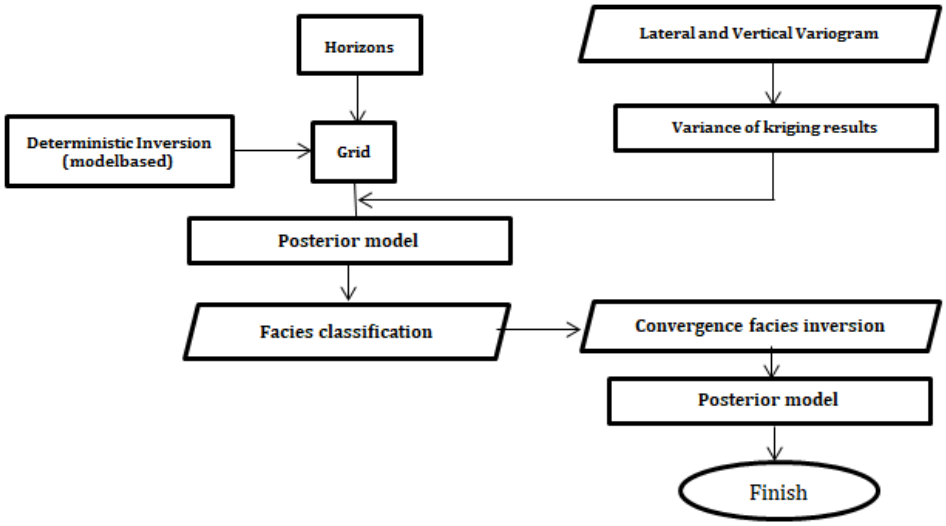

Figure 4. Stochastic inversion flowchart.

Results and Discussion

Wavelet Extraction

Wavelet extraction is very necessary in inversion which aims to equate synthetic seismogram and seismic data in well location (Dikman et al., 2015). Wavelets can be extracted by several methods such as statistical, bandpass, ricker, and usewell. Wavelet extraction in this research, trial and error was carried out to obtain the best. Based on synthetic seismogram analysis, ricker model generates the best model that has the similarity with the observed seismogram.

Well to Seismic Tie

This process aims to change the depth domain into a time domain for the well, so that well data can be linked to seismic data. So, the results of this process can determine the exact whereabouts of the marker data in the seismic data (Kumalasari et al., 2018; Liu et al., 2022). This process requires sonic log and density log data. In the well to seismic tie process, a stretching process is carried out with the aim of obtaining a high correlation, which is more than 0.5 or close to 1 with a time shift value close to 0.

Sensitivity Analysis

Sensitivity analysis can be carried out by carrying out a crossplot between log data to determine the sensitivity of the target well. Crosplots are carried out to separate and determine shale or nonshale lithology and determine the acoustic impedance susceptibility value of the target zone (Pradana et al., 2017; Xue & Mrinal, 2016). This research uses gamma ray logs, P-impedance logs, and porosity logs in lithological separation. Crossplot from well J2 (Figure 5) where the x-axis is a parameter of P-impedance and the y-axis is a parameter of porosity and color index using gamma ray logs. With the gamma ray log cut-off being at 95 API, where if an area with a value of less than 95 API is declared as sand, it is marked with a yellow area with a porosity value ranging from 0.05 – 0.15% and a P-impedance value ranging from 8000 – 9300 (m/s)*(g/cc), while areas with a value of more than 95 API are declared as shale which is marked with a green area with a porosity value ranging from 0.01 – 0.05% and a P-impedance value ranging from 6500 – 8200 (m/s)*(g/cc). And from the crossplot of well J2 there is lithology which is stated as non-shale which is marked by a brown area with a low gamma ray value, which is in the P-impendace value area of 7400 – 8000(m/s)*(g/cc) with porosity values range from 0.15 – 0.23.

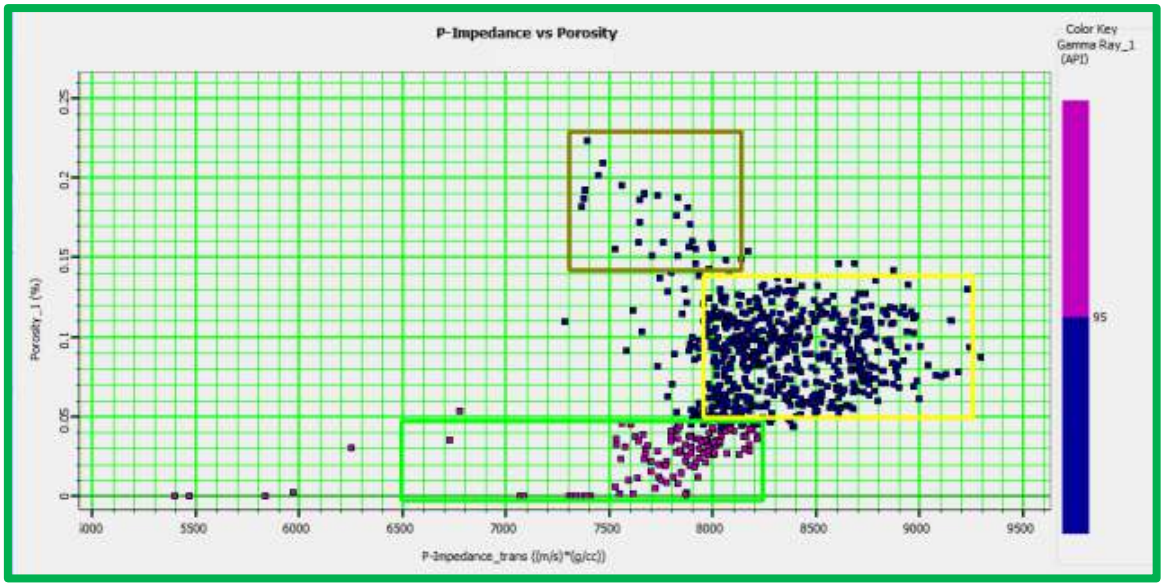

Figure 5. Crossplot well J2.

Fault and Horizon Interpretation

Horizon interpretation is useful in marking the continuity of each formation from a marker that has been well to seismic tied (Novriyani et al., 2016) (Figure 6). So, it can know the correlation between seismic data and well data. Meanwhile, fault interpretation is useful in indicating areas where faults occur in seismic data. So, it can help in determining the horizon in the continuity of the layer structure. In horizon interpretation, this research was carried out in the Otakat water formation.

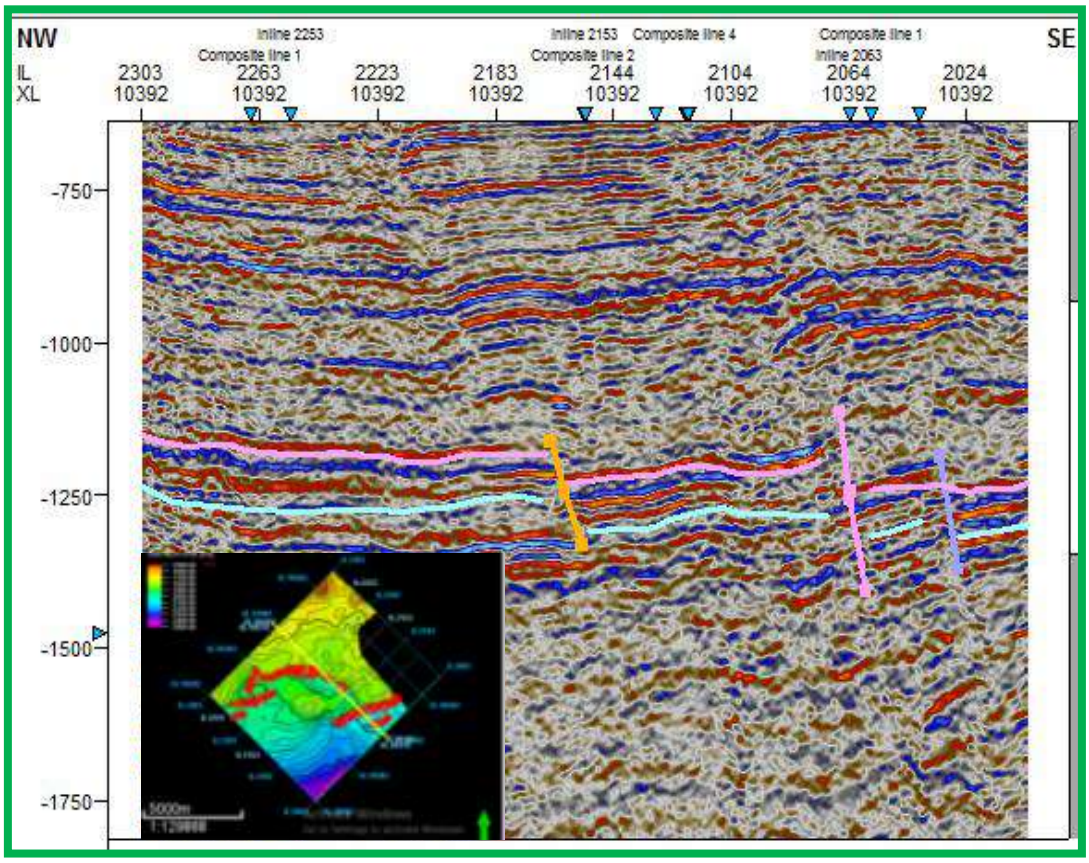

Figure 6. Fault and horizon interpretation.

Initial Model

Seismic inversion is defined as a technique for creating subsurface models using seismic data as input and well data as control. The initial model is the initial model used as a reference in the seismic inversion process (Irvanaya, 2022) (Figure 7). This model was created based on geological information and geophysical data available before the inversion process was carried out. In this study, an initial model was created using a 3D seismic section as input and 3 wells as binding, which are well J2, J5, and J6. This is where the initial model will be used in the process of creating the inversion model.

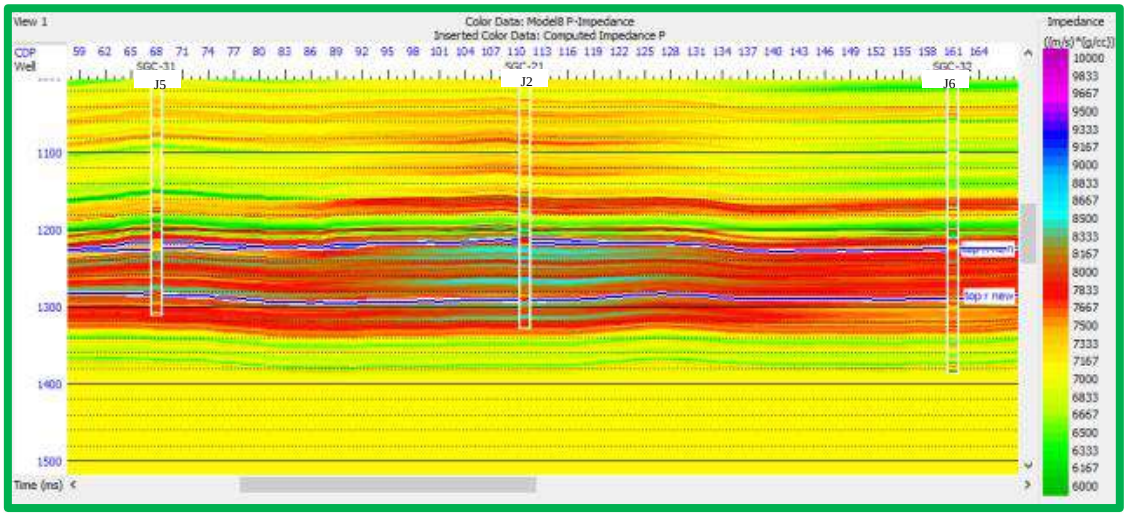

Figure 7. Cross-section of initial model.

Inversion Model-based

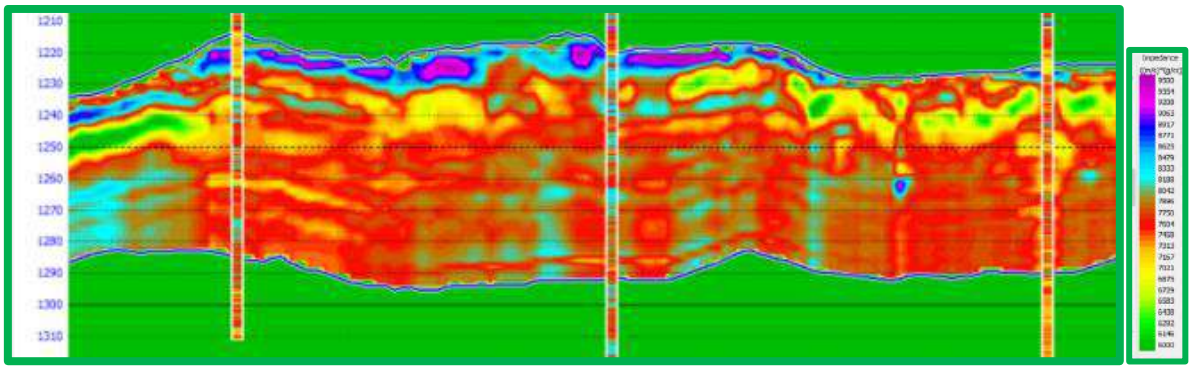

Figure 8. Model-based inversion cross-section.

This research uses model-based post stack deterministic inversion because in this model-based inversion process the modeling results almost resemble the actual geological cross-sectional shape (Figure 8). This method does not perform inversion of seismic data alone, but instead performs inversion of geological models based on well data control (Latifah et al., 2019). The model-based inversion method produces quite good results and is in accordance with the well data, However, the results still tend to be smooth and blocky, so they are not able to resolve thin layers well (Devi, 2018). This research uses data from wells J2, J5, and J6. The model-based cross section shows areas based on acoustic impedance values in the range 6000 – 10000 (m/s)*(g/cc). Areas that have low acoustic impedance value are interpreted in green. Meanwhile, areas that have high acoustic impedance values are interpreted in purple. Zones with high acoustic impedance values indicate denser sandstone reservoirs, while zones with lower acoustic impedance values indicate

more porous sandstone reservoirs. This is because the acoustic impedance value resulting from the P wave velocity and density values describes the nature of the rock, where the P wave that propagates in the rock propagates into the rock matrix through which it passes.

Stochastic inversion

Stochastic seismic inversion is an inversion technique whose basic principle is to use a random simulation algorithm and produce more than one acoustic impedance model (Rashad et al., 2022). The number of realizations is determined based on the size of the data, the duration of the inversion process and the capabilities of the coarse equipment used. The greater the number of realizations will of course affect the statistical calculations, for example reducing uncertainty better (Rohaman, 2017).

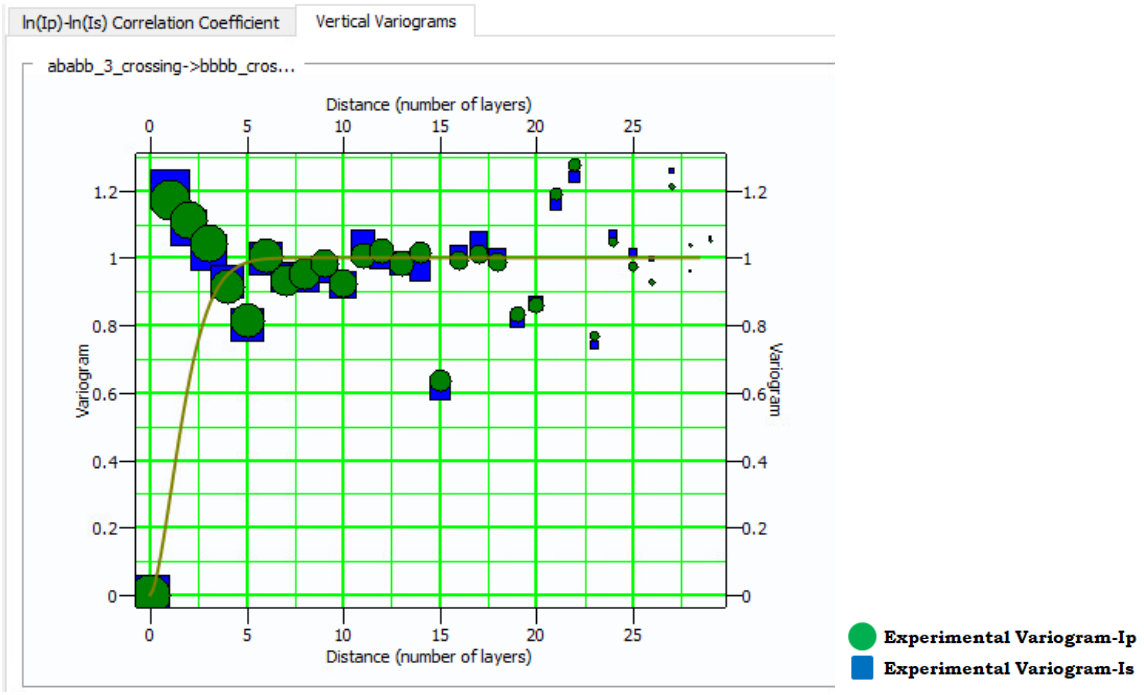

Figure 9. Stochastic inversion variogram.

Variogram analysis is carried out to show the spatial relationship between data in the inversion processstochastic seismic. The variogram analysis carried out is a horizontal variogram (Ekawati & Winardhi, 2018). In Figure 9, the variogram parameters of Ip and Is are used. The Ip value is marked in blue and the Is value is marked in green. At the existing variogram diagram, there is a dissimilarity between each parameter, so it is suspected that there is misalignment.

		Ip	Is	Ip	Is	Ip	Is	Ip	Is
Uncertainty	All Model	4.17 %	6.54 %	3.25 %	5.20 %	4.83 %	7.47 %	4.38 %	6.89 %
	ababb_3_crossing -> bbbb_crossing	4.17 %	6.54 %	3.25 %	5.20 %	4.83 %	7.47 %	4.38 %	6.89 %
Correlation Coefficient	All Model	0.99		0.99		1.00		0.99	
	ababb_3_crossing -> bbbb_crossing	0.99		0.99		1.00		0.99	
Number of samples	All Model	120	120	40	40	40	40	40	40
	ababb_3_crossing -> bbbb_crossing	120	120	40	40	40	40	40	40

Figure 10. Variogram value for each well.

From the values seen (Figure 10), 150 realizations can be seen from the approach taken from the realizations formed on the facies being classified. Where facies are shown on a line that rises from realization 1 to realization 150. From the existing calcification relationships there are values that rise and fall in the process of reducing the ambiguity of the existing facies (Figure 11). So, it get a dominant approach calculation value that is close to the existing facies value.

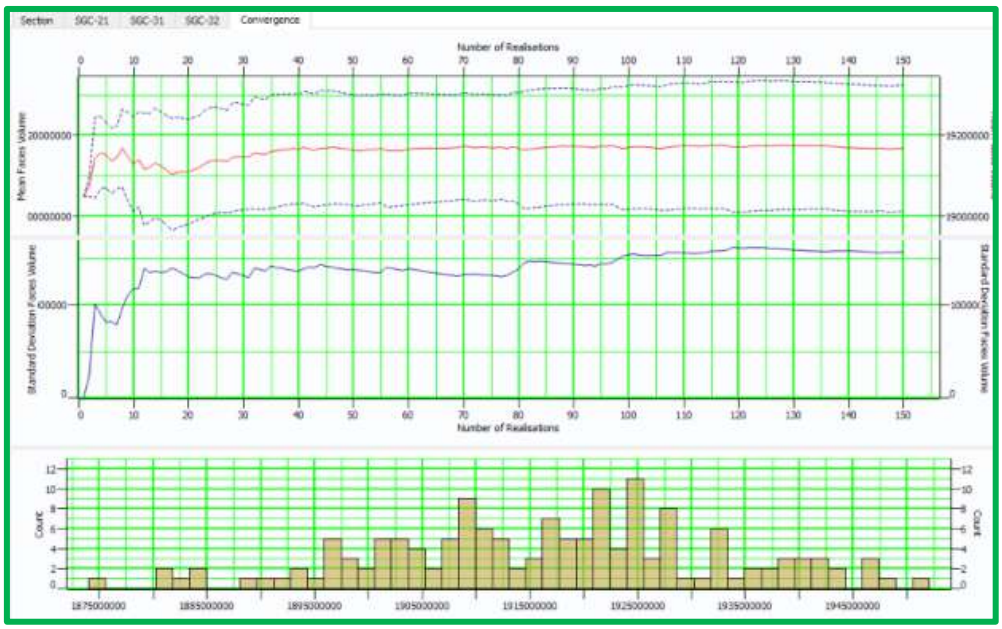

Figure 11. Realization relationships after facies calcification.

In the stochastic inversion seismic section at well J2, the impedance value ranges from 6000 – 10000 (m/s)*(g/cc) with the lowest value in green and the highest value in purple. At the cross-plot values for well J2 (Figure 12), the area marked as shale is at 6500 – 8200 (m/s)*(g/cc) with a light green to pink color range. And the area marked as sand is at impedance 8000 – 9300 (m/s)*(g/cc) with a color range of red to dark blue. So that this area can become a hydrocarbon prospect area. Areas with higher values indicate denser reservoir sand because the impedance value comes from multiplying the wave by density so that it can describe the nature of the rock layers.

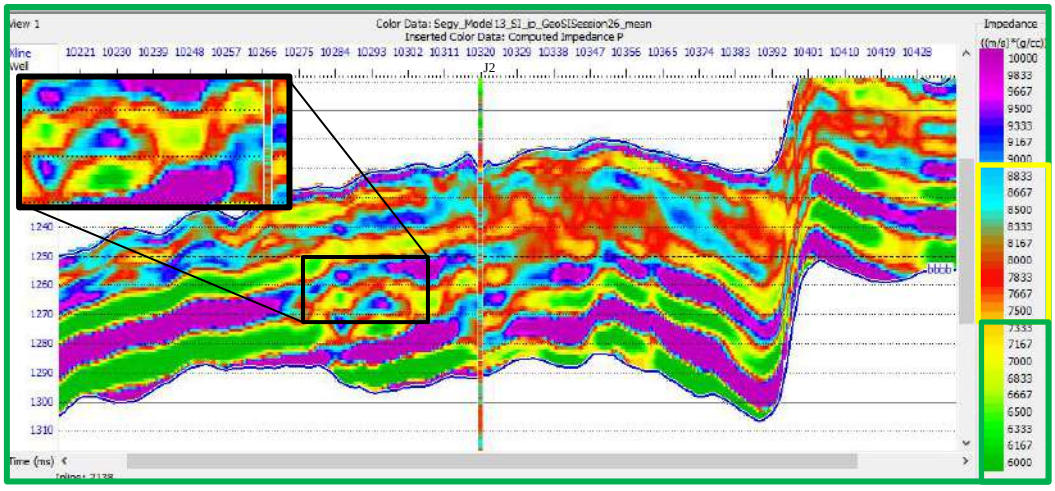

Figure 12. Stochastic inversion seismic section at well J2.

In the oil sand probability cross section (Figure 13), the probability range is from 0.04-0.9 with the lowest value being white while the highest value is purple. The probability value shows the possibility of an oil-bearing layer area. The value closer to 1 indicates that the layer is an oil-bearing area. So this area is included in the area of high hydrocarbon potential.

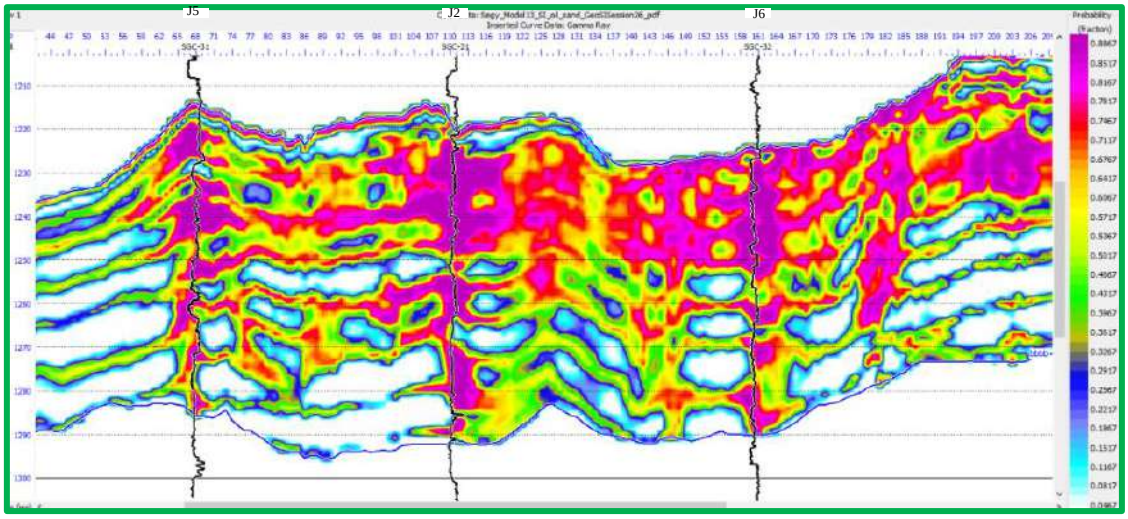

Figure 13. Cross-section based on oil sand probability.

Slice Results

Model-based inversion slices where the range of slices made is around 8,500 – 9,900 (m/s)*(g/cc) which is marked with the smallest value in green and the largest value is marked in purple. So, the results of this slice show that areas of denser sand are purple and areas of less dense sand are green (Figure 14). Because the higher the impendance value of a layer, it can be said that the layer is denser. And from the results of the model-based inversion slice, the hydrocarbon prospect cutoff value ranges from green to yellow.

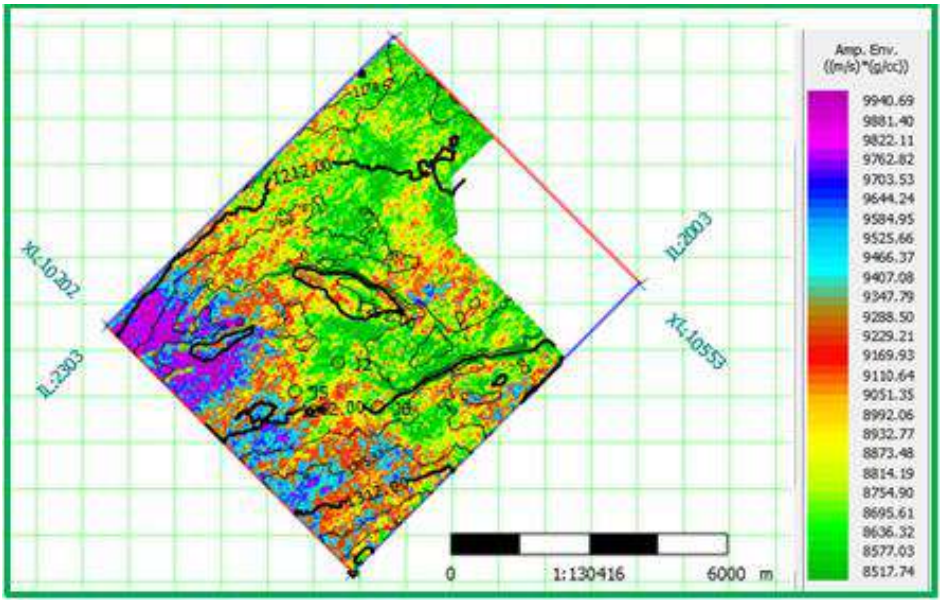

Figure 14. Model-based slice inversion.

Slice from stochastic inversion modeling of the Ip mean cross section which aims to determine the distribution of impendace values in the "JS" field (Figure 15). Based on the cross-plot analysis that has been carried out, the presence of sand has a

value that tends to be high. The values in the slice results obtained impendace values ranging from 8517 – 9940 (m/s)*(g/cc) with the lowest value marked in green to the highest value marked in purple. Meanwhile, the crossplot value results that have been analyzed are around 8000 – 9000 (m/s)*(g/cc) and are marked on the slice results from green to reddish yellow.

The slice results show the areas where oil sands are located (Figure 16). So that the existence of hydrocarbon prospects is known. The range for the slice results is 0.19 – 0.78. where the higher the value of an area, it shows that the area has prospects for oil sands or hydrocarbons. Areas that are suspected to be hydrocarbon prospects are shown in red-purple areas.

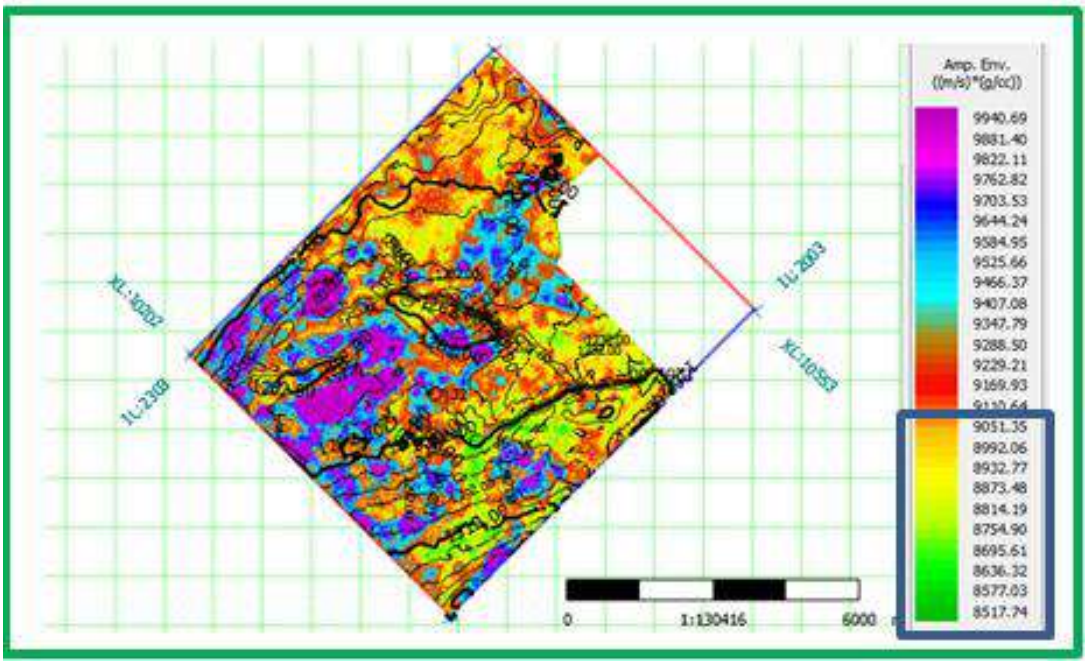

Figure 15. Stochastic inversion slice Ip mean.

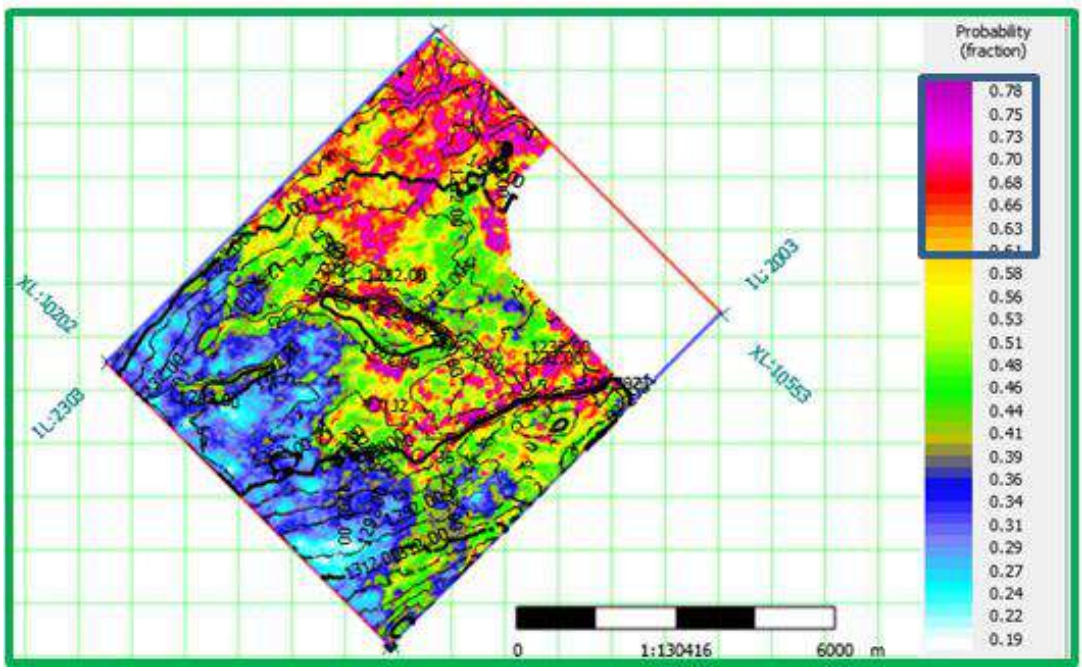

Figure 16. Stochastic inversion slice probability oil sand.

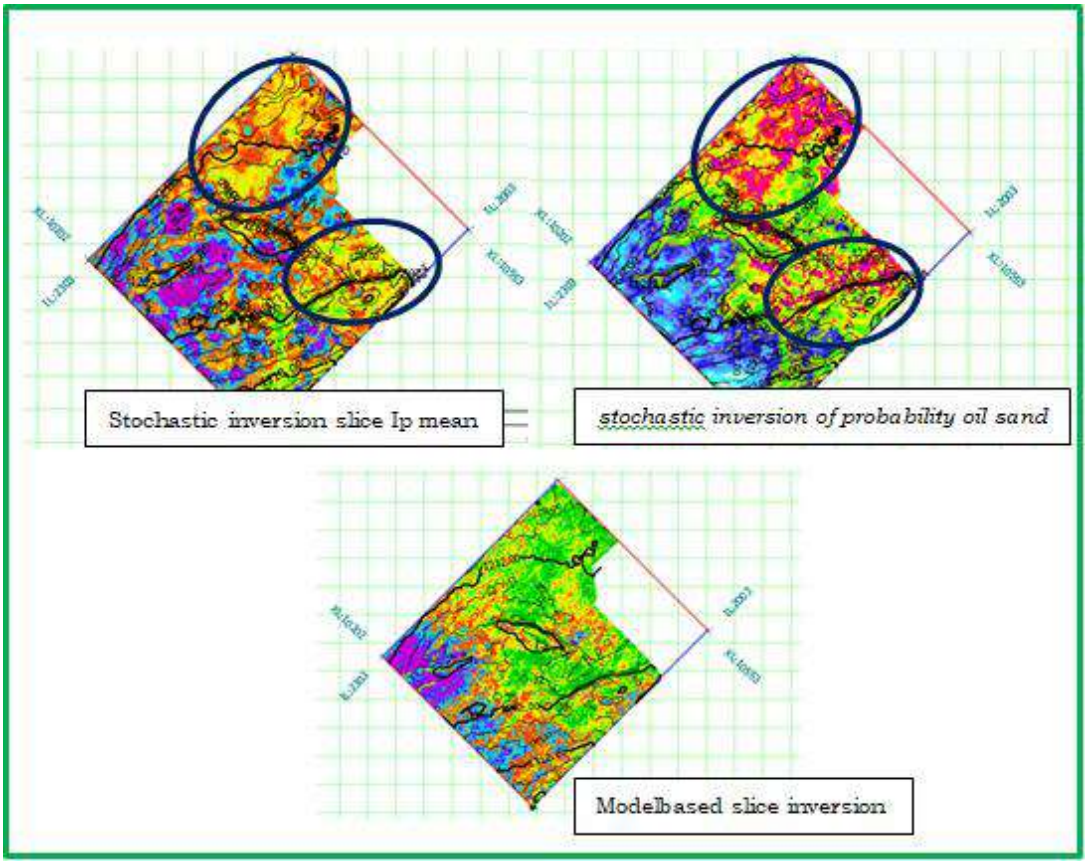

Figure 17. Comparison of slice results.

From the model-based slice with stochastics, the areas that have higher impendance are in the same area, but the results of the stochastic inversion slice show areas that are clearer regarding the existing distribution so that the results obtained are more accurate. If we compare the slice results from the stochastic inversion of Ip mean and the slice results from the stochastic inversion of probability oil sand, we get areas that have quite high hydrocarbon prospects. Where the area marked in Figure 17 is a sandstone distribution area with a vulnerable impendance value of 8000 – 9000 (m/s)* (g/cc) and for probability oil sand at 0.19 – 0.78.

Conclusion

Based on the research findings, the inversion of seismic data has yielded spatial uncertainty values for wells J2, J5, and J6. For well J2, the uncertainty values are (Ip) 3.25% and (Is) 5.20%. For J5, the values are (Ip) 4.83% and (Is) 7.47%. Meanwhile, for J6, the values are (Ip) 4.38% and (Is) 6.89%. Additionally, correlation coefficient values were calculated, with J2 having a coefficient of 0.99, J5 having a coefficient of 1.00, and J6 having a coefficient of 0.99. In the "JS" field, the hydrocarbon zone is identified within the acoustic impedance slice results ranging from 8517 to 9051 (m/s)*(g/cc). Furthermore, the probability values for oil sand in this zone range from 0.61 to 0.78.

Acknowledgements

The authors would like to thank the supervisors who have provided direction and guidance. Thanks to PT Pertamina Hulu Rokan Zona 1 who has provided data access and data processing so that this paper can be presented.

Author Contribution

This paper was completed thanks to the cooperation of all authors. The idea for

this topic was first put forward by Juventa. Data processing and interpretation was carried out by Johannes Kurni Bintang Awan Situmorang who was supervised by Muhammad Suhban and Ghindo Tampubolon helped arrange the background and some editing. Hopefully this kind of collaboration can continue.

Conflict of Interest

No potential conflicts of interest were reported by the authors. This research was entirely carried out by the author under the guidance of the author's lecturer.

References

Dani, I., & Sule, M. R. (2021). Pemodelan Seismik Pada Struktur Geologi Kompleks Menggunakan Metode Common Reflection Surface (CSR). *Jurnal Geofisika Eksplorasi*, 7(3), 164–177. https://doi.org/10.23960/jge.v7i3.135

Devi, G. A. A. (2018). *Analisis Perbandingan Inversi P-Impedance Dengan Metode Deterministik Model Based Dan Metode Stokastik Pada Formasi Lama Lapangan "Ksw" Cekungan Natuna Barat*. UPN Veteran Yogyakarta.

Dikman, T., Susilo, A., & Sabbeq, S. (2015). Korelasi Data Log Sumur dan Seismik untuk Penyebaran Litologi dan Porositas Reservoir Hidrokarbon Formasi Gumai Cekungan Sumatera Selatan, *Natural-B*, 3(2), 166–174. http://dx.doi.org/10.21776/ub.natural-b.2015.003.02.10

Ekawati, G. M., & Winardhi, I. S. (2018). Aplikasi inversi model base dan stokastik untuk memetakan pesebaran reservoir batupasir. *Jurnal of Science and Applicative Technology*, 2(1), 72–85. https://doi.org/10.35472/281451

Fernandes, F. J. D., Teixeira, L., Freire, A. F. M., & Lupinacci, W. M. (2023). Stochastic seismic inversion and Bayesian facies classification applied to porosity modeling and igneous rock identification. *Petroleum Science*, 21(2), 918–935. https://doi.org/10.1016/j.petsci.2023.11.020

Latifah, A., Dwi, P., & Elistia, L. N. (2019). Karakterisasi Recervor Mengunakan Seismik Inversi Deterministik Model Based Pada Lapangan Penobscot Kanada. *Jurnal Fisika Unand*, 8(2), 113–119. https://doi.org/10.25077/jfu.8.2.120-126.2019

Lukman, F., Haryanto, I., Firmansyah, Y., Gani, R. M. G., & Indriyanto, Y. (2019). Tektonostratigrafi Berdasarkan Analisis Seismik 2D Pada Sub Cekungan Jambi, Cekungan Sumatera Selatan. *Padjadjaran Geoscience Jurnal*, 3(1), 18–28. https://jurnal.unpad.ac.id/geoscience/article/view/20838

Irvanaya, S. H. (2022). *Analisis Pesebaran reservoir berdasarkan inversi deterministik dan stokastik serta multi altribut pada lapangan "Neresari" Sub cekungan Jambi*. UPN Veteran Yogyakarta.

Gaol, P. L. (2016). *Karakterisasi Reservoir untuk Menentukan Zona Prospek Berdasarkan Data Seismik dan Data Sumur Menggunakan Metode Inversi Akustik Impedansi (AI) dan Analisa Multiatribut Studi Kasus Formasi Talang Akar Lapangan FL Cekungan Sumatera Selatan*. Universitas Gadjah Mada.

Gahana, A. G., Sjafri, I., Gani, R. M. G., & Firmansyah, S. (2019). Karakterisasi Reservoir Menggunakan Analisis Petrofisika Pada Lapangan Y Formasi Talang Akar Cekungan Sumatera Selatan. *Padjadjaran Geoscience Journal*, 3(1), 29–37.

https://jurnal.unpad.ac.id/geoscience/article/view/20839

Kumalasari, I. N., Dewanto, O., & Mulyanto, B. S. (2018). Identifikasi Persebaran dan Sumur Usulan menggunakan Metode Well Logging, Petrofisika Inversi, Seismik Simultan dan Pemodelan 3D Geometri Reservoir. *Jurnal Geofisika Eksplorasi*, 1(16).

Liu, W., Du, W., Guo, Y., & Li, D. (2022). Lithology prediction method of coal-bearing reservoir based on stochastic seismic inversion and Bayesian classification: a case study on Ordos Basin. *Journal of Geophysics and Engineering*, 19(3), 494–510. https://doi.org/10.1093/jge/gxac033

Liu, X., Li, J., Chen, X., Guo, K., Li, C., Zhou, L., & Cheng, J. (2018). Stochastic inversion of facies and reservoir properties based on multi-point geostatistics. *Journal of Geophysics and Engineering*, 15(6), 2455–2468, https://doi.org/10.1088/1742-2140/aac694

Li, K., Yin, X., Liu, J., & Zong, Z. (2019). An improved stochastic inversion for joint estimation of seismic impedance and lithofacies. *Journal of Geophysics and Engineering*, 16(1), 62–76. https://doi.org/10.1093/jge/gxy005

Novriyani, M., Supriyanto, S., & Hidayat, R. (2016). Pemetaan Penyebaran Resevoar Berdasaran Metode Inversi Stokastik Dengan Integrasi Multiatribut Seismik Lapangan MZ, Cekungan Sumatera Tengah. Seminar Nasional Jurusan Fisika FMIPA UM 2016, FG-1 – FG-9.

Pradana, D. R., Wein, L., & Firman, S. (2017). Analisis Sebara Litologi Batu Pasir Dakota Menggunakan Metode Siesmik Inversi Berbasis Model, Studi Kasis Lapangan Teapot, Wyoming, USA. *Jurnal Sains dan Seni ITS*, 6(2), 2337–3520. http://dx.doi.org/10.12962/j23373520.v6i2.25226

Prasetiyohadi, S. A., Supriatna, J. M., Wirasatia, D., Ilmi, N. N., & Sunardi, E. (2022). Evaluasi Dan Korelasi Batuan Induk-Minyak Bumi Berdasarkan Analisis Geokimia Hidrokarbon Di Lapangan Sp, Sub-Cekungan Jambi. *Padjadjaran Geoscience Journal*, 6(3), 855–875. https://jurnal.unpad.ac.id/geoscience/article/view/45234

Prastika, N., Bagus, S., Ordas, D., Egi,W. (2018). Analsis Perbandingan Metode Seismik Inversi Impedansi Akustik Model Based, Band Limited, Dan Spare Spike Untuk Karaktersisasi Recervoar Karbonat Lapangan "NBL" Pada Cekungan Nias. *Jurnal Geofisika Eksplorasi*.

Rahmadani, E., Ordas. D., Karyanto, K., & Yulianto, N. (2020). Perhitungan Cadangan Hidrokarbon Formasi Talang Akar Menggunakan Analisis Petrofisika Dan Seismik Inversi AI Dengan Pendekatan MAP ALGEBRA Pada Lapangan Bisma Cekungan Sumatera Selatan. *Jurnal Geofisika Eksplorasi*, 4(3), 229–242. https://doi.org/10.23960/jge.v4i3.37

Rashad, O., El-Barkooky, A. N., El-Araby, A., El-Tonbary, M. (2022). Deterministic and Stochastic Seismic Inversion techniques towards a better prediction for the reservoir distribution in NEAG-2 Field, north Western Desert, Egypt. *Egyptian Journal of Petroleum*, 31(1), 15–23. https://doi.org/10.1016/j.ejpe.2021.12.002

Rohaman, M. (2017). *Aplikasi inversi stokastik untuk karakterisasi reservoir batupasir formasi gumai pada lapangan "MR"*. Institut Teknologi Bandung.

Srivastava, R. P., & Sen, M. K. (2009). Fractal-based stochastic inversion of poststack seismic data using very fast simulated annealing. *Journal of Geophysics and Engineering*, 6(4), 412–425. https://doi.org/10.1088/1742-2132/6/4/009

Xue, Y., & Sen, M. K. (2016). Stochastic seismic inversion using greedy annealed importance sampling. *Journal of Geophysics and Engineering*, 13(5), 786–804. https://doi.org/10.1088/1742-2132/13/5/786

Indexing and Abstracting

GEOFISIKA
UNIVERSITAS HASANUDDIN

ISSN 2579-5546